СИБИРСКИЙ ЖУРНАЛ НАУКИ И ТЕХНОЛОГИЙ

SIBERIAN JOURNAL OF SCIENCE AND TECHNOLOGY

CONTENTS

PART 1. INFORMATICS, COMPUTER TECHNOLOGY AND MANAGEMENT

PART 2. AVIATION AND SPACECRAFT ENGINEERING

PART 3. TECHNOLOGICAL PROCESSES AND MATERIAL SCIENCE

СОДЕРЖАНИЕ

ИНФОРМАТИКА,
ВЫЧИСЛИТЕЛЬНАЯ
ТЕХНИКА И УПРАВЛЕНИЕ

INFORMATICS,
COMPUTER TECHNOLOGY
AND MANAGEMENT

THE DEVELOPMENT AND INVESTIGATION OF THE EFFICIENCY OF THE DIFFERENTIAL EVOLUTION ALGORITHM FOR SOLVING MULTI-OBJECTIVE OPTIMIZATION PROBLEMS

D. A. Erokhin*, Sh. A. Akhmedova

Reshetnev Siberian State University of Science and Technology
31, Krasnoyarsky Rabochy Av., Krasnoyarsk, 660037, Russian Federation
*E-mail: erohhaa@mail.ru

In practice problems, which consist in the search of the best (optimal) solution according to the different irredundant and contradictory (conflicting) criteria, called multi-objective problems, are of frequent occurrence. One of the most commonly used methods for solving this kind of problems consists in combination of all criteria into the single one by using some linear relation. However, despite the simplicity of this method, solving problems with its help may cause other problems related to the determination of the mentioned linear combination, namely related to the determination of the weight coefficients for each criterion. The incorrect selection of these coefficients may lead to non-optimal solutions (according to the Pareto theory). In this regard, recently various population-based algorithms have been proposed for solving the described problems, which are the modifications of these population-based algorithms for solving single-objective optimization problems. This article describes the developed modifications of the Differential Evolution algorithm (DE) for solving multi-objective unconstrained optimization problems based on the well-known NSGA (Non-dominated Sorting Genetic Algorithm) and MOEA/D (Multiobjective Evolutionary Algorithm Based on Decomposition) schemes, which use the Pareto theory. The investigation into the efficiency of the Differential Evolution algorithm for solving multi-objective optimization problems in relation to the chosen mutation operator of the original DE algorithm and to the multi-objective scheme was conducted. The developed modifications were tested by using some well-known multi-objective real-valued optimization problems with 30 variables, such as ZDT1, ZDT2, ZDT3, etc. The practical problem of spacecraft control contour variant choice was solved as well. The experimental results show that better results were achieved by the Differential Evolution algorithm with the simplest mutation operators combined with the NSGA scheme. Thus, the applicability of the described modification for solving practical multi-objective optimization problems was demonstrated.

Keywords: optimization, differential evolution, Pareto theory, MOEA/D, NSGA, mutation.
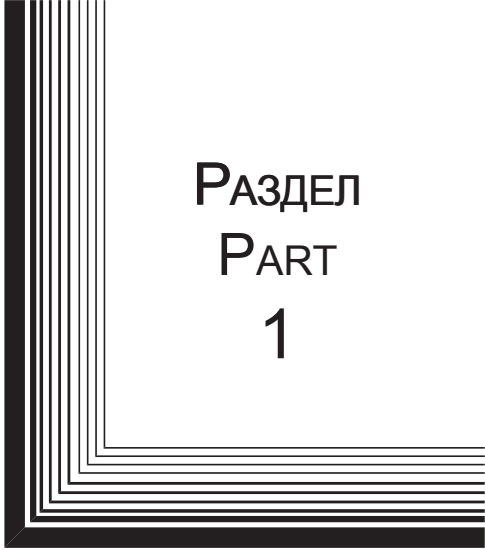
РАЗРАБОТКА И ИССЛЕДОВАНИЕ ЭФФЕКТИВНОСТИ АЛГОРИТМА ДИФФЕРЕНЦИАЛЬНОЙ ЭВОЛЮЦИИ ДЛЯ РЕШЕНИЯ ЗАДАЧ МНОГОКРИТЕРИАЛЬНОЙ ОПТИМИЗАЦИИ

Д. А. Ерохин*, Ш. А. Ахмедова

Сибирский государственный университет науки и технологий имени академика М. Ф. Решетнева
Российская Федерация, 660037, г. Красноярск, просп. им. газ. «Красноярский рабочий», 31
*E-mail: erohhaa@mail.ru

В практической деятельности часто встречаются задачи, заключающиеся в поиске лучшего (оптимального) решения при наличии различных несводимых друг к другу и противоречивых (конфликтующих) критериев оптимальности, называемые задачами многокритериальной оптимизации. Один из наиболее распространенных методов решения подобного рода задач заключается в объединении всех критериев в один, используя некоторое линейное соотношение. Несмотря на простоту метода, при решении задач таким способом могут возникнуть проблемы с определением самого линейного соотношения, а именно весовых коэффициентов каж-

дого критерия, неправильный подбор которых может привести к неоптимальным (в смысле теории Парето доминирования) решениям. В связи с этим в настоящее время предложены различные популяционные алгоритмы для решения описанных задач, которые в свою очередь являются модификациями этих же популяционных алгоритмов для решения задач однокритериальной оптимизации. В данной статье описаны разработанные модификации алгоритма дифференциальной эволюции (Differential Evolution, DE) для решения задач многокритериальной безусловной оптимизации на базе широко известных схем NSGA (Non-dominated Sorting Genetic Algorithm) и MOEA/D (Multiobjective Evolutionary Algorithm Based on Decomposition), использующих теорию Парето доминирования. Исследование эффективности алгоритма дифференциальной эволюции для решения задач многокритериальной оптимизации проводилось в зависимости от выбора оператора мутации исходного алгоритма дифференциальной эволюции и схемы учета множества целевых функций. Разработанные модификации были протестированы с помощью известных задач многокритериальной безусловной оптимизации вещественнозначных функций с 30 независимыми переменными, например, ZDT1, ZDT2, ZDT3 и т. д., также была решена практическая задача выбора эффективного варианта аппаратно-программного комплекса для систем управления космическими аппаратами. В результате экспериментов было установлено, что алгоритм дифференциальной эволюции демонстрирует лучшие результаты при использовании наиболее простых операторов мутации в сочетании со схемой учета целевых функций NSGA, таким образом, показана целесообразность его применения с данными параметрами для решения практических задач.

Ключевые слова: оптимизация, дифференциальная эволюция, теория Парето доминирования, MOEA/D, NSGA, мутация.

Introduction. Complex technical and organizational systems control requires constant decision making taking into consideration various criteria and limited resources. Such kind of problems (multi-objective optimization problems) can be found in different areas, including aerospace industry (for example, [1–3]). For some of them it is possible to find solutions, which would be optimal with respect to all criteria. However, the opposite situation, namely when the criteria conflict with each other, occurs more frequently. In that case there is s a need to determine a set of solutions (best possible variants), where each one of them can be considered as a compromise between all criteria.

There are various ways to determine the mentioned set of solutions, but the most popular among them is the Pareto dominance theory [4]. Generally speaking, a multi-objective optimization problem includes a set of D parameters (variables), a set of K objective functions of these variables, and a set of M constraints. It is necessary to find a solution, that is optimal according to all K criteria, while solving a multi-objective optimization problem; and the problem is formulated as follows:

$$y = f(x) = \left(f_1(x), f_2(x), ..., f_K(x) \right) \rightarrow opt, \qquad (1)$$

$$\begin{cases} g_j(x) \le 0, j = \overline{1, r}, \\ h_j(x) = 0, j = \overline{r+1, M}, \end{cases} \qquad (2)$$

where $x = (x_1, x_2, ..., x_D)$ is possible solution.

Let us consider the multi-objective unconstrained optimization problems. Generally, there are no additional requirements of functions $f_i(x)$, $i = 1, ..., K$, that would be convenient for optimization (for example, convexity, differentiability, etc.). Functions can be defined algorithmically; variables can be continuous, discontinuous, binary and even mixed. This fact significantly reduces the class of optimization algorithms, which could be applied to solving such problems.

In this study modifications of the Differential Evolutions (DE) algorithm [5] for solving multi-objective opti-

mization problems based on the well-known schemes such as MOEA/D (Multiobjective Evolutionary Algorithm Based on Decomposition) [6] and NSGA (Non-dominated Sorting Genetic Algorithm) [7], that use the Pareto theory, are introduced. Moreover, efficiency of these modifications was examined in accordance with the chosen DE's mutation operator [8].

Differential Evolution. Differential evolution or DE is a population-based meta-heuristic approach initially developed for solving multidimensional optimization problems. It was firstly introduced by K. Price and R. Storn in 1995 [5] for solving single-objective optimization problems. The DE algorithm is a direct optimization method, thus it only needs values of the objective function; it uses some of ideas the proposed for the genetic algorithms such as mutation as well.

The DE starts with the random initialization of the population that contains N individuals, to be more specific the set of N vectors is randomly generated. Each individual is represented by its coordinates in the search space with D dimensions. Then a new generation is created in the following way. For each individual x_i^t three different vectors from the old generation are randomly chosen, after that a new mutant vector v_i^t is generated by using the mutation operator.

Nowadays there are various mutation schemes for the differential evolution algorithm [8]. In this study five most popular mutation strategies were used (*rand, best, current_to_best, best2, rand2*):

$$v_j^t = x_{R1,j}^t + F\left(x_{R2,j}^t - x_{R3,j}^t \right); \qquad (3)$$

$$v_j^t = x_{best,j}^t + F\left(x_{R1,j}^t - x_{R2,j}^t \right); \qquad (4)$$

$$v_j^t = x_{i,j}^t + F\left(x_{best,j}^t - x_{i,j}^t \right) + F\left(x_{R1,j}^t - x_{R2,j}^t \right); \qquad (5)$$

$$v_j^t = x_{best,j}^t + F\left(x_{R1,j}^t - x_{R2,j}^t \right) + F\left(x_{R3,j}^t - x_{R4,j}^t \right); \qquad (6)$$

$$v_j^t = x_{R1,j}^t + F\left(x_{R2,j}^t - x_{R3,j}^t \right) + F\left(x_{R4,j}^t - x_{R5,j}^t \right). \qquad (7)$$

In these formulas indexes $R1$, $R2$, $R3$, $R4$ and $R5$ are numbers randomly chosen from the range $[1, N]$, all of them differ from the index i and each other; F is the scaling factor, namely the maximum possible distance by which the search area can be expanded in one variable; x_{best}^t – the best position found by the population during t iterations.

The next step is the crossover, which is performed for the mutant vector. During the crossover its coordinates (or at least a part of them) can be replaced with some probability (CR) by the coordinates of the parent vector. A new obtained vector is called a trial vector. If the value of the objective function calculated for the trial vector is better than the value of the objective function calculated for the parent vector, then the parent vector should be replaced by the trial vector in a new generation, otherwise it stays the same.

Modifications of the DE algorithm for solving multi-objective optimization problems. In this study two well-known schemes for the multi-objective optimization problems were used: Multiobjective Evolutionary Algorithm Based on Decomposition (MOEA/D) [6] and Non-dominated Sorting Genetic Algorithm (NSGA) [7].

Modification of the DE algorithm based on the scheme NSGA works as follows. First of all, in addition to the population of individuals an external archive is generated, in which optimal according to the Pareto theory solutions are saved. This archive is updated at each iteration.

Besides, on every iteration during the crossover the additional second archive of size $2N$, in which initially all individuals from the population are stored, is created. As was mentioned before, during crossover trial vectors, that can replace parent individuals in population, are generated. If the parent individual from the second additional archive is non-dominant with respect to the respective trial vector then the latter is discarded and the parent individual stays the same, and vice versa, if the trial vector is non-dominant then it replaces the parent vector in the second archive. However, if the parent and trial vectors are not comparable then they both are stored in the second additional archive. It should be noted that the trial vectors, which are stored in the mentioned archive, later participate in the crossover, and for them the mutant vectors are generated by using individuals saved in the same archive.

On the next step the second additional archive is truncated to the size N by using the sorting of individuals according to the degree of their non-dominance proposed for the NSGA scheme [7]. Individuals are sorted in the mentioned archive as follows. For each individual its rank, which is denoted as "*rank*", is determined. If an individual is non-dominant with respect to all other individuals from that archive then its *rank* = 0. After that the individual, which is non-dominant with respect to all other individuals from archive except the one with the *rank* = 0, is determined. Therefore, its *rank* is assigned to 1. If there are more than one such an individual, then the same *rank* is assigned to each of them. The process continues until all individuals in the population are ranked.

Next, the ranked individuals are selected according to the Crowding-distance metric (I) described in [9]. For each objective function the solutions with the smallest and largest values of this metric are determined. It is assumed that the metric value for these solutions from the second additional archive reaches its maximum. For other solutions from the archive the distance (metric value) is calculated as follows:

$$I[i] = \sum_{k=1}^{K} \frac{f_k[i+1] - f_k[i-1]}{f_k^{\max} - f_k^{\min}}. \qquad (8)$$

Here parameters $f_k^{\max}$ and $f_k^{\min}$ are the maximum and the minimum values of the k-th objective function, $f_k[i+1]$ and $f_k[i-1]$ are values of the k-th objective function for the $(i+1)$-th and $(i-1)$-th individuals respectively.

After that, the i-th individual is compared with the rest ($i = 1, ..., 2N$) until it is better than any individual according to the rank or to the value of the metric (the higher, the better). In this case, it is saved in a truncated archive, the comparison is stopped and the next individual is considered. These actions are repeated until the number of individuals in the truncated archive is equal to N.

The external archive, in which non-dominated solutions are stored, is updated by the individuals stored in the additional archive. The population that consists of individuals from the truncated archive passes to the next generation.

Now let us consider the modification of the DE algorithm, developed on the basis of the MOEA/D scheme [6]. As for the previous modification, initially an external archive for the non-dominated solutions according to the Pareto theory is generated; moreover, this archive is updated at each iteration. Further, the population of N individuals is initialized randomly.

For each i-th ($i = 1, ..., N$) individual, the vector L_i consisting of weight coefficients for the corresponding objective functions (one coefficient per objective function) is generated. The coefficients are generated randomly within the range $[0, 1]$ and vector L_i is normalized.

Next, the reference vector $z = (z_1, z_2, ..., z_K)$, where z_j is the best currently found value of the j-th ($j = 1, ..., K$) objective function f_j, is determined. In addition, for each i-th individual, a set of indexes $B(i)$ is created, it consists of T indexes of the nearest to L_i neighbors, to be more specific the distances between the vectors L_i and L_j ($j = 1, ..., N$ and $j \neq i$) are calculated using the Euclidean metric, and then T indexes of the nearest neighbors are selected.

Thus, for each i-th individual, where $i = 1, ..., N$, the set of indexes $B(i) = \{i(1), ..., i(T)\}$ is defined such as $L_i(1), ..., L_i(T)$ are the T closest vectors to the vector L_i. Then, during the mutation for the described schemes (3)–(7) indexes $R1$, $R2$, $R3$, $R4$, $R5$ for the i-th individual are randomly chosen from the set $B(i)$.

At the crossover step the trial vector U is generated, after that the vector z is updated. Finally, according to the rule described in [6] the individual in the population is updated (it is replaced by the trial vector U).

Experimental results. The investigation into the efficiency of the DE algorithm with different mutation strategies and schemes for the multi-objective optimization problems was conducted by using the following test problems: ZDT1, ZDT2, ZDT3, ZDT6, Schaffer's Min-Min (SCH) and DTLZ2 [10]. The following parameters were used for testing:

1) S – the maximum number of optimal according to the Pareto theory solutions, which were saved during the algorithm's work; it was set to 100;

2) N – the population size, it was equal to 100;

3) $MaxGen$ – the maximum number of iterations equal to 250;

4) $F = 0.4$;

5) $CR = 0.3$ for modification of the DE approach based on the MOEA/D scheme;

6) $CR = 0.6$ for modification of the DE approach based on the NSGA scheme;

7) $T = 20$;

8) $D = 30$.

Each problem was solved by all modifications 10 times and after each program run the following values were calculated: the E_f error (i. e. the difference between the obtained and real Pareto fronts) and the spread Δ (i. e. the extend of spread achieved among the obtained solutions).

The E_f error was calculated by using the following formula (9):

$$E_f = \left\| PF^e - PF^t \right\|^2 = \sum_{j=1}^{NS} \left(PF_j^e - PF_j^t \right)^2 , \qquad (9)$$

where PF^e is the found Pareto front, PF^t is the actual Pareto front, NS is the number of points in the external archive. The value of the spread Δ was determined using the following formula:

$$\Delta = \frac{d_f + d_l + \sum_{i=1}^{NS-1} \left| d_i - \overline{d} \right|}{d_f + d_l + (NS-1)\overline{d}} , \qquad (10)$$

where d_i is the minimal Euclidean distance between the i-th solution from the obtained Pareto front and other solutions from that front [11] (NS – number of solutions in the external archive), and $\overline{d}$ is the average distance. Parameters d_f and d_l are Euclidean distances between the extreme solutions of the real and obtained Pareto fronts.

Results obtained by the modification of the DE algorithm based on the MOEA/D scheme with different mutation strategies and averaged by the number of program runs are presented in tab. 1.

Thus, it was established that modification of the DE approach based on the MOEA/D scheme demonstrated the best results while using the mutation strategy *best*. Tab. 2 shows how many times this algorithm configuration outperformed others according to four criteria: *Best* – the best obtained values of E_f and Δ respectively, *Worst* – the worst values, *Mean* – the mean values for E_f and Δ, *SD* is the standard deviation for the obtained results.

Results obtained by the modification of the DE algorithm based on the NSGA scheme with different mutation strategies are presented in tab. 3.

Table 1

Results obtained by the DE+MOEA/D algorithm with different mutation schemes

Problem		rand	best	current_to_best	best2	rand2
ZDT1	E_f	0.00384	0.00054	6.59454	0.00119	0.0062
	Δ	0.16367	0.11775	0.489	0.13324	0.16509
ZDT2	E_f	0.00053	0.00041	5.92685	0.00055	0.00199
	Δ	0.09408	0.11174	0.70551	0.105	0.11352
ZDT3	E_f	0.15176	0.08976	4.84475	0.0003	0.00249
	Δ	0.19449	0.16297	0.43173	0.09944	0.15936
ZDT6	E_f	2.08E-07	2.05E-07	0.47384	2.03E-07	0.00391
	Δ	0.04915	0.44263	0.63503	0.04259	0.02977
SCH	E_f	6.85E-07	7.19E-07	0.00019	0.01249	7.19E-07
	Δ	0.40399	0.30593	0.36606	0.32616	0.35382
DTLZ2	E_f	0.00024	0.00022	2.62E-05	0.00056	0.00038
	Δ	0.05619	0.06844	0.0706	0.10307	0.07852

Table 2

The results of the comparison of the mutation schemes for the DE+MOEA/D modification

Scheme	E_f				Δ			
	Worst	*Best*	Mean	SD	*Worst*	*Best*	Mean	SD
rand	0	1	1	0	1	0	2	1
best	3	4	2	3	1	3	4	1
current_to_best	1	1	1	1	0	1	0	0
best2	2	0	2	2	3	2	1	3
rand2	0	0	0	0	1	0	0	1

Thus, it was established that the strategy *best* demonstrated the best results comparing to others in 10 cases, while the strategy *rand* in 14 cases. However, for this modification strategy *rand* outperforms the strategy *best* because it showed the better results according to the second criterion (spread of solutions along the front) more frequently. Tab. 4 shows how many times this algorithm configuration outperformed others according to four criteria: *Best* – the best obtained values of E_f and Δ respectively, *Worst* – the worst values, *Mean* – the mean values for E_f and Δ, *SD* is the standard deviation for the obtained results.

Examples of the Pareto fronts obtained by the developed modifications of the DE algorithm with determined on the previous step best mutation strategies for the listed test problems are demonstrated in fig. 1–6.

The developed modifications of the DE algorithm (DE + NSGA and DE + MOEA/D) are compared with the other methods for solving multi-objective optimization problems: MOPSO [12], NSGA-II [13], SPEA [14] and PAES [15]. Moreover, the comparison was made according to the previously used criteria (error and variation).

Tab. 5 shows the mean values for the criteria obtained by the listed algorithms. The results of the NSGA-II and SPEA, PAES algorithms are taken from the literature [15], and the results of the MOPSO algorithm were obtained independently.

Table 3

Results obtained by the DE+NSGA algorithm with different mutation schemes

Problem		*rand*	*best*	*current_to_best*	*best2*	*rand2*
ZDT1	E_f	0.00733	0.00884	0.00577	0.02993	0.03549
	Δ	0.0775	0.07231	0.28125	0.07318	0.06684
ZDT2	E_f	0.00627	0.00311	0.31043	0.0197	0.03744
	Δ	0.10933	0.603442	0.75164	0.11818	0.12551
ZDT3	E_f	0.00491	0.00628	0.00277	0.0259	0.44998
	Δ	0.06465	0.07346	0.59455	0.0817	0.16594
ZDT6	E_f	0.00058	2.90E-07	0.00212	3.25E-07	0.00324
	Δ	0.05462	0.03373	0.05722	0.0548	0.06761
SCH	E_f	4.93E-05	5.69E-06	5.66E-07	0.00041	7.7E-07
	Δ	0.10595	0.17782	0.18019	0.11755	0.10743
DTLZ2	E_f	11.1832	6.6664	12.164	4.91719	0.01469
	Δ	0.417295	0.27964	0.542015	0.20289	0.05895

Table 4

The results of the comparison of mutation schemes for the DE+NSGA modification

Scheme	E_f				Δ			
	Worst	*Best*	Mean	SD	*Worst*	*Best*	Mean	SD
rand	2	1	1	2	2	1	3	2
best	1	1	2	1	1	1	1	2
current_to_best	1	4	2	0	0	0	0	0
best2	1	0	0	1	2	3	0	1
rand2	1	0	1	2	1	1	2	1
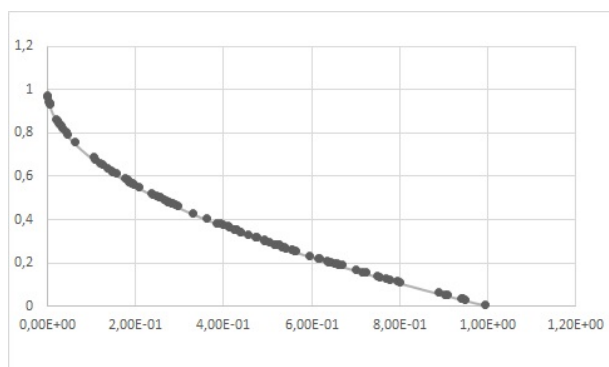
Based on scheme NSGA
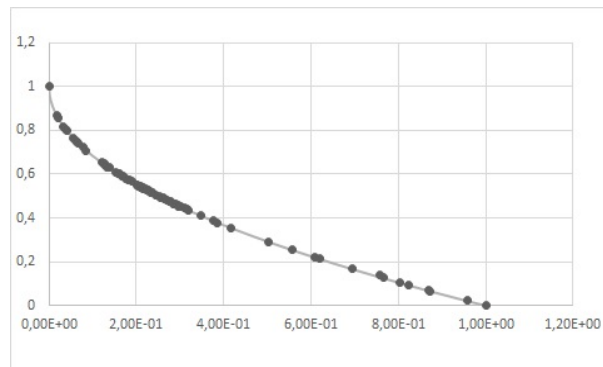
Based on scheme MOEA/D

Fig. 1. Examples of the Pareto front obtained for the ZDT1 problem

Рис. 1. Примеры фронта Парето, полученные для задачи ZDT1

Based on scheme NSGA   Based on scheme MOEA/D
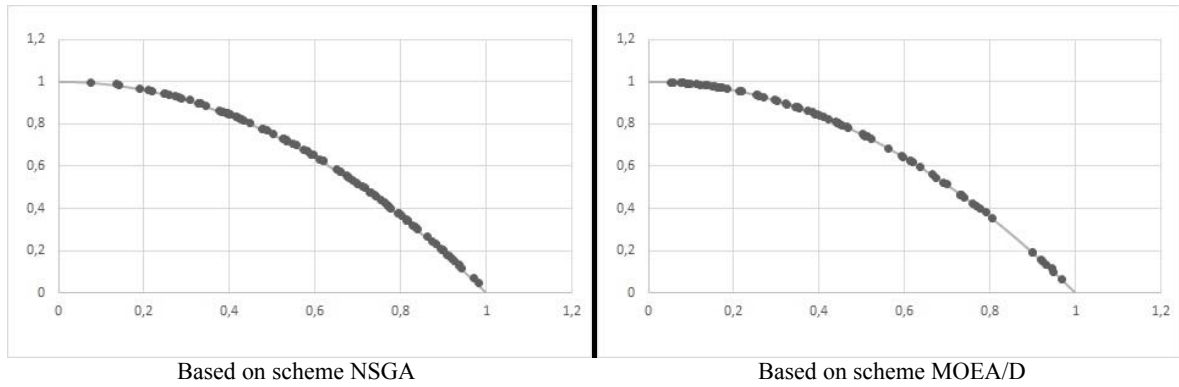
Fig. 2. Examples of the Pareto front obtained for the ZDT2 problem

Рис. 2. Примеры фронта Парето, полученные для задачи ZDT2

Based on scheme NSGA   Based on scheme MOEA/D
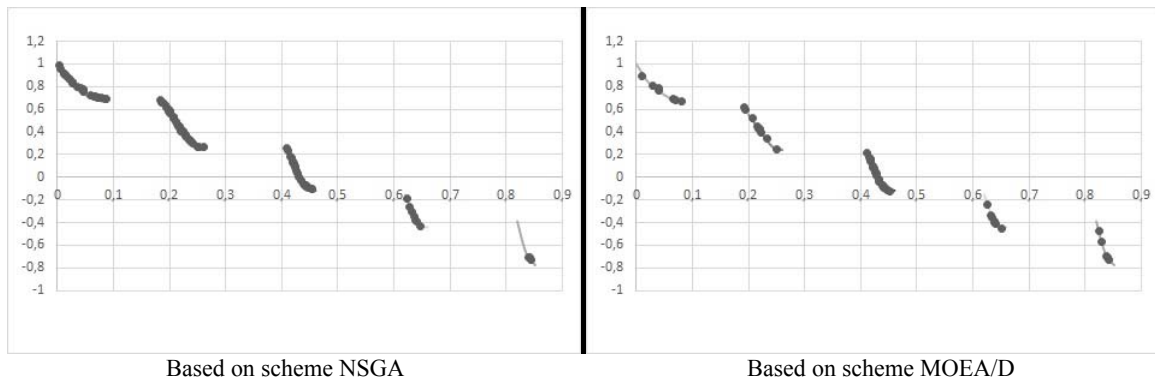
Fig. 3. Examples of the Pareto front obtained for the ZDT3 problem

Рис. 3. Примеры фронта Парето, полученные для задачи ZDT3

Based on scheme NSGA   Based on scheme MOEA/D
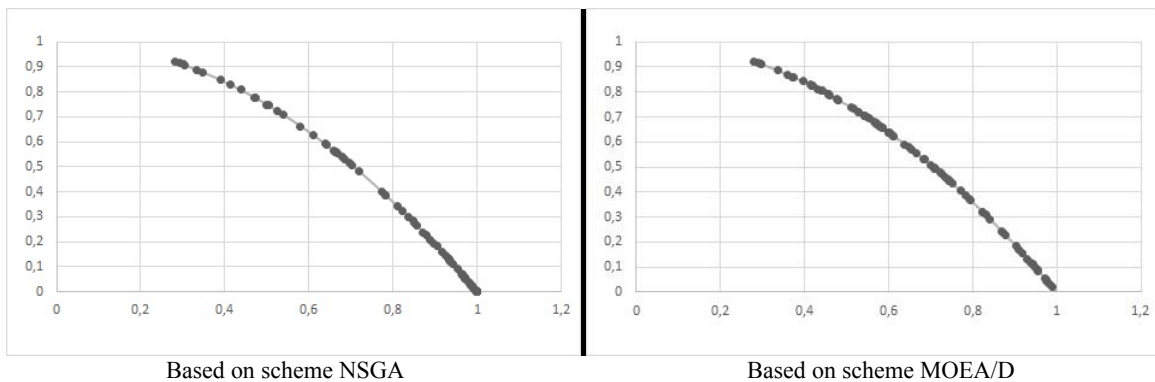
Fig. 4. Examples of the Pareto front obtained for the ZDT6 problem

Рис. 4. Примеры фронта Парето, полученные для задачи ZDT6

Based on scheme NSGA   Based on scheme MOEA/D
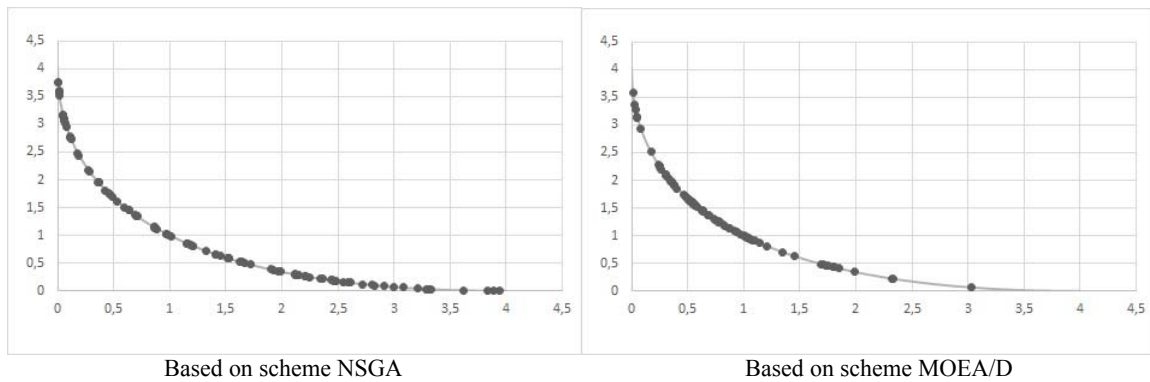
Fig. 5. Examples of the Pareto front obtained for the SCH problem

Рис. 5. Примеры фронта Парето, полученные для задачи SCH

Based on scheme NSGA   Based on scheme MOEA/D
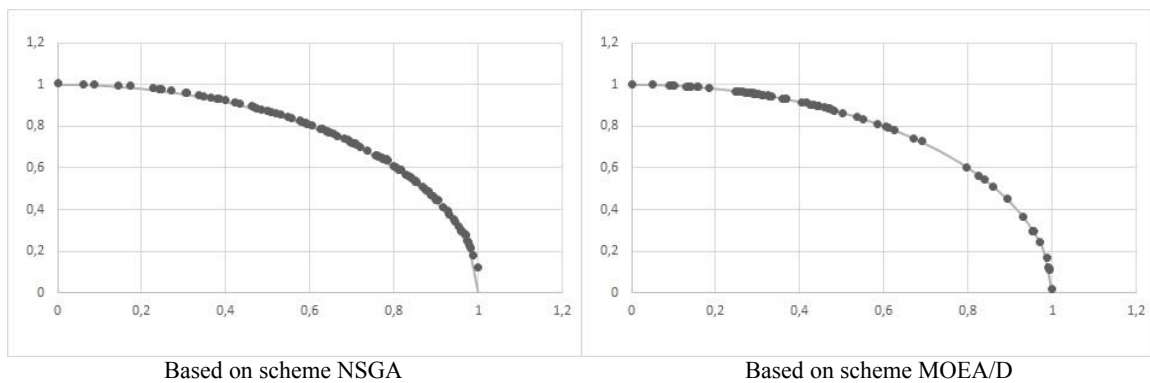
Fig. 6. Examples of the Pareto front obtained for the DTLZ2 problem

Рис. 6. Примеры фронта Парето, полученные для задачи DTLZ2

Table 5

The results of the comparison of the algorithms for solving multi-objective optimization problems

Algorithm	ZDT1		ZDT2		ZDT3		ZDT6		SCH	
	E_f	Δ	E_f	Δ	E_f	Δ	E_f	Δ	E_f	Δ
NSGA-II-r	0.0335	0.3903	0.0724	0.4308	0.1145	0.7385	0.2966	0.668	0.0034	0.4779
NSGA-II-b	0.0009	0.4633	0.0008	0.4351	0.0434	0.5756	7.8068	0.6445	0.0028	0.4493
SPEA	0.0018	0.7845	0.0013	0.7551	0.0475	0.6729	0.2211	0.8494	0.0034	1.0211
PAES	0.0821	1.2298	0.1263	1.1659	0.0239	0.7899	0.0855	1.1531	0.0013	1.0633
MOPSO	0.0605	0.5685	0.0807	0.4045	0.0016	0.415	0.0015	0.1204	8.91E-07	0.6039
DE+NSGA	0.0073	**0.0775**	0.0063	**0.1093**	**0.0049**	**0.0646**	0.5706	**0.1977**	4.93E-05	**0.1059**
DE+MOEA/D	**0.0005**	0.1177	**0.0004**	0.1117	0.0898	0.163	**2.05E-07**	0.4426	**7.19E-07**	0.3059

Thus, as a result of the research, it is established that the best values of objective functions are achieved by modifying the algorithm of differential evolution based on the NSGA scheme with the simplest mutation strategy called *rand*. Moreover, the experiments demonstrate that the modification of the DE algorithm of the NSGA scheme approximates the Pareto front better than the other multi-objective optimization algorithms, namely MOPSO, PAES, NSGA-II, SPEA, DE + MOEA / D.

The problem of the choice of spacecraft control contour variant. In this study the problem of the choice of spacecraft's control contour variant [16] is considered. The functioning process of a spacecraft control subsystems is modeled with Markov chains, while the problem of choosing an effective variant for a spacecraft control system is formulated as a multi-objective discrete optimization problem with algorithmically given functions.

The problem statement and the way the problem of spacecraft's control contour variant choice was modeled are presented in [16]; in this study only a brief description is given.

The system for monitoring and control of an orbital group of telecommunication satellites includes on-board control complexes (BCC) of a spacecraft, a distributed system of telemetry, command and ranging (TCR) stations and data telecommunication systems in each, command measuring systems (CMS) and flight control center (FCC). It should be noted that the last three subsystems are combined into the ground-based control complex (GCC).

Thus, the ground control complex interacts with the onboard control complex using a telecommunication system, as well as command measuring systems and data transmission systems, which include communication centers of a flight control center. BCC is the controlling subsystem of the satellite that ensures real time checking and controlling of on-board systems including pay-load equipment as well as fulfilling program-temporal control. Control functions performed by the automated control system can be divided into subsystems called "control contours". Mentioned contours perform various functions, for example the following contours can be distinguished: a technological contour, a command-program contour, a target contour, etc. [16].

The main task of the command-program contour is the maintenance of the tasks of creating command-programming information, transmitting it to BCC and executing it and control action as well as the realization of the temporal program mode of control. Let us consider the simplified control system, which consists of three subsystems: onboard target equipment, on-board control complexes and ground-based control complex.

If we suppose that BCC can fail and GCC is absolutely reliable, then we can introduce the following notations: λ_1 is the intensity of BCC failures, μ_1 is the intensity of temporal program (TP) computation, μ_2 is the intensity of the command-programming information (CPI) loading into BCC, μ_3 is the intensity of temporal program execution, μ_4 is the intensity of BCC being restored. Therefore, all stochastic flows in the system are Poisson, and there are five possible states for this contour [16]:

1) BCC fulfills TP, GCC is free;
2) BCC is free, GCC computes TP;
3) BCC is free; GCC computes CPI and loads TP;
4) BCC is restored with GCC which is waiting for continuation of TP computation;
5) BCC is restored with GCC which is waiting for continuation of CPI computation.

The corresponding Kolmogorov system of equations for the final probabilities is the following:

$$P_1 \cdot (\lambda_1 + \mu_3) - \mu_2 \cdot P_3 = 0, \qquad (11)$$

$$P_2 \cdot (\mu_1 + \lambda_1) - \mu_3 \cdot P_1 - \mu_4 \cdot P_4 = 0, \qquad (12)$$

$$P_3 \cdot (\lambda_1 + \mu_2) - \mu_1 \cdot P_2 - \mu_4 \cdot P_5 = 0, \qquad (13)$$

$$P_4 \cdot \mu_4 - \lambda_1 \cdot P_1 - \lambda_1 \cdot P_2 = 0, \qquad (14)$$

$$P_5 \cdot \mu_4 - \lambda_1 \cdot P_3 = 0, \qquad (15)$$

$$P_1 + P_2 + P_3 + P_4 + P_5 = 1. \qquad (16)$$

In these formulas P_i is the probability that the system is in the i-th state, where $i = 1, \ldots, 5$. After solving the system (11)–(16), the necessary indexes of control quality for the command-programming contour can be calculated:

1) $T = \dfrac{P_1}{\mu_2 \cdot P_3}$ – the average duration of the independent operating of the spacecraft for this contour;

2) $t_1 = \dfrac{P_3 + P_5}{\mu_1 \cdot P_2}$ – the average duration of BCC and GCC interactions when loading TP for the next interval of independent operation of the spacecraft;

3) $t_2 = \dfrac{P_2 + P_3 + P_4 + P_5}{P_1 \cdot (\lambda_1 + \mu_3)}$ – the average time from the start of TP computation till the start of TP fulfillment by BCC.

Maximizing the first indicator and minimizing the last two indicators leads to the choosing of an effective variant for a spacecraft control system. Thus, the multi-objective optimization problem is formulated with three objective functions. In this study it was solved by the best developed configurations of the DE+NSGA and DE+MOEA/D algorithms. The examples of the obtained Pareto fronts for the described optimization problem are presented in the fig. 7, to be more specific the projection of the Pareto front on the plane $\mu_2 - \mu_4$ (μ_2 – horizontal axis, μ_4 – vertical axis). In addition, on the graphs, the solid points are the points from the Pareto set, obtained by the algorithm, the open points are the true set points (not found respectively).

The problem was solved by each algorithm 10 times, for each program run the number of iterations was set to 30, number of individuals to 20, and for the DE+MOEA/D algorithm parameter was equal to 5. As a result of the research, it was established that modification of the DE algorithm based on the NSGA scheme (DE+NSGA) with the previously found configuration is able to solve the described problem of the choice of spacecraft control contour variant better. Therefore, the workability of that algorithm was verified on real-world problem.

Conclusions. In this paper two developed modifications of the differential evolution algorithm based on the schemes NSGA (DE+NSGA) and MOEA/D (DE+MOEA/D) for solving multi-objective optimization problems are described. First of all, the efficiency of the proposed modifications was examined in accordance with the selected mutation strategy: it was established that for the DE+NSGA algorithm the most useful is the *rand* mutation strategy, while for the DE+MOEA/D algorithm it is the *best* strategy.

Then the results obtained by modifications of the differential evolution algorithm with defined mutation strategies were compared with the results obtained by other well-known population-based algorithms. Finally, it was proved that the modification DE+NSGA described in this study with the *rand* mutation strategy outperforms alternative algorithms for solving multi-objective optimization problems.

Based on scheme NSGA

Based on scheme MOEA/D
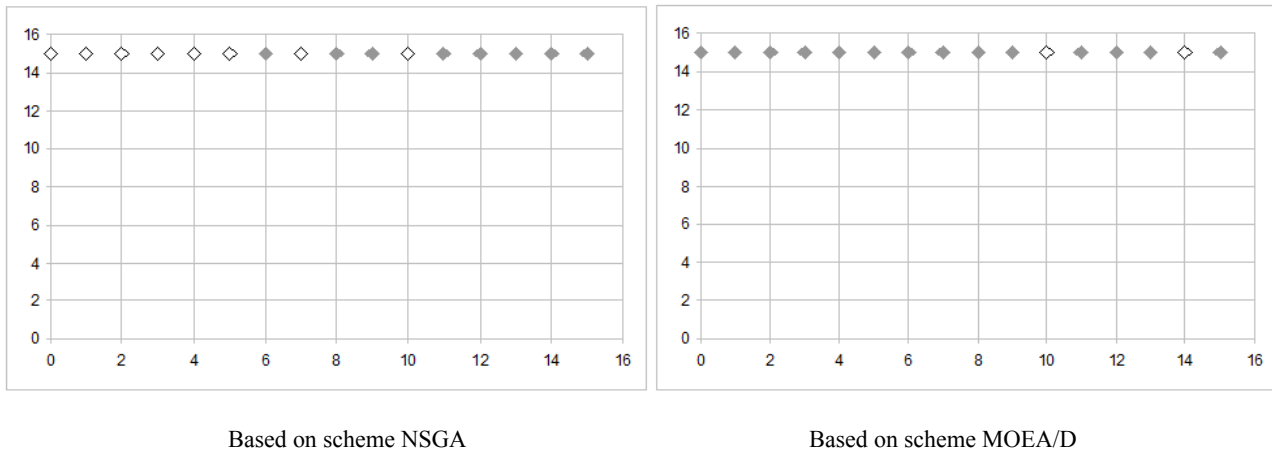
Fig. 7. Examples of the Pareto set obtained for the problem of the spacecraft control contour variant choice

Рис. 7. Примеры множества Парето, полученные для задачи выбора эффективного варианта управления КА

Besides, the problem of the choice of spacecraft control contour variant was solved and the workability of the proposed approaches was demonstrated on the real-world problem.

References

1. Semenkina M., Akhmedova Sh., Brester Ch. et al. Choice of spacecraft control contour variant with self-configuring stochastic algorithms of multi-criteria optimization. *Proceedings of the 13th International Conference on Informatics in Control, Automation and Robotics (ICINCO'2016).* 2016, P. 281–286.

2. Semenkina M., Akhmedova Sh., Semenkin E. et al. Spacecraft solar arrays degradation forecasting with evolutionary designed ANN-based predictors. *Proceedings of the 11th International Conference on Informatics in Control, Automation and Robotics (ICINCO 2014).* 2014, P. 421–428.

3. Akhmedova Sh., Semenkin E. Co-operation of biology related algorithms for multiobective optimization problems. *Proceedings of the International Conference on Computer Science and Artificial Intelligence (ICCSAI).* 2014.

4. Podinovskij V., Nogin V. *Pareto-optimalnye resheniya mnogokriterialnyh zadach* [Pareto Optimal Solutions of the Multiobjective Problems]. Moscow, Nauka Publ., 1982, 256 p.

4. Storn R., Price K. Differential evolution – a simple and efficient heuristic for global optimization over continuous spaces. *Journal of Global Optimization.* 1997, Vol. 11, No. 4, P. 341–359.

6. Zhang Q., Li H. MOEA/D: A multiobjective evolutionary algorithm based on decomposition. *IEEE Trans-actions on Evolutionary Computation.* 2007, Vol. 11, Iss. 6, P. 712–731.

7. Srinivas N., Deb K. Multi-objective function optimization using nondominated sorting genetic algorithms. *Evolutionary Computation.* 1994, Vol. 2, No. 3, P. 221–248.

8. Das S., Suganthan P. N. Differential evolution: A survey of the state-of-the-art. *IEEE Transactions on Evolutionary Computation.* 2011, Vol. 15, Iss. 1, P. 4–31.

9. Deb K., Jain S. Running Performance metrics for evolutionary multi-objective optimization. *Proceedings of the 4th Asia-Pacific Conference on Simulated Evolution and Learning (SEAL'02).* 2002, Vol. 1, P. 13–20.

10. Zitzler E., Thiele L. An evolutionary algorithm for multiobjective optimization: The strength pareto approach. *Technical Report 43, Computer Engineering and Networks Laboratory (TIK), Swiss Federal Institute of Technology (ETH) Zurich.* 1998.

11. Ah King R. T. F., Deb K., Rughooputh H.C.S. Comparison of NSGA-II and SPEA2 on the multiobjective environmental/economic dispatch problem. *University of Mauritius Research Journal.* 2010, Vol. 16, P. 485–511.

12. Moore J., Chapman R. Application of particle swarm to multiobjective optimization. Technical Report, Department of Computer Science and Software Engineering, Auburn University, 1999.

13. A fast and elitist multiobjective genetic algorithm: NSGA–II / K. Deb, A. Pratap, S. Agarwal et al. *IEEE Transactions on Evolutionary Computation.* 2002, Vol. 6, P. 182–197.

14. Zitzler E., Thiele L. Multiobjective evolutionary algorithms: A comparative case study and the strength Pareto approach. *IEEE Transactions on Evolutionary Computation.* 1999, Vol. 3, No. 4, P. 257–271.

15. Knowles J. D., Corne D. W. The Pareto archived evolution strategy: A new baseline algorithm for Pareto multiobjective optimization. *Proceedings of the IEEE Congress on Evolutionary Computation.* 1999, Vol. 1, P. 98–105.

16. Semenkina M., Akhmedova Sh., Brester C., Semenkin E. Choice of spacecraft control contour variant with self-configuring stochastic algorithms of multi-criteria optimization. *Proceedings of the 13th International Conference on Informatics in Control, Automation and Robotics*. 2016, Vol. 1, P. 281–286.

Библиографические ссылки

1. Choice of spacecraft control contour variant with self-configuring stochastic algorithms of multi-criteria optimization / M. Semenkina, Sh. Akhmedova, Ch. Brester [et al.] // Proceedings of the 13th International Conference on Informatics in Control, Automation and Robotics (ICINCO'2016). 2016. P. 281–286.

2. Spacecraft solar arrays degradation forecasting with evolutionary designed ANN-based predictors / M. Semenkina, Sh. Akhmedova, E. Semenkin [et al.] // Proceedings of the 11th International Conference on Informatics in Control, Automation and Robotics (ICINCO 2014). 2014. P. 421–428.

3. Akhmedova Sh., Semenkin E. Co-operation of biology related algorithms for multiobective optimization problems // Proceedings of the International Conference on Computer Science and Artificial Intelligence (ICCSAI). 2014.

4. Подиновский В., Ногин В. Парето-оптимальные решения многокритериальных задач. М. : Наука, 1982. 256 с.

5. Storn R., Price K. Differential evolution – a simple and efficient heuristic for global optimization over continuous spaces // Journal of Global Optimization. 1997. Vol. 11, No. 4. P. 341–359.

6. Zhang Q., Li H. MOEA/D: A multiobjective evolutionary algorithm based on decomposition // IEEE Transactions on Evolutionary Computation. 2007. Vol. 11, Iss. 6. P. 712–731.

7. Srinivas N., Deb K. Multi-objective function optimization using nondominated sorting genetic algorithms // Evolutionary Computation. 1994. Vol. 2, No. 3. P. 221–248.

8. Das S., Suganthan P.N. Differential evolution: A survey of the state-of-the-art // IEEE Transactions on Evolutionary Computation. 2011. Vol. 15, Iss. 1. P. 4–31.

9. Deb K., Jain S. Running Performance metrics for evolutionary multi-objective optimization // Proceedings of the 4th Asia-Pacific Conference on Simulated Evolution and Learning (SEAL'02). 2002. Vol. 1. P. 13–20.

10. Zitzler E., Thiele L. An evolutionary algorithm for multiobjective optimization: The strength pareto approach // Technical Report 43, Computer Engineering and Networks Laboratory (TIK), Swiss Federal Institute of Technology (ETH) Zurich. 1998.

11. Ah King R. T. F., Deb K., Rughooputh H.C.S. Comparison of NSGA-II and SPEA2 on the multiobjective environmental/economic dispatch problem // University of Mauritius Research Journal. 2010. Vol. 16. P. 485–511.

12. Moore J., Chapman R. Application of particle swarm to multiobjective optimization // Technical Report, Department of Computer Science and Software Engineering, Auburn University. 1999.

13. A fast and elitist multiobjective genetic algorithm: NSGA–II / K. Deb, A. Pratap, S. Agarwal [et al.] // IEEE Transactions on Evolutionary Computation. 2002. Vol. 6. P. 182–197.

14. Zitzler E., Thiele L. Multiobjective evolutionary algorithms: A comparative case study and the strength Pareto approach // IEEE Transactions on Evolutionary Computation. 1999. Vol. 3, No. 4. P. 257–271.

15. Knowles J. D., Corne D. W. The Pareto archived evolution strategy: A new baseline algorithm for Pareto multiobjective optimization // Proceedings of the IEEE Congress on Evolutionary Computation. 1999. Vol. 1. P. 98–105.

16. Semenkina M., Akhmedova Sh., Brester C., Semenkin E. Choice of spacecraft control contour variant with self-configuring stochastic algorithms of multi-criteria optimization // Proceedings of the 13th International Conference on Informatics in Control, Automation and Robotics. 2016. Vol. 1. P. 281–286.

Erokhin Danil Aleksandrovich – student; Reshetnev Siberian State University of Science and Technology. E-mail: erohhaa@mail.ru.

Akhmedova Shakhnaz Agasuvar kyzy – Cand. Sc., associate professor of the Department of Higher Mathematics; Reshetnev Siberian State University of Science and Technology. E-mail: shahnaz@inbox.ru.

Ерохин Данил Александрович – студент; Сибирский государственный университет науки и технологий имени академика М. Ф. Решетнева. E-mail: erohhaa@mail.ru.

Ахмедова Шахназ Агасувар кызы – кандидат технических наук, доцент кафедры высшей математики; Сибирский государственный университет науки и технологий имени академика М. Ф. Решетнева. E-mail: shahnaz@inbox.ru.

TO THE TASK OF CONTROLLING A GROUP OF OBJECTS ON THE BASIS OF INFORMATION TECHNOLOGIES

D. A. Zhalnin

LLC "Region Avtomatika"
1b, Glinki St., Krasnoyarsk, 660031, Russian Federation
E-mail: Denis@Zhalnin.com

To participate the TPP with cross-section communications in the general primary frequency control, it is necessary to have a working main regulator. The main regulator is designed to maintain the steam pressure in the major steam line of the TPP at a given level, which is a difficult task. At the TPP with cross-connections, the steam produced by the boilers enters the major steam line. To maintain the pressure in the major steam line, it is necessary to control the heat load of the working boilers. Traditional solutions to construct the main regulator found no use, as have a number of disadvantages, not allowing exploiting a system of automatic control. Looking at the steam pressure control system in the major steam line from the bottom to up, it is possible to identify disadvantages that prevent the effective operation of the main regulator at each level. At the lower level of the main regulator, there are controllers of heat load of boilers, built according to the scheme task-heat. Heat load controllers are designed to maintain heat release in the boiler furnace at the required level. The heat signal is the sum of the signals for the steam flow of the boiler and the rate of change in the steam pressure in the boiler drum. Such a structure does not allow maintaining the invariance of the heat signal under external disturbances effectively, as sharp changes of the steam pressure in the major steam line lead to a "false" operation of the controllers. At the upper level there is the main regulator itself, which maintains the steam pressure in the major steam line at a given level and corrects the tasks to the controllers of the heat load of the boilers. The simultaneous identical effect on the heat load of the boilers cannot be optimal from the point of view of the criteria for assessing the quality of regulation, since the dynamic properties of the boilers, such as the gain, the transition time constant and the transport delay are individual for each boiler.

However, in 2006–2008, the attempt to build an updated main regulator that takes into account the shortcomings of the traditional scheme was made. The basis of the structure of the main regulator is still parametric and, as a result of ten-years' experience, shortcomings in the operation of the updated main regulator were identified. The shortcomings, in most cases, consist in need of frequent corrections of adjusting coefficients of system because of the change of dynamic properties of an object during the operation. In fact, the same problems related to the parametric structure of the regulator remain.

Up-to-date information technologies made it possible to introduce adaptive process control systems that allow to count an extended number of signals entering the system and to form control actions, based on both current and historical data of the technological process. The use of the latest information technologies and modern hardware in the control of complex multi-connected units that solve not only the problems of process control, but also the problem of improving the economic and environmental performance of enterprises, should become a new step in the development of automatic control systems.

Keywords: TPP with cross-section connections, main regulator, heat load controller, pressure regulation in the major steam line.

К ЗАДАЧЕ УПРАВЛЕНИЯ ГРУППОЙ ОБЪЕКТОВ НА ОСНОВЕ ИНФОРМАЦИОННЫХ ТЕХНОЛОГИЙ

Д. А. Жалнин

ООО «Регион Автоматика»
Российская Федерация, 660031, г. Красноярск, ул. Глинки, 1б
E-mail: Denis@Zhalnin.com

Для участия тепловых электростанций (ТЭС) с поперечными связями в общем первичном регулировании частоты необходимо наличие работающего главного регулятора. Главный регулятор предназначен для поддержания давления пара в общем паропроводе ТЭС на заданном уровне, что является сложной задачей. На ТЭС с поперечными связями производимый котлами пар поступает в общий паропровод. Для поддержания давления в общем паропроводе необходимо комплексное управление тепловой нагрузкой работающих котлов. Традиционные решения построения главного регулятора не нашли применения, так как имеют ряд недостатков, не позволяющих эксплуатировать такую систему автоматического регулирования. Если рассматривать систему регулирования давления пара в общем паропроводе снизу вверх, можно на каждом уровне выявить недостатки, мешающие эффективной работе главного регулятора. На нижнем уровне главного регулятора расположены регуляторы тепловой нагрузки котлов, построенные по схеме задание – теплота. Регуляторы тепловой нагрузки предназначены для поддержания тепловыделения в топке котла на требуемом уровне. Сигнал по теплоте представляет собой сумму сигналов по расходу пара за котлом и скорости изменения давления пара в барабане котла. Такая структура не позволяет эффективно поддерживать инвариантность сигнала по теплоте при внешних возмущениях, таких как резкое изменение давления пара в общем паропроводе, что приводит к «ложной» работе регуляторов. На верхнем уровне расположен непосредственно сам главный регулятор, поддерживающий давление пара в общем паропроводе на заданном уровне и корректирующий задания регуляторам тепловой нагрузки котлов. Одновременное одинаковое воздействие на тепловую нагрузку котлов не может быть оптимальным с точки зрения критериев оценки качества регулирования, так как динамические свойства котлов, такие как коэффициент усиления, постоянная времени переходного процесса и транспортное запаздывание, индивидуальные для каждого котла.

Однако в 2006–2008 гг. была осуществлена попытка построения обновленного главного регулятора, учитывающего недостатки традиционной схемы. Основа структуры главного регулятора по-прежнему осталась параметрической, и в результате десятилетнего опыта эксплуатации были выявлены недочеты в работе обновленного главного регулятора. Недочеты в основном состоят в необходимости частой корректировки настроечных коэффициентов системы из-за изменения динамических свойств объекта в процессе эксплуатации. По сути, остались те же самые проблемы, связанные с параметрической структурой регулятора.

С появлением новейших информационных технологий появляется возможность внедрения адаптивных систем управления технологическими процессами, позволяющими обрабатывать расширенное количество поступающих в систему сигналов и формировать управляющие воздействия, основываясь как на текущих, так и на исторических данных технологического процесса. Использование новейших информационных технологий и современных аппаратных средств при управлении сложными многосвязными объектами, решающих не только задачи управления технологическими процессами, но и задачи повышения экономических и экологических показателей предприятий, должно стать новым витком в развитии систем автоматического управления.

Ключевые слова: ТЭС с поперечными связями, главный регулятор, регулятор тепловой нагрузки, регулирование давления в общем паропроводе.

Introduction. One of the conditions of participation of thermal power plants (TPP) with cross-section communications in the general primary regulation of frequency (GPRF) is functioning as the main regulator of steam pressure in the major steam line to control the load of the group of boilers participating in GPRF [1]. Traditional automatic control systems (ACS) of the heat load of boilers used at TPP with cross-connection communications are not able to provide the required dynamics of primary power output at a sudden change in frequency, which can be one of the reasons for emergency fan shutdowns in power systems.

Traditional approach. To maintain the steam pressure in the main steam line at the TPP with cross-connection communications, as a rule, a control scheme is used, when one of the boilers, working in the "regulating" mode, maintains the pressure in the main steam line, and the remaining boilers, working in the "basic" mode, support their specified steam loads.

With this control scheme, the automatic change in the total steam load of the station is limited to the range of possible steam loads of the boiler operating in the "regulating" mode, which is usually 70–100 % of the nominal capacity of the boiler.

Such a range of regulation can not provide a change in the electrical power of the station in 10 % of the nominal frequency deviation, which is necessary for the participation of the station in GPRF.

In order to increase the range of regulation in the "regulating" mode, we can include two boilers and more, but then there is an effect of "pumping" loads of boilers. It is caused by different dynamic properties of boiler equipment and the lack of centralized pressure measurement in the major steam pipe, as well as different values for different boilers job. As a result, some boilers are loaded to the maximum, while others are unloaded to a minimum. This approach makes the process of regulation impossible.

Generally accepted structure of the main regulator (MR), which maintains the pressure in the major steam line at a given value [2], in which one correcting regulator influence the task of the heat load controllers (HLC) of several boilers, has not been used at TPP with cross-connection communications for the following practical reasons:

– the pressure extraction point in the major steam line is the one and does not allow to regulate the pressure at different sets of working boilers and turbines effectively, as well as at the withdrawal of sections of the major steam line for repair;

– when changing the set of working boilers requires reconfiguration of the main regulator;

– the values of the setting coefficients of the main regulator for all boilers can not be the same, since the dynamic properties of the cascade regulator "MR-HLC" are different for each boiler.

Attempts to solve. From 2006 to 2008 at Krasnoyarsk TPP-2 of JSC "Yenisei TGC (TGC-13)" the main regulator that resolves a number of shortcomings of the conventional pressure control structure of the main steam line at

TPP with cross-connection communication was implemented [3]. A significant difference between the updated structure of the main regulator is that instead of one corrective regulator acting on a group of boilers, several corrective regulators are used, separately acting on each boiler.

The technological scheme of the major steam line of Krasnoyarsk TPP-2 is shown in fig. 1. It can be seen from the scheme that the boilers can operate both on the main steam line and separately (block). At block inclusion of boiler units or shutdown of any part of the main steam line, it is necessary to maintain constant pressure in in each its separate part.

Before the implementation of the updated main regulator, boilers heat load regulating systems were used under the scheme of task-heat (fig. 2). The "heat" signal is formed from two signals: steam flow rate and pressure change rate in the boiler drum. The main disadvantage of such a structure of the regulator is that when the pressure in the main steam line (external disturbances) changes, the pressure in the boiler drum changes with a significant delay caused by the capacitive properties of the steam path "drum – steam super heater – steam chamber – main steam line". This effect makes it impossible to achieve invariance of the signal by "heat" to external disturbances.

Fig. 3 shows the steam flow rate of the boiler, the steam pressure in the boiler drum, the reduced rate of change in the steam pressure in the boiler drum and the change in the reduced signal by "heat" with the pressure increase in the major steam line by 0.3 MPa (external perturbation).
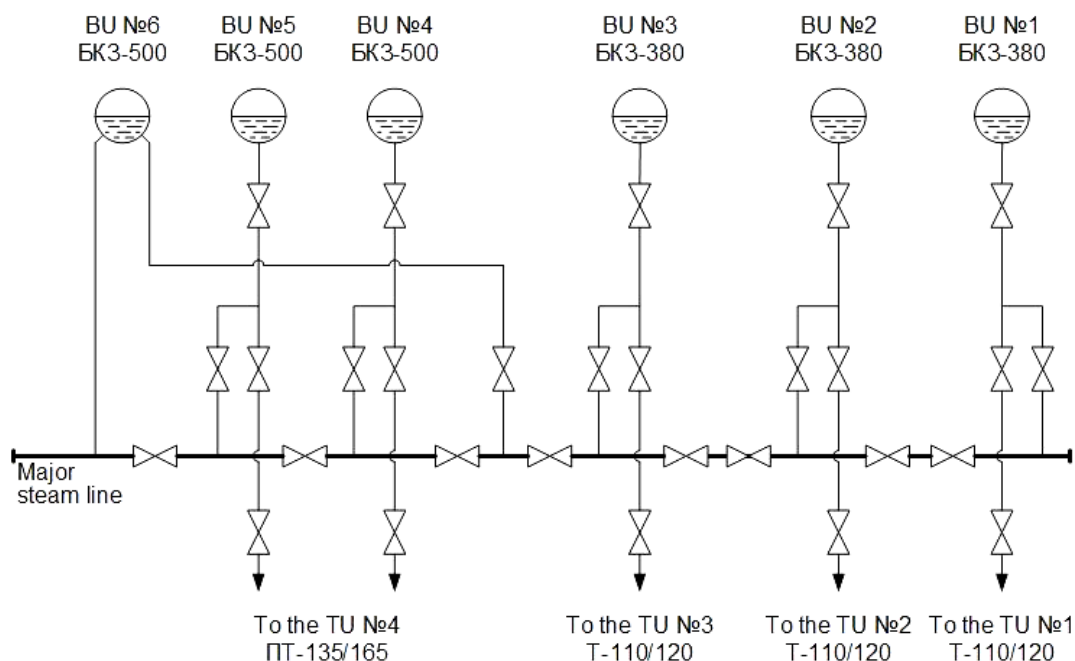
Fig. 1. Major steam line layout of the Krasnoyarsk TPP-2:
BU – boiler unit; TU – turbo unit

Рис. 1. Схема общего паропровода Красноярской ТЭЦ-2:
КА – котлоагрегат; ТА – турбоагрегат
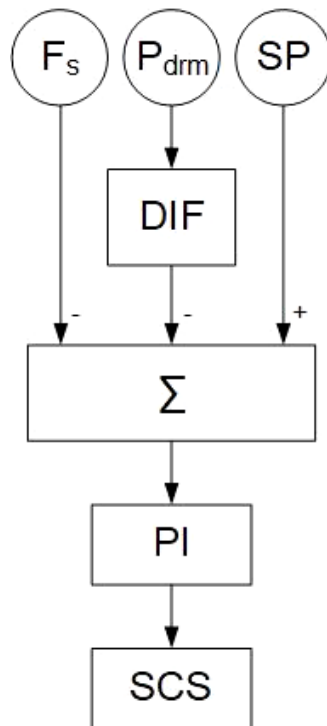
Fig. 2. Structural scheme of the heat load controller:
F_s – steam flow sensor behind the boiler; P_{drm} – boiler drum steam
pressure sensor; SP – setpoint; DIF – differentiator; $\sum$ – adder;
PI – regulator with proportional-integral law of regulation;
SCS – stepless control station

Рис. 2. Структурная схема регулятора тепловой нагрузки:
$F_п$ – датчик расхода пара за котлом; $P_{брб}$ – датчик давления
пара в барабане котла; ЗУ – задающее устройство; ДИФ –
дифференцирующее звено; $\sum$ – сумматор; ПИ – регулятор
с пропорционально-интегральным законом регулирования;
СБР – станция бесступенчатого регулирования
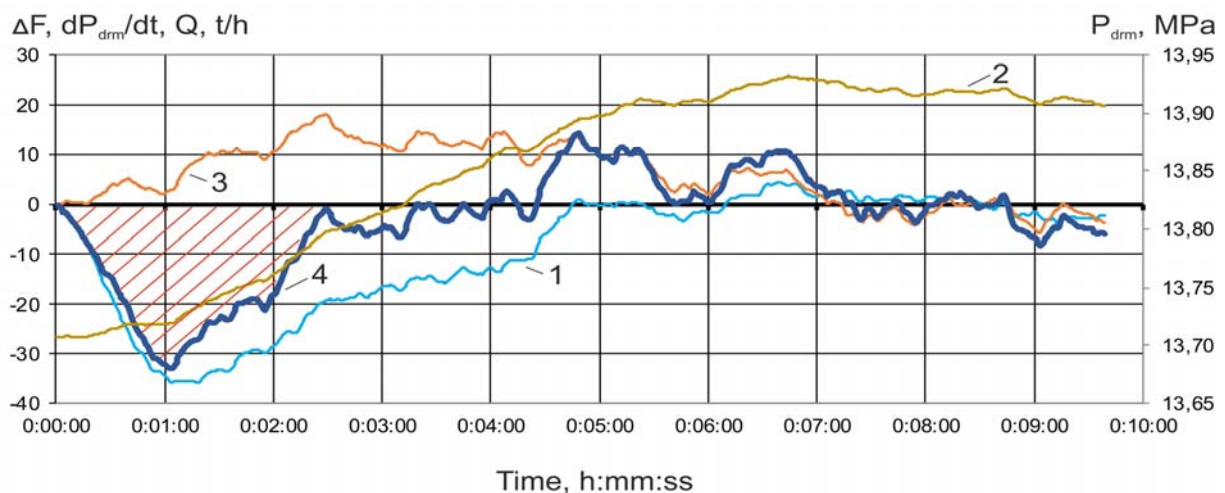
Fig. 3. Graphs of transient processes with increasing pressure in the major steam line by 0.3 MPa (external disturbance):
1 – change of steam flow behind the boiler, t/h; *2* – pressure in the drum of the boiler, MPa; *3* – the reduced rate of pressure change
in the boiler drum, t/h; *4* – change of the reduced signal by "heat" (the sum of the values of graphs 1 and 3), t/h

Рис. 3. Графики переходных процессов при увеличении давления в общем паропроводе на 0,3 МПа (внешнее возмущение):
1 – изменение расхода пара за котлом, т/ч; *2* – давление в барабане котла, МПа; *3* – приведенная скорость изменения давления
в барабане котла, т/ч; *4* – изменение приведенного сигнала по «теплоте» (сумма значений графиков 1 и 3), т/ч

It can be seen from the graphs that the delay in the steam pressure signal in the boiler drum does not allow to adjust the differentiating link to compensate the "failure" in the steam flow rate caused by a change in the pressure in the main steam pipe. As a result, the heat load controller to restore the heat deviation (shaded area on the graph) will increase the fuel supply to of the boiler furnace, although in fact no thermal changes occurred in the boiler. At the same time, to reduce the pressure in the major steam line, it is necessary to reduce the fuel supply of the boiler. This effect of incorrect work of boilers' heat load controllers significantly complicates the process of regulation of the pressure in the main steam line.

To eliminate the described lack of operation of the heat load controllers in the updated main regulator, the structural schemes of the regulators have been changed. The signal of the rate of change of the steam pressure in the steam chamber was used instead of the signal of the rate of change of the steam pressure in the boiler drum. This allows reducing the delay of the change of the steam pressure at external disturbances.

Diagrams of transient processes of the steam flow rate of the boiler, the rate of change of the steam pressure in the steam chamber and the "heat" signal are shown in fig. 4. The graphs show that when the "failure" of the steam flow of the boiler at 13 t/h, the signal "heat" deviates from the original value by 3 t/h. This significantly reduces the effect of "false" operation of the heat load regulator at external disturbances or even eliminate.

The structure of the updated main regulator allows:
– automatically select the necessary pressure sensors in the major steam line, depending on the mode of operation of the TPP;
– calculate (from the readings of the necessary sensors) the average pressure in the major steam line, which is an adjustable parameter for a group of boilers working on a specific section of the major steam line;
– synchronously form the task for corrective regulators working on a specific section of the major steam line;
– to configure a cascade of regulators of MR-HLC separately for each boiler;
– automatically change the coefficients of the corrective regulators, depending on the number of boilers involved in the regulation of pressure in the major steam line;
– randomly select boilers involved in the regulation of pressure in the major steam line;
– enter/output boilers in the mode of pressure regulation in the major steam line shock-free.

The updated main regulator was tested by a discharge and a set of electric power of 50 MWt, which is more than 10 % of the installed electric power of the station. Diagrams of transients at this set of electric power of the station are shown in fig. 5, 6. To restore the pressure, the total steam load of the boilers was increased by 225 t/h. Such a change in the total steam load of boilers in automatic mode with the previous pressure control schemes in the major steam line was impossible.
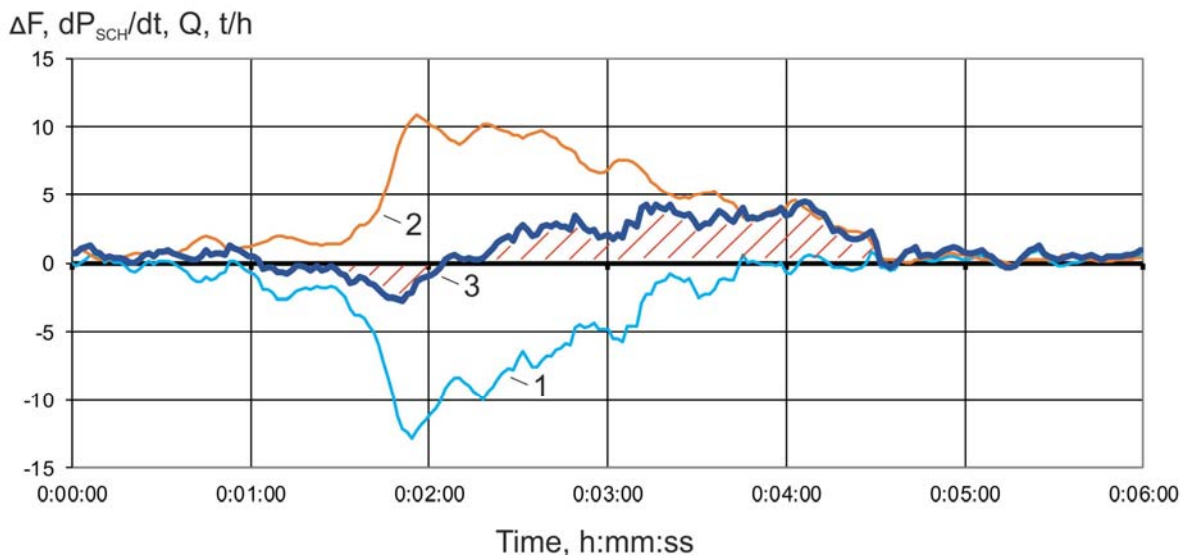
Fig. 4. Graphs of transient processes with the increasing pressure in the major steam line
by 0.15 MPa (external disturbance):
1 – change of steam flow of the boiler, t/h; *2* – the reduced rate of change of steam pressure in the steam chamber
of the boiler, t/h; *3* – change of the reduced signal by "heat" (the sum of the values of graphs 1 and 2), t/h

Рис. 4. Графики переходных процессов при увеличении давления в общем паропроводе
на 0,15 МПа (внешнее возмущение):
1 – изменение расхода пара за котлом, т/ч; *2* – приведенная скорость изменения давления пара в паросборной камере
котла, т/ч; *3* – изменение приведенного сигнала по «теплоте» (сумма значений графиков 1 и 2), т/ч
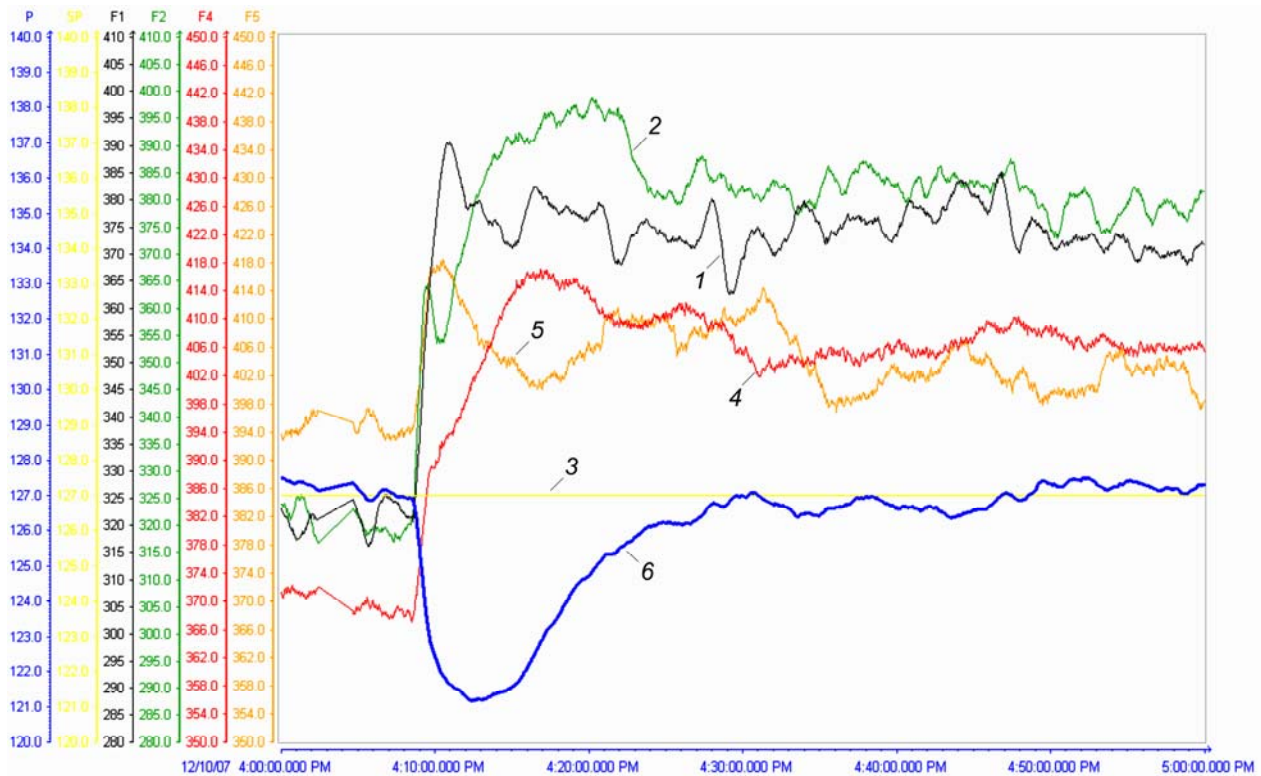
Fig. 5. Graphs of transient processes with increasing electric power output of the Krasnoyarsk TPP-2 by 50 MWt:
1, 2, 4, 5 – steam flow, respectively, of boiler No. 1, 2, 4, 5, t/h; *3* – the set point of the main regulator, bar;
6 – average pressure in the main steam line P_M, bar

Рис. 5. Графики переходных процессов при наборе электрической мощности Красноярской ТЭЦ-2 на 50 МВт:
1, 2, 4, 5 – расход пара соответственно котла № 1, 2, 4, 5, т/ч; *3* – задание главному регулятору, кгс/см^2;
6 – среднее давление в главном паропроводе P_M, кгс/см^2
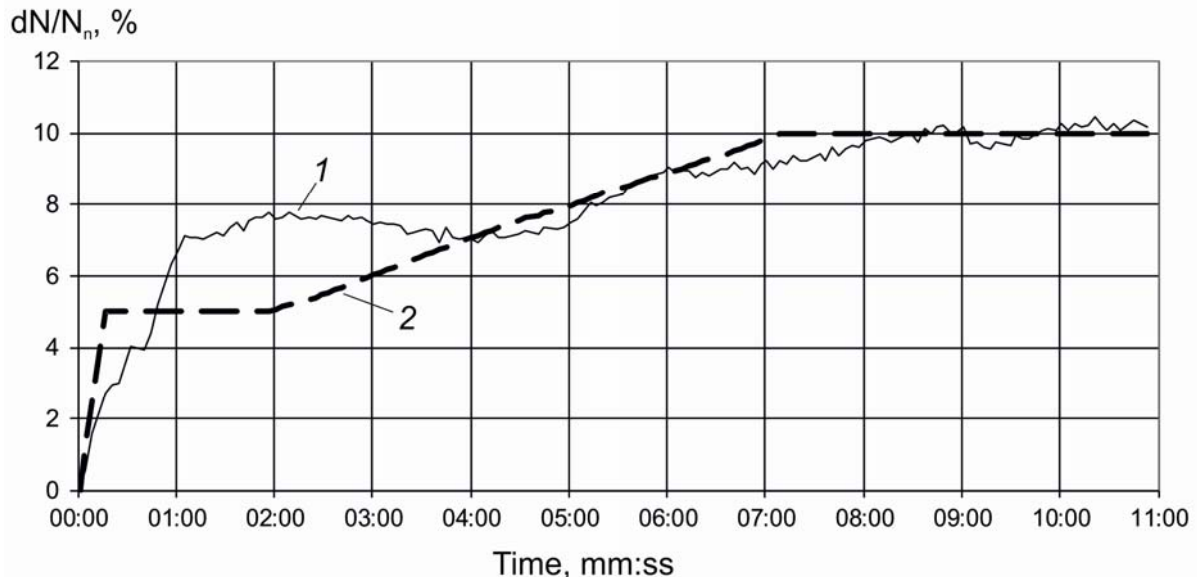
Fig. 6. The graph of the change in the primary power of a TPP when simulating a stepwise decrease in frequency:
1 – station power; *2* – dynamics of primary power output of TPP, according to the technical requirements
for generating equipment of the wholesale market participants [1]

Рис. 6. График изменения первичной мощности ТЭС при имитации скачкообразного снижения частоты:
1 – мощность станции; *2* – динамика выдачи первичной мощности ТЭС, согласно техническим требованиям
к генерирующему оборудованию участников оптового рынка [1]

In the process of operation of the updated main regulator, the following shortcomings in its work were revealed:

– the dynamics of change of pressure in the major steam line and steam flow outside the boiler, when pressure changes in the major steam line, significantly change when transitioning from winter modes of work to the summer, or when partitioning a major steam line. In these cases, it is necessary to adjust the settings of the regulators, conducting tests with a change in the electrical load of the station and the schedules of electrical power generation;

– the use of the steam pressure signal in the steam chamber of the boiler instead of the steam pressure signal in the boiler drum reduces the influence of external disturbances on the heat load regulator, but also slows down the regulator with internal disturbances and, if necessary, rapid changes in the boiler load;

– since the time constants of the transients on the steam flow rate of the boiler and on the steam pressure in the major steam line are comparable values, the cascades of PI-regulators of MR-HLC have oscillatory properties, which slows down the process of regulating the steam pressure in the major steam line.

Possible solution. Parametric control systems at objects that change their dynamic properties during operation require constant reconfiguration, which significantly complicates their operation.

The procedure of setting up control systems includes several stages:

– annulation of the executive authorities' characteristics;

– annulation of transient characteristics of the object;

– preliminary determination of the setting coefficients of the ACS;

– experimental setup of ACS at the object;

– testing of ACS.

Characteristics of the executive authorities, as a rule, are annulled once at starting the operation, or after capital repairs. Changes in the characteristics of the executive authorities in the overhaul interval can occur because of wear and tear of the equipment or its failure, which can significantly affect the quality of the parametric control system.

The transient response of the object allows determining its dynamic properties for the calculation of the setting coefficients of the ACS.

The transient response is removed when applying a single disturbing influence. The main parameters for determining the setting coefficients of the ACS are the dynamic characteristics of the object, such as the gain, the transition time constant and the delay time.

Methods for determining the setting coefficients of the ACS can be divided into accurate and approximate, search and non-search, working in real time or not. A list of some methods for determining the setting coefficients of the ACS is below: E. G. Dudnikov's method [4], V. Ya. Rotach's method [5], V. R. Sabanin and N. I. Smirnov's method [6], method of determining settings by nomograms [7], scaling method [8], Ziegler-Nichols method [9], adaptive method for oscillation by Rotach V. Y. [10], adaptive method using the transient characteristic

of V. Ya. Rotach system [11], method based on the technology of reconfiguration of closed systems [12], VTI method [13], direct adaptive control method [14].

Preliminary determination of the setting factors requires further tests of the ACS at the object with their possible adjustments. This stage causes difficulties in the organization of the experiments, since it is not clear how optimal the values of the setting coefficients of the ACS were in their preliminary determination and how many experiments are necessary for the final configuration of the system. This stage can be optimized using model studies of the system, but this requires an accurate model of the object, reflecting its real technological limitations and the state of the executive authorities.

It is a very complicated task to construct the traditional control systems based on the PI-regulators, using an extended number of parameters that affect the change in steam pressure in the major steam line.

To avoid these disadvantages of traditional automatic control systems, the improved steam pressure control system in the major steam line can be applied. It is based on the use of adaptive non-parametric control algorithms, which use the statistical data obtained from the object during its operation while forming controlled actions [15–17]. Modern computer technology allows not only to accumulate and store large amounts of information received from the object, but also to calculate the control actions in real time.

An example of a block diagram of an improved main regulator is shown in fig. 7. All the necessary controlled parameters related to the effective pressure maintenance in the major steam line are supplied as input to the intelligent control device (CD). The control device, using adaptive control algorithms, forms control actions on regulators of thermal loading of boilers.

The structure of the improved main regulator can additionally solve the following tasks:

– to identify the type of disturbance in the boiler equipment (internal or external) and make the decision to change the current load of the boiler (the correction of the false work of the heat load controllers under external disturbance);

– to form control actions before the pressure change in the major steam pipeline counting the input/output steam balance along the major steam line;

– to distribute the load on the boilers in the most optimal way (in terms of efficiency);

– to track the changes in the dynamic properties of the object and adjust the value of control actions.

Conclusion. Despite the fact that automatic control systems at modern industrial enterprises are based on microprocessor controllers, their algorithmic solutions are still rigid parametric structures that are not able to work effectively when changing the dynamic characteristics of the object. The use of the latest information technologies and modern hardware in the management of complex multi-connected objects that solve not only the problems of process control, but also the problem of improving the economic and environmental performance of enterprises, should become a new ыеуз in the development of automatic control systems.
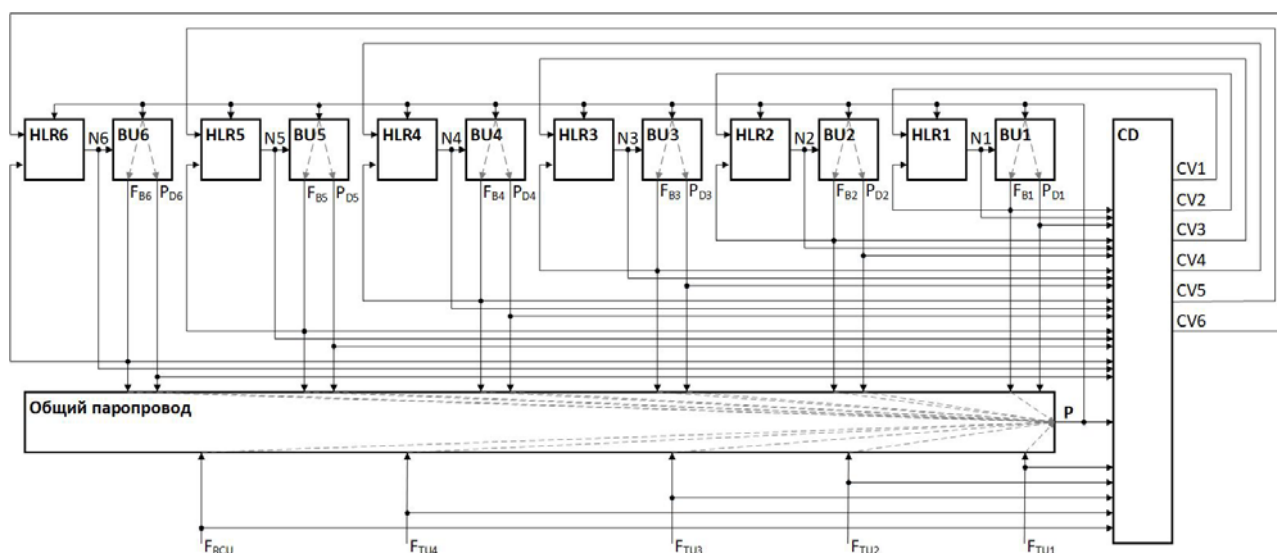
Fig. 7. Block diagram of the improved main regulator:
BU1, BU2, BU3, BU4, BU5, BU6 – boiler units; HLR1, HLR2, HLR3, HLR4, HLR5, HLR6 – boiler heat load regulators; CD – intelligent control device; N1, N2, N3, N4, N5, N6 – coal feeder speed; F_{B1}, F_{B2}, F_{B3}, F_{B4}, F_{B5}, F_{B6} – steam flow at the boiler outlet; P_{D1}, P_{D2}, P_{D3}, P_{D4}, P_{D5}, P_{D6} – boiler drum pressure; F_{TU1}, F_{TU2}, F_{TU3}, F_{TU4} – steam flow for turbine units; F_{RCU} – total steam flow for reduction cooling units and other controlled steam outlets; P – main steam line pressure; CV1, CV2, CV3, CV4, CV5, CV6 – control values to boiler's HLR from the CD

Рис. 7. Структурная схема улучшенного главного регулятора:
КА1, КА2, КА3, КА4, КА5, КА6 – котлоагрегаты; РТН1, РТН2, РТН3, РТН4, РТН5, РТН6 – регуляторы тепловой нагрузки котлов; УУ – интеллектуальное управляющее устройство; N1, N2, N3, N4, N5, N6 – обороты питателей угля; $F_{К1}$, $F_{К2}$, $F_{К3}$, $F_{К4}$, $F_{К5}$, $F_{К6}$ – расход пара на выходе из котла; $Р_{Б1}$, $Р_{Б2}$, $Р_{Б3}$, $Р_{Б4}$, $Р_{Б5}$, $Р_{Б6}$ – давление в барабане котла; $F_{ТА1}$, $F_{ТА2}$, $F_{ТА3}$, $F_{ТА4}$ – расход пара на турбоагрегаты; $F_{РОУ,БРОУ}$ – суммарный расход пара на редукционные установки и прочие контролируемые отборы; Р – давление в общем паропроводе; УВ1, УВ2, УВ3, УВ4, УВ5, УВ6 – управляющие воздействия на РТН котлов от УУ

References

1. Technical requirements for the generated equipment of the wholesale market participants of March 06, 2019. Moscow, 193 p.

2. Kljuev A. S., Lebedev A. T., Novikov S. I. *Naladka sistem avtomaticheskogo regulirovaniya barabannykh parovykh kotlov* [Adjustment of automatic control systems of drum steam boilers]. Moscow, Eenergoatomizdat Publ., 1985, 280 p.

3. Zhalnin D. A., Shorohov V. A., Evdokimov A. N., Bubnovskij O. A., Churinov A. V. [Experience in the implementation of a pressure control system in the main steam line at the Krasnoyarsk TPP-2]. *Elektricheskie stantsii.* 2009, No. 11, P. 18–25 (In Russ.).

4. Pikina G. A., Meshherjakova Ju. S. [Searchless method of calculating the settings of the PID controllers on the minimum of a quadratic criterion]. *Teploenergetika.* 2012, No. 10, P. 58–64 (In Russ.).

5. Rotach V. Ja. *Teoriya avtomaticheskogo upravleniya* [Automatic control theory]. Moscow, Moscow Power Engineering Institute Publ., 2008, 396 p.

6. Sabanin V. R., Smirnov N. I., Repin A. I. [Modified genetic algorithm for optimization and control]. *Exponenta Pro. Matematika v prilozheniyakh.* 2004, No. 3–4, P. 78–85 (In Russ.).

7. Rotach V. Ja., Vishnjakova Ju. N. [Calculation of regulatory systems with two auxiliary control values]. *Teploenergetika.* 2006, No. 2, P. 40–47 (In Russ.).

8. Bazhanov V. L. [The scaling method is an effective tool for practical adjustment of regulators in closed ACS]. *Pribory i sistemy. Upravlenie, kontrol', diagnostika.* 2006, No. 6, P. 1–8 (In Russ.).

9. Ziegler J. G., Nichols N. B. Optimum settings for automatic controllers. *Transactions of the ASME.* 1942, Vol. 64, P. 759–768.

10. Rotach V. Ja., Kuzishhin V. F., Kljuev A. S. *Avtomatizatsiya nastroyki sistem upravleniya* [Automation of control system settings]. Moscow, Jenergoatomizdat Publ., 1984, 294 p.

11. Rotach V. Ja. [Adaptation in process control systems]. *Promyshlennye ASU i kontrollery.* 2005, No. 1, P. 4–10 (In Russ.).

12. Shtejnberg Sh. E., Serjozhin L. P., Zaluckij I. E., Varlamov I. G. [Problems of creating and operating effective regulatory systems]. *Promyshlennye ASU i kontrollery.* 2004, No. 7, P. 1–7 (In Russ.).

13. Novikov S. I. *Optimizatsiya avtomaticheski sistem regulirovaniya teploenergeticheskogo oborudovaniya* [Optimization of automatic control systems for power equipment]. Novosibirsk, Novosibirsk State Technical University Publ., 2006, 108 p.

14. Karl J. Astrom and Bjron Wittenmark. Adaptive Control, second edition. Addison-Wesley Publishing Company, 1995.

15. Sung S. W., Lee J. Modeling and control of Wiener-type processes. *Chemical Engineering Science.* 2004, No. 59, P. 1515–1521.

16. Dorf R. C., Bishop R. H. *Sovremennye sistemy upravleniya* [Modern Control Systems]. Moscow, Laboratoriya bazovykh znaniy Publ., 2002, 832 p.

17. Keesman K. J. System identification. An introduction. London, Springer, 2011, 351 p.

Библиографические ссылки

1. Технические требования к генерирующему оборудованию участников оптового рынка от 06 марта 2019. Москва. 193 с.

2. Клюев А. С., Лебедев А. Т., Новиков С. И. Наладка систем автоматического регулирования барабанных паровых котлов. М. : Энергоатомиздат, 1985. 280 с.

3. Опыт внедрения системы регулирования давления в главной паровой магистрали на Красноярской ТЭЦ-2 / Д. А. Жалнин, В. А. Шорохов, А. Н. Евдокимов [и др.] // Электрические станции. 2009. № 11. С. 18–25.

4. Пикина Г. А., Мещерякова Ю. С. Беспоисковый метод расчета настроек ПИД-регуляторов на минимум квадратичного критерия // Теплоэнергетика. 2012. № 10. С. 58–64.

5. Ротач В. Я. Теория автоматического управления. М. : Изд. дом МЭИ, 2008. 396 с.

6. Сабанин В. Р., Смирнов Н. И., Репин А. И. Модифицированный генетический алгоритм для задач оптимизации и управления // Exponenta Pro. Математика в приложениях. 2004. № 3–4. С. 78–85.

7. Ротач В. Я., Вишнякова Ю. Н. Расчет систем регулирования с двумя вспомогательными регулируемыми величинами // Теплоэнергетика. 2006. № 2. С. 40–47.

8. Бажанов В. Л. Метод масштабирования – эффективный инструмент для практической настройки регуляторов в замкнутых САР // Приборы и системы. Управление, контроль, диагностика. 2006. № 6. С. 1–8.

9. Ziegler J.G., Nichols N.B. Optimum settings for automatic controllers // Transactions of the ASME. 1942, Vol. 64, P. 759–768.

10. Автоматизация настройки систем управления. / В. Я. Ротач, В. Ф. Кузищин, А.С. Клюев [и др.]. М. : Энергоатомиздат, 1984. 294 с.

11. Ротач В. Я. Адаптация в системах управления технологическими процессами // Промышленные АСУ и контроллеры. 2005. № 1. С. 4–10.

12. Проблемы создания и эксплуатации эффективных систем регулирования / Ш. Е. Штейнберг, Л. П. Серёжин, И. Е. Залуцкий [и др.] // Промышленные АСУ и контроллеры. 2004. № 7. С. 1–7.

13. Новиков С. И. Оптимизация автоматически систем регулирования теплоэнергетического оборудования. Новосибирск : Изд-во НГТУ, 2006. 108 с.

14. Karl J. Astrom and Bjron Wittenmark. Adaptive Control, second edition. Addison-Wesley Publishing Company, 1995.

15. Sung S. W., Lee J. Modeling and control of Wiener-type processes. Chemical Engineering Science. 2004. No. 59. P. 1515–1521.

16. Дорф Р., Бишоп Р. Современные системы управления / пер. с англ. Б. И. Копылова. М. : Лаборатория базовых знаний, 2002. 832 с.

17. Keesman K. J. System identification. An introduction. London : Springer, 2011. 351 p.

Zhalnin Denis Aleksandrovich – engineer, Chief Specialist; LLC "Region Avtomatika". E-mail: Denis@Zhalnin.com.

Жалнин Денис Александрович – инженер, главный специалист; ООО «Регион Автоматика». E-mail: Denis@Zhalnin.com.

APPLIED CLASSIFICATION PROBLEMS USING RIDGE REGRESSION

N. V. Kononova[1*], E. S. Mangalova[2], A. V. Stroev[3], D. V. Cherdantsev[3], O. V. Chubarova[4]

[1]Siberian Federal University
79, Svobodny Av., 660041, Krasnoyarsk, Russian Federation
[2]ООО "RD Science"
19, Kirova St., Krasnoyarsk, 660017, Russian Federation
[3]Krasnoyarsk State Medical University named after Prof. V. F. Voino-Yasenetsky
1, Partizana Zheleznyaka St., Krasnoyarsk, 660022, Russian Federation
[4]Reshetnev Siberian State University of Science and Technology
31, Krasnoyarsky Rabochy Av., Krasnoyarsk, 660037, Russian Federation
*E-mail: koplyarovanv@mail.ru

The rapid development of technical devices and technology allows monitoring the properties of different physical nature objects with very small discreteness of the data. As a result, one can accumulate large amounts of data that can be used with advantage to manage an object, a multiply connected system, and a technological enterprise. However, regardless of the field of activity, the tasks associated with small amounts of data remains. In this case the dynamics of data accumulation depends on the objective limitations of the external world and the environment. The conducted research concerns high-dimensional data with small sample sizes. In this connection, the task of selecting informative features arises, which will allow both to improve the quality of problem solving by eliminating "junk" features, and to increase the speed of decision making, since algorithms are usually dependent on the dimension of the feature space, and simplify the data collection procedure (do not collect uninformative data). As the number of features can be large, it is impossible to use a complete search of all features spaces. Instead of it, for the selection of informative features, we propose a two-step random search algorithm based on the genetic algorithm uses: at the first stage, the search with limiting the number of features in the subset to reduce the feature space by eliminating "junk" features, at the second stage - without limitation, but on a reduced set features. The original problem formulation is the task of supervised classification when the object class is determined by an expert. The object attributes values vary depending on its state, which makes it belong to one or another class, that is, statistics has an offset in class. Without breaking the generality, for carrying out simulation modeling, a two-alternative formulation of the supervised classification task was used. Data from the field of medical diagnostics of the disease severity were used to generate training samples.

Keywords: small samples, supervised classification, ridge-regression, quantile transformation, meta-classifier, significance of features, genetic algorithm.

ПРИКЛАДНЫЕ ВОПРОСЫ КЛАССИФИКАЦИИ С ИСПОЛЬЗОВАНИЕМ ГРЕБНЕВОЙ РЕГРЕССИИ

Н. В. Кононова[1*], Е. С. Мангалова[2], А. В. Строев[3], Д. В. Черданцев[3], О. В. Чубарова[4]

[1]Сибирский федеральный университет
Российская Федерация, 660041, г. Красноярск, просп. Свободный, 79
[2]ООО «АрДиСайнс»
Российская Федерация, 660017, г. Красноярск, ул. Кирова, 19
[3]Красноярский государственный медицинский университет имени профессора В. Ф. Войно-Ясенецкого
Российская Федерация, 660022, г. Красноярск, ул. Партизана Железняка, 1
[4]Сибирский государственный университет науки и технологий имени академика М. Ф. Решетнева
Российская Федерация, 660037, г. Красноярск, просп. им. газ. «Красноярский рабочий», 31
*E-mail: koplyarovanv@mail.ru

Бурное развитие технологий и техники обеспечивают возможность мониторинга свойств объектов различной физической природы с очень малой дискретностью. В результате накапливаются большие объемы данных, которые можно использовать с пользой для управления объектом, многосвязной системой, техноло-

гическим предприятием. Однако, вне зависимости от сферы деятельности, остаются задачи, связанные с небольшими объемами данных, динамика их накопления зависит от объективных ограничений внешнего мира и окружающей среды.

Проводимые исследования касаются данных небольших объемов выборок и размерности признаков объектов, которая может считаться высокой относительно количества изучаемых объектов. В связи с этим возникает задача отбора информативных признаков, что позволит как улучшить качество решения задачи за счет исключения «мусорных» признаков, так и повысить скорость принятие решения, поскольку алгоритмы обычно зависимы от размерности признакового пространства, и упростить процедуру сбора данных (не собирать неинформативные данные). Поскольку количество признаков может быть велико, полный перебор всех пространств признаков оказывается невозможным. Вместо этого для отбора информативных признаков предложен двуступенчатый алгоритм случайного поиска, основанный на применении генетического алгоритма: на первом этапе с ограничением количества признаков в подмножестве для сокращения признакового пространства за счет исключения «мусорных» признаков, на втором этапе – без ограничения, но по сокращенному набору признаков.

Исходная формулировка проблемы представляет собой задачу классификации объектов с учителем, когда класс объекта определен экспертом. Значения признаков объектов меняются в зависимости от его состояния, что обусловливает принадлежность тому или иному классу, то есть статистики обладают смещенностью в классе.

Без нарушения общности для проведения имитационного моделирования использовалась двухальтернативная постановка задачи классификации с учителем, для генерации обучающих выборок были использованы данные из области медицинской диагностики степени тяжести заболевания.

Ключевые слова: малые выборки, классификация с учителем, ридж-регрессия, квантильное преобразование, мета-классификатор, значимость признаков, генетический алгоритм.

Introduction. By solving the problem of classification the essential components are objects selection, feature reduction and distance criteria (norming).

For feature reduction it is necessary to pay attention to the following aspects:

– the possible accuracy of classification algorithm which can be valued with cross-validation algorithms for any feature set. If the set is insufficient for model building the accuracy of an examined classification algorithm will be limited by the lack of information;

– time to build a classifier: the size of feature space implicitly defines learning time. Amount of irrelevant features can unnecessary increase classifier building time;

– the number of objects required for learning a sufficiently accurate classifier: other conditions being equal the greater number of features is used in the model the greater number of objects must be which are necessary to achieve the required classification accuracy. With a large number of features and a small number of objects the risk of retraining the model is high;

– the cost of classifying a new object using the trained classifier: in many practical applications, for example, in medical diagnostics features are the observed symptoms as well as the results of diagnostic tests. Different diagnostic test may have various costs and associated risks. For example, an invasive exploratory operation can be much more expensive and riskier than a blood test. This presents us with the problem of choosing a subset of features when training the classifier.

The problem of choosing a feature space is related to the identification task and it is to choose a subset of features from the larger set of often mutually redundant, possibly irrelevant features with different measurement costs and / or risks. An example of such a task of considerable practical interest is the problem of forming the feature space for solving the problem of classifying the disease severity.

The literature suggests various approaches to select a subset of features. Some of them include finding the optimal subset based on a specific quality criterion [1], uses an exhaustive wide search [2], to find the minimum combination of features sufficient to build an accurate model from observations. Since the complete enumeration of all feature combinations is impossible because of the large number of features and combinations, most approaches to the choice of the feature subset imply the monotony of a certain measure – classification accuracy. If it is assumed that adding features does not impair accuracy, then the branch and bound method can be used for searching [3; 4]. However, in many practical applications the monotony assumption is not satisfied.

Some authors consider the use of heuristic search (often in combination with the branch and bound method) [5–11], as well as randomize algorithms [12; 13] and genetic algorithms [14–17], to select a subset of features and its further use with the decision tree or the method of nearest neighbours.

General formulation of the problem. Suppose there are many objects $\left\{ O_i, i = \overline{1, n} \right\}$, where n is a sample size which is described by a known features set $\left\{ p_i, i = \overline{1, m} \right\}$, measured in absolute ($m_1$) and rank ($m_2$) scales: $m_1 + m_2 = m$. For each object there is an indication of the teacher to which class it belongs: $O_i \in Z_l$, $l = \overline{1, L}$, L is a number of classes. Denote feature measurements for each object by a set of values $\left\{ \left(z_i, x_i^j \right), i = \overline{1, s}, j = \overline{1, m} \right\}$, where x_i^j is a value of p_j feature of O_i object, z_i is a number of the class, n_l is a number of class objects Z_l, $\sum_{l=1}^{L} n_l = n$.

It is necessary to build a classification algorithm, develop procedures for setting the parameters of algorithms.

The above task is complicated by the fact that the number of features is comparable to the sample size. In fact, this means data that are highly sparse in multidimensional space and have no pronounced interclass boundaries. That is, it is hardly possible to build a satisfactory quality classifier.

In this case the question arises: what is the ratio of the number of features to the sample size considered as a threshold of significant sparseness and what to do when the set of features is large and the data volume is limited? The first question is the subject of further research and is closely related to the stability characteristic of the classifier. The second question is considered in the further sections of the article.

Due to the small amount of input data leading to the high sparseness in the feature space it is necessary to order the features according to the degree of their influence on the quality of classification, in other words, to reduce the number of features discarding the ones of little significance.

An insignificant feature is proposed to consider the one which, being excepted, does not worsen the classification.

Selection of significant features and classification. Feature reduction experiments were performed using a standard genetic algorithm [18; 19]. The results are based on a sliding exam for the problem of classifying an object with the following parameters of the genetic algorithm:

1. Population size: 100;
2. Number of generations: 200;
3. Selection: ranking method;
4. Crossover probability: 0.6;
5. Mutation probability: 0.001;
6. Probability of choosing an individual with the highest rank: 0.6.

Each individual in the population is a variant of the feature subset to solve the problem of classification. Based on the total number of features m a classification can be made.

To solve the classification problem it is proposed to use its regression formulation. This is possible when objects form different classes according to their states. This means that the class is a group of similar objects in a certain state. The state of the object is classified according to the values of a specific set of features which are the measurements of technological parameters and the results of diagnostic tests. Due to the fact that the transition of an object from one state to another under the influence of various loads, disruptions in work and environmental influences can be interpreted as a sequential transition from one class to another. The classification task is presented as a regression task where the classes are ordered according to the state of the object. Thus, objects with a light form of deviation of technological parameters and a slight wear of resource form class 1; class 2 is made up of objects with a higher (medium) level of inconsistency; objects with significant deviations (severe stage) form class 3.

As a result of building the regression dependence each new object will be assigned a value from 1 to 3 instead of a class number (1 – light, 2 – medium, 3 – severe). For example if forecasts 1.1 and 1.4 are obtained for two objects, the probability that the first object has a slight degree of deviation is higher than for the second one although both of them will be attributed to the state of slight deviation.

If there are m features there are 2^m possible subsets of features. For large values of m the complete search of features takes considerable time which may not be consisted with the restriction of waiting for the result of the algorithm.

Each individual is a binary vector of dimension m. If the bit is 1, it means that the corresponding attribute is selected to build the classifier. The value 0 indicates that the corresponding attribute is excluded from the classifier.

The average square of residual is chosen as a fitness function. Since the classification problem is solved as a regression problem, MSE additionally penalizes (for example, in comparison with MAE) large errors of classification when the forecast deviation from the real value of the class is more than 1.5, i. e. the error is more than one class (instead of the light stage the classifier predicts the severe condition and vice versa).

For numerical modeling and building the regression dependence a ridge regression was used (linear regression with a regularization parameter) [20]. The ridge regression is used if it occurs:

– data redundancy;
– correlated independent variables (multicollinearity);
– strong differences in the eigenvalues of the characteristic equation or the proximity to zero of several of them.

All of the above properties of features quite often take place in practice when the removal of technological parameters is of a distributed nature.

We use a linear model: $y = f(x, \beta)$, where f is a linear operator (linear functional dependence), β is model parameters.

We assume that the vector of coefficients of the linear regression model β is found by the least squares method:

$$\sum_{i=1}^{n} \left(f\left(x_i, \beta\right) - y_i \right)^2 \to \min_{\beta_i}. \qquad (1)$$

Analytical solution of this problem: $\beta = (X^T X)^{-1} X^T Y$, however, when the matrix $X^T X$ is degenerate, the solution is not unique, but if it is poorly conditioned it is not stable. Therefore, regularization of the parameter β is introduced, for example according to the following rule:

$$Q(\beta) = Y - X\beta^2 + \lambda\beta^2 \to \min_{\beta}, \qquad (2)$$

where $\lambda > 0$ regularization parameter.

The regularized least squares solution is as follows:

$$\beta = \left(X^T X + \lambda I \right)^{-1} X^T Y. \qquad (3)$$

The increase in the parameter λ leads to the decrease in the norm of the parameter vector and the increase in the efficiency of the feature space dimension.

The error is estimated using a sliding exam since the size of the training sample is small and the construction of the classifier takes little machine time. This paper proposes the use of two-step feature selection algorithm:

1. At the first step the primary selection of features is carried out. It means the exclusion of the most "junk" ones. We restrict the individuals so that the number of features in subsets is less than 0.2*n, where n is the number of observations in the training set, further additions of features in theory will lead to the increase in the risk of retraining. For example in the task of predicting the severity of the disease 25 features (of 94 in the original sample) are revealed, i.e. no evaluable feature subset can contain more than 25 features. If, as a result of crossing or mutation we get an individual who is not suitable for this condition then such an individual is thrown out and replaced by the following one suitable for this rule.
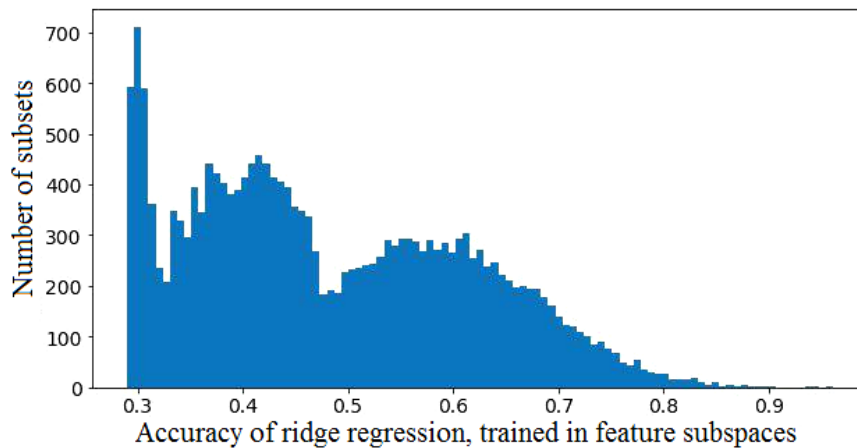
Fig.1. The distribution of the accuracy of classifiers trained on various attribute subspaces
that were individuals in the course of optimization by the genetic algorithm for any generation

Рис. 1. Распределение точности классификаторов, обученных по различным признаковым
подпространствам, которые являются индивидами в ходе оптимизации генетическим
алгоритмом на любом поколении
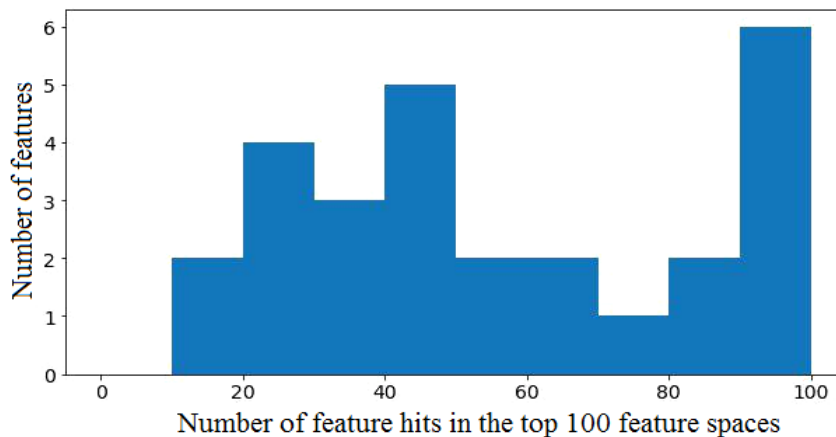
Fig. 2. Distribution of features by the number of hits in the subsets
from the pool of the best subsets

Рис. 2. Распределение признаков по количеству попаданий в подмножества
из пула лучших подмножеств

Using the genetic algorithm we form sets of the best solutions that could be obtained at any iteration. Fig. 1 shows the accuracy distribution of forecasts for MSE. It is to be noted that the accuracy of 0.699 is provided by a simple average for this problem. If a subset of features gives the accuracy worse than 0.699, it means that there is a retraining effect and the subset contains no important features.

From the entire set of features a pool of the best solutions (subsets) is selected from the first (left) peak of the distribution density of the accuracy of classifiers trained in various attribute subspaces. Further, according to this pool, we calculate the number of inclusions of the feature in the feature spaces. The feature distribution by the number of hits is shown in fig. 2

There is a sharp drop in the number of feature hits in the best feature subspaces. All features that fall into a substantially small number of subsets are excluded, provided that the excluded feature does not fall into the top 20 feature spaces.

Thus, 67 features are cut off at this stage. It is also to be noted that one feature gets into the best subsets a lot more times and can be initially included in the best subset.

2. At the second step we launch a new optimization process with no limitation on the number of features. Fig. 3 shows distribution of the feature number in the best in reproducible classification accuracy of feature subspaces.

Fig. 4 shows the accuracy distribution of forecasts for MSE. It should be noted that the proportion of individuals close to the best selected increased, as did the average accuracy of the classifiers and the best accuracy compared to the solutions found at the first step.

Fig. 5 shows the distribution of features by the number of individuals in the top 100 and table contains the number of specific features in the most suitable individuals top 5, top 50 and top 100.
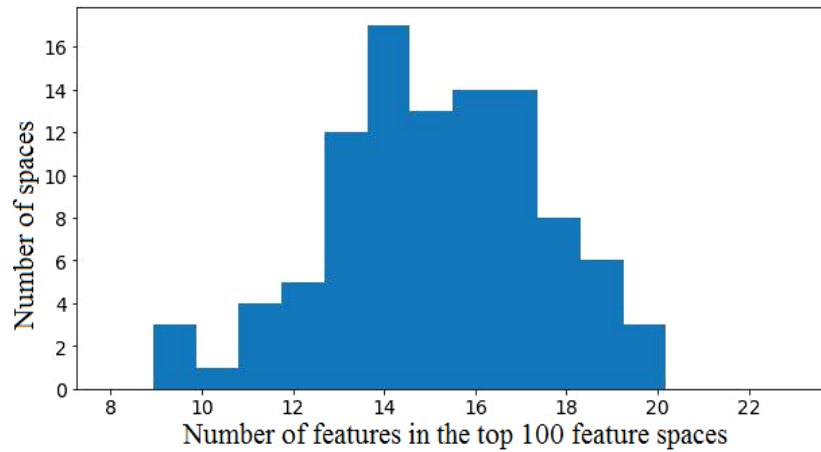
Fig. 3. Distribution of the features number in the best in reproducible classification accuracy of feature subspaces

Рис. 3. Распределение количества признаков в лучших по воспроизводимой точности классификации признаковых подпространствах
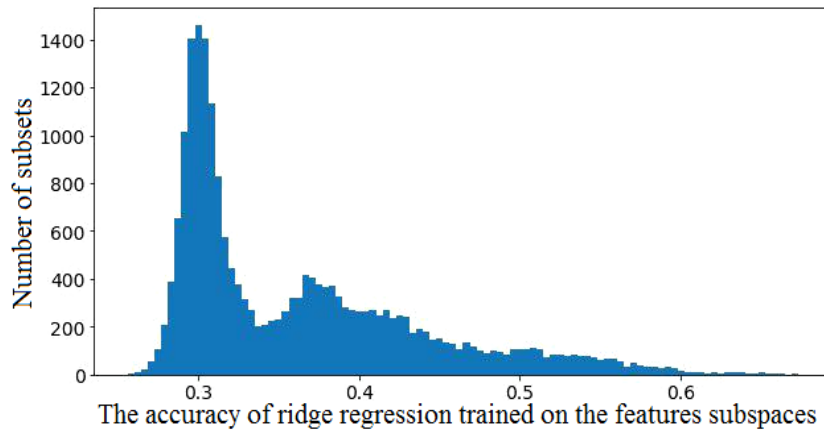
Fig. 4. Accuracy distribution of MSE classifiers after optimization without limitation on the number of features

Рис. 4. Распределение точности классификаторов по MSE после процесса оптимизации без ограничения на количество признаков
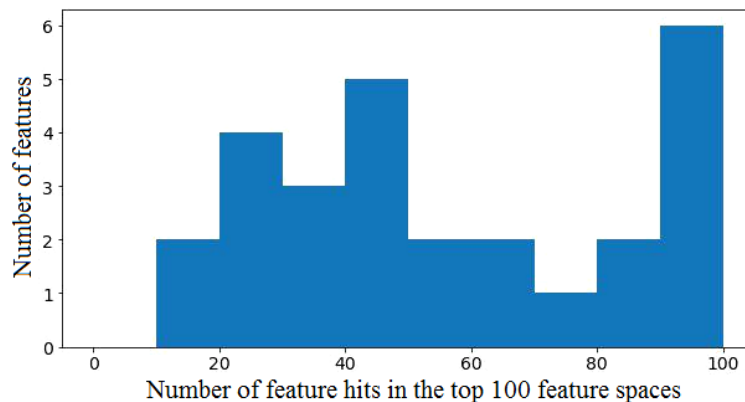
Fig. 5. Distribution of features by the number of hits in the top 100 feature spaces

Рис. 5. Распределение признаков по количеству попаданий в топ-100 признаковых пространств

The number of hits in the top best individuals

Sequence number of the feature	Number of hits in the top 5 best individuals	Number of hits in the top 50 best individuals	Number of hits in the top 100 best individuals
1	5	44	78
2	2	16	35
3	0	7	28
4	0	21	48
5	0	11	30
6	0	12	27
7	5	49	90
8	5	50	100
9	0	18	43
10	1	19	43
11	5	45	91
12	0	13	37
13	5	35	64
14	0	20	47
15	0	5	16
16	5	50	90
17	0	18	41
18	2	30	61
19	2	37	82
20	0	9	18
21	5	45	93
22	1	15	25
23	5	50	100
24	5	45	86
25	3	27	54
26	1	12	26
27	5	30	57

Conclusion. The paper considers the procedure of feature selection for small volumes of the original training set and a significant number of features describing the state of objects. To solve the problem the genetic algorithm for the feature subspaces formation was used. The approach to the classifier construction differs from the classical one and is a construction of the regression dependence of the class value output on the input feature values. Such implementation allows estimating the probability of belonging to a particular class through the regression value. Application of this approach to the classification problem is possible in cases when the class of an object depends on its state and the classes can be ordered (ranked). Data on the state of human health were taken as a basis of simulation samples generation for numerical experiments but without violation of generality the approach can be extended to other industries and fields of activity including the diagnosis of changes in the state of equipment during its operation.

References

1. Vafaie H., De Jong K. Robust Feature Selection Algorithms. *Proceedings of the IEEE International Conference on Tools with Artificial Intelligence.* 1993, P. 356–363.

2. Cormen T. H., Leiserson C. E., Rivest R. L., Stein C. Introduction to Algorithms. 3rd edition. The MIT Press. 2009, 1320 p.

3. Narendra P., Fukunaga K. A Branch and Bound Algorithm for Feature Subset Selection. *IEEE Transactions on Computers.* 1977, Vol. 26, P. 917–922.

4. Foroutan I., Sklansky J. Feature Selection for Automatic Classification of non- Gaussian Data. *IEEE Transactions on Systems, Man and Cybernetics.* 1987, Vol. 17, P. 187–198.

5. Kira K., Rendell L. A Practical Approach to Feature Selection. *Proceedings of the Ninth International Conference on Machine Learning (Morgan Kaufmann).* 1992, P. 249–256.

6. Modrzejewski M. Feature Selection Using Rough Sets Theory. *Proceedings of the European Conference on Machine Learning (Springer).* 1993, P. 213–226.

7. Liu H., Setiono R. Chi2: Feature Selection and Discretization of Numeric Attributes. *Proceedings of the Seventh IEEE International Conference on Tools with Artificial Intelligence.* 1995.

8. John G., Kohavi R., Peger K. Irrelevant Features and the Subset Selection Problem. *Machine Learning: Proceedings of the Eleventh International Conference (Morgan Kaufmann).* 1994, P. 121–129.

9. Kohavi R., Frasca B. Useful Feature Subsets and Rough Set Reducts. Third International Workshop on Rough Sets and Soft Computing. 1994.

10. Kohavi R. Feature Subset Selection as Search with Probabilistic Estimates. AAAI Fall Symposium on Relevance. 1994 .

11. Koller D., Sahami M. Toward Optimal Feature Selection. *Machine Learning: Proceedings of the Thirteenth International Conference (Morgan Kaufmann)*. 1996.

12. Liu H., Setiono R. A Probabilistic Approach to Feature Selection – A Filter Solution. *Proceedings of the Thirteenth International Conference on Machine Learning (Morgan Kaufmann)*. 1996.

13. Liu H., Setiono R. Feature Selection and Classification – A Probabilistic Wrapper Approach. *Proceedings of the Ninth International Conference on Industrial and Engineering Applications of AI and ES*. 1996.

14. Siedlecki W., Sklansky J. A Note on Genetic Algorithms for Large-scale Feature Selection. *IEEE Transactions on Computers*. 1989, Vol. 10, P. 335–347.

15. Punch W., Goodman E., Pei M., Chia-Shun L., Hovland P., Enbody R. Further Research on Feature Selection and Classification Using Genetic Algorithms. *Proceedings of the International Conference on Genetic Algorithms (Springer)*. 1993, P. 557–564.

16. Brill F., Brown D., Martin W. Fast Genetic Selection of Features for Neural Network Classiers. *IEEE Transactions on Neural Networks*. 1992, Vol. 3(2), P. 324–328.

17. Richeldi M., & Lanzi P. Performing Effective Feature Selection by Investigating the Deep Structure of the Data. *Proceedings of the Second International Conference on Knowledge Discovery and Data Mining (AAAI Press)*. 1996, P. 379–383.

18. Goldberg D. Genetic Algorithms in Search, Optimization, and Machine Learning. New York, Addison-Wesley, 1989.

19. Mitchell M. An Introduction to Genetic algorithms. Cambridge, MA: MIT Press. 1996.

20. Dreiper N., Smit G. Applied regression analysis. 1986, 351 p.

Kononova Nadezhda Vladimirovna – Cand. Sc., associate professor; Informational systems department, Siberian Federal University. E-mail: koplyarovanv@mail.ru.

Mangalova Ekaterina Sergeevna – software developer; "RD Scienc" (Research. Development. Science.). E-mail: e.s.mangalova@hotmail.com.

Stroev Anton Vladimirovich – Postgraduate Student; Krasnoyarsk State Medical University named after Prof. V. F. Voino-Yasenetsky. E-mail: antoxa134@mail.ru.

Cherdantsev Dmitry Vladimirovich – Dr. Sc., Professor; Krasnoyarsk State Medical University named after Prof. V. F. Voino-Yasenetsky. E-mail: gs7@mail.ru**.**

Chubarova Olesya Victorovna – Cand. Sc., associate professor; System analysis and operations research department, Reshetnev Siberian State University of Science and Technology. E-mail: kuznetcova_o@mail.ru.

Кононова Надежда Владимировна – кандидат технических наук, доцент; кафедра информационных систем, Сибирский федеральный университет. E-mail: koplyarovanv@mail.ru.

Мангалова Екатерина Сергеевна – программист-разработчик; ООО «АрДиСайнс» (Research. Development. Science.). E-mail: e.s.mangalova@hotmail.com.

Строев Антон Владимирович – аспирант; Красноярский государственный медицинский университет имени профессора В. Ф. Войно-Ясенецкого. E-mail: antoxa134@mail.ru.

Черданцев Дмитрий Владимирович – доктор медицинских наук, профессор; заведующий кафедрой хирургических болезней, Красноярский государственный медицинский университет имени профессора В. Ф. Войно-Ясенецкого. E-mail: gs7@mail.ru.

Чубарова Олеся Викторовна – кандидат технических наук, доцент, доцент; кафедра системного анализа и исследования операций, Сибирский государственный университет науки и технологий имени академика М. Ф. Решетнева. E-mail: kuznetcova_o@mail.ru.

NONPARAMETRIC IDENTIFICATION OF DYNAMIC SYSTEMS UNDER NORMAL OPERATION

M. E. Kornet, A. V. Shishkina[*]

Siberian Federal University, Space and information technology Institute
26b, Academic Kirensky St., Krasnoyarsk, 660074, Russian Federation
*E-mail: nastya.shishkina95@mail.ru

The research gives nonparametric identification algorithms under the conditions of incomplete a priory information. The identification case differs from the previously known ones due to the fact that, besides the control action, an uncontrollable variable, but a measurable one, impacts on the object input. In contrast to parametric identification, the research considers the situation when the equations describing dynamic objects are not given with accuracy to the parameters. In this case, there are some features to study while getting the recovery characteristics of various object channels. The main characteristic is that the transition response of a channel is taken when the other channel is in a stable position. Moreover, the identification problem is analyzed under normal object operation, opposite to the previously known nonparametric approach based on Heaviside function input to the object and further Duhamel integral application. An arbitrary signal is input to the object during normal operation as a result we have a corresponding response of the object output. It should be noted that the measurements of the input and output variables are carried out with random noise. As a result, we have a sample of input-output variables. As linear dynamical system can be described by the Duhamel integral, with known input and output object variables, corresponding values of the weight function can be found. This is achieved by discrete representation of the latter. Having such realization, nonparametric estimate of the weight function in the form of the nonparametric Nadaraya-Watson estimate is used later. Substituting this with the Duhamel integral, we obtain a nonparametric model of a linear dynamical system of unknown order.

The article also describes the case of constructing nonparametric model when a delta-shaped function is input to the object. It is interesting to find out how delta-shaped function might differ from the delta function. The weight function is determined in the class of nonparametric Nadaraya-Watson estimates. Previously proposed nonparametric algorithms consider the case when Heaviside function is applied to the object; this narrows the scope of nonparametric identification practical use. It is important to construct nonparametric model of the dynamic object under conditions of normal operation.

Keywords: Duhamel integral, transient function, weight function, delta-shaped input, Nadarya-Watson estimate, nonparametric model.

О НЕПАРАМЕТРИЧЕСКОЙ ИДЕНТИФИКАЦИИ ДИНАМИЧЕСКИХ СИСТЕМ В УСЛОВИЯХ НОРМАЛЬНОГО ФУНКЦИОНИРОВАНИЯ

М. Е. Корнет, А. В. Шишкина[*]

Сибирский федеральный университет, Институт космических и информационных технологий
Российская Федерация, 660074, г. Красноярск, ул. Академика Киренского, 26б
*E-mail: nastya.shishkina95@mail.ru

Приводятся непараметрические алгоритмы идентификации в условиях неполной информации. Существенное отличие самой задачи идентификации от известных предыдущих задач состоит в том, что на вход объекта, кроме управляющего воздействия, действует неуправляемая переменная, но контролируемая. В отличие от параметрической идентификации, рассматривается ситуация, когда уравнения, описывающие динамические объекты, не заданы с точностью до параметров. В этом случае появляются некоторые особенности, которые необходимо учитывать при снятии переходных характеристик объектов по различным каналам. Основная особенность состоит в том, что переходная характеристика по одному каналу снимается при стабильном положении другого канала. Более того, задача идентификации рассматривается в условиях нормаль-

ного функционирования объекта в отличие от ранее известного подхода к непараметрической идентификации, основанного на подаче на вход объекта функции Хевисайда и дальнейшем применении интеграла Дюамеля. В условиях нормального функционирования на вход объекта подают сигнал произвольной формы. При этом на выходе объекта наблюдается соответствующий отклик. Измерения входной и выходной переменных осуществляются со случайными помехами. В итоге имеем реализацию (выборку) входных–выходных переменных. Поскольку линейная динамическая система может быть описана интегралом Дюамеля, то при известных входных и выходных переменных объекта могут быть найдены соответствующие значения весовой функции. Это достигается при дискретной записи последнего. Располагая подобной реализацией, в дальнейшем используется непараметрическая оценка весовой функции в виде непараметрической оценки Надарая – Ватсона. Подставляя ее в интеграл Дюамеля, получаем тем самым непараметрическую модель линейной динамической системы неизвестного порядка.

В статье приведен так же любопытный случай построения непараметрической модели при подаче на вход дельтаобразной функции. Было интересно выяснить, насколько дельтаобразная функция может отличаться от дельта-функции. Оценка весовой функции и в этом случае определялась в классе непараметрических оценок Надарая – Ватсона. Ранее были предложены непараметрические алгоритмы идентификации для случая, когда на вход объекта подавалась функция Хевисайда. Это несколько сужает рамки практического использования самой идеи непараметрической идентификации. Естественно, важным является случай построения непараметрической модели динамического объекта, находящегося в условиях нормальной эксплуатации. Эта особенность является наиболее важной из рассматриваемых приемов идентификации в условиях непараметрической неопределенности.

Ключевые слова: интеграл Дюамеля, переходная функция, весовая функция, дельтаобразное входное воздействие, оценка Надарая – Ватсона, непараметрическая модель.

Introduction. The main objective of identification theory is the model construction based on input and output process variables observations while data about the object is incomplete [1–3]. The article considers dynamic object identification under nonparametric uncertainty [4; 5], when the dynamical model cannot be identified up to parameter vector due to the lack of a priori data. In this case getting transient response and following estimation of an object weight function are reasonable. The basis of this paper is Duhamel integral use, due to the principle of superposition [6; 7]. Identification algorithms of the object in normal operation conditions are described. The research analyses three methods of obtaining weight function estimation using Heaviside function [8; 9], delta-shaped input and arbitrary input.

Problem formulation. We assume that an object is a dynamic system described by equation [1], $x_t = f(u_t, \mu_t)$ where $f(\cdot)$ – is unknown function; u_t – control input variable; μ_t – uncontrolled, but measured variable; x_t – output variable.

Fig. 1 illustrates a block diagram of the dynamic process [1; 10], with the following notations: $\hat{x}_t$ – output of model; u_t – control variable; μ_t – uncontrolled, but measured variable; (t) – continuous time; t – discrete time; ξ_t, h_t – random noise influencing the object and output variable measuring channel, with zero mathematical expectation and limited dispersion.

Variables control is carried out at time interval Δt. Thus, it is possible to obtain initial input – output variable sample $\{x_i, u_i, \mu_i, i = \overline{1, s}\}$, where s – a sample size.

Non-parametric identification algorithm when standard signals can be input to the object. We could assume that the object is described by a linear differential equation of unknown order. In this case, for zero initial conditions, $x(t)$ is found as

where

$$x(t) = x_u(t) + x_\mu(t),$$

$$x_u(t) = \int_0^t h_u(t-\tau)u(\tau)d\tau, \tag{1}$$

$$x_\mu(t) = \int_0^t h_\mu(t-\tau)\mu(\tau)d\tau.$$

Where $h_u(t-\tau), h_\mu(t-\tau)$ – weight functions of u and μ channels. Weight function is a derivative of the transition function $h(t) = k'(t)$.

This problem becomes the weight function estimation, so, first, the transition function needs to be obtained.

As it is mentioned, weight function can be obtained by various means.

First case. We suppose that the object is described by linear differential equation of unknown order. Under zero initial conditions, $x(t)$ is found as (1). Transition function is an object reaction to input impact, namely as Heaviside function $u(t) = 1(t)$.

$$1(t) = \begin{cases} 0, u(t) < 0 \\ 1, u(t) \geq 0 \end{cases}. \tag{2}$$

After obtaining transition function, to find its non-parametric estimation is required [11; 12]:

$$\overline{k}(t) = \frac{T}{sc_s} \sum_{i=0}^{s} k_i H\left(\frac{t-t_i}{c_s}\right), \tag{3}$$

where $\overline{k}_i$ – transition function estimate, k_i – transition function, t_i – discrete time of measurements, s – sample size, c_s – kernel smoothing, H – kernel function, T – time observation period [2].
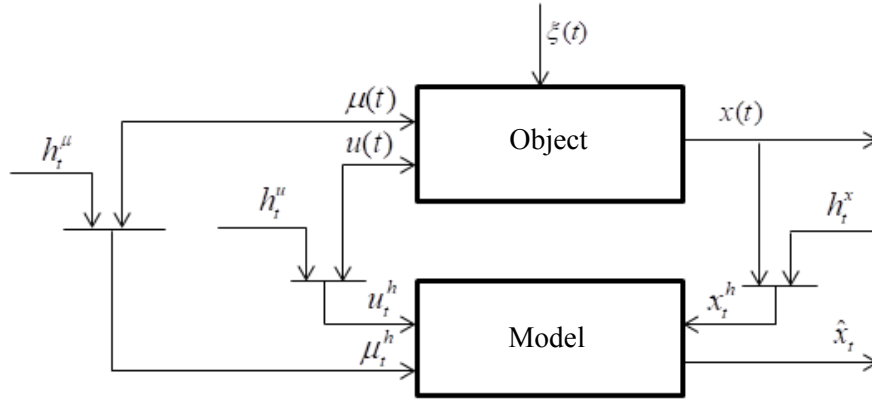
Fig. 1. Identification scheme

Рис. 1. Схема идентификации

We note that kernel function and kernel smoothing satisfy following terms [11; 12]:

$$\frac{1}{c_s}\int\limits_{-\infty}^{\infty} H\left(\frac{t-t_i}{c_s}\right)dt = 1, \quad \lim_{s\to 0}\frac{1}{c_s}\int\limits_{-\infty}^{\infty}\phi(t)H\left(\frac{t-t_i}{c_s}\right)dt = \phi(t_i),$$

$$H\left(\frac{t-t_i}{c_s}\right) \geq 0, \quad c_s > 0, \quad \lim_{c_s\to\infty} sc_s \to \infty, \quad \lim_{s\to\infty} c_s \to 0, \tag{4}$$

where $\phi(t_i)$ – an arbitrary function.

In particular, kernel function would be considered as Sobolev function (5):

$$H = \begin{cases} 0, |t-t_i| > c_s \\ \dfrac{0.827}{c_s}e^{\left(\frac{-(t-t_i)^2}{(t-t_i)^2 - c_s{}^2}\right)}, & |t-t_i| \leq c_s. \end{cases} \tag{5}$$

Since weight function $h(t)$ is derivative of transition function $k(t)$, then

$$\bar{h}(t) = \frac{T}{sc_s}\sum_{i=0}^{s}\bar{k}_i H'\left(\frac{t-t_i}{c_s}\right), \tag{6}$$

where $\bar{k}_i$ – transition function estimation, k_i – transition function, t_i – discrete time of measurements, s – sample size, c_s – kernel smoothing, H – kernel function, T – time observation period.

Second case. The weight function could be obtained when a delta-shaped function is input, shown in fig. 2. It has got step function type (7), Δt – discretization interval

$$\delta^\Delta(t) = \begin{cases} \dfrac{1}{\Delta t}, t \in \Delta t, \end{cases} \tag{7}$$

where Δt, for example, is an equation $\Delta t = t' - t''$.

Identification algorithm under normal object operation. Constructing an adaptive object model often requires identification of measuring channels under normal object operation [2; 8; 13]

Therefore, the third case has got the priority in solving the problem of nonparametric identification [4; 6]. The following algorithm when input impact has got sinusoidal type function (as an example) is analyzed below.
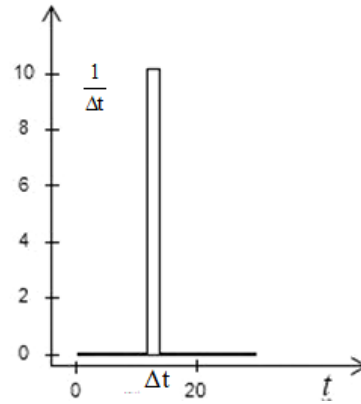
Fig. 2. Delta-shaped function example

Рис. 2. Пример дельтаобразного входного воздействия

Third case. If control action and object output are known, weight function may be described by (1).

In a discrete form:

$$h_i = \left(x_t^u - \left(\sum_{i=1}^{s} u_i \Delta\tau + \sum_{i=1}^{s} h_0\right)\right) +$$

$$+ \left(x_t^\mu - \left(\sum_{i=1}^{s}\mu_i\Delta\tau + \sum_{i=1}^{s} h_0\right)\right), \quad i = \overline{1,s}, \tag{8}$$

where s – sample size; $\Delta\tau$ – variables control time interval; u_i – control variable; μ_t – uncontrolled, but measured variable; x_t – object output; h_0 – value of the weight function on previous iteration steps.

Therefore, nonparametric process model is:

$$x_s(t) = \frac{T}{sc_s}\left(\int\limits_0^t\sum_{i=1}^{s} k_i H'\left(\frac{t-t_i}{c_s}\right)u(\tau)d\tau + \int\limits_0^t\sum_{i=1}^{s} k_i H'\left(\frac{t-t_i}{c_s}\right)\mu(\tau)d\tau\right)$$

or

$$x_s(t) = \frac{T}{sc_s}\left(\int\limits_0^t\sum_{i=1}^{s} h_i^u u(\tau)d\tau + \int\limits_0^t\sum_{i=1}^{s} h_i^\mu \mu(\tau)d\tau\right), \tag{9}$$

where k_i – transition function, h_i – weight function, c_s – kernel smoothing, s – sample size, T – observation period.

Computer experiment. We suggest that dynamical an object is described by a second-order differential equation. It can be represented as:

$$x_t = x_t^u + x_t^\mu,$$

$$x_t^u = 0.25x_{t-1}^u - 0.33x_{t-2}^u + 0.33u_t, \qquad (10)$$

$$x_t^\mu = 0.25x_{t-1}^\mu - 0.33x_{t-2}^\mu + 0.33u_t.$$

We could suppose that the equation (10) is used to obtain sampling points. Nonparametric algorithm does not mean the known form of the differential equation, only information on the linearity of an object is known, in contrast with [14; 15]. It should be noted once again that certain equations accepted in this computational experiment remain unknown. Only a priori information about its linearity is known as well as the presence of the principle of a super position. It is important, that taking the transient characteristics for each object channel occurs when the other channel stabilizes [16; 17].

As an arbitrary input signal in the conditions of normal operation of the object, we give a sinusoidal input action $u(t)$, it is not a controlling action, but a measured one $\mu(t)$:

$$\begin{aligned} u_t &= \sin(0.1t) \\ \mu_t &= \sin(0.05t) \end{aligned} \qquad (11)$$

Fig. 3 uses following notations: $u(t)$ − sinusoidal input action, $\mu(t)$ − uncontrolling, but a measured variable.

We could add a random noise h, that arising in the channel of output signal $x(t)$ measurement

$$h_t = lx_t\xi_t, \qquad (12)$$

where $\xi_t \in [-1;1]$, noise level $l = 10\%$.

We calculate a recovery error − w according to the

$$w = \frac{\sum_{i=1}^{s} |x_t - \hat{x}_t|}{\sum_{i=1}^{s} |x_t - \overline{x}|}, \qquad (13)$$

where $\overline{x} = \dfrac{1}{s}\sum_{i=1}^{s} x_t$ − arithmetic mean, $x_s(t)$ − model output.

Implementing the algorithm (1), we construct a model of the object, shown in fig. 4.

Fig. 4 uses the following notations: $x(t)$ − object output; $\hat{x}(t)$ − model output; noise level $l = 0\%$; recovery error w − 0.047, according to the chart and recovery error, this model could be considered as satisfactory.
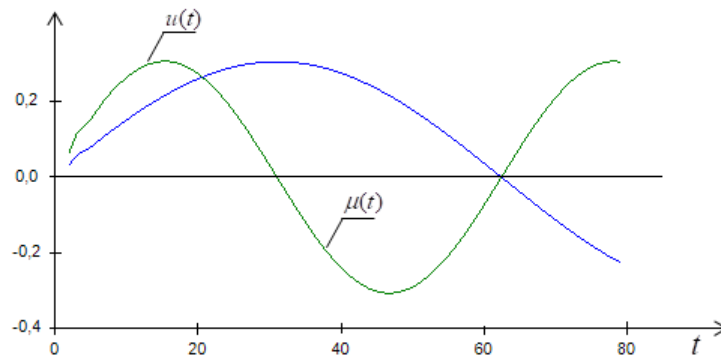
Fig. 3. Arbitrary input actions u and μ

Рис. 3. Произвольные входные воздействия u и μ
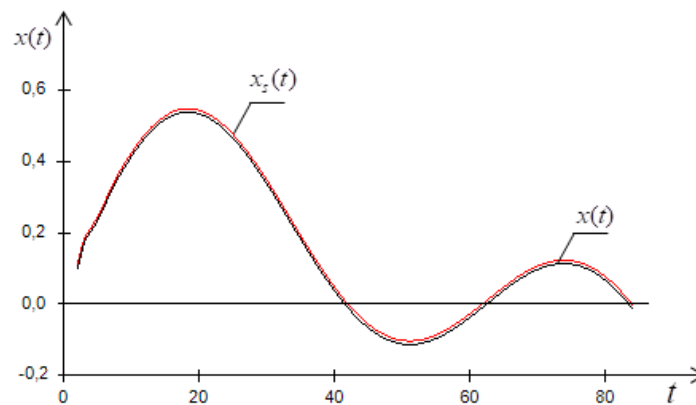
Fig. 4. Object output $x(t)$ when the input is an arbitrary sinusoidal signal

Рис. 4. Реакция выхода объекта *x*(*t*) и модели,
при синусоидальном входном воздействии
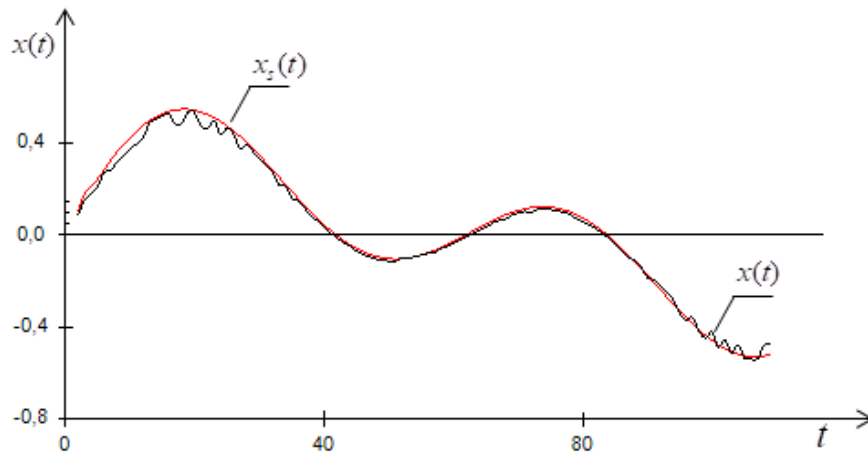
Fig. 5. Object output when the input is an arbitrary sinusoidal signal and noise level 10 %

Рис. 5. Результаты выхода объекта, при синусоидальном входном
воздействии при уровне помех равном 10 %

The case when $l = 10$ % and recovery error $w – 0.112$ is shown on fig. 5.

Conclusion. The research analyzes the problem of nonparametric identification of linear dynamical objects under the conditions of incomplete data. The main result of this paper is resolution of identification problem in an object normal operation conditions. The paper submits nonparametric linear dynamical system models based on Duhamel integral estimation by means of Nadaraya-Watson statistics.

The main conclusions based on the extensive numerical research of nonparametric models are following: although in practice delta function cannot be submitted to the object input, sometimes it is possible to submit delta-shaped input signal and then construct a satisfactory model. Undoubtedly, noise increase in input-output variables measurement and increase in discreteness of input-output variables control deteriorate an accuracy of nonparametric models.

In addition, it is important to note that a researcher does not know a particular object equation and a differential equation order; moreover, all equations described are analyzed as examples. Therefore, algorithm does not depend on the type of input impact, the main condition is observance of the superposition principle.

References

1. Tsypkin Ya. Z. *Informatsionnaya teoriya identifikatsii* [Information theory of identification]. Moscow, Nauka, Fizmatlit Pabl., 1995, 336 p.

2. Raibman N. N. *Chto takoe identifikatsiya* [What is identification]. Moscow, Nauka Pabl., 1970, 119 p.

3. Eykhoff P. *Osnovy identifikatsii sistem upravleniya* [Fundamentals of identification of control systems]. Moscow, Mir Publ., 1975, 681 p.

4. Medvedev A. V. *Neparametricheskie sistemy adaptatsii* [Nonparametric adaptation systems]. Novosibirsk, Nauka Publ., 1983, 174 p.

5. Medvedev A. V. [Adaptation under conditions of non-parametric uncertainty]. *Adaptivnye sistemy i ikh prilozheniya* [Adaptive systems and their applications]. Novosibirsk, Nauka Publ., 1978, P. 4–34.

6. Medvedev A. V. [The theory of nonparametric systems. Modeling]. *Vestnik SibGAU.* 2010, No. 4 (30), P. 4–9 (In Russ.).

7. Medvedev A. V. [Elements of the theory of nonparametric control systems]. *Aktual'nye problemy informatiki, prikladnoy matematiki i mekhaniki. Informatika* [Actual problems of computer science, applied mathematics and mechanics. Information technologies]. Novosibirsk, Krasnoyarsk, Izd-vo Sib. otd-niya Ros. akad. Nauk Publ., 1996, P. 87–112.

8. *Metody klassicheskoy i sovremennoy teorii avtomaticheskogo upravleniya. T. 1: Matematicheskie modeli, dinamicheskie kharakteristiki i analiz sistem upravleniya* [Methods of classical and modern theory of automatic control. Vol. 1. Mathematical models, dynamic characteristics and analysis of control systems]. Ed. K. A. Pupkova, N. D. Egupova. Moscow, MSTU named after N.E. Bauman Publ., 2004, 656 p.

9. *Metody klassicheskoy i sovremennoy teorii avtomaticheskogo upravleniya. T. 2: Statisticheskaya dinamika i identifikatsiya sistem avtomaticheskogo upravleniya* [Methods of classical and modern theory of automatic control. Vol. 2. Statistical dynamics and identification of automatic control systems]. Ed. K. A. Pupkova, N. D. Egupova. Moscow, MSTU named after N. E. Bauman Publ., 2004, 640 p.

10. Shishkina A. V., Agafonov E. D., Shishkina A. V. [Nonparametric control of a dynamical system]. *Siberian Journal of Science and Technology.* 2018. Vol. 19, No. 4, P. 711–718 (In Russ.).

11. Nadaraya E. A. *Neparametricheskoe otsenivanie plotnosti veroyatnostey i krivoy regressii* [Nonparametric estimation of the probability density and the regression curve]. Tbilisi, Izd. Tbil. University Publ., 1983.

12. Kotkinik V. Ya. *Neparametricheskaya identifikatsiya i sglazhivanie dannykh* [Nonparametric identification and data smoothing]. Moscow, Nauka Publ., 1985, 336 p.

13. Grop D. *Metody identifikatsii system* [Methods of identification of systems]. Moscow, Mir Publ., 1979, 304 p.

14. Tse E., Bar-Shalom Y. An actively adaptive control for linear systems with random parameters via the dual control. Automatic Control. *IEEE Transactions.* 2003, Vol. 18, Is. 2, P. 109–117.

15. Wenk C. J. Bar-Shalom, Y. A multiple model of an adaptive dual control algorithm for stochastic systems with unknown parameters Automatic Control. *IEEE Transactions.* 2003, Vol. 25, Is. 4, P. 703–710.

16. Liung L. *Identifikatsiya sistem* [Identification of systems]. Moscow, Nauka Pudl., 1991, 423 p.

17. *Metody klassicheskoy i sovremennoy teorii avtomaticheskogo upravleniya. T. 3: Sintez regulyatorov sistem avtomaticheskogo upravleniya* [Methods of classical and modern theory of automatic control. Vol. 3. Synthesis of regulators of automatic control systems]. Ed. K. A. Pupkova, N. D. Egupova. Moscow, MSTU named after N. E. Bauman Publ., 2004, 656 p.

Библиографический список

1. Цыпкин Я. З. Информационная теория идентификации. М. : Наука ; Физматлит, 1995. 336 с.

2. Райбман Н. С. Что такое идентификация. М. : Наука, 1970. 119 с.

3. Эйкхофф П. Основы идентификации систем управления. М. : Мир, 1975. 681 с.

4. Медведев А. В. Непараметрические системы адаптации. Новосибирск : Наука, 1983. 174 с.

5. Медведев А. В. Адаптация в условиях непараметрической неопределенности // Адаптивные системы и их приложения. Новосибирск : Наука ; СО АНССР, 1978. С. 4–34.

6. Медведев А. В. Теория непараметрических систем. Моделирование // Вестник СибГАУ. 2010. № 4 (30). С. 4–9.

7. Медведев А. В. Элементы теории непараметрических систем управления // Актуальные проблемы информатики, прикладной математики и механики. Информатика. Новосибирск ; Красноярск : Изд-во Сиб. отд-ния РАН, 1996. С. 87–112.

8. Методы классической и современной теории автоматического управления. Т. 1: Математические модели, динамические характеристики и анализ систем управления / под ред. К. А. Пупкова, Н. Д. Егупова. М. : МГТУ им. Н. Э. Баумана, 2004. 656 с.

9. Методы классической и современной теории автоматического управления. Т. 2: Статистическая динамика и идентификация систем автоматического управления / под ред. К. А. Пупкова, Н. Д. Егупова. М. : МГТУ им. Н. Э. Баумана, 2004. 640 с.

10. Шишкина А. В., Агафонов Е. Д., Шишкина А. В. О непараметрическом управлении динамической системой // Сибирский журнал науки и технологий. 2018. Т. 19, № 4. С. 711–718.

11. Надарая Э. А. Непараметрическое оценивание плотности вероятностей и кривой регрессии. Тбилиси : Изд-во Тбил. ун-та. 1983.

12. Катковник В. Я. Непараметрическая идентификация и сглаживание данных. М. : Наука, 1985. 336 с.

13. Гроп Д. Методы идентификации систем : пер. с англ. М. : Мир , 1979. 304 с.

14. Tse E., Bar-Shalom Y. An actively adaptive control for linear systems with random parameters via the dual control approach Automatic Control // IEEE Trans. 2003. Vol. 18, Is. 2. P. 109–117.

15. Wenk C. J. Bar-Shalom, Y. A multiple model adaptive dual control algorithm for stochastic systems with unknown parameters Automatic Control // IEEE Trans. 2003. Vol. 25, Is. 4. P. 703–710.

16. Льюнг Л. Идентификация систем. М. : Наука, 1991. 423 p.

17. Методы классической и современной теории автоматического управления. Т. 3. Синтез регуляторов систем автоматического управления / под ред. К. А. Пупкова, Н. Д. Егупова. М. : МГТУ им. Н. Э. Баумана, 2004. 656 с.

Kornet Maria Evgenievna – applicant of the Department of System Analysis and Operations Research; Reshetnev Siberian State University of Science and Technology, Institute of Informatics and Telecommunications. E-mail: marya.kornet@gmail.com.

Shishkina Anastasia Vasilyevna – graduate student; Siberian Federal University, Institute of space and information technologies. E-mail: nastya.shishkina9666@mail.ru.

Корнет Мария Евгеньевна – соискатель кафедры системного анализа и исследования операций; Сибирский государственный университет науки и технологий имени академика М. Ф. Решетнева, Институт информатики и телекоммуникаций. E-mail: marya.kornet@gmail.com.

Шишкина Анастасия Васильевна – магастрант; Сибирский федеральный университет, Институт космических и информационных технологий. E-mail: nastya.shishkina9666@mail.ru.

APPLYING SOFTWARE-MATHEMATICAL MODELS OF ONBOARD EQUIPMENT TO DEVELOP ONBOARD SOFTWARE

Yu. S. Lomaev, I. A. Ivanov, A. V. Tolstykh, E. V. Islent'ev

JSC "Academician M. F. Reshetnev "Information Satellite Systems"
52, Lenina St., Zheleznogorsk, Krasnoyarsk region, 662972, Russian Federation
E-mail: lomaif@rambler.ru

This paper deals with the testing of the functioning logic of spacecraft subsystems at the stage of developing system onboard software. The increasing complexity of the structure and operation logic of spacecraft due to the increased requirements in terms of providing consumers with information services (navigation, satellite monitoring of transport, geodesy, communications etc.) demands maintaining the reliability of uninterrupted operation, the implementation of automated parrying of emergency situations during the operation of spacecraft onboard equipment. In order to meet these requirements, it is necessary to test the interaction of onboard equipment and onboard integrated computing complex software that implements the target-oriented operation of spacecraft onboard systems. In such a case, meeting the requirements for reliability increase of onboard software should not lead to the increase of the manufacturing period of spacecraft.

In this work we propose the approach for testing information and logical interaction between onboard equipment and software of a spacecraft onboard integrated computing complex with the use of a laboratory testing sample unit and a software-mathematical model. We described the basic concepts of conducting two-stage testing of onboard software, involving autonomous and system testing on the ground testing complex. The proposed approach is applied as part of the onboard software development cycle in accordance with the standards of the JSC "Academician M.F. Reshetnev "Information Satellite Systems".

The approach proposed in this work helps reduce the number of errors during onboard software development and testing of information and logical interaction between onboard equipment and a spacecraft as a whole in every operation mode.

Keywords: spacecraft, onboard equipment, onboard software, software-mathematical model, laboratory testing, ground testing complex.

ПРИМЕНЕНИЕ ПРОГРАММНО-МАТЕМАТИЧЕСКИХ МОДЕЛЕЙ БОРТОВОЙ АППАРАТУРЫ ПРИ РАЗРАБОТКЕ БОРТОВОГО ПРОГРАММНОГО ОБЕСПЕЧЕНИЯ

Ю. С. Ломаев, И. А. Иванов, А. В. Толстых, Е. В. Ислентьев

АО «Информационные спутниковые системы» имени академика М. Ф. Решетнева»
Российская Федерация, 662972, г. Железногорск Красноярского края, ул. Ленина, 52
E-mail: lomaif@rambler.ru

Работа посвящена отработке логики функционирования подсистем космического аппарата на этапе разработки бортового программного обеспечения системы. Усложнение структуры и логики функционирования космических аппаратов в связи с повышением требований в части обеспечения потребителей информационными услугами (навигации, спутникового мониторинга транспорта, геодезии, связи и т.д.) требует поддержания надежности и бесперебойного функционирования, реализации автоматизированного парирования нештатных ситуаций при работе бортовых аппаратур космических аппаратов. Для достижения поставленных требований необходима отладка взаимодействия бортовой аппаратуры и программного обеспечения бортового интегрированного вычислительного комплекса, реализующего целевое функционирование бортовых систем космического аппарата. При этом выполнение требований по увеличению надёжности бортового программного обеспечения не должно приводить к увеличению сроков изготовления космического аппарата.

В настоящей работе предложен подход для отработки информационно-логического взаимодействия бортовой аппаратуры и программного обеспечения бортового интегрированного вычислительного комплекса космического аппарата с применением лабораторно-отработочного изделия и программно-математической модели. Описаны основные идеи проведения двухуровневого тестирования бортового программного обеспечения, включающего в себя автономное и системное тестирование на наземном отладочном комплексе. Указанный подход применен в рамках реализации цикла разработки бортового программного обеспечения, проводимого согласно стандартам АО «Информационные спутниковые системы» имени академика М. Ф. Решетнева».

Предложенный в работе подход способствует сокращению ошибок при разработке бортового программного обеспечения и проверке информационно-логического взаимодействия бортовой аппаратуры и космического аппарата в целом во всех режимах функционирования.

Ключевые слова: космический аппарат, бортовая аппаратура, бортовое программное обеспечение, программно-математическая модель, лабораторно-отработочные испытания, наземный отладочный комплекс.

Introduction. Currently, spacecraft have a crucial role in providing consumers with communications, television broadcasting and navigation services. Depending on the purpose, spacecraft contain a specific set of onboard equipment. The problems solved by individual instruments determine the functioning and logic of the operation of individual systems and a spacecraft as a whole. To ensure a reliable uninterrupted operation [1] and automated management of emergency situations arising from the operation of onboard equipment, it is necessary to adjust the interaction with the software of the onboard integrated computing system of spacecraft [2; 3].

The development of onboard software. A spacecraft includes a number of target and auxiliary equipment (spacecraft systems), which is determined according to the purpose of a spacecraft. For all onboard equipment, specialists develop software as part of the onboard software, as well as software as a part of equipment ensuring the interaction of this equipment with the onboard control complex of a spacecraft.

Onboard software is a combination of the software of onboard systems operating in single hardware and software environment of the onboard integrated computing system of a spacecraft [4]. Each component of the onboard software is a functional part of its onboard system and, together with its hardware, solves the problems assigned to this onboard system.

There are many approaches to software development related to its design. The development, autonomous and system testing of onboard software are key stages of the lifecycle of a spacecraft [5], which provide the interaction and logic of functioning data and instruments within its systems.

Let us consider the standard cycle of the development of onboard software:

1) defining the requirements to system software;

2) developing the architectural design of system software;

3) developing and autonomous testing of system software;

4) system testing of system software in system modes;

5) testing system software in spacecraft modes;

6) fit testing of software and onboard equipment as part of a spacecraft at the stage of electrical and radio tests and flight tests;

7) maintaining system software at the stage of normal operation.

If necessary, we return to the previous stages in the standard cycle of developing onboard software. In case of the successful completion of these stages we use the developed onboard software for work with spacecraft equipment and maintain the onboard software operation with the equipment in the spacecraft until the end of its active life. The onboard software architecture has the following form in general terms (fig. 1).

While developing the onboard software, it is necessary to conduct detailed testing of the interaction of software that is part of a spacecraft system and onboard equipment in order to detect errors before conducting integration tests of software and equipment as part of a spacecraft. Frequently, when errors are detected, changing the software of onboard equipment is no longer possible, since it may contain one-time programmable memories, or error correction may take much time, which leads to an increase in the duration of spacecraft testing. In this case, when abnormal situations occur, there is a possibility of correcting software failures of the onboard equipment from an onboard control complex by modifying its software.

The use of a mathematical software model. One of the ways to test software in the development of onboard software is to simulate the logic of the equipment by creating its software and mathematical model.

Software and mathematical model is a complex of the implemented logic of equipment operation in the form of a program code, through which we receive and transmit information when interacting with the onboard software.

When creating a software model of equipment, it is not necessary to have a high specification of the description of its internal structure and logic of functioning, but only to imitate those features of the equipment that are important from the point of view of its interaction with the external environment.

Fig. 2 shows the scheme of testing onboard software and software-mathematical model.

In the onboard software the logic of the interaction of equipment and the onboard control complex is implemented. The input information is the initial data, which contain the requirements for the development of onboard software.

The output information comprises the results of the stand-alone testing of the onboard software through debugging packages. The debug package is a pseudo-code for checking whether it is possible to achieve the

execution of a certain branch of the logic of onboard software.

As a result of package debugging, we determine the execution time, the size of the stack used, the coverage of the logic of the executable program code.

The essence of the debugging of information interaction between the software-mathematical model and the onboard control complex is to check the reception and transmission of various types of information messages, such as control commands, telemetry information, onboard time, software arrays, receipts, etc. Information exchange between the equipment and the BUD is performed via a multiplex exchange channel according to GOST R 52070–2003 (ГОСТ Р 52070–2003) [6] in accordance with the protocol of information and logic interaction with this equipment, developed by the equipment manufacturer and agreed with the developer of the onboard software.

In case of the successful normal operation of the interaction between the onboard control complex and the software-mathematical model, we check the occurrence of abnormal situations in information exchange: hardware malfunctions, failures of the multiplex exchange channel, errors in information messages, temperature failures, failures in signal power, current strength, voltage and other malfunctions.

System testing on the ground debugging complex. The result of the procedures described above is the integration of the onboard software and the software-mathematical model with the aim of conducting system testing on the ground debugging complex [7; 8]. A ground testing complex is the integrated environment for testing the onboard software and the software-mathematical model instruments within a spacecraft. The testing of the interaction occurs by checking the execution of the program logic using sequence diagrams [9].
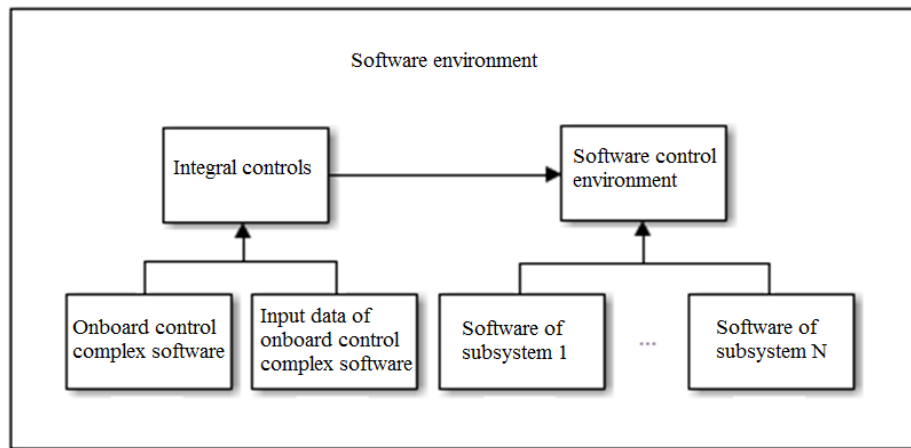
Fig. 1. Onboard software architecture

Рис. 1. Архитектура бортового программного обеспечения
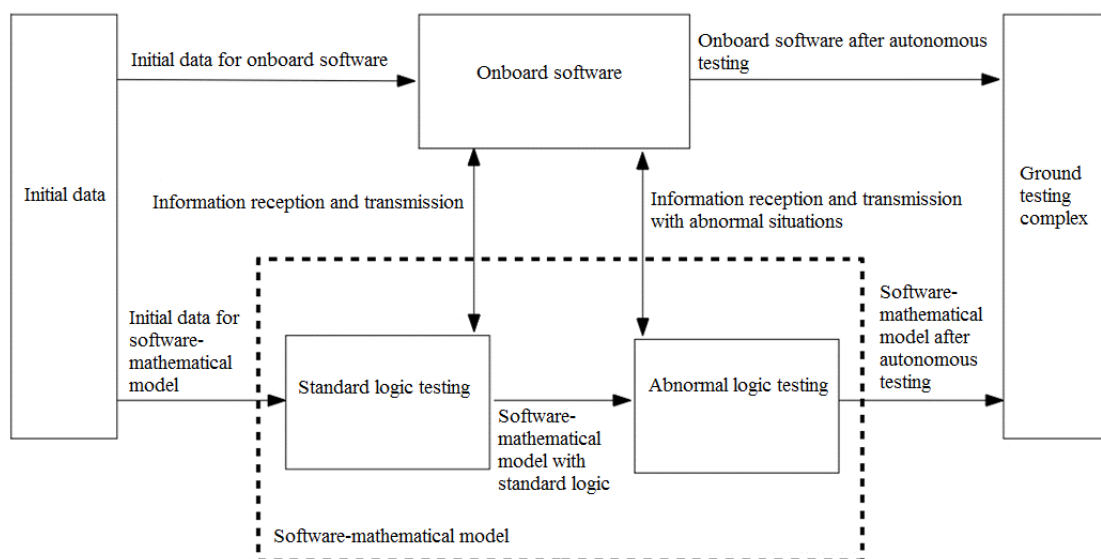
Fig. 2. Testing of onboard software and of a software-mathematical model

Рис. 2. Отработка бортового программного обеспечения
и программно-математической модели

A sequence diagram is a pseudo-code for system testing, based on a graphical formalized language describing the procedures and test options, allowing automating a testing process.

The result of this stage is the onboard software of the equipment, ready for testing in the spacecraft mode on the ground testing complex.

In addition, the ground testing complex has the ability to specify various initial data of the spacecraft operation, both in general and each spacecraft system in particular; that allows testing the onboard software for the whole set of its functionality. Fig. 3 shows the ground testing complex architecture.

Sample application for laboratory testing. Another way to test the onboard software is to use a laboratory testing sample [10; 11]. A laboratory testing sample is a special sample of equipment for testing, which is a prototype of standard equipment in terms of functionality and basic technical characteristics, on which we develop software and technical solutions. Such a product is cheaper than standard equipment and it is manufactured faster, therefore there is a possibility of the onboard software testing before the completion of the production of a standard sample. Fig. 4 shows the scheme for testing the interaction of onboard software with the laboratory testing sample.
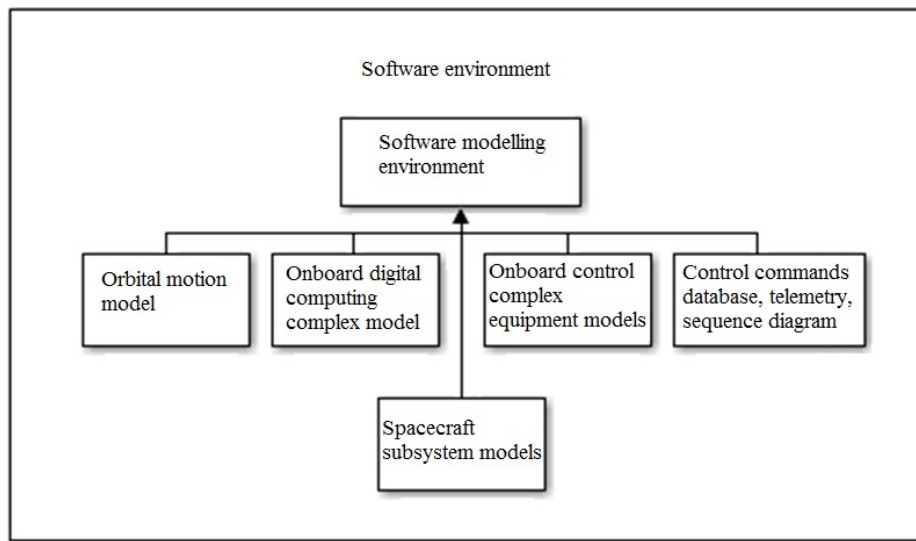
Fig. 3. Ground testing complex architecture

Рис. 3. Архитектура наземного отладочного комплекса
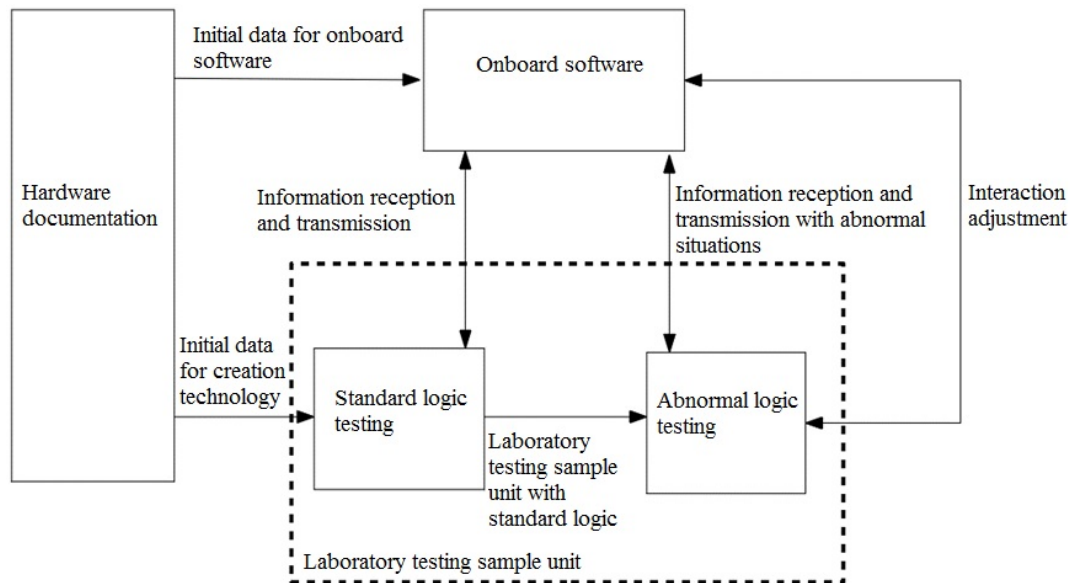
Fig. 4. Testing the interaction between onboard software and a laboratory testing sample unit

Рис. 4. Отработка взаимодействия бортового программного обеспечения с образцом
для лабораторно-отработочных испытаний
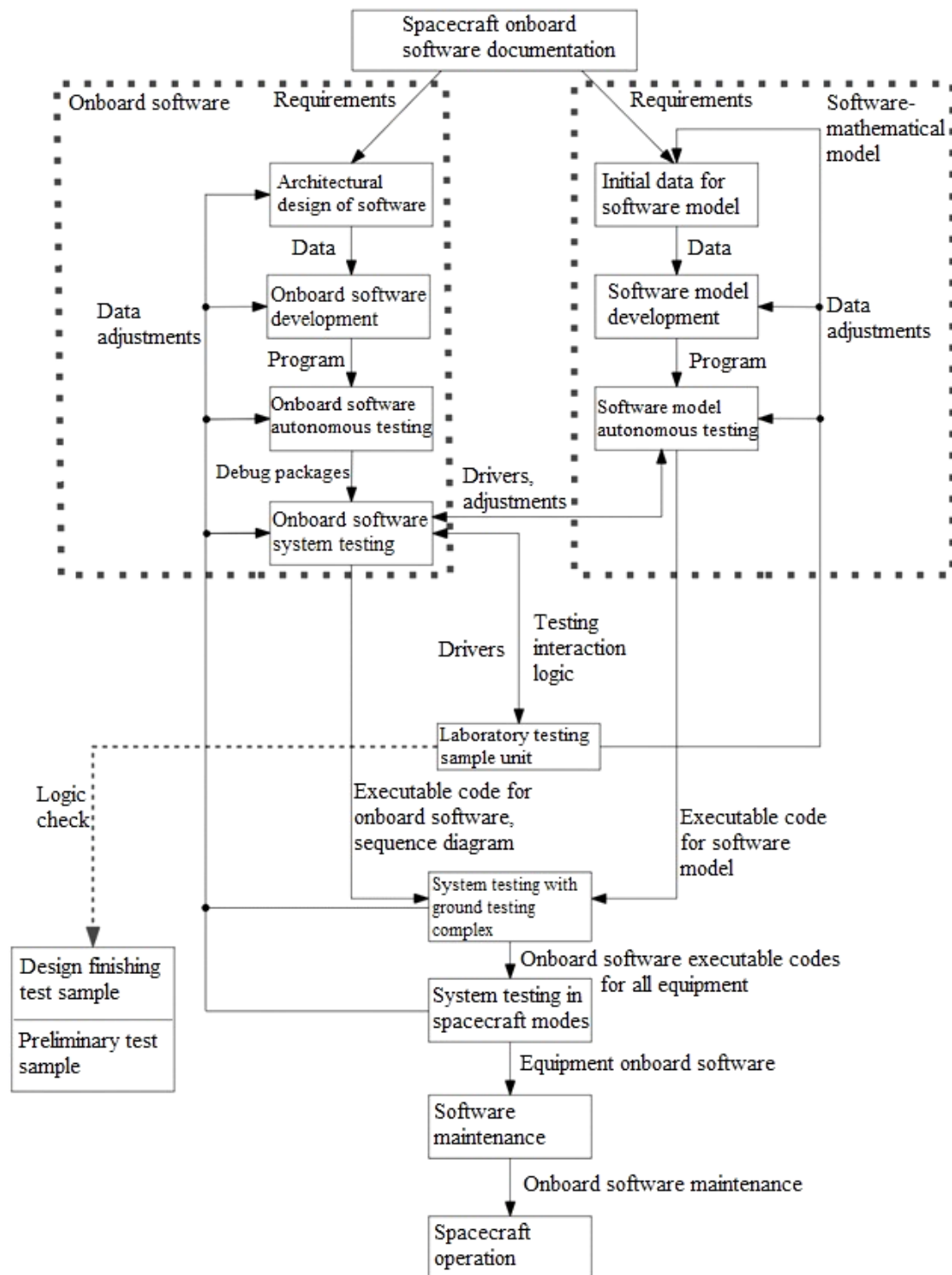
Fig. 5. The general scheme of the development of onboard software with the application
of a software-mathematical model, and laboratory testing sample unit

Рис. 5. Общая схема разработки БПО с использованием ПММ, образца ЛОИ

The input information is the logic of the functioning of the sample, which is governed by the requirements for the creation of an experimental product. The output information is the executable code of the onboard software for testing with the ground testing complex.

As part of the development of software interaction with the equipment, we conduct testing to check the standard and abnormal logic of the laboratory testing sample.

The result is a corrected logic of the equipment, which we take into account at further stages of the development of onboard software. Fig. 5 shows the proposed software development scheme for onboard spacecraft systems [12; 13].

The particularities of using a software-mathematical model and a laboratory testing sample. We develop the onboard software and the software-mathematical model in parallel, and we pair them with the help of software drivers.

The peculiarity of using the software-mathematical model is to simulate the logic of the equipment in both regular and abnormal situations in which there are predictable failures in information exchange between it and the onboard control complex [14; 15]. We perform testing of the docking of the onboard software and the software-mathematical model during the delivery of the software to the ground testing complex, which allows us to prevent errors in the logic of the functioning of the onboard software at subsequent stages.

The use of the laboratory testing sample contributes to the accurate reflection of the procedures for recording and reading information from the point of view of the logic of operation of the device.

Testing on the laboratory testing sample gives a complete picture of the logic of the equipment, the physical component of the equipment, the processor, the runtime and the number of operations for a given time, which allows us to work out the hardware software and onboard software. In this case, there is information about real-time execution of operations, making it possible to adjust the system resources in advance (allocated memory, execution time, pauses during operation, etc.).

The use of the laboratory testing sample allows to reduce the time for making changes to the code of the onboard software, since the introduction of changes at the system testing stage in spacecraft modes requires consistency in working with the developers of other systems. The laboratory testing sample serves as a prototype for design finishing test sample and preliminary test sample, we take into account the adjustments for the laboratory testing sample on the indicated samples.

The advantages of the described methods in the development of onboard software. The use of the proposed methodology for the development of system software, including direct interaction with the laboratory testing sample and the use of the software-mathematical model, contributes to the reduction of time and parity of errors in the development cycle, autonomous and system testing of software.

The benefits of using a software-mathematical model is to organize the development of regular and emergency situations in the flight control center, to provide training for operation personnel, which contributes to rapid response when such situations occur during the operation of products.

Conclusion. The need to develop and use a software-mathematical model to test the onboard software of spacecraft is determined by several factors. Firstly, with the help of the software-mathematical model at the NOC, we sreated and tested the sequence diagrams, which are later used in testing and final adjusting actual onboard equipment and spacecraft systems, which can significantly reduce the time required for software testing and final adjustment. Secondly, the development stages of software and hardware run in parallel, therefore the possibility of developing software with real hardware is not available. Consequently, there is a need for its software simulation. The use of a software-mathematical model when testing onboard software allows us to produce better and more complete development of the logic of the operation of the equipment and various emergency situations. Thirdly, it is necessary to envisage the possibility of making changes in the onboard software after launching the spacecraft, changes can be preliminarily worked out on software models of spacecraft systems before they are installed in the onboard integrated computing complex; that helps prevent emergency situations and increases the overall reliability of spacecraft.

The modified methodology for the development of onboard software is used in the development of software of systems in the process of the creation of the "Glonass-K" spacecraft.

References

1. Tyugashev A. A., Iljin I. A., Ermakov I. E. [Ways of increasing software reliability and quality in space industry]. *Upravlenie bolshimi sistemami.* 2012, No. 39, P. 288–299 (In Russ.).

2. Tzapko G. P., Martynov Ya. A. [Unified information environment for creating and supporting onboard software of navigation and communication satellites]. *Doklady TUSURa.* 2015, No. 3(37), P. 97–102 (In Russ.).

3. Koltashev A. A. [Main principles of system testing and confirmation of satellite onboard software]. *Vestnik SibGAU.* 2010, No. 1(27), P. 4–7 (In Russ.).

4. Antamoshkin A. A., Koltashev A. A. [Technological aspects of creating communication satellite onboard software]. *Vestnik SibGAU.* 2005, No. 6, P. 93–95 (In Russ.).

5. Koltashev A. A. [Effective technology for controlling onboard software lifecycle of communication and navigation satellites]. *Aviakosmicheskoe priborostroenie.* 2006, No. 12, P. 20–25 (In Russ.).

6. *GOST R 52070–2003. Interfeis magistralniy posledovatelniy sistemy electronnykh moduley* [State standard R 52070-2003. Trunk serial interface for electronic modules system]. Moscow, Standartinform Publ., 2003. 24 c.

7. Mostovoi Ya. A. [Simulation mathematical model of the external environment in the life cycle of the onboard sowtware for managing the space platform]. *Komp'yuternaya optika.* 2012, No. 3(36), P. 412–418 (In Russ.).

8. Lomaev Yu. S. [Application of onboard software system testing]. *Aktualnye problemy aviatsii i kosmonavtiki.* 2016, No. 1, P. 531–532 (In Russ.).

9. Shoshmina I. V. [Design of software onboard control systems with verification support]. *Modelirovanie i analiz informatsionnyh system.* 2010, No. 4, P. 125–136 (In Russ.).

10. Lomaev Yu. S., Ivanov I. A. [Usage of laboratory testing sample unit for reducing time costs for onboard software development and testing]. *Sbornik tezisov IV nauchno-technicheskoy konferentsii molodyh spetsialistov "Razrabotka, proizvodstvo, ispytaniya i ekspluatatsiya*

kosmicheskih apparatov i sistem" [Theses compilation of IV science-technical conference of young specialists "Development, manufacturing, testing and operation of spacecrafts and systems"]. JSC "ISS", Zheleznogorsk, 2017, P. 99–101 (In Russ.).

11. Lomaev Yu. S., Ivanov I. A. [Usage of laboratory testing sample unit for optimization of onboard software development]. *Sbornik tezisov IV Vserossiyskoy nauchno-technicheskoy konferentsii "Sistemy svyazi i radionavigatsii"* [Theses compilation of IV All-Russian science-technical conference "Communication and radionavigation systems"]. JSC "NPP Radiosvyaz", Krasnoyarsk, 2017, P. 339–342 (In Russ.).

12. Lomaev Yu. S., Tolstykh A. V., Zvonar V. D. [Modification of onboard software development stages]. *VIII ezhegodnaya nauchno-technicheskaya konferentsiya molodyh uchenyh i spetsialistov FGUP TSNIIMASH* [VIII annual science-technical conference of FGUP TSNII-MASH young scientists and specialists]. Moscow, 3–6 April 2018, P. 41–43 (In Russ.).

13. Lomaev Yu. S., Tolstykh A. V. [Software testing approach modification for onboard software development]. *Tezisy dokladov X Obscherossiyskoy molodezhnoy nauchno-tekhnicheskoy konferentsii "Molodezh. Tekhnika. Kosmos"* [Report theses of X All-Russian youth science-technical conference "Youth. Technics. Space."]. Saint-Petersburg, 18–20 April 2018, P. 30–31 (In Russ.).

14. Lomaev Yu. S., Tolstykh A. V. [Usage of software-mathematical model for onboard software complex development]. *Aktualnye problemy aviatsii i kosmonavtiki"*. 2018, Vol. 1, P. 119–120 (In Russ.).

15. Ivanov I. A., Antropov N. R., Deryshev R. A. [Usage of program models for testing spacecraft onboard software]. *Trudy X Obsherossiyskoy molodezhnoy nauchno-tekhnicheskoy konferentsii "Molodezh. Tekhnika. Kosmos"* [Report theses of X All-Russian youth science-technical conference "Youth. Technics. Space."]. Saint-Petersburg, 18–20 April 2018, Vol. 2, P. 69–73 (In Russ.).

Библиографические ссылки

1. Тюгашев А. А., Ильин И. А., Ермаков И. Е. Пути повышения надежности и качества программного обеспечения в космической отрасли // Управление большими системами. 2012. № 39. С. 288–299.

2. Цапко Г. П., Мартынов Я. А. Единая информационная среда создания и сопровождения бортового программного обеспечения спутников навигации и связи // Доклады ТУСУРа. 2015. № 3(37). С. 97–102.

3. Колташев А. А. Основные принципы системного тестирования и подтверждения бортового программного обеспечения спутников // Вестник СибГАУ. 2010. № 1(27). С. 4–7.

4. Антамошкин А. А., Колташев А. А. Технологические аспекты создания бортового программного обеспечения спутников связи // Вестник СибГАУ. 2005. № 6. С. 93–95.

5. Колташев А. А. Эффективная технология управления циклом жизни бортового программного обеспечения спутников связи и навигации // Авиакосмическое приборостроение. 2006. № 12. С. 20–25.

6. ГОСТ Р 52070–2003. Интерфейс магистральный последовательный системы электронных модулей. М. : ИПК Издательство стандартов, 2003. 24 с.

7. Мостовой Я. А. Имитационная математическая модель внешней среды в жизненном цикле бортового программного обеспечения управления космической платформой // Компьютерная оптика. 2012. № 3(36). С. 412–418.

8. Ломаев Ю. С. Применение системного тестирования бортового программного обеспечения // Актуальные проблемы авиации и космонавтики : сб. тез. Всеросс. науч.-практич. конф. 2016. № 1. С. 531–532.

9. Шошмина И. В. Проектирование программных бортовых систем управления с поддержкой верификации // Моделирование и анализ информационных систем. 2010. № 4. С. 125–136.

10. Ломаев Ю. С., Иванов И. А. Применение лабораторно-отработочного изделия для сокращения временных затрат на разработку и тестирование бортового программного обеспечения // Разработка, производство, испытания и эксплуатация космических аппаратов и систем : сб. тез. IV науч.-техн. конф. молодых специалистов / «АО «ИСС». Железногорск, 2017. С. 99–101.

11. Ломаев Ю. С., Иванов И. А. Применение лабораторно-отработочного образца для оптимизации разработки бортового программного обеспечения // Системы связи и радионавигации : сб. тез. IV Всеросс. науч.-техн. конф. / АО «НПП «Радиосвязь». Красноярск, 2017. С. 339–342.

12. Ломаев Ю. С., Толстых А. В., Звонарь В. Д. Модификация этапов разработки бортового программного обеспечения // Тез. докладов VIII ежегодной науч.-техн. конф. молодых ученых и специалистов ФГУП ЦНИИМАШ. Москва, 3–6 апреля 2018 г. С. 41–43.

13. Ломаев Ю. С., Толстых А. В. Модификация подходов проведения тестирования программного обеспечения при разработке бортового программного обеспечения // Молодежь. Техника. Космос : тез. докладов X Общеросс. молодежной науч.-техн. конф. СПб, 18-20 апреля 2018 г. С. 30–31.

14. Ломаев Ю. С., Толстых А. В. Применение программно-математической модели при разработке бортового программного комплекса // Актуальные проблемы авиации и космонавтики : материалы III междунар. науч.-практич. конф. творческой молодежи. Красноярск, 9–13 апреля 2018 г. Т. 1. С. 119–120.

15. Иванов И. А., Антропов Н. Р., Дерышев Р. А. Применение программных моделей для отработки бортового программного обеспечения космических аппаратов // Молодежь. Техника. Космос : тр. X Общеросс. молодежной науч.-техн. конф. СПб, 2018. Т. 2. С. 69–73.

Lomaev Yuri Sergeevich – an engineer of the second category; JSC "Academician M. F. Reshetnev "Information Satellite Systems". E-mail: lomaif@rambler.ru.

Ivanov Ilia Andreievich – Cand. Sc., an engineer of the second category; JSC "Academician M. F. Reshetnev "Information Satellite Systems". E-mail: ilyaiv92@gmail.com.

Tolstykh Anastasia Vladimirovna – technician; JSC "Academician M. F. Reshetnev "Information Satellite Systems". E-mail: avtolstykh1@gmail.com.

Islentev Eugene Vladimirovich – Cand. Sc., a head of sector; JSC "Academician M. F. Reshetnev "Information Satellite Systems". E-mail: islentev@iss-reshetnev.ru.

Ломаев Юрий Сергеевич – инженер второй категории; АО «Информационные спутниковые системы» имени академика М. Ф. Решетнева». E-mail: lomaif@rambler.ru.

Иванов Илья Андреевич – кандидат технических наук, инженер второй категории; АО «Информационные спутниковые системы» имени академика М. Ф. Решетнева». E-mail: ilyaiv92@gmail.com.

Толстых Анастасия Владимировна – техник; АО «Информационные спутниковые системы» имени академика М. Ф. Решетнева». E-mail: avtolstykh1@gmail.com.

Ислентьев Евгений Владимирович – начальник сектора; АО «Информационные спутниковые системы» имени академика М. Ф. Решетнева». E-mail: islentev@iss-reshetnev.ru.

MULTI-GRID FINITE ELEMENTS IN CALCULATIONS OF MULTILAYER OVAL CYLINDRICAL SHELLS

N. V. Pustovoi[1], A. N. Grishanov[1], A. D. Matveev[2*]

[1]Novosibirsk State Technical University
20, Karl Marx Av., Novosibirsk, 630073, Russian Federation
[2]Institute of Computational Modeling SB RAS
50/44, Akademgorodok, Krasnoyarsk, 660036, Russian Federation
*E-mail: mtv241@mail.ru

The method of finite elements (FEM) is actively used in calculations of composite shell constructions (rotation shells, circle and oval cylindrical shells), which are widely used in space-rocket and aviation equipment. To calculate multi-layer oval cylindrical shells three-dimensional curvilinear Lagrange multi-grid finite elements (MGFE) are suggested. When building a k-grid finite element (FE), k nested grids are used. The fine grid is generated by the basic split of MGFE that takes into account its complex heterogeneous structure and shape. On k-1 large grids the move functions used for decreasing MGFE dimension are determined. The stress-strain state in MGFE is described by the elasticity theory three-dimensional task equations (without introduction of additional hypotheses) in local Cartesian coordinates systems. The procedure of building shell-type Lagrange MGFE with the use of Lagrange polynomials presented in curvilinear coordinate systems is demonstrated. With the size reduction of discrete models MGFE have constant thickness equal to the thickness of the shell. The Lagrange polynomials nodes coincide in thickness with the MGFE large grid nodes and are located on the shared borders of different module layers. The use of such MGFE generates approximate solutions sequences that uniformly and quickly converge to precise solutions.

The main advantages of MGFE are as follows: they form discrete models with the dimension 10^2–10^6 times smaller than the basic models dimension and they generate small error solutions. Examples of calculations are given for four- and three-layer oval shells of various thickness and shape under both uniform and local loading with the use of 3-grid FE. Comparative analysis of the obtained solutions with the solutions built with the help of the software package ANSYS shows high efficiency of the suggested MGFE in calculations of multi-grid oval shells.

Keywords: elasticity, composite, oval cylindrical shell, multi-grid finite elements, Lagrange polynomials, convergence of the solution sequence, software package ANSYS.

МНОГОСЕТОЧНЫЕ КОНЕЧНЫЕ ЭЛЕМЕНТЫ В РАСЧЕТАХ МНОГОСЛОЙНЫХ ОВАЛЬНЫХ ЦИЛИНДРИЧЕСКИХ ОБОЛОЧЕК

Н. В. Пустовой[1], А. Н. Гришанов[1], А. Д. Матвеев[2*]

[1]Новосибирский государственный технический университет
Российская Федерация, 630073, г. Новосибирск, просп. К. Маркса, 20
[2]Институт вычислительного моделирования СО РАН
Российская Федерация, 630036, г. Красноярск, Академгородок, 50/44
*E-mail: mtv241@mail.ru

Метод конечных элементов (МКЭ) активно используется в расчетах композитных оболочечных конструкций (оболочки вращения, круговые и овальные цилиндрические оболочки), которые широко применяются в ракетно-космической и авиационной технике. Для расчета многослойных овальных цилиндрических оболочек предложены трехмерные криволинейные лагранжевые многосеточные конечные элементы (МнКЭ). При построении k-сеточного конечного элемента (КЭ) используется k вложенных сеток. Мелкая сетка порождена базовым разбиением МнКЭ, которое учитывает его сложную неоднородную структуру и форму. На k–1 круп-

ных сетках определяются функции перемещений, применяемые для понижения размерности МнКЭ. Напряженно-деформированное состояние в МнКЭ описывается уравнениями трехмерной задачи теории упругости (без введения дополнительных гипотез) в локальных декартовых системах координат. Показана процедура построения лагранжевых МнКЭ оболочечного типа с применением полиномов Лагранжа, представленных в криволинейных системах координат. При измельчении дискретных моделей МнКЭ имеют постоянную толщину, равную толщине оболочки. Узлы полиномов Лагранжа по толщине совпадают с узлами крупных сеток МнКЭ и расположены на общих границах разномодульных слоев. Применение таких МнКЭ порождает последовательности приближенных решений, которые равномерно и быстро сходятся к точным.

Основные достоинства МнКЭ состоят в том, что они образуют дискретные модели, размерность которых в 10^2–10^6 раз меньше размерности базовых моделей, и порождают решения с малой погрешностью. Представлены примеры расчетов четырех- и трехслойных овальных оболочек различной толщины и формы при равномерном и локальном нагружениях с применением 3-сеточных КЭ. Сравнительный анализ полученных решений с решениями построенных с помощью программного комплекса ANSYS показывает высокую эффективность предлагаемых МнКЭ в расчетах многослойных овальных оболочек.

Ключевые слова: упругость, композиты, овальная цилиндрическая оболочка, многосеточные конечные элементы, полиномы Лагранжа, сходимость последовательности решений, программный комплекс ANSYS.

Introduction. When studying the stress-strain state (SSS) of elastic homogeneous and composite shells, various numerical methods are widely used [1–8]. Traditionally, in the theory of shells, displacements are decomposed into power series with respect to a coordinate normal to the middle surface. However, in this case, in the numerical study of the SSS of thick shells, it is necessary to take into account a large number of terms in the corresponding expansions [1; 2]. Effective numerical approaches to the study of elastic shells are mainly based on the finite element method (FEM) [3–5]. The construction of finite elements (FE) in curvilinear coordinates creates a number of difficulties [5], in particular, related to the fulfillment of conformance conditions, which is necessary for the monotonic convergence of the sequence of FEM solutions [6].

When calculating shells using the FEM, there are three main approaches: approximation of the shell by flat FE, using curvilinear two-dimensional FE and construction of three-dimensional FE. As shown by numerical experiments, in the latter case, the calculation of shells with inhomogeneous (micro-inhomogeneous) structure by FEM using the equations of three-dimensional elasticity theory without introducing additional simplifying hypotheses leads to systems of linear algebraic equations (SLAE) of high order (10^9 – 10^{12}). As a result, it becomes necessary to develop such FEM variants in which the corresponding SLAE has a small order and its solution provides an acceptable small error for displacements and stresses.

In [9; 10], the calculation of circular cylindrical shells with a fibrous structure using multi-grid finite elements (MGFE), in which displacements are approximated by Lagrangian polynomials of various orders, is proposed. When building a k-grid-based FE ($k \geq 2$) k nested grids are used. The fine mesh is generated by the base partition of the MGFE, which consists of homogeneous single-grid FE (SGFE) of the 1st order and takes into account the non-uniform structure and shape of the MGFE. The remaining $k-1$ large grids are used to reduce the dimension of the base partition, that is, the dimension of the MGFE. In [11], Lagrangian MGFEs are used to calculate

multilayer circular cylindrical shells. The order of the Lagrange polynomials in the height of the MGFE was arbitrary and was not related to the number of layers.

In [12–14], the method of reference surfaces was proposed for calculating homogeneous and layered shells in the three-dimensional formulation. As unknowns, functions of displacements of these surfaces are chosen as functions of curvilinear coordinates. Displacements across the shell thickness are approximated using Lagrange polynomials of various orders, and displacements in the reference surfaces are given by functions that satisfy the boundary conditions. For displacements and deformations of reference surfaces, standard bilinear approximations and four-node curvilinear FEs are used [15], which distinguishes this approach from the analysis of the SSS of the shell using three-dimensional MGFE [10; 11].

In [16], it is noted that the use of non-circular cylindrical shells in aircraft industry allows to reduce the mass of the structure, effectively using the internal volume of pressurized cabins. The variability of the radius of curvature in the cross section of such shells in the general case creates certain difficulties in calculating the SSS using FEM. These difficulties are reduced if the noncircular cross section of the middle surface of the shell consists of several conjugate arcs of circles [16]. In this case, the three-dimensional Lagrangian MGFE developed in [10; 11] can be used to calculate multi-layer oval shells of different thickness, which greatly simplifies the application of FEM to analyze the SSS of oval shells.

The features of the MGFE in the calculation of oval shells are associated with the discretization rule, which is as follows. The proposed MGFEs with any partition have a constant thickness equal to the thickness of the oval shell. The nodes of the large MGFE mesh coincide with the nodes of Lagrange polynomials in the thickness of the shell and are located at the boundaries of the multimodular layers. When refining discrete models, such MGFEs generate sequences of approximate solutions that converge uniformly and quickly to exact solutions.

The advantages of the proposed MGFEs are that they generate multigrid discrete models of oval cylindrical shells, which require 10^2 – 10^6 times less computer memory than for the basic models. The calculations for

multi-layer oval cylindrical shells of various thickness and shape show that the solutions obtained using the MGFE and using the ANSYS software package differ by a small value.

Multi-layer Lagrangian multi-grid finite elements. In [16], construction of the cross section of the middle surface of an oval shell with semi-axes a, b was shown (fig. 1). B – the point of conjugation of the arcs AB and BC with centers O_R, O_r and radii R, r. For given a, b the radii of circles R, r of the middle surfaces of circular cylindrical shells, fragments of which form an oval shell, are determined by the formulas

$$r = a\frac{1+k^2-\sqrt{1+k^2}}{1+k-\sqrt{1+k^2}}, \ R = a\frac{1-k(\sqrt{1+k^2}-k)}{1+k-\sqrt{1+k^2}},$$

$$k = \text{tg}\alpha = \frac{b}{a}, \ \gamma = \frac{\pi}{2}-\alpha. \qquad (1)$$

For the procedure of constructing a multi-grid discrete model for calculating a multilayer oval cylindrical shell we will consider the example of a 4-layer shell of constant thickness h, located in the Cartesian coordinate system $Oxyz$, Oy – the axis of the shell. We have $h = \sum_{i=1}^{4} h_i$, h_i – the thickness of the i-th layer of the shell, let $h_i = \text{const}$, $i = 1,...,4$.
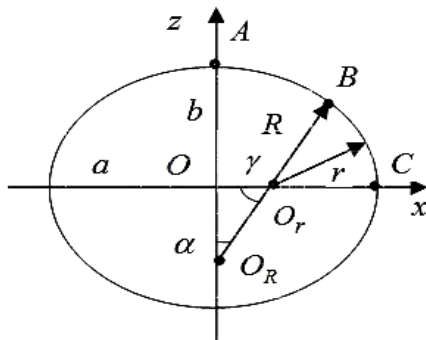
Fig. 1. Section of the shell middle surface

Рис. 1. Сечение срединной поверхности овальной оболочки

Without losing commonality of views, for simplicity, we assume that the geometric shape, physical characteristics, the discrete model, and the fixing of the oval shell are symmetrical with respect to the planes Oyz and Oxy. Therefore, we will consider a $1/4$ part of the oval shell, that is, a cylindrical panel, which we denote by V^0. The panel V^0 consists of subregions (panels) V_1 and V_2 of circular cylindrical shells, respectively, with radii R and r (their middle surfaces, fig. 1). We believe that bonds between the components of the inhomogeneous structure of the shell are ideal. The procedure of constructing an MGFE for calculating a 4-layer panel V^0 is considered on the example of a 4-layer three-grid FE (3GFE) $V_{e,p}^{(3)}$ (fig. 2), where the superscript

in brackets corresponds to the number of nested grids that are used in the construction of 3GFE [10; 11].
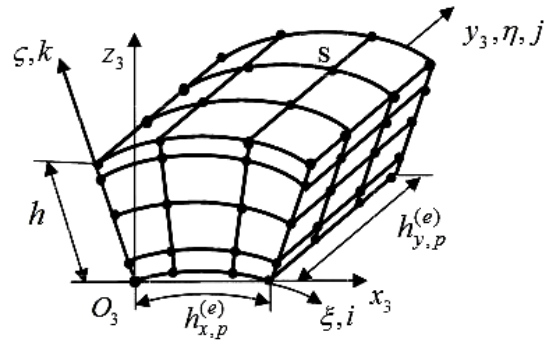
Fig. 2. Three-grid FE $V_{e,p}^{(3)}$ for 4-layer oval shell

Рис. 2. Четырехслойный ТрКЭ $V_{e,p}^{(3)}$ овальной оболочки

The circular cylindrical panel V_p consists of 3GFE $V_{e,p}^{(3)}$, where $e = 1,...N_p$, N_p is the total number of 3GFE in the panel V_p, $p = 1.2$. Each 3GFE $V_{e,p}^{(3)}$ consists of two-grid FE (2GFE) $V_{m,p}^{(2)}$, where $m = 1,...,M_p$, M_p is the total number of 2GFE. For simplicity, we assume that $M_1 = M_2 = M$. The area of 2GFE $V_{m,p}^{(2)}$ of the panel V_p consists of curvilinear homogeneous single-grid FE (SGFE) $V_{n,p}^{(1)}$ of the 1st order ($p = 1.2$), $n = 1,...,K_p$ is the total number of SGFE. Fig. 3 shows the eight-node SGFE $V_{n,p}^{(1)}$ with characteristic dimensions $h_{x,p}^{(n)} \times h_{y,p}^{(n)} \times h_{z,p}^{(n)}$, $O_1 x_1 y_1 z_1$ is a local Cartesian coordinate system. SGFEs $V_{n,p}^{(1)}$ take into account the inhomogeneous structure and shape of 2GFE $V_{m,p}^{(2)}$. The stress state in SGFE $V_{n,p}^{(1)}$ is described by the equations of the three-dimensional problem of the theory of elasticity, which are represented in the local Cartesian coordinate system $O_1 x_1 y_1 z_1$, that is, a three-dimensional SSS is realized in SGFE.
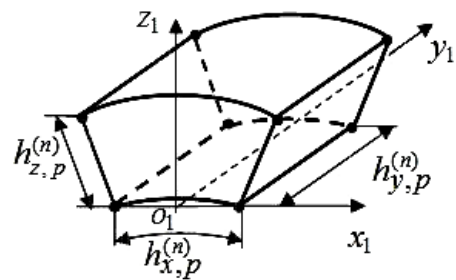
Fig. 3. Single-grid FE $V_{n,p}^{(1)}$

Рис. 3. Односеточный КЭ $V_{n,p}^{(1)}$

The procedures of constructing SGFE and 2GFE for circular cylindrical panels are described in detail in [9]. For 3GFE $V_{e,p}^{(3)}$, $p = 1.2$ we introduce three local coordinate systems: Cartesian $O_3 x_3 y_3 z_3$, curvilinear $O_3 \xi \eta \zeta$, and for nodes of a coarse 3GFE $V_{e,p}^{(3)}$ grid H_3 – integer-valued ijk, where $i, j = 1, ..., 4$, $k = 1, ..., 5$, the nodes of the coarse grid H_3 in fig. 2 are marked by dots, 80 nodes. The special feature of the 3GFE $V_{e,p}^{(3)}$ is that it has a constant thickness h equal to the thickness of the shell, that is, the thickness of the 3GFE $V_{e,p}^{(3)}$ does not change when the partitioning of the discrete model is refined. Herewith, the nodes of the coarse grid H_3 of 3GFE $V_{e,p}^{(3)}$ lie at the boundaries of the multi-modular layers by thickness, fig. 2. The 3GFE $V_{e,p}^{(3)}$ with the characteristic dimensions $h_{x,p}^{(e)} \times h_{y,p}^{(e)} \times h$ has the 3rd order in the coordinates x_3, y_3, and the 4th order in thickness h, that is, in the coordinate z_3 (fig. 2). Note that when calculating the n-layer oval shell n-layer Lagrangian 3GFEs of the n-th order in thickness are used, the order of MGFE in the direction of each of the three coordinates is determined by the order of the corresponding Lagrange polynomial constructed on its coarse nodal grid.

3GFEs $V_{e,1}^{(3)}$, $V_{e,2}^{(3)}$, which differ from each other only in geometric dimensions and physical characteristics and correspond respectively to circular cylindrical panels V_1 and V_2, are designed according to a single algorithm [10; 11], the brief essence of which is as follows. On the coarse grid H_3 of the 3GFE $V_{e,p}^{(3)}$, we determine the functions of displacements $u^{(3)}$, $v^{(3)}$, $w^{(3)}$, which are used to reduce the dimension of the 3GFE $V_{e,p}^{(3)}$. The base function N_{ijk} for a node S with integer coordinates i, j, k of a coarse grid H_3 of the 3GFE $V_{e,p}^{(3)}$ (fig. 2) is represented as [10; 11]

$$N_{ijk}(\alpha, \eta, \zeta) = L_i(\alpha) L_j(\eta) L_k(\zeta), \qquad (2)$$

where α is the central angle corresponding to the arc $h_{x,p}^e$ (fig. 2), $i, j = 1, ..., 4$, $k = 1, ..., 5$, $L_i(\alpha)$, $L_j(\eta)$, $L_k(\zeta)$ are Lagrange polynomials having the form

$$L_i(\alpha) = \prod_{n=1, n \neq i}^{n_1} \frac{\alpha - \alpha_n}{\alpha_i - \alpha_n}, \quad L_j(\eta) = \prod_{n=1, n \neq j}^{n_2} \frac{\eta - \eta_n}{\eta_j - \eta_n},$$

$$L_k(\zeta) = \prod_{n=1, n \neq k}^{n_3} \frac{\zeta - \zeta_n}{\zeta_k - \zeta_n}. \qquad (3)$$

Let the coarse grid node H_3 with coordinates i, j, k ($i, j = 1, ..., 4$, $k = 1, ..., 5$) correspond to an integer β, $\beta = 1, ..., 80$. Using (2), (3), we will present functions of displacements $u^{(3)}$, $v^{(3)}$, $w^{(3)}$ in the form

$$u^{(3)} = \sum_{\beta=1}^{80} N_\beta^{(3)} u_\beta^{(3)}, \quad v^{(3)} = \sum_{\beta=1}^{80} N_\beta^{(3)} v_\beta^{(3)}, \quad w^{(3)} = \sum_{\beta=1}^{80} N_\beta^{(3)} w_\beta^{(3)}, \qquad (4)$$

where $u_\beta^{(3)}$, $v_\beta^{(3)}$, $w_\beta^{(3)}$, $N_\beta^{(3)}$ are displacements and shape functions of β-th node of the H_3 grid

The functional of the total potential energy $\Pi_p^{(3)}$ ($p = 1, 2$) for the 3GFE $V_{e,p}^{(3)}$ is written as

$$\Pi_p^{(3)} = \sum_{m=1}^{M} (\frac{1}{2} (\delta_{m,p}^{(2)})^T \mathbf{K}_{m,p}^{(2)} \delta_{m,p}^{(2)} - (\delta_{m,p}^{(2)})^T \mathbf{P}_{m,p}^{(2)}),$$

$$p = 1, 2, \qquad (5)$$

where $\mathbf{K}_{m,p}^{(2)}$ is the stiffness matrix, $\mathbf{P}_{m,p}^{(2)}$, $\delta_{m,p}^{(2)}$ are the vectors of the nodal forces and displacements of the 2GFE $V_{m,p}^{(2)}$ corresponding to the coordinate system $O_3 x_3 y_3 z_3$, T is the transposition.

Using (4), we express the vector of displacements $\delta_{m,p}^{(2)}$ of 2GFE $V_{m,p}^{(2)}$ through the vector of nodal displacements $\delta_p^{(3)}$ of the coarse grid H_3 of the 3GFE $V_{e,p}^{(3)}$, thus obtaining the relation

$$\delta_{m,p}^{(2)} = \mathbf{A}_{m,p}^{(3)} \delta_p^{(3)}, \qquad (6)$$

where $\mathbf{A}_{m,p}^{(3)}$ is a rectangular matrix, $\delta_p^{(3)} = \{u_\beta^{(3)}, v_\beta^{(3)}, w_\beta^{(3)}\}^T$.

Substituting (6) into (5) and, following the principle of minimum total potential energy $\partial \Pi_p^{(3)} (\delta_p^{(3)}) / \partial \delta_p^{(3)} = 0$, we obtain the relation $\mathbf{K}_p^{(3)} \delta_p^{(3)} = \mathbf{P}_p^{(3)}$, where

$$\mathbf{K}_p^{(3)} = \sum_{m=1}^{M} (\mathbf{A}_{m,p}^{(3)})^T \mathbf{K}_{m,p}^{(2)} \mathbf{A}_{m,p}^{(3)},$$

$$\mathbf{P}_p^{(3)} = \sum_{m=1}^{M} (\mathbf{A}_{m,p}^{(3)})^T \mathbf{P}_{m,p}^{(2)}, \quad p = 1, 2, \qquad (7)$$

where $\mathbf{K}_p^{(3)}$, $\mathbf{P}_p^{(3)}$ is the stiffness matrix and the vector of nodal forces of the 3GFE $V_{e,p}^{(3)}$.

So, 3GFEs $V_{e,p}^{(3)}$ correspond to the circular cylindrical panel V_p, where $p = 1, 2$, $e = 1, ... N_p$, N_p is the total number of 3GFEs $V_{e,p}^{(3)}$, representing the area of the panel V_p.

Remark. The dimension of the vector $\delta_p^{(3)}$ (i. e., the dimension of the 3GFE $V_{e,p}^{(3)}$) does not depend on the total number M of 2GFE $V_{m,p}^{(2)}$ that make the 3GFE $V_{e,p}^{(3)}$. Consequently, the partitioning of the 3GFE $V_{e,p}^{(3)}$ into 2GFEs $V_{m,p}^{(2)}$, and therefore also into SGFE $V_{n,p}^{(1)}$, can be arbitrarily small, which makes it possible to take into ac-

count the complex heterogeneous (micro-inhomogeneous) structure and shape of the circular cylindrical panels V_1 and V_2.

Calculations show that the introduction of additional nodes of polynomials inside the layers allows reducing the error of the SSS values, but it increases the order of the SLAE and increases the estimated time of the problem.

The number of layers of 2GFE may be less than the number of layers of the shell. For example, when constructing a 4-layer 3GFE, one can use 2-layer 2GFE. This reduces the time costs in the calculation of the SSS with an insignificant change in the solution error.

In order to reduce the dimensionality of discrete models of shells, according to the procedure similar to the one discussed above, it is possible to construct 4-grid FE, and k-grid FE, $k \geq 4$. The described method can be used to calculate multi-layer oval cylindrical shells with layers of both equal and different thickness.

Examples of the calculation of 4-layer oval shells of various thickness. Thick-walled shell. In the Cartesian coordinate system $Oxyz$ we consider the solution of the FEM problem of deformation of a 4-layer oval cylindrical shell V^1 of constant thickness $h^1 = 12$ cm with semi-axes $a = 90$ cm; $b = 72$ cm (fig. 1), Oy is an axial coordinate of the shell. The length of the shell is equal to $2L = 1200$ cm. We have: $\dfrac{a}{h^1} = \dfrac{90}{12} = 7.5 < 10$, i. e. the shell V^1 is thick-walled. The thicknesses of the homogeneous isotropic layers of the shell (starting from the inner layer) are equal: $h_1 = h^1 / 12 = 1$ cm, $h_2 = h^1 / 2 = 6$ cm, $h_3 = h^1 / 4 = 3$ cm, $h_4 = h^1 / 6 = 2$ cm, which Young's moduli are equal: $E_1 = 10E$ kg/cm^2, $E_2 = 3E$ kg/cm^2, $E_3 = 5E$ kg/cm^2, $E_4 = 20E$ kg/cm^2, where $E = 10^4$, Poisson's ratio is equal $\nu = 0.3$. For $y = 0$; $2L$, we have $u = v = w = 0$. Pressure $q_0 = 10$ kg/cm^2 is applied to the outer surface of the shell. In the calculations we use 1/8 of the oval shell, which we denote by V_0, of length L. A cylindrical panel V_0 consists of two circular cylindrical panels V_1, V_2 (conjugated along a common lateral bor-

der) of length L with radii (their middle surfaces) R and r (fig. 1) defined by the formula (1).

For the panel V_p we use 5 discrete models $R_{1,p}$, …, $R_{5,p}$, which consist of 3GFE $V_{e,p}^{(3)}$, $p = 1.2$. The base grid of the model $R_{n,p}$ has the dimension $m_n^1 \times m_n^2 \times m_n^3$, where

$$m_n^1 = 162n + 1, \quad m_n^2 = 649n + 1,$$
$$m_n^3 = 24n + 1, \quad n = 1,...,5, \qquad (8)$$

where m_n^1 is the dimension of the grid in the circumferential direction of the panel V_p, m_n^2 – in the axial direction, m_n^3 – in the radial direction. SGFE $V_{n,p}^{(1)}$ has dimensions $h_{x,p}^{(n)} \times h_{y,p}^{(n)} \times h_{z,p}^{(n)}$, fig. 3, where $h_{x,p}^{(n)} = \alpha_{n,p} r_{n,p}$, $r_{n,p}$ is the radius of the lower surface of the SGFE, $\alpha_{n,p} = \alpha_p / m_n^1$, corner angle α_1 (α_2) of the panel V_1 (V_2), according to (1) we have $\operatorname{tg}\alpha_1 = \dfrac{b}{a}$, $\alpha_2 = \dfrac{\pi}{2} - \alpha_1$, $h_{y,p}^{(n)} = L / m_n^2$, $h_{z,p}^{(n)} = h^1 / m_n^3$. The 3GFE $V_{e,p}^{(3)}$ with characteristic dimensions $81 h_{x,p}^{(n)} \times 81 h_{y,p}^{(n)} \times h^1$ consists of Lagrangian 2GFEs $V_{m,p}^{(2)}$ with characteristic dimensions $9 h_{x,p}^{(n)} \times 9 h_{y,p}^{(n)} \times h^1$. In 2GFE and 3GFE, Lagrange polynomials of the form (3) have the third order in the circumferential and axial directions and the fourth order in the radial one. The nodes of the Lagrange polynomials (nodes of the coarse grids of 2GFE and 3GFE) lie on the common boundaries of the multi-modular layers by the shell thickness.

Tab. 1 shows the results of calculations of a cylindrical panel V_0. Characteristic points A (in the plane Oyz) and C (in the plane Oxy) lie at the intersection of the extension of the semi-axes b and a with the outer surface of the shell in cross section $y = L$, in which we define displacements w_n. Equivalent stresses σ_n (in the vicinity of points A, C) are determined by the 4th theory of strength.

Table 1

The results of calculations of a thick oval shell ($a / h = 7.5$; $b / a = 0.8$)

n	$\dfrac{(w_n)_A}{(w_n)_C}$ (mm)	$\begin{array}{c}\delta_{w,n}(\%)_A\\ \delta_{w,n}(\%)_C\end{array}$	$\dfrac{(\sigma_n)_A}{(\sigma_n)_C}$ (kg/cm^2)	$\begin{array}{c}\delta_{\sigma,n}(\%)_A\\ \delta_{\sigma,n}(\%)_C\end{array}$
1	7.511 4.487	–	371.43 144.21	–
2	7.601 4.564	1.181 1.689	377.19 146.87	1.527 1.811
3	7.620 4.580	0.251 0.356	378.37 147.78	0.312 0.616
4	7.627 4.587	0.097 0.142	378.88 148.19	0.135 0.277
5	7.631 4.590	0.051 0.072	379.16 148.41	0.074 0.148

Table 2

The results of calculations of the oval shell for the model R_5 and the ANSYS software package ($b/a = 0.9$)

a/h	$\dfrac{w_A}{w_C}$ (mm)	$\dfrac{w_A^0}{w_C^0}$ (mm)	$\dfrac{\delta_w(\%)_A}{\delta_w(\%)_C}$	$\dfrac{\sigma_A}{\sigma_C}$ (kg/cm^2)	$\dfrac{\sigma_A^0}{\sigma_C^0}$ (kg/cm^2)	$\dfrac{\delta_\sigma(\%)_A}{\delta_\sigma(\%)_C}$
15	12.429 7.942	12.444 7.964	0.12 0.28	544.23 302.74	544.29 301.42	0.01 0.44
30	28.674 19.785	28.678 19.857	0.01 0.36	963.17 768.26	962.45 766.19	0.07 0.27

The relative errors at $n = 2,...,5$ are found by the formulas

$$\delta_{\sigma,n}(\%) = 100\% \times |\sigma_n - \sigma_{n-1}| / \sigma_n,$$

$$\delta_{w,n}(\%) = 100\% \times |w_n - w_{n-1}| / w_n. \qquad (9)$$

The nature of the change $\delta_{w,n}(\%)$, $\delta_{\sigma,n}(\%)$ in values (tab. 1) shows the rapid convergence of stresses σ_n and displacements w_n. Therefore, the values w_5, σ_5 at the points A and C can be taken as exact values with an error of less than 0.15 %. A comparison of the obtained results with the results of the task calculation in the ANSYS software package (SP) was conducted. Values of equivalent stresses and normal displacements, which are obtained using ANSYS SP, are equal to $\sigma_A^0 = 380.05$ kg/cm^2, $\sigma_B^0 = 149.52$ kg/cm^2 and $w_A^0 = -7.655$ mm, $w_B^0 = 4.609$ mm.

The difference in results between the two variants of calculations is less than 0.5 % for displacements and less than 0.8 % for stresses.

The shell is of medium thickness and thin-walled shell. In the global Cartesian coordinate system $Oxyz$, we consider the solution by the FEM of the problem of deforming a 4-layer oval shell V^2 (V^3) with semi-axes $a = 90$ cm; $b = 81$ cm, thickness $h^2 = 6$ cm ($h^3 = 3$ cm) with the same ratios of the layer thicknesses as in the shell V^1 of p. 2.1, Oy is the axial coordinate of the shell V^2 (V^3). The shell V^2 (V^3) has a length of $2L = 1200$ cm, uniform loading $q_0 = 10$ kg/cm^2 on the outer surface and is rigidly fixed on the ends. We have: $\dfrac{a}{h^2} = \dfrac{90}{6} = 15 < 20$, i. e. V^2 is a shell of average thickness, $\dfrac{a}{h^3} = \dfrac{90}{3} = 30 > 20$, which means V^3 is a thin-walled shell. In the calculations we consider 1/8 of the oval shell V^2 (V^3). When constructing solutions using the FEM, we use the previously considered 3GFE (fig. 2) and the grinding law (8). The calculation results are given in tab. 2, where designations are introduced: w_A, w_C, σ_A, σ_C are the displacements and equivalent stresses found at the points A, C (see p. 2.1); w_A^0, w_C^0, σ_A^0, σ_C^0 are displacements and equivalent stresses calculated in points A, C using SP ANSYS.

Relative errors are determined by the formulas

$$(\delta_w(\%))_A = 100\% \times |w_A^0 - w_A| / w_A^0,$$
$$(\delta_\sigma(\%))_A = 100\% \times |\sigma_A^0 - \sigma_A| / \sigma_A^0,$$
$$(\delta_w(\%))_C = 100\% \times |w_C^0 - w_C| / w_C^0,$$
$$(\delta_\sigma(\%))_C = 100\% \times |\sigma_C^0 - \sigma_C| / \sigma_C^0. \qquad (10)$$

The performed calculations show a small error (less than 1%) in the spread of the results obtained using the 3GFE and ANSYS software package for thin, medium and thick 4-layer oval shells.

The dimension of the base model, which is represented by SGFE, is approximately 1.9×10^9 node unknowns, the width of the SLAE tape is 588550. The corresponding three-grid model has 108295 node unknowns, the width of the SLAE tape is 2775. Realizing the FEM reduces the order of SLAE by a factor of 1.76×10^4 and requires 3.73×10^6 times less computer memory capacity than for the base model. The number of 3GFE (160 FE) used for the calculation is approximately 80 times less (depending on the value a/h) than the total amount of FEs ($1.2 \times 10^4 - 1.4 \times 10^4$) used in ANSYS.

An example of the calculation of a 3-layer oval shell of complex shape with local loading. In the Cartesian coordinate system $Oxyz$ we consider the problem of deforming a 3-layer oval cylindrical shell with semi-axes $a = 90$ cm, $b = 63$ cm, thickness $h = 3$ cm, Oy is the axial coordinate of the shell. The length of the shell is $2L = 400$ cm. At $y = 0$; $2L$ the ends of the shell are clamped. All isotropic homogeneous layers of the shell have thickness of $h/3$. The Young's moduli of the layers (starting from the inner) are: $E_1 = 6E$ kg/cm^2, $E_2 = 2E$ kg/cm^2, $E_3 = 10E$ kg/cm^2, where $E = 10^4$, the Poisson's ratio for all layers is $\nu = 0.3$. The form, loading and fixing of the shell are symmetrical with respect to the Oyz and $y = L$ planes, therefore in calculations we use 1/4 of the shell, which we denote: panel V^4, fig. 4 shows its median surface. A panel area V^4 of length L consists of two circular cylindrical panels V_3 and V^4 (of length L), respectively, with corner angles $\alpha = 35^0$; $\gamma = 55^0$. The panel V^4 has two holes (rectangular in plan) with dimensions $1 = L/6$, $S_1 = r\gamma/2$ (fig. 4). On the outer surface of the panel V_3 in the local area of dimensions $L/3 \le y \le 2L/3$, $S_2 = R\alpha$, pressure

$q_0 = -1$ kg/cm^2 is applied, as shown in fig. 4. When calculating a cylindrical panel V^4, we use a three-layer 3GFE with parameters, which were introduced earlier, and discrete models R_n ($n = 1,...,5$), for which the grids of basic partitions R_n^0 have the dimension

$$m_n^1 = 324n + 1, \ m_n^2 = 486n + 1,$$
$$m_n^3 = 6n + 1, \ n = 1,...,5. \tag{11}$$

Tab. 3 shows the calculation results for the models R_n, $n = 1,...,5$. Values w_5, σ_5 for the model R_5, defined in points A, C (fig. 4, 5), can be taken as accurate values with an error of less than 0.2% for displacements and less than 0.1% for stresses. The values of equivalent stresses σ^0 and normal displacements w^0 obtained in ANSYS are $\sigma_A^0 = 75.16$ kg/cm^2, $\sigma_C^0 = 43.52$ kg/cm^2 and $w_A^0 = -6.210$ mm, $w_C^0 = 2.534$ mm. The difference

in the results of the two calculations is less than 0.3% for displacements and less than 0.6 % for stresses.
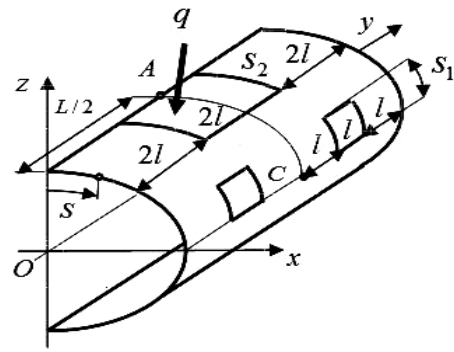
Fig. 4. Design scheme for 1/4 of the shell, panel V^4

Рис. 4. Расчетная схема 1/4 части оболочки, панель V^4

Table 3

The results of calculations of a thin oval shell with holes ($a / h = 30$; $b / a = 0.9$)

R_n	$\dfrac{(w_n)_A}{(w_n)_C}$ (mm)	$\begin{array}{c}\delta_{w,n}(\%)_A\\\delta_{w,n}(\%)_C\end{array}$	$\dfrac{(\sigma_n)_A}{(\sigma_n)_C}$ (kg/cm^2)	$\begin{array}{c}\delta_{\sigma,n}(\%)_A\\\delta_{\sigma,n}(\%)_C\end{array}$
R_1	−6.041 2.390	− 	78.21 39.92	−
R_2	−6.155 2.491	1.852 4.055	74.57 42.88	4.881 6.903
R_3	−6.182 2.513	0.437 0.875	74,91 43.13	0.454 0.580
R_4	−6.193 2.522	0.178 0.357	75.05 43.23	0.187 0.231
R_5	−6.198 2.527	0.081 0.198	75.12 43.26	0.093 0.069

a

b
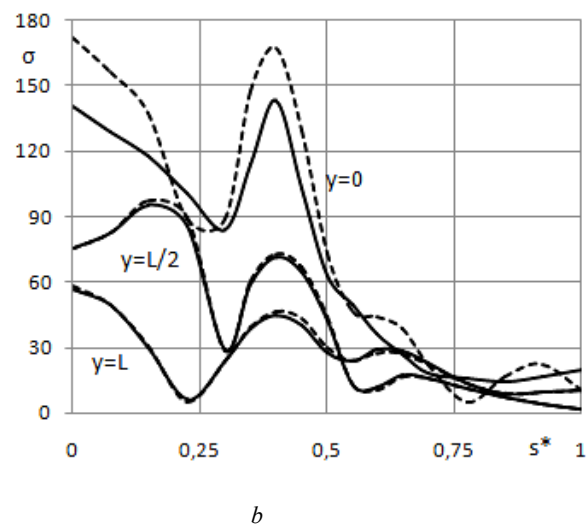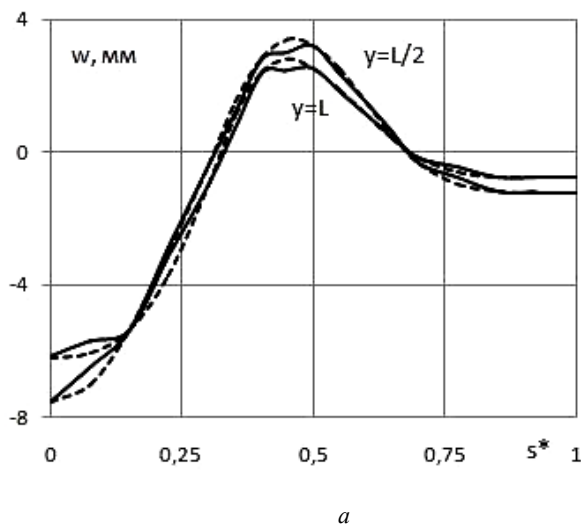
Fig. 5. Distribution of deflections w (*a*) and of stress σ (*b*) over the upper shell surface in cross-sections: $y = 0$; $L/2$; L. Three-grid FE – solid line; SP ANSYS – dashed line

Рис. 5. Распределение прогибов w (*a*) и напряжений σ (*b*) по верхней поверхности оболочки в поперечных сечениях: $y = 0$; $L/2$; L. ТрКЭ – сплошная линия; ПК ANSYS – штриховая линия

Fig. 5 shows the distribution of displacements ($w = w_5$) in sections $y = L / 2$; L and stresses ($\sigma = \sigma_5$) in sections $y = 0$; $L / 2$; L on the outer surface of the shell, depending on the parameter $s^* = s / P$; s, P is the distance from the axis Oz to the point on the outer surface of the shell and to the point C (fig. 4). The SSS calculation was fulfilled using the 3GFE (full line) and using ANSYS (dashed line).

A noticeable discrepancy in the stress distribution is observed only in the clamping area. In the rest of the complex shell structure, one can observe an acceptable in engineering calculations coincidence of the SSS, obtained by means of 3GFE and ANSYS SP.

The FEM implementation for the multigrid model R_5 reduces the order of the SLAE solved by 5625 times and requires 3.88×10^5 times less computer memory than for the basic model R_5^0, which uses only SGFE. The number of 3GFE used for calculation in a discrete model R_5 (240 FE) is approximately 300 times less than the number of FE used for calculation in ANSYS (73892 FE).

Thus, the use of 3GFE in the analysis of SSS allows saving computer resources significantly, which greatly expands the possibilities of FEM in a variant of multigrid modeling.

Conclusion. The high efficiency of using curvilinear Lagrangian MGFE in the analysis of three-dimensional SSS of multilayer oval cylindrical shells is shown. The implementation of the FEM using MGFE requires $10^2 - 10^6$ times less computer memory than with the use of SGFE or ANSYS SP, and allows analysis of the SSS of shells with a small error of results.

References

1. Noor A. K., Burton W. S. Assessment of computational models for multilayered composite shells. *Applied Mechanics Reviews*. 1990, Vol. 43, P. 67–97.

2. Reddy J. N. Mechanics of laminated composite plates and shells: theory and analysis. 2004, CRC Press, 858 p.

3. Zienkiewicz O. C., Taylor R. L., Zhu J. Z. The finite element method: its basis and fundamentals. Oxford: Elsevier Butterworth-Heinemann, 2013, 715 p.

4. Norrie D. H., de Vries G. *Vvedenie v metod konechnykh elementov* [An introduction to finite element analysis]. Moscow, Mir Publ., 1981, 304 p

5. Golovanov A. I., Tyuleneva O. I., Shigabutdinov A. F. *Metod konechnykh elementov v statike i dinamike tonkostennykh konstruktsiy* [Finite element method in statics and dynamics of thin-wall constructions]. Moscow, Fizmatlit Publ., 2006, 392 p.

6. Bate K., Wilson E. *Chislennye metody analiza i metod konechnykh elementov* [Numerical methods in finite element analysis]. Moscow, Stroyizdat Publ., 1982, 448 p.

7. Obraztsov I. F., Savelyev L. M., Khazanov Kh. S. *Metod konechnykh elementov v zadachakh stroitelnoy mekhaniki letatelnykh apparatov* [Finite element method

in aircraft structural mechanics problems]. Moscow, Vysshaya shkola Publ., 1985, 392 p.

8. Sekulovich M. *Metod konechnyh ehlementov* [Finite element method]. Moscow, Stroyizdat Publ., 1993, 664 p.

9. Matveev A. D., Grishanov A. N. [Single and double grid curvilinear elements of three-dimensional cylindrical plates and shells]. *Izvestiya AltGU.* 2014, No. 1/1, P. 84–94 (In Russ.).

10. Matveev A. D., Grishanov A. N. [Multi-grid Lagrange curvilinear elements in three-dimensional analysis of composite cylindrical plates and shells]. *Vestnik KrasGAU.* 2015, No. 1, P. 75–85 (In Russ.).

11. Matveev A. D., Grishanov A. N. [Three-dimensional composite multigrid finite elements of shell type]. *Izvestiya AltGU.* 2017, No. 4, P. 120–125 (In Russ.).

12. Kulikov G. M. Plotnikova C. V. [Solution of the problem of statics for an elastic shell in a spatial statement]. *Doklady RAN.* 2011, Vol. 439, No. 5, P. 613–616 (In Russ.).

13. Kulikov G. M. Plotnikova C. V. [Solution of three-dimensional problems for thick elastic shells based on the method of reference surfaces]. *Mekhanika tverdogo tela.* 2014, No. 4, P. 54–64 (In Russ.).

14. Kulikov G. M., Plotnikova S. V. On the use of a new concept of sampling surfaces in shell theory. *Advanced Structured Materials.* 2011, Vol. 15, P. 715–726.

15. Kulikov G. M., Plotnikova S. V. [Calculation of composite constructions under tracking load using geometrically accurate shell element]. *Mekhanika kompozitnykh materialov.* 2009, Vol. 45, No. 6, P. 789–804 (In Russ.).

16. Zheleznov L. P., Kabanov V. V., Boyko D. V. [Nonlinear deformation and stability of oval cylindric shells under pure bending and internal pressure]. *Prikladnaya mekhanika i tekhnicheskaya fizika.* 2006, Vol. 47, No. 3, P. 119–125 (In Russ.).

Библиографические ссылки

1. Noor A. K., Burton W. S. Assessment of computational models for multilayered composite shells // Applied Mechanics Reviews. 1990. Vol. 43. P. 67–97.

2. Reddy J. N. Mechanics of laminated composite plates and shells: theory and analysis. CRC Press, 2004. 858 p.

3. Zienkiewicz O. C., Taylor R. L., Zhu J. Z. The finite element method: its basis and fundamentals. Oxford: Elsevier Butterworth-Heinemann, 2013. 715 p.

4. Норри Д., де Фриз Ж. Введение в метод конечных элементов. М. : Мир, 1981. 304 с.

5. Голованов А. И., Тюленева О. И., Шигабутдинов А. Ф. Метод конечных элементов в статике и динамике тонкостенных конструкций. М. : Физматлит, 2006. 392 с.

6. Бате К., Вилсон Е. Численные методы анализа и метод конечных элементов. М. : Стройиздат, 1982. 448 с.

7. Образцов И. Ф., Савельев Л. М., Хазанов Х. С. Метод конечных элементов в задачах строительной

механики летательных аппаратов. М. : Высшая школа, 1985. 392 с.

8. Секулович М. Метод конечных элементов. М. : Стройиздат, 1993. 664 с.

9. Матвеев А. Д., Гришанов А. Н. Одно- и двухсеточные криволинейные элементы трехмерных цилиндрических панелей и оболочек // Известия АлтГУ. 2014. № 1/1. С. 84–94.

10. Матвеев А. Д., Гришанов А. Н. Многосеточные лагранжевые криволинейные элементы в трехмерном анализе композитных цилиндрических панелей и оболочек // Вестник КрасГАУ. 2015. № 2. С. 75–85.

11. Матвеев А. Д., Гришанов А. Н. Трехмерные композитные многосеточные конечные элементы оболочечного типа // Известия АлтГУ. 2017. № 4. С. 120–125.

12. Куликов Г. М., Плотникова С. В. Решение задачи статики для упругой оболочки в пространственной постановке // Доклады РАН. 2011. Т. 439, № 5. С. 613–616.

13. Куликов Г. М., Плотникова С. В. Решение трехмерных задач для толстых упругих оболочек на основе метода отсчетных поверхностей // Механика твердого тела. 2014. № 4. С. 54–64.

14. Kulikov G. M., Plotnikova S.V. On the use of a new concept of sampling surfaces in shell theory // Advanced Structured Materials. 2011. Vol. 15. P. 715–726.

15. Куликов Г. М., Плотникова С. В. Расчет композитных конструкций под действием следящих нагрузок с использованием геометрически точного элемента оболочки // Механика композитных материалов. 2009. Т. 45, № 6. С. 789–804.

16. Железнов Л. П., Кабанов В. В., Бойко Д. В. Нелинейное деформирование и устойчивость овальных цилиндрических оболочек при чистом изгибе с внутренним давлением // Прикладная механика и техническая физика. 2006. Т. 47, № 3. С. 119–125.

Pustovoi Nikolai Vasilevich – Dr. Sc., Professor; Novosibirsk State Technical University. E-mail: pla@craft.nstu.ru.

Grishanov Aleksandr Nikolaevich – applicant of the Department of aircraft strength; Novosibirsk State Technical University. E-mail:a_grishanov@ngs.ru.

Matveev Aleksandr Danilovich – Cand. Sc., senior researcher; Institute of computational modeling SB RAS. E-mail: mtv241@mail.ru.

Пустовой Николай Васильевич – доктор технических наук, профессор кафедры прочности летательных аппаратов; Новосибирский государственный технический университет. E-mail: pla@craft.nstu.ru.

Гришанов Александр Николаевич – соискатель кафедры прочности летательных аппаратов; Новосибирский государственный технический университет. E-mail: a_grishanov@ngs.ru.

Матвеев Александр Данилович – кандидат физико-математических наук, доцент, старший научный сотрудник; Институт вычислительного моделирования СО РАН. E-mail: mtv241@mail.ru.

STRICT AVALANCHE CRITERION OF FOUR-VALUED FUNCTIONS AS THE QUALITY CHARACTERISTIC OF CRYPTOGRAPHIC ALGORITHMS STRENGTH

A. V. Sokolov[1], O. N. Zhdanov[2]

[1]Odessa National Polytechnic University
1, Shevchenko Av., Odessa, 65044, Ukraine
[2]Reshetnev Siberian State University of Science and Technology
31, Krasnoyarsky Rabochy Av., Krasnoyarsk, 660037, Russian Federation
E-mail: onzhdanov@mail.ru

The S-box is the most important component of modern cryptographic algorithms which largely determines the quality of cryptographic transformation. The modern method of estimating the S-boxes quality employs their representation as component Boolean functions to which cryptographic quality criteria are applied. Such criteria include: nonlinearity, correlation immunity, an error propagation criterion, and a strict avalanche criterion. Nevertheless, it is obvious that a cryptanalyst is not constrained in the ways of representing the cipher components, in particular, using the functions of many-valued logic. The design features of modern cryptographic algorithms allow their representation in the form of 4-logic functions, which determines the need to research cryptographic properties of the S-boxes represented as component 4-functions. In the literature today there are methods for measuring the nonlinearity of 4-functions; nevertheless, there are no similar methods for researching the differential properties of 4-functions, in particular, involving their compliance with the strict avalanche criterion. In this paper the strict avalanche criterion is generalized to the case of 4-functions and the compliance of the S-boxes component 4-functions of the "Magma" cryptoalgorithm to the strict avalanche criterion has been researched. All balanced 4-functions of length N = 16 satisfying the strict avalanche criterion were synthesized using the restricted brute-force method. The basic properties of the constructed class of 4-functions are determined, and bijective S-boxes based on them are constructed. It has been established that S-boxes of length N = 16 satisfying the strict avalanche criterion, both in terms of component Boolean functions and in terms of 4-functions, also possess optimal nonlinear properties. This circumstance allows us to recommend S-boxes satisfying the strict avalanche criterion of component 4-functions for use in modern cryptographic algorithms.

Keywords: many-valued logic functions, strict avalanche criterion, S-box.

СТРОГИЙ ЛАВИННЫЙ КРИТЕРИЙ ФУНКЦИЙ ЧЕТЫРЕХЗНАЧНОЙ ЛОГИКИ КАК ХАРАКТЕРИСТИКА СТОЙКОСТИ КРИПТОАЛГОРИТМОВ

А. В. Соколов[1], О. Н. Жданов[2]

[1]Одесский национальный политехнический университет
Украина, 65044, г. Одесса, просп. Шевченко, 1
[2]Сибирский государственный университет науки и технологий имени академика М. Ф. Решетнева
Российская Федерация, 660037, г. Красноярск, просп. им. газ. «Красноярский рабочий», 31
E-mail: onzhdanov@mail.ru

Важнейшим компонентом современных криптографических алгоритмов, который во многом определяет качество криптопреобразования, является S-блок. Современная методика оценки качества S-блоков предполагает их представление в виде компонентных булевых функций, к которым применяются критерии криптографического качества, такие как нелинейность, критерий распространения ошибки, строгий лавинный критерий, корреляционный иммунитет. Тем не менее очевидным является тот факт, что криптоаналитик не стеснен в способах представления компонент шифра, в частности и с помощью функций многозначной логики. Конструктивные особенности современных криптоалгоритмов допускают их представление в виде функций 4-логики, что диктует необходимость исследования криптографических свойств S-блоков, представленных

в виде компонентных 4-функций. В литературе сегодня имеются методы измерения нелинейности 4-функций, тем не менее отсутствуют подобные методы для изучения дифференциальных свойств 4-функций, в частности, их соответствия строгому лавинному критерию. В настоящей статье строгий лавинный критерий обобщен на случай 4-функций, проведены исследования соответствия строгому лавинному критерию компонентных 4-функций S-блоков криптоалгоритма «Магма». Методом ограниченного перебора синтезированы все сбалансированные 4-функции длины N = 16, удовлетворяющие строгому лавинному критерию. Определены базовые свойства построенного класса 4-функций, а также построены биективные S-блоки на их основе. Установлено, что S-блоки длины N = 16, удовлетворяющие строгому лавинному критерию как с точки зрения компонентных булевых функций, так и с точки зрения 4-функций, обладают также оптимальными нелинейными свойствами. Данное обстоятельство позволяет рекомендовать S-блоки, удовлетворяющие строгому лавинному критерию компонентных 4-функций, к использованию в современных криптоалгоритмах.

Ключевые слова: функции многозначной логики, строгий лавинный критерий, S-блок.

Introduction and problem formulation. The problem of further improvement of modern cryptographic information protection systems is closely related to the tasks of constructing higher quality cryptographic primitives. In many ways the strength of a symmetric cryptographic algorithm is determined by a substitution box (*S*-box) [1].

Currently, the quality of *S*-boxes is determined by the following main criteria for cryptographic quality [2]:

1. The algebraic degree of nonlinearity.

2. The distance of nonlinearity.

3. The error propagation criterion, a particular case of which is the strict avalanche criterion (SAC), as well as the criterion of maximum avalanche effect.

4. The matrix of the correlation coefficients of the S-box output and input, as well as the associated criterion of the component Boolean functions correlation immunity.

All of these criteria are based on the representation of the *S*-box as a set of Boolean functions. However, other mathematical constructions describing a cryptoalgorithm, in particular, the apparatus of many-valued logic functions can be used to launch an attack.

This circumstance requires the research of all possible forms of *S*-boxes representation, in particular, using the component functions of many-valued logic.

The cryptoalgorithms used in practice often have S-boxes of length N multiple of 4, for example, $N = 16$ as in the "Magma" cryptoalgorithm [3] or $N = 256$ as in the Nyberg S-boxes [4; 5] in the AES cryptoalgorithm [6]. Thus, the research of the cryptographic quality of S-boxes represented as component 4-functions is of practical value.

The 4-nonlinearity criterion for S-boxes was introduced and a method for synthesizing S-boxes with a maximum 4-nonlinearity value was proposed in [7] on the basis of the Vilenkin–Chrestenson transformation. However, at present in the literature there is no definition of the strict avalanche criterion as applied to the representation of S-boxes as 4-logic functions.

This paper is devoted to the research of the strict avalanche criterion of 4-functions, as well as the synthesis of S-boxes whose component 4-functions satisfy the strict avalanche criterion.

The propagation criterion of the Boolean functions. The strict avalanche criterion is one of the main criteria which characterize resistance to differential cryptanalysis [8]. Methods for the synthesis of S-boxes that satisfy the strict avalanche criterion are practically in demand, and well-known [8–10].

The research of the Boolean function compliance with the strict avalanche criterion is based on the following definitions.

Definition 1 [11]. A derivative in the direction $u \in V_n$ of the Boolean function f is the Boolean function

$$D_u f(x) = f(x) \oplus f(x \oplus u), \qquad (1)$$

where V_n is the linear vector space of binary vectors of length n, $\oplus$ is the modulo 2 addition.

Definition 2 [11]. The Boolean function $f(x)$ satisfies the propagation criterion with respect to the vector $u \in V_n - PC(u)$ if its derivative in the direction u is a balanced function, i. e.

$$p\{f(x) = f(x \oplus u)\} = 0,5. \qquad (2)$$

Definition 3 [11]. The Boolean function $f(x)$ satisfies the propagation criterion of the degree $k - PC(k)$ if it satisfies the propagation criterion $PC(u)$ with respect to all vectors u of weight $1 \le wt(u) \le k$, i. e.

$$p\{f(x) = f(x \oplus u)\} = 0.5, \quad \forall u \in V_n, \quad 1 \le wt(u) \le k. \quad (3)$$

Definition 4 [11]. The Boolean function f satisfies the strict avalanche criterion (SAC) if it satisfies the propagation criterion of the degree $1 - PC(1)$

$$p\{f(x) = f(x \oplus u)\} = 0.5, \quad \forall u \in V_n, \quad wt(u) = 1. \quad (4)$$

Let us consider the S-box synthesized in [10] and its decomposition into component Boolean functions

$$S = \begin{cases} 4 & 7 & 2 & 14 & 1 & 13 & 8 & 11 & 15 & 12 & 6 & 10 & 5 & 9 & 3 & 0 \\ 0 & 1 & 0 & 0 & 1 & 1 & 0 & 1 & 1 & 0 & 0 & 0 & 1 & 1 & 1 & 0 \\ 0 & 1 & 1 & 1 & 0 & 0 & 0 & 1 & 1 & 0 & 1 & 1 & 0 & 0 & 1 & 0 \\ 1 & 1 & 0 & 1 & 0 & 1 & 0 & 0 & 1 & 1 & 1 & 0 & 1 & 0 & 0 & 0 \\ 0 & 0 & 0 & 1 & 0 & 1 & 1 & 1 & 1 & 1 & 0 & 1 & 0 & 1 & 0 & 0 \end{cases}.$$

$$(5)$$

Let us give an example of researching the Boolean function of four variables which is the first component function of the S-box (5) on compliance with the strict avalanche criterion

$$f(x_1, x_2, x_3, x_4) =$$
$$= \{0 \ 1 \ 0 \ 0 \ 1 \ 1 \ 0 \ 1 \ 1 \ 0 \ 0 \ 0 \ 1 \ 1 \ 1 \ 0\}. \quad (6)$$

Example of finding derivatives of the Boolean function

$f(X)$	$f(X \oplus 0001)$	$D_{0001}f$	$f(X \oplus 0010)$	$D_{0010}f$	$f(X \oplus 0100)$	$D_{0100}f$	$f(X \oplus 1000)$	$D_{1000}f$
$f(0000)=0$	$f(0001)=1$	1	$f(0010)=0$	0	$f(0100)=1$	1	$f(1000)=1$	1
$f(0001)=1$	$f(0000)=0$	1	$f(0011)=0$	1	$f(0101)=1$	0	$f(1001)=0$	1
$f(0010)=0$	$f(0011)=0$	0	$f(0000)=0$	0	$f(0110)=0$	0	$f(1010)=0$	0
$f(0011)=0$	$f(0010)=0$	0	$f(0001)=1$	1	$f(0111)=1$	1	$f(1011)=0$	0
$f(0100)=1$	$f(0101)=1$	0	$f(0110)=0$	1	$f(0000)=0$	1	$f(1100)=1$	0
$f(0101)=1$	$f(0100)=1$	0	$f(0111)=1$	0	$f(0001)=1$	0	$f(1101)=1$	0
$f(0110)=0$	$f(0111)=1$	1	$f(0100)=1$	1	$f(0010)=0$	0	$f(1110)=1$	1
$f(0111)=1$	$f(0110)=0$	1	$f(0101)=1$	0	$f(0011)=0$	1	$f(1111)=0$	1
$f(1000)=1$	$f(1001)=0$	1	$f(1010)=0$	1	$f(1100)=1$	0	$f(0000)=0$	1
$f(1001)=0$	$f(1000)=1$	1	$f(1011)=0$	0	$f(1101)=1$	1	$f(0001)=1$	1
$f(1010)=0$	$f(1011)=0$	0	$f(1000)=1$	1	$f(1110)=1$	1	$f(0010)=0$	0
$f(1011)=0$	$f(1010)=0$	0	$f(1001)=0$	0	$f(1111)=0$	0	$f(0011)=0$	0
$f(1100)=1$	$f(1101)=1$	0	$f(1110)=1$	0	$f(1000)=1$	0	$f(0100)=1$	0
$f(1101)=1$	$f(1100)=1$	0	$f(1111)=0$	1	$f(1001)=0$	1	$f(0101)=1$	0
$f(1110)=1$	$f(1111)=0$	1	$f(1100)=1$	0	$f(1010)=0$	1	$f(0110)=0$	1
$f(1111)=0$	$f(1110)=1$	1	$f(1101)=1$	1	$f(1011)=0$	0	$f(0111)=1$	1

To do this, in accordance with *Definition 3* and *Definition 4*, we need to find the derivatives of the Boolean function (6) in all directions of the Hamming weight $wt(u)=1$, i.e. in directions $\{001\}$, $\{010\}$ and $\{001\}$. The results are shown in tab. 1.

The presented results lead to the conclusion: all derivatives $D_i f$ are balanced, i.e. $wt(D_i f) = N/2$, where N is the length of the truth table of the Boolean function. Thus, the Boolean function (6) satisfies the SAC.

Extension of the strict avalanche criterion to the case of 4-functions. However, in the case of attacking the cryptographic algorithm a cryptanalyst is not constrained by the means used and can use the approximation of cipher elements by any available means including methods of many-valued logic as it is shown in research carried out in [12]. Thus, when constructing S-boxes it makes sense to consider not only binary affine functions, but also affine functions of many-valued logic through which the S-box of a given size can be represented.

Definition 5 [13]. The mapping $\{0,1,2,...,q-1\}^n \to \{0,1,2,...,q-1\}$ is called the function of the q-valued logic of n variables.

Definition 5 is the definition of Boolean functions when $q=2$. *Definition 5* is the definition of 4-functions as mappings $\{0,1,2,3\}^k \to \{0,1,2,3\}$ when $q=4$. Thus, a 4-function is a rule that uniquely associates the vector of k coordinates that take values 0, 1, 2, 3 with a value of 0, 1, 2 or 3.

For example, the *S*-box (5) can be represented using two component 4-functions

$$S = \left\{ \begin{array}{cccccccccccccccc} 4 & 7 & 2 & 14 & 1 & 13 & 8 & 11 & 15 & 12 & 6 & 10 & 5 & 9 & 3 & 0 \\ \hline 0 & 3 & 2 & 2 & 1 & 1 & 0 & 3 & 3 & 0 & 2 & 2 & 1 & 1 & 3 & 0 \\ 1 & 1 & 0 & 3 & 0 & 3 & 2 & 2 & 3 & 3 & 1 & 2 & 1 & 2 & 0 & 0 \end{array} \right\},$$
(7)

the cryptographic properties of which also determine the properties of the S-box itself but at the level of quaternary logic.

We propose a general scheme for which the Boolean function and 4-function will be special cases.

Let us consider the q-function of n variables $f(x)$. Let $u = (u_1, u_2, ..., u_n)$.

Definition 6. The weight $\varpi(u)$ of a q-valued vector is the number of its nonzero components.

Definition 7. The derivative of the function f with respect to the direction of the vector u is the function

$$D_u f(x) = f(x \underset{q}{\oplus} u) - f(x) \pmod{q} ,$$
(8)

where $\underset{q}{\oplus}$ means the modulo q addition.

Definition 8. The function of q-valued logic $f(x)$ satisfies the propagation criterion with respect to the vector $u \in V_n - PC(u)$ if its derivative in the direction u is a balanced function, i. e. values $0,1,...,q-1$ are taken with equal probabilities: $p(D_u f(x) = i \pmod{q}) = \dfrac{1}{q}$ for all $i = 0,1,...,q-1$. In other words, $K^0 = K^1 = ... = K^{q-1}$, where K^i is the number of sets of variable values for which the derivative takes the value i.

Definition 9. The function of q-valued logic $f(x)$ satisfies the propagation criterion of degree $k - PC(k)$ if it satisfies the propagation criterion $PC(u)$ with respect to all vectors u of weight $1 \le \varpi(u) \le k$.

Definition 10. The function of q-valued logic $f(x)$ satisfies the strict avalanche criterion (SAC) if it satisfies the propagation criterion of degree $1 - PC(1)$.

In accordance with the definitions introduced, we consider the example of researching the first

4-function of the *S*-box (7) for compliance with the strict avalanche criterion.

Data analysis in tab. 2 allows us to say that the first component 4-function of the *S*-box (7) does not satisfy the strict avalanche criterion. Thus*, being optimal in terms of the strict avalanche criterion in a binary sense, the S-box (7) is not optimal in terms of the strict avalanche criterion in a quaternary sense.*

We illustrate our reasoning with examples of well-known cryptoalgorithms.

Research of *S*-boxes of the "Magma" cryptographic algorithm. The approach in which *S*-boxes were considered as a long-term key was used in the common GOST 28147–89 cryptoalgorithm. In the new edition of the standard GOST R 34.12–2015 the following set of *S*-boxes was defined [3]

$$S = \begin{bmatrix}
12 & 4 & 6 & 2 & 10 & 5 & 11 & 9 & 14 & 8 & 13 & 7 & 0 & 3 & 15 & 1 \\
6 & 8 & 2 & 3 & 9 & 10 & 5 & 12 & 1 & 14 & 4 & 7 & 11 & 13 & 0 & 15 \\
11 & 3 & 5 & 8 & 2 & 15 & 10 & 13 & 14 & 1 & 7 & 4 & 12 & 9 & 6 & 0 \\
12 & 8 & 2 & 1 & 13 & 4 & 15 & 6 & 7 & 0 & 10 & 5 & 3 & 14 & 9 & 11 \\
7 & 15 & 5 & 10 & 8 & 1 & 6 & 13 & 0 & 9 & 3 & 14 & 11 & 4 & 2 & 12 \\
5 & 13 & 15 & 6 & 9 & 2 & 12 & 10 & 11 & 7 & 8 & 1 & 4 & 3 & 14 & 0 \\
8 & 14 & 2 & 5 & 6 & 9 & 1 & 12 & 15 & 4 & 11 & 0 & 13 & 10 & 3 & 7 \\
1 & 7 & 14 & 13 & 0 & 5 & 8 & 3 & 4 & 15 & 10 & 6 & 9 & 12 & 11 & 2
\end{bmatrix}.$$

$$(9)$$

Tab. 3 shows the values of the basic criteria for the cryptographic quality of *S*-boxes (9).

The data analysis in tab. 3 dictates the need for further improvement of the substitution constructions of the cryptoalgorithm "Magma" and similar ones.

Table 2

Example of finding the derivative of 4-function

$f(X)$	$u=01$	$D_{01}f$	$u=02$	$D_{02}f$	$u=03$	$D_{03}f$	$u=10$	$D_{10}f$	$u=20$	$D_{20}f$	$u=30$	$D_{30}f$
$f(00)=0$	3	3	2	2	2	2	1	1	3	3	1	1
$f(01)=3$	2	3	2	3	0	1	1	2	0	1	1	2
$f(02)=2$	2	0	0	2	3	1	0	2	2	0	3	1
$f(03)=2$	0	2	3	1	2	0	3	1	2	0	0	2
$f(10)=1$	1	0	0	3	3	2	3	2	1	0	0	3
$f(11)=1$	0	3	3	2	1	0	0	3	1	0	3	2
$f(12)=0$	3	3	1	1	1	1	2	2	3	3	2	2
$f(13)=3$	1	2	1	2	0	1	2	3	0	1	2	3
$f(20)=3$	0	1	2	3	2	3	1	2	0	1	1	2
$f(21)=0$	2	2	2	2	3	3	1	1	3	3	1	1
$f(22)=2$	2	0	3	1	0	2	3	1	2	0	0	2
$f(23)=2$	3	1	0	2	2	0	0	2	2	0	3	1
$f(30)=1$	1	0	3	2	0	3	0	3	1	0	3	2
$f(31)=1$	3	2	0	3	1	0	3	2	1	0	0	3
$f(32)=3$	0	1	1	2	1	2	2	3	0	1	2	3
$f(33)=0$	1	1	1	1	3	3	2	2	3	3	2	2

Table 3

The values of the main criteria for the cryptographic quality of the "Magma" cryptoalgorithm *S*-boxes

S-box	Algebraic degree of nonlinearity $\deg(S)$	Nonlinearity distance *SNl*	Maximum absolute values of the matrix of correlation coefficients $\max_{i,j}\{|c_{i,j}|\}$	Compliance with the SAC in a binary sense	Compliance with the SAC in a quaternary sense
S_1	2	4	0.5	–	–
S_2	2	4	0.5	–	–
S_3	3	4	0.5	–	–
S_4	3	4	0.25	–	–
S_5	2	4	0.5	–	–
S_6	3	4	0.5	–	–
S_7	2	4	0.5	–	–
S_8	3	4	0.5	–	–

Experimental search for S-boxes satisfying SAC in a quaternary sense. The problem of finding S-boxes that satisfy the SAC in a quaternary sense is important from a practical point of view. Nevertheless, we note that even the search for 4-functions of length $N = 16$ (that is, the smallest of those having practical sense) satisfying the SAC in a quaternary sense is associated with considerable computational difficulties because the number of 4-functions of this length is 4 294 967 296.

However, it is known that the construction of bijective S-boxes is possible only on the basis of balanced 4-functions [14].

Obviously, the total number of balanced 4-functions of length $N = 16$ is $J = C_{16}^4 \cdot C_{12}^4 \cdot C_8^4 \cdot C_4^4 = 1820 \cdot 495 \cdot 70 \cdot 1 = 63\,063\,000$, which is significantly less than the total number of 4-functions of length $N = 16$.

We experimentally (by exhaustive search of all variants) established that in a given volume of balanced 4-functions there are 7680 functions satisfying the SAC in a quaternary sense.

Direct verification established the properties of the functions of this set.

Definition 11. Let us call a new sequence $T_2 = \{t_j\}$, $j = N-1, N-2, \ldots, 0$ a mirror image of the sequence $T1 = \{t_i\}$, $i = 0, 1, \ldots, N-1$.

Property 1. The sequence obtained as a result of mirroring a balanced sequence satisfying the SAC in a quaternary sense also satisfies the SAC in a quaternary sense.

For example, let us consider one of the 4-functions satisfying SAC in a quaternary sense

$$f_0 = \{0001023212312133\}. \tag{10}$$

Performing its mirroring we obtain a new 4-function, which also satisfies the SAC in a quaternary sense

$$f_1 = \{3312132123201000\}. \tag{11}$$

Property 2. Sequences obtained by applying the following 8 of the 24 possible single-valued mappings of the alphabet of the sequence satisfying the SAC in a quaternary sense also satisfies the SAC in a quaternary sense

$$\begin{Bmatrix} 0 & 1 & 2 & 3 \\ 0 & 1 & 2 & 3 \end{Bmatrix}; \quad \begin{Bmatrix} 0 & 1 & 2 & 3 \\ 0 & 3 & 2 & 1 \end{Bmatrix}; \quad \begin{Bmatrix} 0 & 1 & 2 & 3 \\ 1 & 0 & 3 & 2 \end{Bmatrix};$$

$$\begin{Bmatrix} 0 & 1 & 2 & 3 \\ 1 & 2 & 3 & 0 \end{Bmatrix}; \quad \begin{Bmatrix} 0 & 1 & 2 & 3 \\ 2 & 1 & 0 & 3 \end{Bmatrix}; \quad \begin{Bmatrix} 0 & 1 & 2 & 3 \\ 2 & 3 & 0 & 1 \end{Bmatrix}; \tag{12}$$

$$\begin{Bmatrix} 0 & 1 & 2 & 3 \\ 3 & 0 & 1 & 2 \end{Bmatrix}; \quad \begin{Bmatrix} 0 & 1 & 2 & 3 \\ 3 & 2 & 1 & 0 \end{Bmatrix}.$$

Let us consider an increasing sequence of non-negative integers from 0 to $n-1$

$$u = \{0, 1, 2, 3, \ldots, n-1\}. \tag{13}$$

Definition 12 [15]. By the dyadic shift operator we shall mean the matrix of the size $n \times n$, each row of which is obtained in accordance with the following rule

$$Dyad_i(n) = u_i \oplus i, \tag{14}$$

where the sign $\oplus$ means addition modulo 2.

Thus, the 16th order dyadic shift operator has the following form

$$Dyad(16) = \begin{bmatrix}
0 & 1 & 2 & 3 & 4 & 5 & 6 & 7 & 8 & 9 & 10 & 11 & 12 & 13 & 14 & 15 \\
1 & 0 & 3 & 2 & 5 & 4 & 7 & 6 & 9 & 8 & 11 & 10 & 13 & 12 & 15 & 14 \\
2 & 3 & 0 & 1 & 6 & 7 & 4 & 5 & 10 & 11 & 8 & 9 & 14 & 15 & 12 & 13 \\
3 & 2 & 1 & 0 & 7 & 6 & 5 & 4 & 11 & 10 & 9 & 8 & 15 & 14 & 13 & 12 \\
4 & 5 & 6 & 7 & 0 & 1 & 2 & 3 & 12 & 13 & 14 & 15 & 8 & 9 & 10 & 11 \\
5 & 4 & 7 & 6 & 1 & 0 & 3 & 2 & 13 & 12 & 15 & 14 & 9 & 8 & 11 & 10 \\
6 & 7 & 4 & 5 & 2 & 3 & 0 & 1 & 14 & 15 & 12 & 13 & 10 & 11 & 8 & 9 \\
7 & 6 & 5 & 4 & 3 & 2 & 1 & 0 & 15 & 14 & 13 & 12 & 11 & 10 & 9 & 8 \\
8 & 9 & 10 & 11 & 12 & 13 & 14 & 15 & 0 & 1 & 2 & 3 & 4 & 5 & 6 & 7 \\
9 & 8 & 11 & 10 & 13 & 12 & 15 & 14 & 1 & 0 & 3 & 2 & 5 & 4 & 7 & 6 \\
10 & 11 & 8 & 9 & 14 & 15 & 12 & 13 & 2 & 3 & 0 & 1 & 6 & 7 & 4 & 5 \\
11 & 10 & 9 & 8 & 15 & 14 & 13 & 12 & 3 & 2 & 1 & 0 & 7 & 6 & 5 & 4 \\
12 & 13 & 14 & 15 & 8 & 9 & 10 & 11 & 4 & 5 & 6 & 7 & 0 & 1 & 2 & 3 \\
13 & 12 & 15 & 14 & 9 & 8 & 11 & 10 & 5 & 4 & 7 & 6 & 1 & 0 & 3 & 2 \\
14 & 15 & 12 & 13 & 10 & 11 & 8 & 9 & 6 & 7 & 4 & 5 & 2 & 3 & 0 & 1 \\
15 & 14 & 13 & 12 & 11 & 10 & 9 & 8 & 7 & 6 & 5 & 4 & 3 & 2 & 1 & 0
\end{bmatrix}. \tag{15}$$

Property 3. Sequences obtained by applying the dyadic shift operator to the original sequence satisfying the SAC in a quaternary sense also satisfies the SAC in a quaternary sense.

For example, the following 16 sequences that satisfy the SAC in a quaternary sense can be obtained by applying the dyadic shift operator (15) on the basis of the sequence (11) satisfying the SAC in a quaternary sense

$$
\begin{aligned}
&\{0001023212312133\}; \quad \{1231213300010232\};\\
&\{0010202321131233\}; \quad \{2113123300102023\};\\
&\{0100320231123321\}; \quad \{3112332101003202\};\\
&\{1000232013213312\}; \quad \{1321331210002320\};\\
&\{0232000121331231\}; \quad \{2133123102320001\};\\
&\{2023001012332113\}; \quad \{1233211320230010\};\\
&\{3202010033213112\}; \quad \{3321311232020100\};\\
&\{2320100033121321\}; \quad \{3312132123201000\}.
\end{aligned}
\tag{16}
$$

Definition 13. By the 4-shift operator we shall mean the matrix of the size $n \times n$ each row of which is obtained in accordance with the following rule

$$
4ad(n) = u_i \underset{4}{\oplus} i , \tag{17}
$$

where the sign $\underset{4}{\oplus}$ means addition modulo 4.

Thus, the 16th order 4-shift operator has the following form

$$
4ad(16) =
\begin{bmatrix}
0 & 1 & 2 & 3 & 4 & 5 & 6 & 7 & 8 & 9 & 10 & 11 & 12 & 13 & 14 & 15\\
1 & 2 & 3 & 0 & 5 & 6 & 7 & 4 & 9 & 10 & 11 & 8 & 13 & 14 & 15 & 12\\
2 & 3 & 0 & 1 & 6 & 7 & 4 & 5 & 10 & 11 & 8 & 9 & 14 & 15 & 12 & 13\\
3 & 0 & 1 & 2 & 7 & 4 & 5 & 6 & 11 & 8 & 9 & 10 & 15 & 12 & 13 & 14\\
4 & 5 & 6 & 7 & 8 & 9 & 10 & 11 & 12 & 13 & 14 & 15 & 0 & 1 & 2 & 3\\
5 & 6 & 7 & 4 & 9 & 10 & 11 & 8 & 13 & 14 & 15 & 12 & 1 & 2 & 3 & 0\\
6 & 7 & 4 & 5 & 10 & 11 & 8 & 9 & 14 & 15 & 12 & 13 & 2 & 3 & 0 & 1\\
7 & 4 & 5 & 6 & 11 & 8 & 9 & 10 & 15 & 12 & 13 & 14 & 3 & 0 & 1 & 2\\
8 & 9 & 10 & 11 & 12 & 13 & 14 & 15 & 0 & 1 & 2 & 3 & 4 & 5 & 6 & 7\\
9 & 10 & 11 & 8 & 13 & 14 & 15 & 12 & 1 & 2 & 3 & 0 & 5 & 6 & 7 & 4\\
10 & 11 & 8 & 9 & 14 & 15 & 12 & 13 & 2 & 3 & 0 & 1 & 6 & 7 & 4 & 5\\
11 & 8 & 9 & 10 & 15 & 12 & 13 & 14 & 3 & 0 & 1 & 2 & 7 & 4 & 5 & 6\\
12 & 13 & 14 & 15 & 0 & 1 & 2 & 3 & 4 & 5 & 6 & 7 & 8 & 9 & 10 & 11\\
13 & 14 & 15 & 12 & 1 & 2 & 3 & 0 & 5 & 6 & 7 & 4 & 9 & 10 & 11 & 8\\
14 & 15 & 12 & 13 & 2 & 3 & 0 & 1 & 6 & 7 & 4 & 5 & 10 & 11 & 8 & 9\\
15 & 12 & 13 & 14 & 3 & 0 & 1 & 2 & 7 & 4 & 5 & 6 & 11 & 8 & 9 & 10
\end{bmatrix}. \tag{18}
$$

Property 4. Sequences obtained by applying the 4-shift operator of the original sequence satisfying the SAC in a quaternary sense also satisfies the SAC in a quaternary sense.

For example, the following 16 sequences that satisfy the SAC in a quaternary sense can be obtained by applying the 4-shift operator (18) on the basis of the sequence (11) satisfying the SAC in a quaternary sense

$$
\begin{aligned}
&\{0001023212312133\}; \quad \{1231213300010232\};\\
&\{0010232023111332\}; \quad \{2311133200102320\};\\
&\{0100320231123321\}; \quad \{3112332101003202\};\\
&\{1000202311233213\}; \quad \{1123321310002023\};\\
&\{0232123121330001\}; \quad \{2133000102321231\};\\
&\{2320231113320010\}; \quad \{1332001023202311\};\\
&\{3202311233210100\}; \quad \{3321010032023112\};\\
&\{2023112332131000\}; \quad \{3213100020231123\}.
\end{aligned}
\tag{19}
$$

Cryptographic properties of the proposed set of *S*-boxes

S-box	Algebraic degree of nonlinearity $\deg(S)$	Nonlinearity distance *SNl*	Maximum absolute values of the matrix of correlation coefficients $\max\limits_{i,j}\left\{\left|c_{i,j}\right|\right\}$	Compliance with the SAC in a binary sense	Compliance with the SAC in a quaternary sense
$S_1...S_8$	3	4	0.5	+	+

On the basis of the obtained 7680 balanced 4-functions which satisfy SAC in a quaternary sense it was possible to construct 245760 bijective S-boxes. 8192 of them simultaneously satisfy the SAC in a binary sense. It was established experimentally that in addition to compliance with the SAC in a quaternary and binary sense each of the 8192 built S-boxes of length $N=16$ has the maximum nonlinearity distance $SNl=4$, the algebraic degree of nonlinearity $\deg(S)=3$, and the maximum absolute values of the correlation coefficient matrix $\max\limits_{i,j}\left\{\left|c_{i,j}\right|\right\}=0.5$.

Thus, the high cryptographic quality of S-boxes simultaneously satisfying the SAC in a quaternary and in a binary sense is proven. It seems to us reasonable to recommend them for practical use in cryptoalgorithms, for example, in "Magma". We present one of the possible replacement tables composed of the S-boxes constructed by us and satisfying the SAC in a quaternary and binary sense

$$S=\begin{bmatrix} 0 & 1 & 3 & 7 & 14 & 2 & 10 & 9 & 6 & 12 & 11 & 4 & 13 & 8 & 15 & 5 \\ 1 & 0 & 2 & 6 & 15 & 3 & 11 & 8 & 7 & 13 & 10 & 5 & 12 & 9 & 14 & 4 \\ 3 & 2 & 0 & 4 & 13 & 1 & 9 & 10 & 5 & 15 & 8 & 7 & 14 & 11 & 12 & 6 \\ 2 & 3 & 1 & 5 & 12 & 0 & 8 & 11 & 4 & 14 & 9 & 6 & 15 & 10 & 13 & 7 \\ 8 & 9 & 12 & 0 & 3 & 7 & 2 & 1 & 15 & 5 & 13 & 10 & 11 & 6 & 4 & 14 \\ 9 & 8 & 13 & 1 & 2 & 6 & 3 & 0 & 14 & 4 & 12 & 11 & 10 & 7 & 5 & 15 \\ 11 & 10 & 15 & 3 & 0 & 4 & 1 & 2 & 12 & 6 & 14 & 9 & 8 & 5 & 7 & 13 \\ 10 & 11 & 14 & 2 & 1 & 5 & 0 & 3 & 13 & 7 & 15 & 8 & 9 & 4 & 6 & 12 \end{bmatrix}. \quad (20)$$

Tab. 4 shows the cryptographic properties of the set of S-boxes proposed for practical use, which are the same for the entire set.

Conclusions. We note the main results obtained in the paper:

1. The strict avalanche criterion is extended to the case of functions of q-valued logic for an arbitrary value of q.

2. The S-boxes of the "Magma" cryptographic algorithm were researched. The research showed that they do no satisfy the strict avalanche criterion both in terms of Boolean functions and in terms of 4-logic functions.

3. All balanced 4-functions that satisfies the strict avalanche criterion were found experimentally. The class of S-boxes which satisfies the strict avalanche criterion both in terms of Boolean functions and in terms of 4-logic functions is constructed on the basis of the found set of 4-functions. These *S*-boxes also have the maximum possible distance of non-linearity and the algebraic degree of non-linearity, as well as an acceptable level of correlation of the output and input vectors. Thus, the constructed S-boxes can be recommended for practical use including the use in the "Magma" cryptoalgorithm.

References

1. Zhdanov O. N. *Metodica vibora kluchevoi informacii dla algoritmov blochnoigo shifrovania* [The method of selecting key information for the block cipher algorithm]. Moscow, INFRA-M Publ, 2013, 97 p.

2. Sokolov A. V. New methods for synthesizing nonlinear transformations of modern ciphers. Germany, Lap Lambert Academic Publishing, 2015, 100 p.

3. GOST R 34.12–2015. *Kriptograficheskaya zashhita informacii blochnye shifry* [State Standard R 34.12–2015. Cryptographic information protection block ciphers]. Moscow, Standartinform Publ., 2015, P. 21.

4. Nyberg K. Differentially uniform mappings for cryptography. Advances in cryptology, Berlin, Heidelberg, New York, *Proc. of EUROCRYPT'93*, Lecture Notes in Compuer Springer Verlag, 1994, P. 55–65.

5. Mazurkov M. I., Sokolov A. V. [Cryptographic properties of the nonlinear transformation of the cipher Rijndael on the basis of complete classes of irreducible polynomials]. *Trudy Odesskogo politekhnicheskogo universiteta.* 2012, No. 2 (39), P. 183–189 (In Russ.).

6. FIPS 197. Advanced encryption standard. Available at: http://csrc.nist.gov/publications (accessed 07.06.2019).

7. Sokolov A. V., Krasota N. I. [Very nonlinear permutations: synthesis method for S-boxes with maximal 4-nonlinearity]. *Naukovi praczi ONAZ im. O. S. Popova.* 2017, No. 1, P. 145–154.

8. Kim K. Matsumoto T., Imai H. A recursive construction method of S-boxes satisfying strict avalanche criterion. *Proc. of CRYPTO'90*, Springer, Verlag, 1990, P. 565–574.

9. Gao S., Ma W., Shen D. Design of bijective S-boxes satisfying the strict avalanche criterion. *USA: Journal of computer information systems*. 2011, No. 6, P. 1967–1973.

10. Sokolov A. V. [Constructive method for the synthesis of nonlinear S-boxes satisfying the strict avalanche criterion]. *Izvestiya vysshikh uchebnykh zavedeniy. Radioelektronika.* 2013, Vol. 56, No. 8, P. 43–52 (In Russ.).

11. Logachev O. A., Salnikov A. A., Yashhenko V. V. *Bulevy funkcii v teorii kodirovaniya i kriptologii* [Boolean functions in coding theory and cryptology]. Moscow, MCzNMO Publ., 2004, 472 p.

12. Sokolov A. V., Zhdanov O. N. Prospects for the Application of Many-Valued Logic Functions in Cryptog-

raphy. *International Conference on Theory and Applications of Fuzzy Systems and Soft Computing, Springer, Cham.* 2018, P. 331–339.

13. Zhdanov O. N., Sokolov A. V. [Extending Nyberg construction on Galois fields of odd characteristic]. *Izvestiya vysshikh uchebnykh zavedeniy. Radioelektronika.* 2017, Vol. 60, No. 12, P. 696–703 (In Russ.).

14. Kim K. Construction of DES-like S-boxes Based on Boolean Functions Satisfying the SAC. *Proc. of Asiacrypt'91.* Springer Verlag, 1991, P. 59–72.

15. Mazurkov M. I., Sokolov A. V. [Fast orthogonal transforms based on bent-sequences]. *Informatika ta matematichni metodi v modelyuvanni.* 2014, No. 1, P. 5–13.

Библиографические ссылки

1. Жданов О. Н. Методика выбора ключевой информации для алгоритма блочного шифрования. М. : ИНФРА-М, 2013. 97 с.

2. Sokolov A. V. New methods for synthesizing nonlinear transformations of modern ciphers. Germany, Lap Lambert Academic Publishing, 2015, 100 p.

3. ГОСТ Р 34.12–2015 Криптографическая защита информации. Блочные шифры. М. : Стандартинформ, 2015. 21 с.

4. Nyberg K. Differentially uniform mappings for cryptography. Advances in cryptology // Proc. of EUROCRYPT'93. Berlin, Heidelberg, New York. Lecture Notes in Compuer Springer-Verlag. 1994. Vol. 765. P. 55–65.

5. Мазурков М. И., Соколов А. В. Криптографические свойства нелинейного преобразования шифра Rijndael на базе полных классов неприводимых полиномов // Тр. Одесского политехн. ун-та. 2012. № 2(39). С. 183–189.

6. FIPS 197. Advanced encryption standard [Электронный ресурс]. URL: http://csrc.nist.gov/publications (дата обращения: 07.06.2019).

7. Соколов А. В., Красота Н. И. Сильно нелинейные подстановки: метод синтеза S-блоков, обладающих максимальной 4-нелинейностью // Наукові праці ОНАЗ ім. О. С. Попова. 2017. № 1. С. 145–154.

8. Kim K. Matsumoto T., Imai H. A recursive construction method of S-boxes satisfying strict avalanche criterion // Proc. of CRYPTO'90, Springer, Verlag. 1990. P. 565–574.

9. Gao S., Ma W., Shen D. Design of bijective S-boxes satisfying the strict avalanche crierion // USA: Journal of computer information systems. 2011, № 6. P. 1967–1973.

10. Соколов А. В. Конструктивный метод синтеза нелинейных S-блоков подстановки, соответствующих строгому лавинному критерию // Известия высших учебных заведений. Радиоэлектроника. 2013. Т. 56, № 8. С. 43–52.

11. Логачев О. А., Сальников А. А., Ященко В. В. Булевы функции в теории кодирования и криптологии. М. : МЦНМО, 2004. 472 с.

12. Sokolov A. V., Zhdanov O. N. Prospects for the Application of Many-Valued Logic Functions in Cryptography. International Conference on Theory and Applications of Fuzzy Systems and Soft Computing, Springer, Cham. 2018. P. 331–339.

13. Жданов О. Н., Соколов А. В. О распространении конструкции Ниберг на поля Галуа нечетной характеристики // Известия высших учебных заведений. Радиоэлектроника. 2017. Т. 60, № 12. С. 696–703.

14. Kim K. Construction of DES-like S-boxes Based on Boolean Functions Satisfying the SAC // Proc. of Asiacrypt'91, Springer Verlag. 1991. P. 59–72.

15. Мазурков М. И., Соколов А. В. Быстрые ортогональные преобразования на основе бент-последовательностей // Інформатика та математичні методи в моделюванні. 2014. № 1. Р. 5–13.

Sokolov Artem Viktorovich – Cand. Sc., Senior Lecturer of the Department of Informatics and Information Security Management; Odessa National Polytechnic University. E-mail: radiosquid@gmail.com.

Zhdanov Oleg Nikolaevich – Cand. Sc., Associate Professor at the Department of Information Technology Security; Reshetnev Siberian State University of Science and Technology. E-mail: onzhdanov@mail.ru.

Соколов Артем Викторович – кандидат технических наук, старший преподаватель кафедры информатики и управления защитой информационных систем; Одесский национальный политехнический университет. E-mail: radiosquid@gmail.com.

Жданов Олег Николаевич – кандидат физико-математических наук, доцент кафедры безопасности информационных технологий; Сибирский государственный университет науки и технологий имени академика М. Ф. Решетнёва. E-mail: onzhdanov@mail.ru.

LIBRARY OF MATHEMATICAL FUNCTIONS WITH PARALLELISM AT THE OPERATIONAL LEVEL IN THE PYTHAGOR LANGUAGE

J. V. Udalova[*], D. A. Kuzmin

Siberian Federal University
79, Svobodny Av., Krasnoyarsk, 660041, Russian Federation
[*]E-mail: judalova@sfu-kras.ru

At present, developed tools and libraries have been designed for imperative and functional programming languages that provide parallelism through processes or threads. There are other alternative approaches to the organization of parallel computing, one of which is implemented in Pythagor – the language of functional-streaming parallel programming, and involves parallelism at the level of operations.

The tools of the Pythagor programming language are actively developing, and the repository of predefined functions is expanding. Many mathematical functions have been designed to provide a developer with no less functionality than the math library math.h of the C programming language. A large part of the mathematical functions have been implemented using the Maclaurin's series. It is both used as an approach of faster and less accurate calculations, in which a predetermined number of elements of the series is calculated without cycles and recursions with the substitution of pre-calculated coefficients in the function code, and as an approach of less rapid and more accurate calculations, in which the elements of the series are calculated dynamically until the desired accuracy is achieved.

The development of a library of mathematical functions of a programming language is an applied algorithmic task already implemented in one way or another for a number of existing programming languages. But in many languages, the implementation of algorithms for mathematical functions is hidden from the user, while modern tools of the Pythagor language support an open repository of functions. Additional interest is the possibility of parallelism at the level of operations in the calculation of mathematical formulas in the Pythagor language.

Keywords: parallelism at the operation levels, functional-stream programming, algorithms of mathematical functions.

РЕАЛИЗАЦИЯ БИБЛИОТЕКИ МАТЕМАТИЧЕСКИХ ФУНКЦИЙ С ПАРАЛЛЕЛИЗМОМ НА УРОВНЕ ОПЕРАЦИЙ НА ЯЗЫКЕ ПИФАГОР

Ю. В. Удалова[*], Д. А. Кузьмин

Сибирский федеральный университет
Российская Федерация, 660041, г. Красноярск, просп. Свободный, 79
[*]E-mail: judalova@sfu-kras.ru

К настоящему времени параллельное программирование обеспечивается большим объемом развитых инструментов и библиотек, базирующихся на императивном программировании с применением параллельных процессов или потоков (нитей), также развиваются средства распараллеливания и для функциональных языков программирования. Вместе с перечисленными инструментами существуют и альтернативные подходы к организации параллельных вычислений, один из которых реализуется языком функционально-потокового параллельного программирования Пифагор, поддерживающим параллелизм на уровне операций.

И теоретические концепции, и инструментальные средства обозначенного языка программирования активно развиваются, расширяется репозиторий разработанных функций. Разработано множество математических функций, без встроенной реализации которых затруднено комфортное программирование многих задач, способное предоставить разработчику не меньшую функциональность, чем математическая библиотека math.h языка С. Большая часть математических функций реализована с помощью рядов Маклорена. Используется как подход, предоставляющий более быстрые и менее точные вычисления, при котором без циклов и рекурсий вычисляется предопределенное количество элементов ряда с подстановкой в код функции заранее вычисленных коэффициентов, так и подход, предоставляющий менее быстрые и более точные вычисления, при котором элементы ряда вычисляются динамически до достижения нужной точности. Для части функций ряд Маклорена имеет ощутимо разный уровень точности в рамках своей области определения, тогда в окре-

стностях точек, отрицательно влияющих на точность ряда, искомая функция уточняется с помощью дополнительных математических формул, например, формул приведения.

Задача описания библиотеки математических функций языка является прикладной алгоритмической задачей, уже реализованной тем или иным образом для ряда существующих языков программирования. При этом во многих языках реализация алгоритмов математических функций скрыта от пользователя, последнему предоставляется только возможность программного вызова такой функции, тогда как современные инструментальные средства языка Пифагор поддерживают открытый репозиторий функций. Применительно к языку программирования Пифагор интерес представляют особенности и возможности распараллеливания на уровне операций при вычислении математических формул, представленные в статье.

Ключевые слова: параллелизм на уровне операций, функционально-потоковое программирование, алгоритмы математических функций.

Introduction. The Pythagor language of functional-stream parallel programming [1–6] maintaining overlapping at the level of operations and assuming the organization of architecture-independent parallel calculations represents alternative approach to parallel calculations. Now the language and its tools are actively developing [7–14]. The article is devoted to realization of mathematical functions library for the Pythagor language and illustrates features of stream parallel calculations with overlapping at the level of operations.

Considerable part of mathematical functions is calculated by means of Makloren's series [15]. Both a faster and less accurate calculations, at which the predetermined number of elements of a series with pre-calculated coefficients, and a less fast and more accurate calculations, at which elements of series are calculated dynamically before achievement of the desired accuracy, are used.

Approximate calculation of mathematical functions and their program realization in a number of the known programming languages are the tasks that have been solved by now. As for the Pythagor language and its original calculation pattern the task has been solved for the first time. Besides, realization of mathematical functions in many known languages is hidden from the developer: he can cause function performance, but cannot know by means of what method and algorithm the calculation of result is done. Thus, the basic principles of mathematical library design described in the article can be useful to those readers who need to solve a similar problem for their own calculation system.

Fast approximate calculation of Makloren's series on the example of a sine, a cosine and exponent. Makloren's series for the sine is written as:

$$\sin(x) \approx x - x^3/3! + x^5/5! - x^7/7! + \ldots,$$
$$\text{where } |x| \leq 1. \tag{1}$$

In calculation of a sine for a random angle = x radian, it is required to give an argument to an interval $[-\pi, \pi]$. In case the argument belongs to $[-\pi, -\pi/2) \cup (\pi/2, \pi]$, it moves to the interval $[-\pi/2, \pi/2]$, whereupon remembered is the indicator of the subsequent multiplication of the result by –1. For the argument x from $[-\pi/2, \pi/2]$ calculated is $x' = 2x/\pi$, approximate formula (1) is written as follows:

$$\sin(x) = \sin(\pi x'/2) \approx (\pi/2)x' - (\pi/2)^3 x'^3/3! +$$
$$+ (\pi/2)^5 x'^5/5! - (\pi/2)^7 x'^7/7! + \ldots,$$
$$\text{where } |x| \leq \pi/2, |x'| \leq 1 \tag{2}$$

For fast calculation of an acceptable result the first six summands in a series are taken and their numerical coefficients are pre-calculated external to the program code: 1) k1 = $\pi/2$ = 1.570796326794, 2) k2 = $-(\pi/2)^3/3!$ = = –0.645964097505, 3) k3 = $(\pi/2)^5/5!$ = 0.079692626245, 4) k4 = $-(\pi/2)^7/7!$ = –0.0046817541, 5) k5 = $(\pi/2)^9/9!$ = = 0.00016044118, 6) k6 = $-(\pi/2)^{11}/11!$ = –0.0000035988432.

In the course of the function operation, argument degrees are calculated; multiplication by coefficients and summation of a required formula are performed. Such algorithm is comparable to a similar consecutive imperative algorithm except the fact that the Pythagor language calculation pattern assumes potential parallel performance of all those operations relating to one or different functions with the available input data. Realization of the designated algorithm by means of the Pythagor language forms the following sequences of operators potentially available for parallel calculation (fig. 1).

Fig. 1 shows that a great number of operators of one branch, for example, calculation of argument degrees x2, x3, x5, etc. can be performed only consistently since they need the results of smaller degrees, whereas operators of one layer, for example, «(x2, x5):*>>x7», «(0.079692626245,x5):*>>p3», «(p1,p2):+>>S1» can be potentially available for parallel performance.

When illustrating the graph in fig. 1 selection of auxiliary identifiers was generally used – x2, … x11, p1, … p6, S1, … S5. The program code of function can be realized in the same style, or by means of combining formulas in one expression. For example, calculation of the required sum in the code is written as «(((((p1,p2):+,p3):+,p4):+,p5):+,p6):+ >> return», whereby the operators calculation pattern remains the same (fig. 1). But, for example, selection in the code of identifier x2 is desirable, its existence prevents performing operation 'x*x' several times when calculating argument degrees.

Comparison of results of a sine fast approximate calculation in the Pythagor language and calculations of a sine by means of a sin function call from math.h library in language C is presented in tab. 1.

Other trigonometrical functions can be calculated similarly via their Makloren's series or by means of substitution of sine values in reduction formulas, for example, of $\cos(x) = 1 - 2\sin^2(x/2)$.

When realizing the mathematical functions library for the Pythagor language, reduction formulas were used. Therefore tables of comparison of cosine and a tangent calculations in the Pythagor and C languages accurately correlate with tab. 1, i. e. for example, cos(1.2) will be closer to a similar call of a cosine from math.h than cos(1.6).
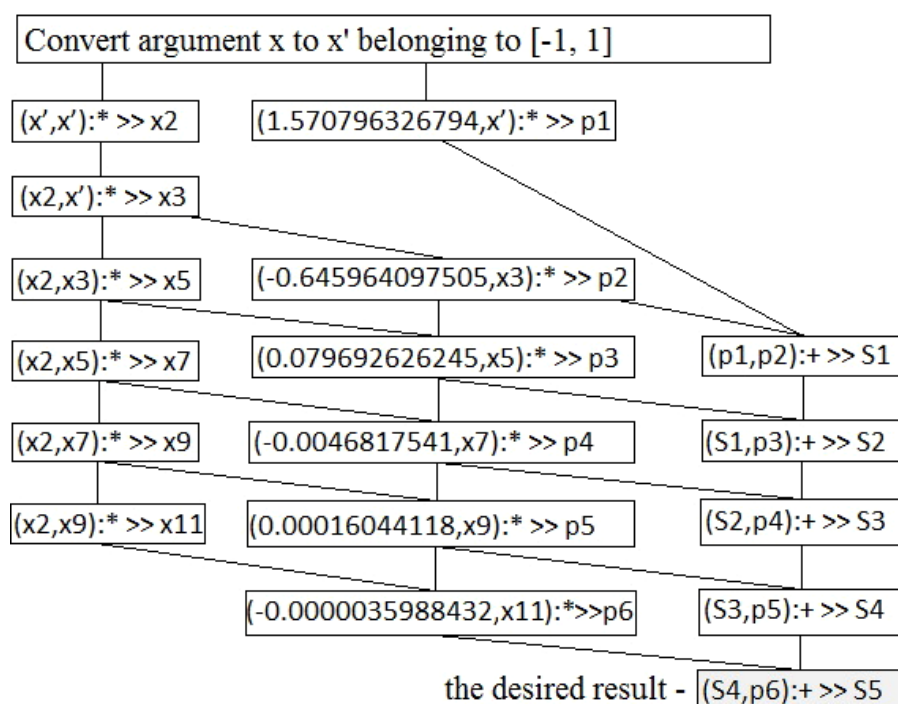
Fig. 1. Simplified information and control graph of the function sin

Рис. 1. Упрощенный информационно-управляющий граф функции sin

Sine calculation in the Pythagor language and C language (library math.h)

Argument x	math.h	Pythagor	Argument x	math.h	Pythagor
0.2	0.198668	0.198669	5.2	−0.883455	−0.883455
0.4	0.389417	0.389418	5.4	−0.772766	−0.772764
0.6	0.564641	0.564642	5.6	−0.631268	−0.631266
0.8	0.717355	0.717356	5.8	−0.464604	−0.464602
1.0	0.841470	0.841471	6.0	−0.279418	−0.279416
1.2	0.932039	0.932039	10.0	−0.544021	−0.544021
1.4	0.985450	0.985452	50.0	−0.262375	−0.262375
1.6	0.999574	0.999578	100.0	−0.506366	−0.506370

Under approximate calculation of given functions by means of Makloren's series a considerable decrease in accuracy in the neighborhood of separate points, lying in the series range of definition can be observed, as a rule, it is 1 and-1. The arcsine belongs to such functions. For an arcsine the range of definition of function and series coincide, it is [-1, 1] therefore argument transformation, similar to the one performed to the sine, is not required. Under approximate calculation of an arcsine the following formula based on its Makloren's series with the coefficients calculated out of the program code is used:

$$\arcsin(x) \approx x + 0.166666666666x^3 + 0.075x^5 +$$
$$+ 0.044642857142x^7 + 0.030381944444x^9 +$$
$$+ 0.022372159090x^{11} + 0.017352764423x^{13} +$$
$$+ 0.01396484375x^{15} + 0.011551800896x^{17} +$$
$$+ 0.009666219208x^{19} + 0.008390335809x^{21} +$$
$$+ 0.007312525873x^{23} + 0.000011679728x^{25},$$
$$\text{where } |x| \leq 1 \qquad (3)$$

While for a sine acceptable accuracy it is enough to take first six summands, for an arcsine it is desirable to calculate not less than twelve. In addition, supposing x is located in the neighborhood of points 1 or −1, the accuracy of an approximate formula considerably decreases. In realization of an arcsine for the Pythagor language at x belonging to [−1, −0.93) U (0.93, 1], the auxiliary formula $\arcsin(x) = \pi/2 - \arcsin$ is used $((1 - x^2)^{1/2})$.

Comparison of the arcsine fast approximate calculation in the Pythagor language and calculations of the arcsine by means of the sin function call from math.h library in language C is presented in tab. 2.

When calculating the exponent the following formula with preliminary calculated coefficients based on Makloren's series is used:

$$e^x \approx 1 + x + 0.5x^2 + 0.166666666666\ x^3 +$$
$$+ 0.041666666666\ x^4 + 0.008333333333x^5 +$$
$$+ 0.001388888888x^6 + 0.00019841269841x^7,$$
$$\text{where } |x| \leq 0.7 \qquad (4)$$

Makloren's series of exponent is defined on [−1, 1], but as at fast approximate calculation the final small number of elements is used, for acceptable accuracy the domain [−0.7, 0.7] is chosen. The domain of exponent

definition includes all numerical axis, therefore for random argument x the exponent property is used $e^{a+b} = e^a e^b$. The argument x is divided into the integral and fractional parts, e in fractional degree is calculated with the help of formula (4), e in the integral degree is calculated by multiplication of constants e or 1/e, at the same time additional values, calculated external the program code, are applied to speed up calculations, for example, $e^2 = 7.389056098930649$, $e^8 = 2980.957987041726$, $e^{64} = 6.235149080811582e + 027$, used in multiplication.

Comparison of results of fast approximate calculation of exponent in the Pythagor language and exponent calculations by means of an exp function call from math.h library in language C is presented in tab. 3.

The accurate recursive calculation of Makloren's series on the example of a logarithm. Makloren's series for the natural logarithm is written as:

$$\ln(x + 1) \approx x - x^2/2 + x^3/3 - x^4/4 + ...,$$
$$\text{where } -1 < x \leq 1. \qquad (5)$$

Formula (5) includes higher coefficients than Makloren's series of the above considered functions, therefore fast calculation of the natural logarithm is not realized as it would demand enumeration of a significant number of summands (up to several hundreds or thousands). Instead, recursive calculation of formula (5) before achievement of the desired accuracy of 10-8 is used, in imperative language it could be realized by means of a cycle, in the Pythagor language cyclic algorithms are realized by means of recursive functions.

The definition domain of the natural logarithm is a set of positive numbers, therefore for any argument x the property of the natural logarithm is used $\ln(b*10^a) = \ln(b) + a*\ln(10) = \ln(b) + a*2.302585092994046$, where b can be chosen so as to suit the calculation of ln(b) with the help of formula (5).

Recursive function expects the argument type of (number 1, number 2, number 3) where number is b, number 2 in the first recursion call coincides with b, number 3 is a series denominator, in the first recursion call equals one. One iteration of the recursion calculates four summands of Makloren's series. The simplified information and control graph of the natural logarithm function is written as (fig. 2).

The expressions in braces, for example {(S, (b, (b4,b):*, (z,4):+):recursion):+} in fig. 2, belong to the delayed calculations and will be carried out only if the condition of stop is true: - i.e. when the fourth command s4 in the current iteration taken according to module are more than 10^{-8}. Commands (b, (b4,b):*,(z,4):+) form the argument (number1, number2, number3) for the iteration following the same recursive function. Presented here recursive calculation of formula (5) can be realized via Pythagor language tools or other recursion ways, however, when realizing the library of mathematical functions the suggested method was chosen.

Comparison of the natural logarithm in the Pythagor language and natural logarithm by means of a log function call from math.h library in language C is presented in tab. 4.

Table 2

Calculation of the arcsine in the Pythagor and C languages (library math.h)

Argument x	math.h	Pythagor	Argument x	math.h	Pythagor
0.1	0.100167	0.100167	0.91	1.143284	1.140812
0.2	0.201358	0.201358	0.92	1.168081	1.164584
0.3	0.304693	0.304693	0.93	1.194413	1.189442
0.4	0.411517	0.411517	0.94	1.222630	1.229622
0.5	0.523599	0.523599	0.95	1.253236	1.258546
0.6	0.643501	0.643501	0.96	1.287002	1.290796

Table 3

Exponent calculation in the Pythagor and C languages (library math.h)

Argument x	math.h	Pythagor	Argument x	math.h	Pythagor
−25	0.000000	0.000000	0.5	1.648721	1.648721
−13.7	0.000001	0.000001	1.1	3.004166	3.004166
−9.6	0.000068	0.000068	6.6	735.095093	735.094910
−7.9	0.000371	0.000371	8.8	6634.245117	6634.240234
−1.5	0.223130	0.223130	16.3	11994985.0	11994990.0
−0.8	0.449329	0.449329	25	72004902912	72004902912

Table 4

Calculation of natural logarithm in Pythagor and C languages

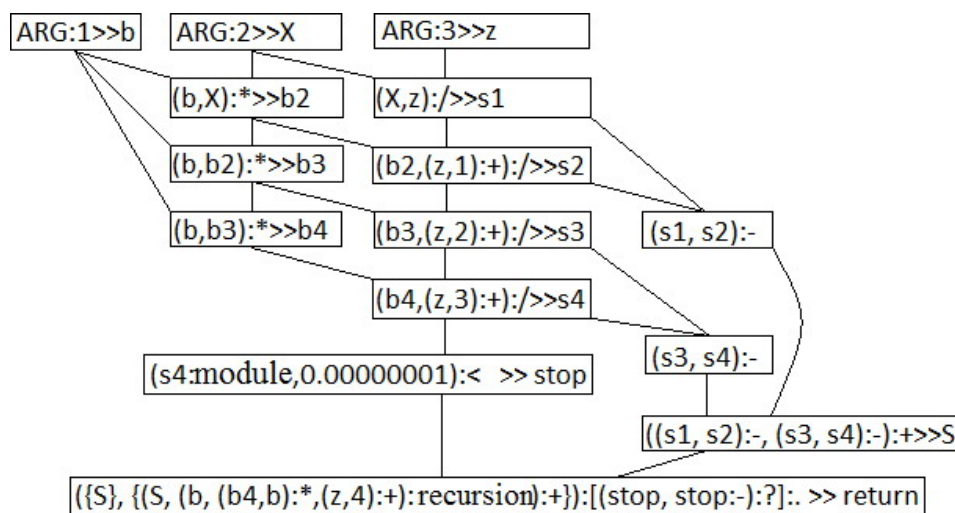| Argument x	math.h	Pythagor	Argument x	math.h	Pythagor
0.07	−2.659260	−2.659260	15	2.708050	2.708050
0.15	−1.897120	−1.897120	40	3.688879	3.688879
0.47	−0.755023	−0.755023	200	5.298317	5.298317
0.88	−0.127833	−0.127833	400	5.991465	5.991465
1.85	0.615186	0.615186	10500	9.259130	9.259131
8	2.079442	2.079442	100000	11.512925	11.512930

Fig. 2. Simplified information and control graph of the function ln

Рис. 2. Упрощенный информационно-управляющий граф функции ln

Having realization of natural logarithm calculation it becomes possible to calculate a logarithm on a random basis, using $\log_a$ (b) property $= \ln(b)/\ln(a)$, for a decimal logarithm in a denominator a constant 2.302585092994046 calculated exclusive the code is substituted. Exponentiation is realized by means of the formula $x^y = e^{y*\ln(x)}$.

Conclusion. The problem of the Pythagor language mathematical library development has been completely realized and is one of the subtasks which are successfully executed with the RFFI grant "Architecture-independent Development of Parallel Programs on the basis of the Functional and Stream Paradigm".

The list of the realized mathematical functions. Module. Sine. Cosine. Tangent. Cotangent. Arcsine. Arccosine. Arctangent. Arc cotangent. Secant. Cosecant. Square root. Cubic root. Rounding. Rounding down. Rounding up. Integral and fractional parts of number. Exponent. Hyperbolic sine, cosine, tangent, cotangent. Natural logarithm. Decimal logarithm. A logarithm on the specified basis. Exponentiation. The integral part from division and a remainder of division (arguments of function can be numbers, both integral, and material). Mantissa and exponent of the two marking. Multiplication of number to the power of two. Number sign. Inverse hyperbolic: cosine, sine, tangent, cotangent, secant, cosecant. Rising of the two to the power. Maximum from couple of numbers. Minimum from couple of numbers. Hypotenuse. Difference module.

All realized functions are included in the open repository of the Pythagor language, thus, the developer can not only execute and look through their code, but also borrow it for creation of own algorithms or alternative realization of mathematical functions.

References

1. Legalov A. I., Ushakova M. S. [Features of the development and transformation of functional data-flow parallel programs]. *Superkomp'yuternye dni v Rossii. Trudy mezhdunarodnoy konferentsii* [Supercomputer days in Russia. Proceedings of the international conference]. 2018, P. 999–1000.

2. Legalov A. I. et al. [Change of computing management strategies in architecture-independent parallel programming]. *Nauchnyy servis v seti Internet. Trudy XIX Vserossiyskoy nauchnoy konferentsii* [Scientific service on the Internet. Proceedings of the XIX all-Russian scientific conference]. 2017. P. 341–350 (In Russ.).

3. Legalov A. I. [Language support for architecture-independent parallel programming]. *Yazyki programmirovaniya i kompilyatory. Trudy konferentsii* [Programming languages and compilers. Proceedings of the conference]. 2017, P. 169–172 (In Russ.).

4. Legalov A. I. et al. [Technological aspects of creation, transformation and execution of functional-stream parallel programs]. *Nauchnyy servis v seti Internet: vse grani parallelizma. Trudy Mezhdunarodnoy superkomp'yuternoy konferentsii* [Scientific service on the Internet: all facets of parallelism. Proceedings of the International supercomputer conference]. 2013, P. 443–447 (In Russ.).

5. Legalov A. I. et al. [Storage of functional data-flow parallel programs]. *Vestnik SibGAU*. 2013, No. 4 (50), P. 53–57 (In Russ.).

6. Legalov A. I. et al. [Event-driven computing model that supports the execution of functional-stream parallel programs] *Sistemy. Metody. Tekhnologii*. 2012, No. 1 (13), P. 113–119 (In Russ.).

7. Romanova D.S. [Organization of testing to check the correctness of Pythagor's tools]. *Prospekt Svobodnyy – 2018. Materialy Mezhdunarodnoy konferentsii molodykh uchenykh* [Prospect Free – 2018. Proceedings of the International conference of young scientists]. Siberian Federal University, 2018, P. 25–28 (In Russ.).

8. Udalova U. V. [Verification of functional-stream parallel programs using interval formulas]. *Obra-*

zovatel'nye resursy i tekhnologii. 2016, No. 2 (14), P. 259–262 (In Russ.).

9. Ushakova M. S., Legalov A. I. [Verification of programs with mutual recursion in Pythagor]. *Modelirovanie i analiz informatsionnykh sistem.* 2018, Vol. 25, No. 4 (76), P. 358–381 (In Russ.).

10. Vasiliev V. S., Legalov A. I. [Optimization of loop invariant in the language of Pythagor]. *Modelirovanie i analiz informatsionnykh sistem.* 2018, Vol. 25, No. 4 (76), P. 347–357 (In Russ.).

11. Legalov A. I. et al. A toolkit for the development of data-driven functional parallel programmes. *Communications in Computer and Information Science.* 2018, Vol. 910, P. 16–30.

12. Legalov A. I. et al. [Tool support for the creation and transformation of functional data-flow parallel programs]. *Trudy Instituta sistemnogo programmirovaniya RAN* [Proceedings of Institute for system programming of the Russian Academy of Sciences]. 2017, Vol. 29, No. 5, P. 165–184 (In Russ.).

13. Ushakova M. S., Legalov A. I. [Instrumental support for formal verification of programs written in the language of functional-streaming parallel programming]. *Vestnik Yuzhno-Ural'skogo gosudarstvennogo universiteta. Seriya: Vychislitel'naya matematika i informatika.* 2015, Vol. 4, No. 2, P. 58–70 (In Russ.).

14. Udalova U. V., Legalov A. I. [Verification of functional-stream parallel programs by inductive assertions]. *Doklady Akademii nauk vysshey shkoly Rossiyskoy Federatsii.* 2014, No. 2-3 (23-24), P. 125–132 (In Russ.).

15. Lusternik L. A. *Matematicheskii analiz. Funkcii, predeli, rydi, chepnie drobi* [Mathematical analysis. Functions, limits, series, continued fractions]. Moscow, IL Publ., 2012, 442 p.

Библиографические ссылки

1. Легалов А. И., Ушакова М. С. Особенности разработки и преобразования функционально-потоковых параллельных программ // Суперкомпьютерные дни в России. Тр. Междунар. конф. 2018. С. 999–1000.

2. Изменение стратегий управления вычислениями при архитектурно-независимом параллельном программировании / А. И. Легалов [и др.] // Научный сервис в сети Интернет : тр. XIX Всеросс. науч. конф. 2017. С. 341–350.

3. Легалов А. И. Языковая поддержка архитектурно-независимого параллельного программирования // Языки программирования и компиляторы : тр. конф. 2017. С. 169–172.

4. Технологические аспекты создания, преобразования и выполнения функционально-потоковых параллельных программ / А. И. Легалов [и др.] // Научный сервис в сети Интернет: все грани параллелизма : тр. Междунар. суперкомпьютерной конф. 2013. С. 443–447.

5. Особенности хранения функционально-потоковых параллельных программ / А. И. Легалов [и др.] // Вестник СибГАУ. 2013. № 4 (50). С. 53–57.

6. Событийная модель вычислений, поддерживающая выполнение функционально-потоковых параллельных программ / А. И. Легалов [и др.] // Системы. Методы. Технологии. 2012. № 1 (13). С. 113–119.

7. Романова Д. С. Организация тестирования для проверки корректности инструментальных средств языка Пифагор // Проспект Свободный – 2018 : материалы Междунар. конф. молодых учен. / Сиб. федер. ун-т. 2018. С. 25–28.

8. Удалова Ю. В. Верификация функционально-потоковых параллельных программ с помощью интервальных формул // Образовательные ресурсы и технологии. 2016. № 2 (14). С. 259–262.

9. Ушакова М. С., Легалов А. И. Верификация программ со взаимной рекурсией на языке Пифагор // Моделирование и анализ информационных систем. 2018. Т. 25, № 4 (76). С. 358–381.

10. Васильев В. С., Легалов А. И. Оптимизация инварианта цикла в языке Пифагор // Моделирование и анализ информационных систем. 2018. Т. 25, № 4 (76). С. 347–357.

11. A toolkit for the development of data-driven functional parallel programmes / А. И. Легалов [и др.] // Communications in Computer and Information Science. 2018. Т. 910. Р. 16–30.

12. Инструментальная поддержка создания и трансформации функционально-потоковых параллельных программ / А. И. Легалов [и др.] // Тр. Ин-та систем. программирования РАН. 2017. Т. 29, № 5. С. 165–184.

13. Инструментальная поддержка формальной верификации программ, написанных на языке функционально-потокового параллельного программирования / М. С. Ушакова, А. И. Легалов // Вестник Южно-Уральского гос. ун-та. Серия: Вычислительная математика и информатика. 2015. Т. 4, № 2. С. 58–70.

14. Удалова Ю. В., Легалов А. И. Верификация функционально-потоковых параллельных программ методом индуктивных утверждений // Доклады АН ВШ РФ. 2014. № 2–3 (23-24). С. 125–132.

15. Люстерник Л. А. Математический анализ. Функции, пределы, ряды, цепные дроби. М. : ИЛ, 2012. 442 с.
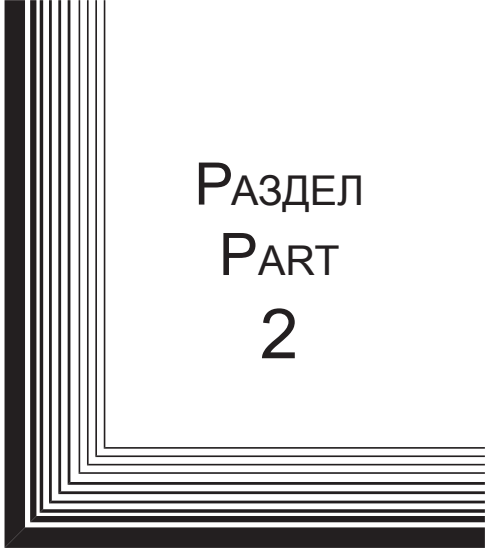
Udalova Julia Vasilyevna – Ph. D., associate professor, Siberian Federal University. E-mail: judalova@sfu-kras.ru.
Kuzmin Dmitry Alexandrovich – Ph. D., associate professor, Siberian Federal University. E-mail: dkuzmin@sfu-kras.ru.

Удалова Юлия Васильевна – кандидат технических наук, доцент, Сибирский федеральный университет. E-mail: judalova@sfu-kras.ru.
Кузьмин Дмитрий Александрович – кандидат технических наук, доцент, Сибирский федеральный университет. E-mail: dkuzmin@sfu-kras.ru.

АВИАЦИОННАЯ
И РАКЕТНО-
КОСМИЧЕСКАЯ ТЕХНИКА

AVIATION
AND SPACECRAFT
ENGINEERING

DEVELOPING THE LABORATORY TEST BENCH OF FUEL THREE-POINT MEASUREMENT

R. A. Akzigitov*, N. S. Pisarev, N. I. Statsenko, A. R. Glukharev, I. B. Tsar'kov

Reshetnev Siberian State University of Science and Technology
31, Krasnoyarsky Rabochy Av., Krasnoyarsk, 660037, Russian Federation
*E-mail: balals@mail.ru

The development of digital technology allows continuous improvements in many areas. This paper reflects the development of a new fuel measurement method. To measure the fuel, the authors propose three fuel sensors and a computational element to simulate the position of the fuel level in space with further calculating the volume of fuel, to reduce errors due to the fuel meters operation. The main advantage of this system is the elimination of errors arising from the evolution of an aircraft, as well as its uneven movement.

The paper demonstrates a phased development of a laboratory test bench to study the three-point method to measure fuel. In the course of the work, a vessel is assembled to simulate the fuel tank of the aircraft. The vessel is a glass container with submersible measuring sensors. Also, the research contains calculation of the bridge electrical circuit to compute a voltage value at each sensor. In the test, transformer fluid substitutes fuel, since it acted as a dielectric. The program code for the microcontroller is recorded.

The proposed method has several advantages in comparison with traditional methods of measuring the fuel level; a mathematical model is presented, on the basis of which the level of fuel in the aircraft fuel tank is measured.

Keywords: laboratory test bench, fuel gauge, fuel tank, error, aviation.

РАЗРАБОТКА ЛАБОРАТОРНОЙ УСТАНОВКИ ТРЕХТОЧЕЧНОГО ИЗМЕРЕНИЯ ТОПЛИВА

Р. А. Акзигитов*, Н. С. Писарев, Н. И. Стаценко, А. Р. Глухарев, И. Б. Царьков

Сибирский государственный университет науки и технологий имени академика М. Ф. Решетнева
Российская Федерация, 660037, просп. им. газ. «Красноярский рабочий», 31
*E-mail: balals@mail.ru

Развитие цифровых технологий позволяет непрерывно производить улучшения во многих сферах деятельности. Данная работа посвящена разработке нового, несуществующего на данный момент метода измерения топлива. Для измерения топлива предлагается использовать три топливных датчика и вычислительный элемент для моделирования положения уровня топлива в пространстве с дальнейшим расчетом объёма топлива, что позволит уменьшить погрешности, возникающие при эксплуатации топливомеров. Главным преимуществом данной системы будет устранение погрешности, возникающей при эволюциях воздушного судна, а также при его неравномерном движении.

В данной работе проводится поэтапная разработка лабораторного стенда для исследования трехточечного метода измерения топлива. В ходе работы был собран сосуд, моделирующий топливный бак воздушного судна. Сосуд представляет собой стеклянную емкость с погружными измерительными датчиками. Также был проведен расчет мостовой электрической схемы, рассчитывающей значение напряжения на каждом датчике. В качестве замены топлива использовалось трансформаторное масло, выступающее в качестве диэлектрика. Был записан программный код для микроконтроллера.

Предложенный способ обладает рядом преимуществ в сравнении с традиционными способами замера уровня топлива. В работе представлена математическая модель, на основе которой производилось измерение уровня топлива в топливном баке воздушного судна.

Ключевые слова: лабораторная установка, топливомер, топливный бак, погрешность, авиация.

Introduction. The main objective of the method is to eliminate an error in case the surface of the fuel deviates from the position when the fuel is not affected by external forces [1].

The three-point method of fuel measurement involves the use of three fuel meters that determine the coordinates of the points located on the surface of the fuel and the electronic computing device with the geometric characteristics of the fuel tank introduced into it [2–4].

The obtained spatial coordinates of the three points located in the fuel tank in the computing device can be used to simulate the plane at the fuel surface (fig. 1). The resulting plane isolates the upper (empty) part of the fuel tank [5–8]. Using the mathematical apparatus of the resulting truncated figure (truncated fuel tank), we can calculate its volume.

The development of the pilot plant includes four stages:

1. Fuel tank model design;
2. Calculation and installation of electrical circuits of the fuel gauge;
3. Firmware of the microcontroller;
4. Test and adjustment of the installation.

Fuel tank model design. The result of the first stage of constructing a fuel tank model is a vessel that is a glass flask with a square section and a wooden cover with holes to install submersible fuel meter sensors [9–11]. We use aluminum pipes with a diameter of 10 mm and 16 mm assembled in the form of coaxial capacitors as submersible sensors (fig. 2).

For the calculation, the inner lower surface of the vessel is divided into similar sectors (fig. 3).
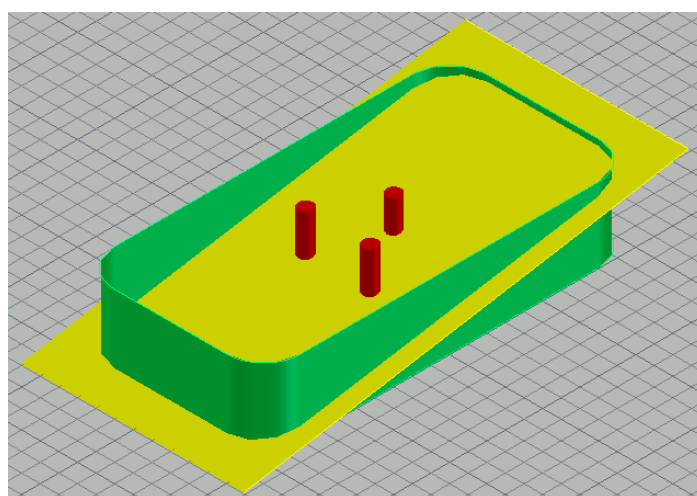
Fig. 1. The cross section of the fuel tank by the plane of the fuel level

Рис. 1. Сечение топливного бака плоскостью уровня топлива

Fig. 2. A vessel to measure liquids

Рис. 2. Сосуд для измерения жидкости

Fig. 3. Selected sectors of the surface

Рис. 3. Выделенные сектора поверхности

The second stage consists of the calculation and installation of the measuring bridge generating a misalignment signal from 0V to 5V.

Calculation and installation of electrical circuits of the fuel gauge. For the calculation and simulation of the scheme, we use an "online electric" resource for the interactive calculations of power supply systems (fig. 4).

Based on the modeled scheme, we install three schemes of the measuring bridges for each sensor separately to a prototyping board. Further, elements are connected to the submersible sensor as a capacitive element [12; 13].

Firmware of the microcontroller. Microcontroller "WAVGAT" (fig. 5) is chosen to be a computing device due to its docile computing performance and ease of firmware.

Microcontroller firmware is performed according to the following code; and an integrated development environment Arduino is used as the development environment.

Fig. 6 shows a part of the code, responsible for creating a program code with unchanged values to be used for the future mathematical calculations of the fuel level.

Fig. 7 demonstrates a section of the program code, designed to indicate the analog inputs, which are supplied with an analog signal in the form of voltage from 0 V to 5 V. This signal comes from the bridge circuit of the measuring unit.

At this stage (fig. 8) analog-to-digital conversion of the input signal is performed to facilitate further mathematical calculations [14; 15]. The calculated values as well as the constant values are used to continuous computation of the secant plane.
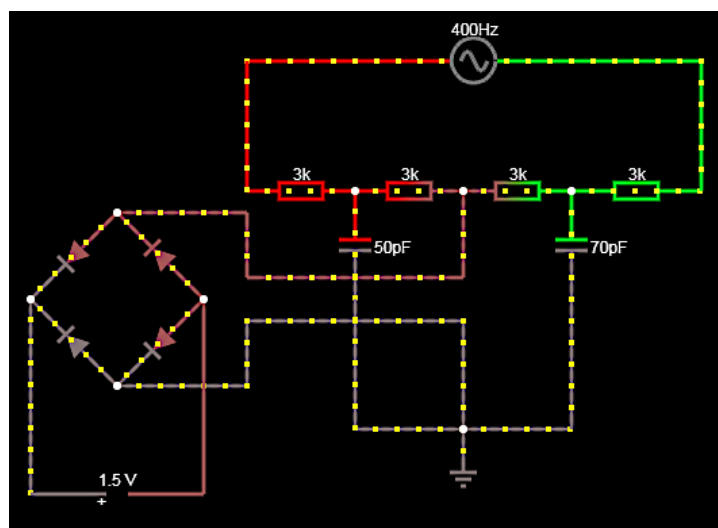
Fig. 4. Electrical diagram of the measuring bridge

Рис. 4. Электрическая схема измерительного моста
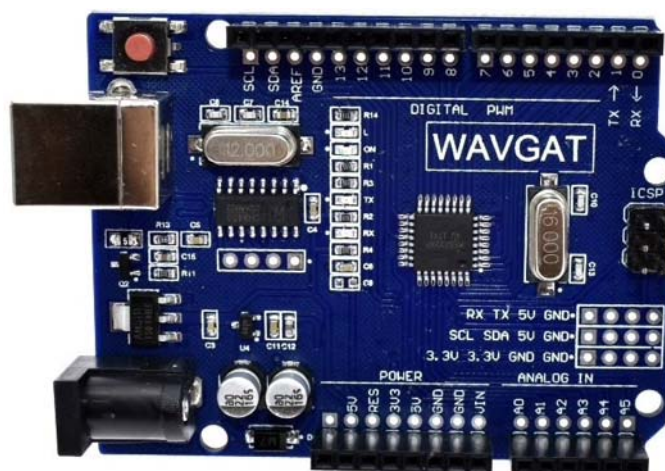
Fig. 5. Microcontroller WAVGAT

Рис. 5. Микроконтроллер WAVGAT

```
//Const: size
    int xMax = 120;
    int yMax = 120;
    int zMax = 200;
    int S = 12;

    int z0;
    int z1;
    int z2;

//Const: coordinate
    float x0 = xMax * 0.15;
    float y0 = yMax * 0.15;
    float x1 = xMax * 0.85;
    float y1 = yMax * 0.15;
    float x2 = xMax * 0.15;
    float y2 = yMax * 0.85;
```

Fig. 6. The designation of the model vessel dimensions
and the position of the submersible sensors

Рис. 6. Обозначение размеров модели сосуда
и положение погружных датчиков

```
void setup() {
  // put your setup code here, to run once:
  Serial.begin(9600);

//Height
  pinMode(A0, INPUT);
  pinMode(A1, INPUT);
  pinMode(A2, INPUT);
}
```

Fig. 7. Designation in the code of analog inputs

Рис. 7. Обозначение в коде аналоговых входов

```
z0 = analogRead(A0);
z0 = map(z0, 0, 1023, 0, 200);
//z0 = constrain(z0, 0, 200);

z1 = analogRead(A1);
z1 = map(z1, 0, 1023, 0, 200);
//z1 = constrain(z1, 0, 200);

z2 = analogRead(A2);
z2 = map(z2, 0, 1023, 0, 200);
//z2 = constrain(z2, 0, 200);

int A = ((y1 + y0) * (z2 - z0)) - ((y2 - y0) * (z1 - z0));
int B = ((x1 + x0) * (z2 - z0)) - ((x2 - x0) * (z1 - z0));
int C = ((x1 + x0) * (y2 - y0)) - ((x2 - x0) * (y1 - y0));
int D = (-x0 * A) + (y0 * B) - (z0 * C);

int V = 0;
int z = 0;
```

Fig. 8. Analog-to-digital conversion and computation
of the secant plane equation

Рис. 8. Аналогово-цифровое преобразование
и вычисление уравнения секущей плоскости

Nested loop (fig. 9) calculates the height of the fuel level in each sector of the fuel tank model.

```
for (int x = 1; x <= xMax; x++) {

    for (int y = 1; y <= yMax; y++) {
        z = ((-x * A) + (y * B) - D) / C;
        V += S * z;
    }
}
```

Fig. 9. Nested loop

Рис. 9. Вложенный цикл

After the firmware, the output channels of bridge circuit rectifiers are connected to the microcontroller analog inputs and the operation of this system is tested. Transformer oil is used as a dielectric to replace aviation fuel; this eliminates the need to do insulation for submersible sensors.

Conclusion. By applying these corrections in the calculations, it becomes possible to perform computations with higher accuracy. It is possible to notice, the virtual truncated model corresponds to the real level of fuel tank filling factor, and the error in case of external forces does not occur, since the section plane will tilt in the virtual model while maintaining the volume.

The system shows some deviations during the measurements, but in general, the reliability of this measurement method has been confirmed and has got prospects for further development with more accurate measuring devices for better measurement accuracy.

References

1. Grigorovskiy B. K., Katsyuba O. A., Priputnikov A. P. [Display a variety of information and measurement process by a model number of fuel engineers. Representativeness of the display]. *Vestnik SAMGUPS.* 2015, Vol. 2, No. 2, P. 150–155 (In Russ.).

2. Dzhezhora A. A., Rubanik V. V., Savchuk V. K., Kuz'minich A. V. [Capacitive level sensors for electroconductive liquid]. *Datchiki i sistemy.* 2008, No. 12, P. 26–29 (In Russ.).

3. Mastepanenko M. A., Vorotnikov I. N., Anikuev S. V. *Matematicheskie modeli i metody obrabotki izmeritel'nykh signalov emkostnykh preobrazovateley na postoyannom toke* [Mathematical models and methods of processing measuring signals of capacitive DC converters]. Stavropol', Agrus, 2015, 232 p.

4. Dzhezhora A. A., Rubanik V. V., Savchuk V. K. [Fuel level control]. *Vestnik Polotskogo gosudarstvennogo universiteta.* 2009, No. 2, P. 21–25 (In Russ.).

5. Bogoyavlenskiy A. A. [Instrumental control of the stock and flow of working fluids during technical operation of aircraft]. *Mir izmereniy.* 2017, No. 4, P. 16–23 (In Russ.).

6. Rechkin A. G., Kraynikov V. A., Sablin A. S. [To the question of measuring the fuel stock on board an aircraft] *II shkola-seminar molodykh uchenykh "Fundamental'nye problemy sistemnoy bezopasnosti"* [II school-seminar of young scientists "Fundamental problems of system security"]. Yelets, 2015, P. 196–202 (In Russ.).

7. Danilov V. G., Shemsedinov I. Sh. [Training system for solving problems in analytical geometry with generating tasks based on generating grammars]. *Kachestvo. Innovatsii. Obrazovanie.* 2009, No. 47, P. 5–10 (In Russ.).

8. Kenmoku Masakatsu [Analytic solutions of the wheeler-dewitt equation in spherically symmetric geometry]. *Gravity and cosmology.* 2009, Vol. 5, No. 4, P. 289–296

9. Pylilo I. S., Klybik V. K. [Selecting a prospective sensor type for continuous fuel level measurement]. *Mekhanizatsiya i elektrifikatsiya sel'skogo khozyaystva.* 2012, No. 4, P. 160–166 (In Russ.).

10. Goncharov D. S., Dzhezhora A. A. [Influence of coaxiality of cylindrical shells of circular section on the capacity of fuel level sensors]. *50 mezhdunarodnaya nauchno-tekhnicheskaya konferentsiya prepodavateley i studentov, posvyashchennaya godu nauki* [50th International Scientific and Technical Conference of Teachers and Students, dedicated to the Year of Science]. Vitebsk, 2017, P. 105–106 (In Russ.).

11. Koshevoy N. D., Matveev A. G. [Development of algorithms for modeling the operation of fuel consumption sensors and interaction with the fuel main]. *Radioelektronika, informatika, upravlenie.* 2011, No. 2, P. 54–59 (In Russ.).

12. Vershinin O. S., Sharov V. V. [Experimental method for estimating the error of an automobile fuel level sensor]. *Izvestiya vysshikh uchebnykh zavedeniy. Problemy energetiki.* 2008, Vol. 2, No. 3, P. 116–121 (In Russ.).

13. Gurtovtsev A. L. [About Metrology of Electronic Power Meters]. *Elektro. Elektrotekhnika, elektroenergetika, elektrotekhnicheskaya promyshlennost'.* 2008, No. 2, P. 44–52 (In Russ.).

14. Buzhinskiy V. A. [About fluid oscillations in fuel tanks with damping gratings]. *Kosmonavtika i raketostroenie.* 2007, No. 46, P. 110–120 (In Russ.).

15. Pisarev N. S., Statsenko N. I. [Three-point aviation fuel gauge]. *Materialy XXI Mezhdunar. nauch. konf. "Reshetnevskie chteniya"* [Materials XXI Intern. Scientific. Conf. "Reshetnev reading"]. Krasnoyarsk, 2017, Vol. 1, P. 468–469 (In Russ.).

Библиографические ссылки

1. Григоровский Б. К., Кацюба О. А., Припутников А. П. Отображение модельным рядом топливомеров многообразия информационно-измерительного процесса. Репрезентативность отображения // Вестник САМГУПС. 2015. Т. 2, № 2. С. 150–155.

2. Емкостные датчики уровня электропроводящей жидкости / А. А. Джежора, В. В. Рубаник, В. К. Савчук, А. В. Кузьминич // Датчики и системы. 2008. № 12. С. 26–29.

3. Мастепаненко М. А., Воротников И. Н., Аникуев С. В. Математические модели и методы обработки измерительных сигналов емкостных преобразователей на постоянном токе. Ставрополь : Агрус, 2015. 232 с.

4. Джежора А. А., Рубаник В. В., Савчук В. К. Контроль уровня топлива // Вестник Полоцкого гос. ун-та. 2009. № 2. С. 21–25.

5. Богоявленский А. А. Инструментальный контроль запаса и расхода рабочих жидкостей при технической эксплуатации воздушных судов // Мир измерений. 2017. № 4. С. 16–23.

6. Речкин А. Г., Крайников В. А., Саблин А. С. К вопросу измерения запаса топлива на борту воздушного судна // Фундаментальные проблемы системной безопасности : II шк.-семинар молодых учен. Елец, 2015, Р. 196–202.

7. Данилов В. Г., Шемседдинов И. Ш. Обучающая система для решения задач по аналитической геометрии с генерацией заданий на основе порождающих грамматик // Качество. Инновации. Образование. 2009. № 47. С. 5–10.

8. Kenmoku Masakatsu. Analytic solutions of the wheeler-dewitt equation in spherically symmetric geometry // Gravity and cosmology. 2009. Vol. 5, No. 4. P. 289–296.

9. Пылило И. С., Клыбик В. К. Выбор перспективного типа датчика для непрерывного измерения уровня топлива // Механизация и электрификация сельского хозяйства. 2012. № 4. С. 160–166.

10. Гончаров Д. С., Джежора А. А. Влияние соосности цилиндрическихоболочек кругового сечения на емкость датчиков уровня топлива // 50-я Междунар. науч.-техн. конф. преподавателей и студентов, посвящённая году науки. Витебск, 2017. С. 105–106

11. Кошевой Н. Д., Матвеев А. Г. Разработка алгоритмов моделирования работы датчиков расхода топлива и взаимодействия с топливной магистралью // Радиоэлектроника, информатика, управления. 2011. №. 2. С. 54–59.

12. Вершинин О. С., Шаров В. В. Экспериментальный метод оценки погрешности автомобильного датчика уровня топлива // Известия высших учебных заведений. Проблемы энергетики. 2008. Т. 2, № 3. С. 116–121.

13. Гуртовцев А. Л. О метрологии электронных электросчетчиков // Электро. Электротехника, электроэнергетика, электротехническая промышленность. 2008. № 2. С. 44–52.

14. Бужинский В. А. О колебаниях жидкости в топливных баках с демпфирующими решетками // Космонавтика и ракетостроение. 2007. № 46. С. 110–120.

15. Писарев Н. С., Стаценко Н. И. Трехточечный авиационный топливомер // Решетневские чтения : материалы XXI Междунар. науч. конф. Красноярск, 2017. Т. 1. С. 468–469.

Akzigitov Revo Avkhadievich – senior lecturer, professor; Reshetnev Siberian State University of Science and Technology, navigation system department. E-mail: akzigitov-r@mail.ru.

Pisarev Nikita Sergeyevich – student; Reshetnev Siberian State University of Science and Technology, navigation system department. E-mail: nike0996@gmail.com.

Statsenko Nikolay Ivanovich – student; Reshetnev Siberian State University of Science and Technology, navigation system department. E-mail: stacenkoni@mail.ru.

Glukharev Artem Renatovich – student; Reshetnev Siberian State University of Science and Technology, navigation system department. E-mail: aptemka.dt@gmail.com.

Tsar'kov Ivan Borisovich – student; Reshetnev Siberian State University of Science and Technology, navigation system department. E-mail: ivan.tsarkov.1996@mail.ru.

Акзигитов Рево Авхадиевич – доцент; Сибирский государственный университет науки и технологий имени академика М. Ф. Решетнева, кафедра пилотажно-навигационных комплексов. E-mail: akzigitov-r@mail.ru.

Писарев Никита Сергеевич – студент; Сибирский государственный университет науки и технологий имени академика М. Ф. Решетнева, кафедра пилотажно-навигационных комплексов. E-mail: nike0996@gmail.com.

Стаценко Николай Иванович – студент; Сибирский государственный университет науки и технологий имени академика М. Ф. Решетнева, кафедра пилотажно-навигационных комплексов. E-mail: stacenkoni@mail.ru.

Глухарев Артем Ренатович – студент; Сибирский государственный университет науки и технологий имени академика М. Ф. Решетнева, кафедра пилотажно-навигационных комплексов. E-mail: aptemka.dt@gmail.com.

Царьков Иван Борисович – студент; Сибирский государственный университет науки и технологий имени академика М. Ф. Решетнева, кафедра пилотажно-навигационных комплексов. E-mail: ivan.tsarkov.1996@mail.ru.

INTER-SATELLITE OPTICAL COMMUNICATION LINK

A. V. Aleksandrov [1]*, A. V. Vasilenko [2], D. O. Korolev [3]

[1] Kirensky Institute of Physics – Federal Research Center "Krasnoyarsk Scientific Center"
Siberian Branch of the Russian Academy of Sciences
50, bldg. 38, Akademgorodok St., Krasnoyarsk, 660036, Russian Federation
[2] JSC "Academician M. F. Reshetnev "Information Satellite Systems"
52, Lenin St., Zheleznogorsk, Krasnoyarsk region, 662972, Russian Federation
[3] Siberian Federal University
79, Svobodny Av., Krasnoyarsk, 660041, Russian Federation
*E-mai: alexa820@mail.ru

A two-level system of data transmission in the optical range is considered between a low-orbit spacecraft located in a sun-synchronous orbit and a repeater satellite located in a geostationary orbit. This topic is rather relevant due to the fact that the rapid development of remote sensing satellites resulted in the increase of the amount of transmitted information, which in consequence introduced new requirements for communication systems. The increase of data transmission rate and severization of requirements for communication systems contributed to the development of one of the most promising areas of space communications, based on the information transmission via a laser channel, due to a high energy concentration and a much higher carrier frequency. The prospects for the application of optical communication systems are designated by lower power consumption, dimensional specifications and the mass of the transceiver equipment of the optical range (compared to radiofrequency range systems).

The article describes the solution of application of optical communication link between a low-orbit spacecraft and a repeater satellite. The main factors that contribute to the attenuation in the process of signal propagation along the route are presented and analyzed. A model of a communication channel between a low-orbit spacecraft and a repeater satellite is provided for a visual image. Two different approaches of mutual guidance and tracking of laser terminals are described for using beacons and without ones. EDRS foreign system is considered as an analogue. The estimation of the main parameters of the communication link is given.

The communication system considered in the article will allow for greater carrier capacity of the data transmission in the optical range between the low-orbit spacecraft and repeater satellite. The application of this system will allow solving problems, including in the interests of any departments and structures of the Ministry of Defense of the Russian Federation, for which the rate of obtaining information is one of the basic requirements for a satellite communication system. The tasks of precise targeting of receiving and transmitting devices arising as a result of narrow beam patterns can be solved with current technical means.

Keywords: optical communication, low-orbit spacecraft, repeater satellite, channel parameters.

МЕЖСПУТНИКОВАЯ ОПТИЧЕСКАЯ ЛИНИЯ СВЯЗИ

А. В. Александров[1]*, А. В. Василенко[2], Д. О. Королев[3]

[1] Институт физики им. Л. В. Киренского СО РАН – обособленное подразделение ФИЦ КНЦ СО РАН
Российская Федерация, 660036, г. Красноярск, Академгородок, 50, стр. 38
[2] АО «Информационные спутниковые системы» имени академика М. Ф. Решетнёва»
Российская Федерация, 662972, г. Железногорск Красноярского края, ул. Ленина, 52
[3] Сибирский федеральный университет
Российская Федерация, 660041, г. Красноярск, просп. Свободный, 79
*E-mai: alexa820@mail.ru

Рассмотрена двухуровневая система передачи данных оптического диапазона между низкоорбитальным космическим аппаратом (НКА), находящимся на солнечно-синхронной орбите, и спутником-ретранслятором (СР), находящимся на геостационарной орбите. Данная тема является весьма актуальной в связи с тем, что стремительное развитие спутников дистанционного зондирования земли привело к повышению объемов пере-

даваемой информации, что в следствии привело к новым требованиям к системам связи. Увеличение скорости передачи данных, повышение требований к системам связи способствовало развитию одного из перспективных направлений космической связи, основанного на передаче информации по лазерному каналу благодаря высокой концентрации энергии и гораздо более высокой частоте несущей. Меньшее энергопотребление, габаритные размеры и масса приемопередающей аппаратуры оптического диапазона (по сравнению с системами радиодиапазона) определяют перспективы применения оптических систем связи.

В статье описано решение использования между НКА и СР оптической линии связи. Приведены и проанализированы основные факторы, вносящие ослабление в процессе распространения сигнала на трассе. Приведена модель для наглядного отображения канала связи между НКА и СР. Описаны два разных подхода взаимного наведения и сопровождения лазерных терминалов с использованием маяков и без маяков. В качестве близкого аналога рассмотрена зарубежная система EDRS. Приведена оценка основных параметров линии связи.

Рассмотренная в статье система связи сможет обеспечить большую пропускную способность при передаче данных в оптическом диапазоне между НКА и СР. Применение данной системы позволит решать задачи, в том числе в интересах любых ведомств и структур МО РФ, для которых скорость получения информации является одним из основных требований, предъявляемых к системе спутниковой связи. Задачи точного наведения приемных и передающих устройств, возникающие как следствие узких диаграмм направленности, можно решить современными техническими средствами.

Ключевые слова: оптическая связь, низкоорбитальный космический аппарат, спутник ретранслятор, параметры канала.

Introduction. One of the promising areas for the development of space communication systems is the application of an optical communication system (OCS). These systems allow for greater carrier capacity with less power consumption, dimensional specifications and weight of transceiver equipment than the radiofrequency range systems currently in use. Wireless laser communication is a type of optical communication using electromagnetic waves of the optical range (light) generated by a laser source transmitted in free space.

Potentially, optical communication systems can provide a high rate of information flow – up to 1–10 Gbit/s and higher, with onboard equipment weight of 35–70 kg [1].

These advantages of optical communication systems in comparison with radiofrequency range systems cause a growing interest to transmitting data between spacecraft in the optical range in the space industry.

At the same time, the application of optical antennas with narrow radiation patterns in laser terminals of low-orbit spacecraft (LOS) and repeater satellites (RS) defines firm requirements for the mutual guidance of antennas axes, which results in a number of technical difficulties.

System description. Fig. 1 shows a schematic image of the considered communication system, which solves the problem of delivering the information from a low-orbit spacecraft (LOS) to a ground information receiving station (GIRS) via a repeater satellite (RS). Information is delivered from the LOS to the RS in the optical range, and from the RS to the GIRS – in the radiofrequency range.

An Earth remote sensing satellite is considered in the function of a LOS. The Earth remote sensing satellite receives the information about the Earth's surface and objects on it, the atmosphere, the ocean, and the upper layer of the earth's crust by means of noncontact methods, when the data recorder is distant from the object under study.

Requests of military departments serve as an effective stimulus for the development of Earth remote sensing systems [2; 3]. In this case, the speed of information delivery to the consumer plays a particularly important role.

The system in question operates in a session mode. The duration of communication sessions is limited by the time of a line-of-sight coverage of laser terminals. In addition, the time of communication sessions is limited by the possible exposure of a solar radiation into the optical receivers, as well as by arrangement features of the communication terminal on the LOS.

Ensuring of mutual detection and guidance of LOS and RS is carried out by using lasers-beacons installed on each spacecraft. These lasers-beacons emit at a wavelength close to 800 nm, ensuring a high visibility of the spacecraft. The use of this wavelength is due to the convenience of recording by means of widely available charge coupled device (CCD) matrices, as well as the possibility of application of spectral separation of the target information (TI) transmitter signal and the beacon signal [4; 5].

During the procedure of mutual detection, the antennas axes of both laser terminals are turned to the calculated angles, the RS laser terminal switches on a beacon radiation source. The LOS laser terminal generates a response in the RS direction during the registration of the beacon beam from the RS at a wavelength close to 800 nm as well. This signal is received by the RS and the system entries into a tracking mode. The tracking mode requires using beacons to maintain the spatial orientation of both spacecraft [6; 7].

The use of beacons is not always necessary, thus in a foreign EDRS system, spatial guidance is performed by means of a collimated beam (TI at 1.06 μm) with using of quadrature detectors instead of an additional beacon [8; 9]. The application of such an approach imposes some limitations – the measurement of the spacecraft orientation requires a very high accuracy.

The system under consideration uses an amplitude modulation of the radiation, which makes it possible to apply the methods of incoherent signal reception. This approach allows reducing the requirements for the applied component base, since it eliminates the need for a device that compensates for the Doppler shift of the carrier wave of the optical range.

In the mutual tracking mode, the LOS laser terminal starts transmitting the TI via the transmitting optical system at a wavelength of 1.55 μm.

At the RS, the optical signal is fed to the avalanche photodetector, then data processing takes place, the useful signal is extracted and formed for delivering to the ground station (GS) in a radiofrequency range. The schematic block diagram of the LOS laser terminal is presented in fig. 2.

The presented parameters of the communication link (table) are calculated for the case when the LOS moves in a sun-synchronous orbit of 700 km in altitude, and the RS is at an altitude of 35.786 km.

Below there are the calculated formulas of the communication channel of LOS – RS.

The power supplied to the receiver is calculated by formula (1) [10]:

$$P_{rec} = P_{tr} G_{tr} G_{rec} L_{weak} L_{sist}, \qquad (1)$$

where P_{tr} is the transmitter power, G_{rec} is the effective gain of the receiving antenna, G_{tr} is the effective gain of the transmitting antenna, L_{weak} is the signal attenuation coefficient in free space, L_{sist} is the path loss of the transmitting and receiving equipment.

The diagram of the radiation power and the power supplied at the receiver input (taking into account the attenuation of the communication link) is presented in fig. 3

The effective gain of the receiving antenna is calculated by formula (2) and depends on the wavelength, and the diameter of the receiving telescope [10]:

$$G_{rec} = \left(\frac{\pi \cdot D}{\lambda} \right)^2, \qquad (2)$$

where λ is the wavelength, D is diameter of the receiving telescope.

The effective gain of the transmitting antenna:

$$G_{tr} = \frac{32}{\theta^2}, \qquad (3)$$

where θ is the width of the angular pattern.

GS - ground station
LOS - low-orbit spacecraft
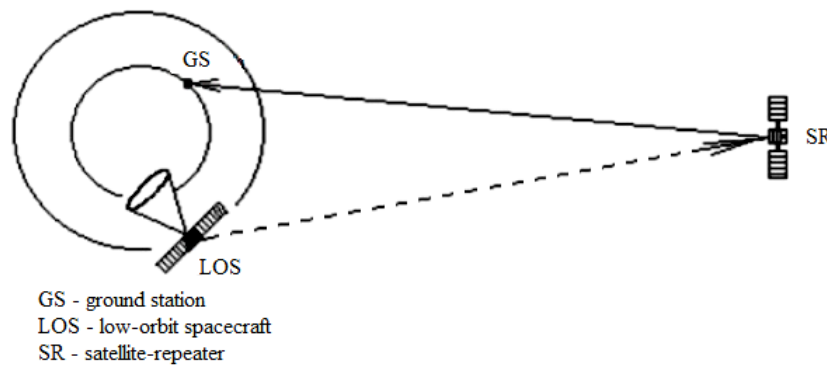SR - satellite-repeater

Fig. 1. Schematic block diagram of a transmission channel
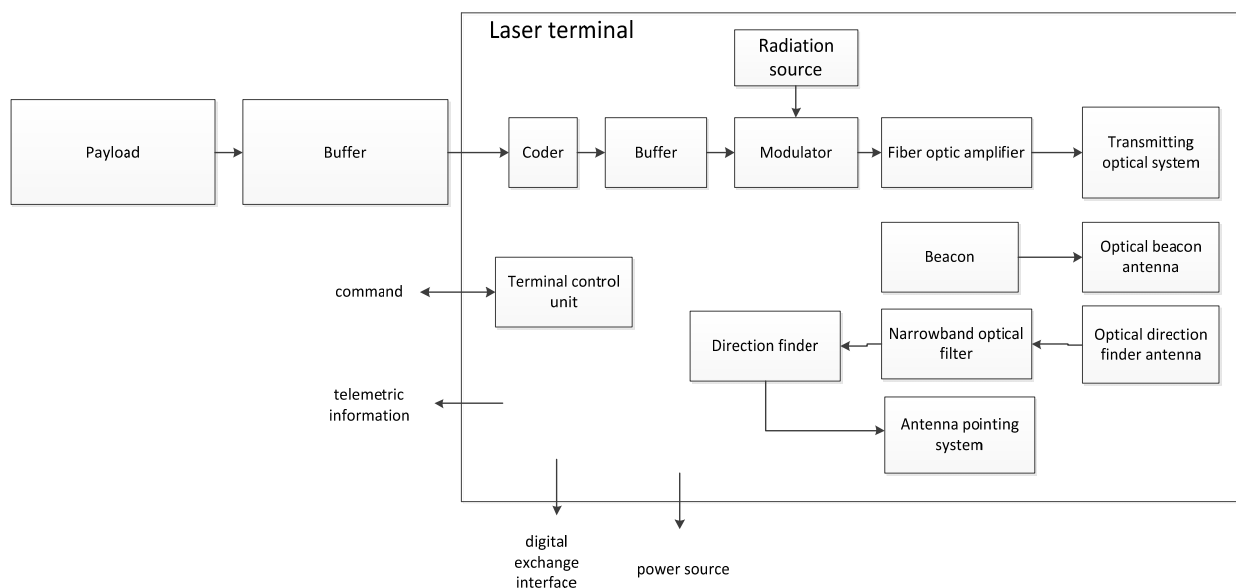
Рис. 1. Структурная схема канала передачи

Fig. 2. Schematic block diagram of the LOS laser terminal

Рис. 2. Структурная схема лазерного терминала НКА

Channel parameters of low-orbit spacecraft – repeater satellite

Parameters	Designation	Value	Units
Wavelength	λ	1.55	um
Transmitting antenna diameter	D_{tr}	0.05	m
Receiving antenna diameter	D_{rec}	0.25	m
Link length of LOS-RS	R	35086 – 41000	km
Transmitter power	P_{tr}	3	dbw
Radiation power at the receiver	P_{rec}	−79.8	dbw
Effective gain of transmitting antenna	G_{tr}	114.4	w
Effective gain of receiving antenna	G_{rec}	105.5	db
Attenuation caused by link length	L_{weak}	−289.08/ −290.4	db
Path loss of receiver, transmitter	L_{sist}	5	db
Receiver bandwidth	dF	200	MHz
Angular pattern width	θ	6.18	sec
Noise power equivalent	NEP	−86.4	db
NEP	M	6.6	db
Number of photons studied in 1 sec	N_{stud}	$3.89 \cdot 10^{18}$	amount
Number of photons arriving at the receiver in 1 sec	N_{rec}	$1.09 \cdot 10^{11}$/ $8.04 \cdot 10^{10}$	amount
Number of photons in 1 bit	N	549.5/402.4	amount
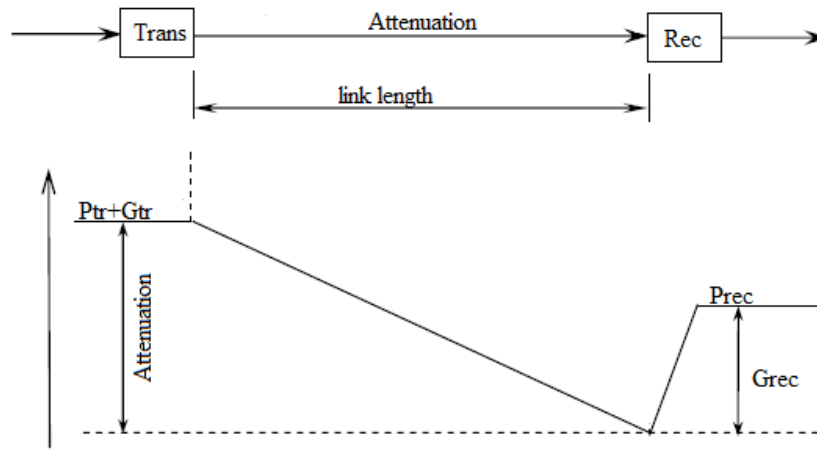
Fig. 3. Diagram representing a communication channel

Рис. 3. Диаграмма представления канала связи

Attenuation in free space depends only on the length of the link [10]:

$$L_{weak} = \left(\frac{\lambda}{4\pi R} \right)^2, \qquad (4)$$

where R is the length of the communication link.

For a complete analysis of the system, we calculate the number of photons emitted by the transmitter and received by the receiver per unit of time.

The number of emitted photons is calculated by formula (5) [10]:

$$N_{bm} = \frac{A}{E}, \qquad (5)$$

where $A = P_{tr} \cdot t$, t is time, E is a quantum energy, calculated by formula (6) [10]:

$$E = \frac{hc}{\lambda}, \qquad (6)$$

where h is Planck's constant ($h = 6{,}63 \cdot 10^{-34}$ J·с), c is the speed of light ($c = 3 \cdot 10^8$ m/s).

The number of photons received during the time t is calculated as follows [10]:

$$N_{rec} = \frac{P_{rec} \cdot t}{h \cdot f}, \qquad (7)$$

where f is a radiation frequency.

Since the relative velocity of a low-orbit spacecraft and a geostationary spacecraft can reach $8 \cdot 10^3$ m/s, and the distance between them is $3.086 \cdot 10^7$ m, it becomes necessary to take into account such effects as light aberration and the Doppler effect [11; 12].

Light aberration. Light aberration refers to the difference in a visible direction of a light source from the real direction to it which is caused by the finiteness of light speed [13]. Let us consider fig. 4, which shows the exchange of signals by LOS and RS. Suppose, at time A, the LOS emits a signal in the direction of the RS. At time B, when the RS receives a signal from the LOS, the latter will have time to move some distance l, and at time B, when the signal from the RS reaches the LOS orbit, it will have time to move from position A to $2l$. In order to "get"

into the LOS, the RS must send a response at a certain angle θ with respect to the direction of the received signal. The angle θ can be calculated as:

$$\theta = 2\arcsin\left(\frac{l}{R}\right), \qquad (8)$$

where *R* is the distance between the LOS and RS at time *B*.

Fig. 4. Aberration of the speed of light

Рис. 4. Аберрация скорости света

When the LOS is moving along a sun-synchronous orbit, its relative speed can be estimated from above as 8 km/s, and the angle which the transmitting antenna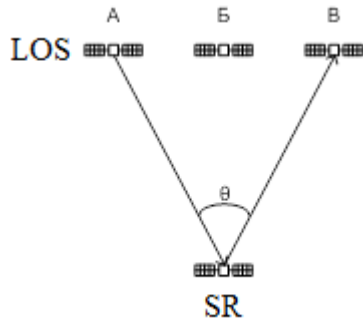 of the RS should be deflected at, relative to the visible direction to the LOS, is 11 arc/s. To account for this effect, it is necessary to install a high-speed corrector for light aberration, which is an additional device.

Doppler effect

Let us consider the longitudinal "linear" Doppler effect as the strongest [14; 15], which is described by formula (9):

$$\nu' = \nu\sqrt{\frac{1-V/c}{1+V/c}}, \qquad (9)$$

where *ν'* and *ν* are radiation frequencies in fixed and moving coordinate systems, *V* is the velocity of a mutual motion of the coordinate systems, *c* is the speed of light.

The change in wavelength caused by the longitudinal Doppler effect can be written as:

$$\Delta\lambda = \frac{c}{\nu} - \frac{c}{\nu'}. \qquad (10)$$

For an optical channel using a wavelength of 1.55 μm, the calculated change in wavelength caused by the Doppler effect was 0.04 nm.

Conclusion. The considered two-level communication system will provide greater carrier capacity, with less power consumption, dimensional specifications and weight of the transceiver equipment, than the radiofrequency range systems being currently in use. The application of this system will allow solving problems, including in the interests of any departments and structures of the Ministry of Defense of the Russian Federation, for which the rate of obtaining information is one of the basic requirements for a satellite communication system.

The communication channel of LOS – RS is a homogeneous medium, where signal attenuation is determined by the length of the communication link in the process of propagation.

However, there is a number of technical problems which have to be solved for the implementation of laser communication channels between LOS and RS:

– high guidance accuracy, mutual tracking at long distances and at space velocities of carriers are necessary;

– electrooptical equipment is becoming more complex: precision optics, micrometrical mechanics, semiconductor and fiber lasers, highly sensitive receivers.

The following conditions are to be considered as well:

– the influence of solar illumination, resulting from exposure of sun beams directly into the viewing sector of the optical receiver;

– ensuring the thermal mode of antennas.

References

1. Maral G. Satellite communication system. John Wiley & Sons Ltd, Publication, 2009, 743 p.

2. Atrohov A. Yu. [Problems of remote sensing of the earth by modern radar methods]. *XXXVI mezhdunarodnaya nauchno-prakticheskaya konferentsiya "Nauchnoe soobshchestvo studentov XXI stoletiya. Tekhnicheskie nauki"* [XXXVI International Scientific and Practical Conference "Scientific community of students of the XXI century. Technical Sciences]. Novosibirsk, 2015, No. 9 (35), P. 168 (In Russ.).

3. Akimov A., Terekhov S., Danilov D., Shevchuk D. [Prospects for increasing the frequency of observation by space remote sensing Systems]. *Tekhnologii i sredstva svyazi.* 2016, No. 6 (117), P. 85–91 (In Russ.).

4. Heine F., Troendle D. Heine F. Progressing towards an operational optical data relay service. Free-Space Laser Communication and Atmospheric Propagation XXIX, 2017. P. 7.

5. Glindemann A., Hippler S. Adaptive optics on large telescopes. Germany, Heidelberg, 1999, 44 p.

6. Zuev V. E. *Rasprostranenie lazernogo izlucheniya v atmosfere* [Propagation of laser radiation in the atmosphere]. Moscow, Radio i Svyaz' Publ., 1981, 288 p.

7. Henniger H., Wilfert O. An introduction to free-space optical communications. Germany, Wessling, 2010, 10 p.

8. Sodnik Z., Sans M. Extending EDRS to Laser Communication from Space to Ground. *Proc. International Conference on Space Optical Systems and Applications (ICSOS)*, 2012, October 9–12 P. 6.

9. Maini A., Agrawal V. Satellite Technology. John Wiley & Sons Ltd, Publication. 2011, P. 696.

10. Wilfert O., Kolka Z. Statistical model on free-space optical data link. *Proceedings of SPIE.* 2004, Vol. 5550, P. 203.

11. Vasilenko A. V., Kashkin V. B. [Evaluation of the influence of astronomical refraction on an optical satellite link]. *Zhurnal Sibirskogo federal'nogo universiteta. Inzheneriya i tekhnologiya.* 2012, Vol. 5, No. 3, P. 353–357 (In Russ.).

12. Aleksandrov A. V., Melnikov P. V., Tverdochlebov S. S., Reshetnikov S. Yu., Milko D. S. [Protected satellite communication model based on System Vue]. *Nauchnaya sessiya TUSUR* [Scientific session TUSUR]. Tomsk, 2015, P. 60–62 (In Russ.).

13. Caplan D. Laser communication transmitter and receiver design. *Journal Optical and fiber communication report.* 2007, P. 138.

14. Roddy D. Satellite communication, Prentice-Hall Inc., Publication, 1989, P. 656.

15. Heine F., Troendle D. Progressing towards an operational optical data relay service. Free-Space Laser Communication and Atmospheric Propagation XXIX, 2017. P. 7.

Библиографические ссылки

1. Maral G. Satellite communication system / John Wiley & Sons Ltd, Publication, 2009. 743 p.

2. Атрохов А. Ю. Проблемы дистанционного зондирования земли современными радиолокационными методами // XXXVI международная научно-практическая конференция «Научное сообщество студентов XXI столетия. Технические науки», Новосибирск, 2015. №9(35) 168 с.

3. Перспективы повышения периодичности наблюдения космическими системами дистанционного зондирования Земли / А. Акимов, С. Терехов, Д. Данилов, Д. Шевчук // Технологии и средства связи. 2016. № 6 (117). С. 85–91.

4. Heine F., Troendle D. Heine F. Progressing towards an operational optical data relay service // Free-Space Laser Communication and Atmospheric Propagation XXIX. 2017. 7 p.

5. Glindemann A., Hippler S. Adaptive optics on large telescopes. Germany, Heidelberg. 1999. 44 p.

6. Зуев В. Е. Распространение лазерного излучения в атмосфере. М. : Радио и связь, 1981. 288 с.

7. Henniger H., Wilfert O. An introduction to free-space optical communications. Germany, Wessling, 2010. 10 p.

8. Sodnik Z., Sans M. Extending EDRS to Laser Communication from Space to Ground // Proc. International Conference on Space Optical Systems and Applications (ICSOS). 2012, October 9–12. 6 p.

9. Maini A., Agrawal V. Satellite Technology. John Wiley & Sons Ltd, Publication. 2011. 696 p.

10. Wilfert O., Kolka Z. Statistical model on free-space optical data link // Proceedings of SPIE. 2004. Vol. 5550. P. 203.

11. Василенко А. В., Кашкин В. Б. Оценка влияния астрономической рефракции на оптическую спутниковую линию // Журнал Сиб. федер. ун-та. Инженерия и технология. 2012. Т. 5, № 3. С. 353–357.

12. Защищенная модель спутниковой связи на базе System Vue / А. В. Александров, П. В. Мельников, С. С. Твердохлебов [и др.] // Научная сессия ТУСУР. Томск, 2015. С. 60–62.

13. Caplan D. Laser communication transmitter and receiver design // Journal Optical and fiber communication reports. 2007. 138 p.

14. Roddy D. Sattelite communication. Prentice-Hall Inc., Publication, 1989. 656 p.

15. Heine F. Progressing towards an operational optical data relay service / F. Heine, D. Troendle // Free-Space Laser Communication and Atmospheric Propagation XXIX. 2017. 7 p.

Aleksandrov Aleksandr Vladimirovich – Postgraduate student; Kirensky Institute of Physics – Federal Research Center "Krasnoyarsk Scientific Center" Siberian Branch of the Russian Academy of Sciences. E-mail: alexa820@mail.ru.

Vasilenko Aleksandr Vladimirovich – Leading Engineer; JSC "Academician M. F. Reshetnev "Information Satellite Systems". E-mail: a.v.vasilenko@mail.ru.

Korolev Dmitry Olegovich – Postgraduate student; Siberian Federal University. E-mail: korolyov.93@gmail.com.

Александров Александр Владимирович – аспирант; Институт физики им. Л. В. Киренского СО РАН – обособленное подразделение ФИЦ КНЦ СО РАН. E-mail: alexa820@mail.ru.

Василенко Александр Владимирович – ведущий инженер; АО «Информационные спутниковые системы» имени академика М. Ф. Решетнёва». E-mail: a.v.vasilenko@mail.ru.

Королев Дмитрий Олегович – аспирант; Сибирский федеральный университет. E-mail: korolyov.93@gmail.com.

INVESTIGATION OF THE METROLOGICAL CHARACTERISTICS OF THE PULSESPI SYSTEM APPLIED TO THE PRECISION INSPECTION OF THERMAL DEFORMATIONS

P. S. Zavyalov[1], M. S. Kravchenko[1*], V. V. Urzhumov[1], V. A. Kuklin[2], V. M. Mikhalkin[2]

[1]Technological Design Institute of Scientific Instrument Engineering SB RAS
41, Russkaya St., Novosibirsk, 630058, Russian Federation
[2] JSC "Academician M. F. Reshetnev "Information Satellite Systems"
52, Lenin St., Zheleznogorsk, Krasnoyarsk region, 662972, Russian Federation
[*]E-mail: max@tdisie.nsc.ru

High-precision and reliable inspection of thermal deformations is necessary in terms of simulating the effects of space in the ground-based experimental processing of antennas and mirror systems of spacecrafts. Inspection of objects up to 1.5 m in size is considered in the paper. In practice, it can reach sizes up to 10 m. Requirements for thermal deformation are in range of 10–200 micrometers. The deformable surface is rough (Ra » λ_{optic}). The measurement error, however, should not exceed ± 1 micron.

The electronic speckle pattern interferometry (ESPI) method is the most suitable for solving this problem. The method allows to inspection objects with a randomly inhomogeneous surface. The method assumes that it is necessary to calculate the wave phase values from the recorded picture by the digital matrix. It is the phase that contains information about the deformation, and the spatial phase shift method is used to calculate it.

One of the measuring systems based on this method is the measuring system PulsESPI (Carl Zeiss Optotechnik GmbH production, Germany). It has a high sensitivity which is about 50 nm. However, this measuring system is designed for single measurements. In this regard, an additional software module for processing and visualization the result of a series of several hundred measurements has been developed.

The experimental test bench with a test object has been developed to research the metrological characteristics of the PulsESPI system in accordance with thermal deformations measurements (multiple determinations). The PulsESPI system and the Renishaw XL-80 interferometer introduced into register of measuring instrumentation of Russian Federation were located on different sides of the object 1.5 m in size. As a result of measuring the surface displacement measured by the Renishaw XL-80 interferometer and its corresponding point from the PulsESPI system deformation map are compared. Three types of tests were carried out at the developed bench. The root-mean-square deviation of single measurements was no more than ± 0.2 μm. Error was no more than ± 1 μm when the series of measurements was conducted in which a total strain of 200 μm was obtained. The results obtained suggest the possibility of using this system for high-precision inspection of thermal deformations of large objects.

Keywords: electronic speckle pattern interferometry, method of spatial phase shift, measurement system for thermal deformations, thermal deformations measurement.

ИССЛЕДОВАНИЕ МЕТРОЛОГИЧЕСКИХ ХАРАКТЕРИСТИК СИСТЕМЫ PULSESPI ПРИМЕНИТЕЛЬНО К ПРЕЦИЗИОННОМУ КОНТРОЛЮ ТЕРМОДЕФОРМАЦИЙ

П. С. Завьялов[1], М. С. Кравченко[1*], В. В. Уржумов[1], В. А. Куклин[2], В. М. Михалкин[2]

[1]Конструкторско-технологический институт научного приборостроения СО РАН
Российская Федерация, 630058, г. Новосибирск, ул. Русская, 41
[2]АО «Информационные спутниковые системы» имени академика М.Ф. Решетнёва»
Российская Федерация, 662972, г. Железногорск Красноярского края, ул. Ленина, 52
*E-mail: max@tdisie.nsc.ru

В условиях имитации воздействия космического пространства при наземной экспериментальной обработке антенн и зеркальных систем космических аппаратов необходим высокоточный и надёжный контроль термодеформаций. В работе рассматривается контроль объектов размером до 1,5 м, но на практике размер

может достигать 10 м. Требования по величине измеряемой термодеформации находится в пределах 10–200 мкм. Деформируемая поверхность обычно является шероховатой (Ra » $\lambda_{оптич}$). Погрешность измерений при этом должна быть порядка 1 мкм.

Методом, отвечающим требованиям данной задачи, является метод электронной спекл-интерферометрии (ESPI). Данный метод позволяет контролировать объекты со случайно-неоднородной поверхностью. При использовании данного метода вычисляют значение фазы волнового фронта, регистрируемого цифровой матрицей камеры. Фаза содержит информацию о деформации, а для ее вычисления используется метод пространственного фазового сдвига.

Одной из измерительных систем, основанных на данном методе, является измерительная система Puls-ESPI (производство Carl Zeiss Optotechnik GmbH, Германия). Она обладает высокой чувствительностью, которая составляет порядка 50 нм. Однако данная измерительная система предназначена для выполнения единичных измерений. В связи с этим разработан дополнительный программный модуль для обработки и визуализации серии из нескольких сотен измерений.

Для исследования метрологических характеристик системы PulsESPI, применительно к измерению термодеформаций (многократные измерения), разработан экспериментальный стенд с тестовым объектом размером 1,5 м. С разных сторон объекта размещались система PulsESPI и интерферометр Renishaw XL-80, внесенный в Госреестр средств измерений РФ. В качестве результатов сравнивались смещение поверхности, измеренное интерферометром Renishaw XL-80, и соответствующая ей точка с карты деформаций системы PulsESPI. На разработанном стенде проведено три вида испытаний. Среднеквадратическое отклонение единичных измерений составило не более ± 0,2 мкм. При проведении серии измерений, в которых получена суммарная деформация 200 мкм, ошибка составила не более ± 1 мкм. Полученные результаты позволяют говорить о возможности применения данной системы для высокоточного контроля термодеформаций крупногабаритных объектов.

Ключевые слова: электронная спекл-интерферометрия, метод пространственного фазового сдвига, система измерения термодеформаций, измерение термодеформаций.

Introduction. To determine the temperature effect on the geometrical parameters of spacecraft elements under conditions of simulation influence of space factors, high-precision and reliable inspection of thermal deformations of objects about 1.5 m in size is necessary. Special attention is paid to reflectors and mirror systems, which thermal deformations should be measured with an accuracy of 1 micrometers. The maximum deformation for the entire test period is about 200 μm, and the error of its measurement should be no more than 1 μm.

The objects to be used in tests to determine thermal deformations of surfaces are carbon fiber reflectors, the surface of which is usually rough (Ra » λ_{optic}). The diameter of the objects does not exceed 1.5 m, and the depth of its central part relative to the edges is no more than 0.5 m. At the same time, the distance between the object and the measurement system is in the range from 1 to 6 m. Horizontal vacuum installation unit with the capacity size of 600 m^3 will be used to simulate the effects of space. Tests are conducted under conditions of simulation influence of space factors ($p \approx 1.333 * 10{-}3$ Pa; $t \pm 150\,°$ C).

The measurements of a test object made of aluminum with dimensions of 1.5 x 1.5 m and having thickness of 5 mm were made as part of this work. The surface of the object was rough. Tests were conducted under normal conditions.

Method of measurement. A review of contactless methods for measuring large-sized objects with a rough surface showed that the required metrological characteristics of the inspection are provided by the speckle-interferometry method [1–3]. In order to inspection the thermal deformations of spacecraft elements, it is necessary to use the modification of the method with the use of electronic image registration devices – the method of electronic speckle pattern interferometry (ESPI). This method has been widely used for non-destructive testing of deformations [4], displacements [5], vibrations [6] of various kinds of the studied environments, and also, unlike standard methods of interferometry, this method makes it possible to inspection objects with an optically rough surface (randomly heterogeneous), which most of the elements of the apparatus in the aerospace industry possess.

The method of speckle interferometry makes relative measurements, at which changes in the surface shape between the initial and final states are recorded. Wherein, the shape of the object can be arbitrary. The interference pattern is obtained both on flat and on volumetric objects. At the same time, the depth of the object should not exceed the value of half the coherence length of the laser interferometer.

In the optical scheme of a speckle interferometer, the coherent radiation of the laser 1 is guided by the mirror 3 and scattered by the lens 4 on the surface of the object 7 (fig. 1) [7].

The spatial separation of the reference and object arm occurs on the beam splitter 2. Then, the addition of the reference wave passing through the lens 5 and directed by the beam splitter 8 is performed with the object scattered by the object formed by the lens 6. The intensity of final speckle pattern distribution depends on relative phase shift of these waves formed as a result of the deformations on the object 7.

Digital camera 9 registers the initial and deformed state of the object in the form of speckle images, which are described by formula (1) [8]. The difference of the illumination vector $\vec{k}_o$ and the observation vector $\vec{k}_н$ gives the sensitivity vector $\vec{s}$ of the whole system. Deformations are recorded in the direction of this vector. As

a result of performing a number of arithmetic operations, computer 10 forms a picture of interference fringes (fig. 2), which is decoded and transformed into the field of displacements of the test surface.

$$I_{result} = I_{obj} + I_{refer} + 2\sqrt{I_{obj}I_{refer}}\cos(\varphi + \Delta\varphi). \qquad (1)$$

Information about the change in the surface of the object carries a change in the phase φ of the object wave. To calculate it from formula (1), it is also necessary to know two other unknowns: the intensity of the reference I_{refer} and the intensity of the subject I_{obj} waves.

Thus, to determine these three variables, it is necessary to register two more images that will have a known phase shift $\Delta\varphi$. At the same time, during the acquisition of all three images, the object must remain stationary and not undergo any changes (fig. 3).
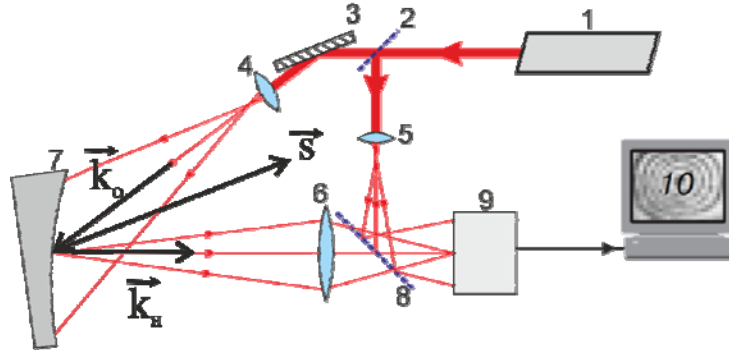

Fig. 1. Key diagram of the speckle interferometer

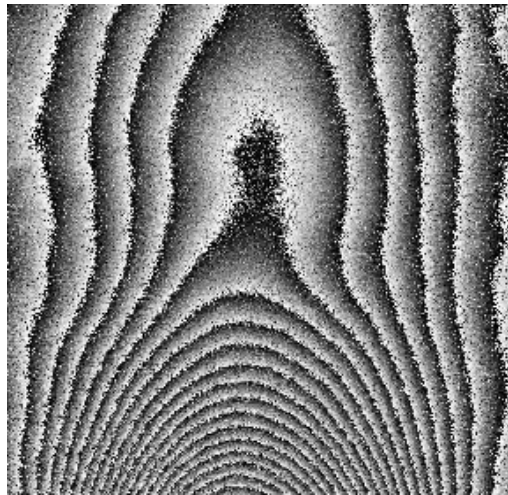Рис. 1. Принципиальная схема спекл-интерферометра

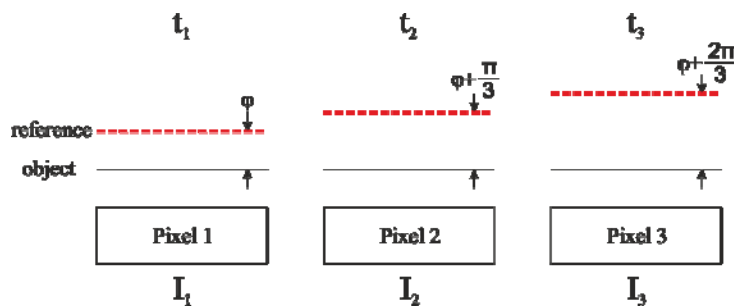Fig. 2. Interference fringes

Рис. 2. Интерференционные полосы

Fig. 3. Temporal phase shift method
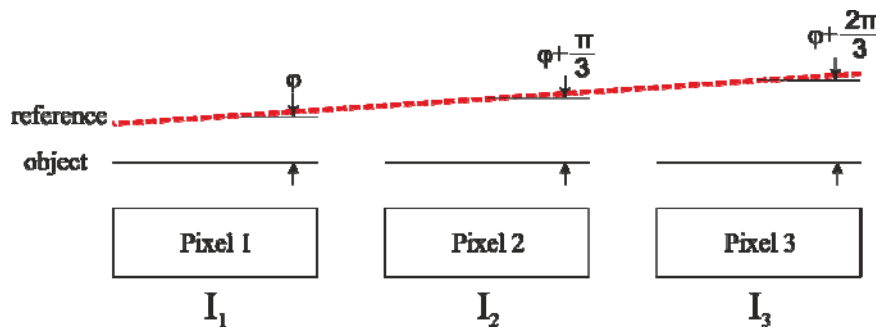
Рис. 3. Метод временного сдвига

Fig. 4. Spatial phase shift method

Рис 4. Метод пространственного сдвига

For the π/3 shift, we obtain a system of three equations 1. Solving it, we obtain formula (2) for determining the phase. This is the time shift method. In practice, the sequential acquisition of three images with a motionless object is often impossible.

$$\varphi = \arctan \sqrt{3}\, \frac{I_{\text{result 1}} - I_{\text{result 2}}}{2I_{\text{result 1}} - I_{\text{result 2}} - I_{\text{result 3}}} \,. \qquad (2)$$

Another way to obtain a system of three equations for calculating the phase is the spatial phase shift method [9]. Reference wave $I_{\text{refer.}}$ is projected onto the matrix at a certain angle, thereby setting the known phase shift between adjacent pixels. As a result, you can get one image and, moving it pixel-by-pixel, get the values of $I_{\text{result 1}}$, $I_{\text{result 2}}$, $I_{\text{result 3}}$. Substituting the obtained values of illumination in expression 2, we obtain the phase φ (fig. 4).

The composition of the measuring system. One of the measuring systems based on this method is the system for measuring thermal deformations of surfaces PulsESPI (hereafter – PulsESPI), manufactured by Carl Zeiss Optotechnik GmbH, Germany (fig. 5). Its work is based on the spatial phase shift method. The sensitivity of this system is less than the value of the wavelength of optical radiation and is about 50 nm. It shows good results in the quantitative analysis of the correlation fringes of high contrast obtained using a pulsed laser [10; 11]. Moreover, for work in conditions of a thermal pressure chamber simulating the climatic conditions of a spacecraft, it is not always possible to create ideal conditions for the stability of the base. In this case, the application of the double-pulse laser mode [12–14] is also important. It is also known that the PulsESPI system was used to measure the deformations of the reflector in the thermal vacuum chamber in the DLR in Berlin [15; 16].

The main components of the PulsESPI system are: synchronization unit 1, data analysis system 2 (FRAMESplus), HLS-R20 ruby pulsed laser 3 (wavelength 694 nm, pulse energy 1 J, pulse duration 20 ns, coherence length 1 m), optics 4, CCD camera 5 (resolution 1280 × 1024 pixels, pixel size 6.7 x 6.7 microns).

The data analysis system (FRAMESplus) is designed to work with a single measurement of deformation. Cycle processing from several single measurements is possible using additional software packages. At the same time, this processing takes a long time. Therefore, for processing and analyzing a series of measurements, an additional software module has been developed that allows one to load source data into FRAMESplus automatically and save the results in a separate file. With this software module it is possible to process and visualize a series of several hundred measurements with minimal operator involvement.

System testing. To test the PulsESPI system in order to determine its metrological characteristics, a bench has been developed, the scheme of which is shown in fig. 6.

An aluminum sheet 2 with dimensions of 1.5 × 1.5 m and a thickness of 5 mm is used as the test object. The elements of the spacecraft, in turn, may have a reflectivity different from aluminum. Therefore, in the process of setting up the PulsESPI system, one of the stages of adjustment is to adjust the brightness of the object beam. The reference beam in all experiments has a similar intensity, and the object beam is adjusted to it. For this, the possibility of changing the object beam diameter and the diameter of the aperture diaphragm of the camera lens is provided.

The PulsESPI 1 system is placed at a distance of no more than 6 m on one side of the object, and on the other side of the sheet a reflector 3 and the Renishaw XL-80 4 displacement interferometer are placed. The object is rigidly fixed to the inflexible columns 5, thereby providing the necessary rigidity. The surface area measured by the Renishaw XL-80 is deformed by the actuator 6. The measurement results compare the displacement readings recorded by the Renishaw XL-80 and the corresponding point from the deformation map obtained by the PulsESPI system. This is possible due to the fact that the sensitivity vector $\vec{s}$ of the PulsESPI system and the direction of measurement of the linear movement of the Renishaw XL-80 coincide.

The Renishaw XL-80 interferometer and object columns are mounted on a massive base 7, which ensures their immobility relative to each other during the tests. To ensure the accuracy of measurements, external sources of vibrations and fluctuations of the measuring point were eliminated, optical paths were isolated, the synchronicity of reading registration and the PulsESPI system at the level of not more than 0.01 s. was provided.

Three types of tests were carried out:

1. *Determination of measurement error between adjacent frames.* In the process of testing the object is stationary, it has no effect. One hundred and twenty frames are recorded. Fig. 7 shows an example of a decoded interference pattern and a color matching scale in the image of

the deformation value. It can be seen that the right, left and lower parts of the object are not deformed. These areas correspond to the columns and the area measured by the Renishaw XL-80 (indicated by a white mark), which is stressed by the actuator. The upper and central parts of the object are free and can oscillate, which can be observed on the deformation map.

Fig. 8 shows a histogram of the measurement error distribution frequencies: the difference in measurements at a point obtained from the deformation map of the PulsESPI system and measured by the Renishaw XL-80 interferometer. The standard deviation was 0.17 μm.

2. Determination of the measurement range between two adjacent frames. The object is stationary, the area measured by the Renishaw XL-80 is deformed (indicated by a white mark). The magnitude of the deformation during the test is constantly increasing. It starts with a value of 0.5 μm between adjacent frames and ends with a value of 10 μm. It is necessary to determine at what amount of deformations the interferograms will be correctly processed.

Fig. 9 shows an example of a decoded interference pattern and a color matching scale in the image of the deformation value.

It can be seen that the right and left parts of the object corresponding to the columns, are not deformed. At the same time, the area measured by the Renishaw XL-80 is deformed by an actuator by a value of about 10 μm. Because of this, there is a pass of the fringes in the lower part of the object when decoding the deformation map (areas are marked with white rectangles). When an object is deformed by an actuator of about 5 μm, no pass of the friges is observed (fig. 10).

Fig. 11 shows the difference between the readings of the Renishaw XL-80 interferometer and the PulsESPI system. The difference is random up to a deformation value of 6 μm, and its value is similar to the error value of test 1. However, with a deformation of 7 μm or more, when a pass of the fringes occurs, the error increases and begins to be systematic.

3. Determination of the total range of deformation measurements at which the measurement error does not exceed 1 μm. The object is stationary, the area measured by the Renishaw XL-80 is deformed (indicated by a white mark). The value of the deformation during the test is constant and equal to 5 μm (fig. 10). Seventy frames are registered and thus the total deformation obtained for the entire test is of about 350 microns.

Fig. 12 shows the difference between the accumulated readings of the Renishaw XL-80 interferometer and the PulsESPI system. It can be seen that the difference in readings is less than 1 μm up to a value of 230 microns.
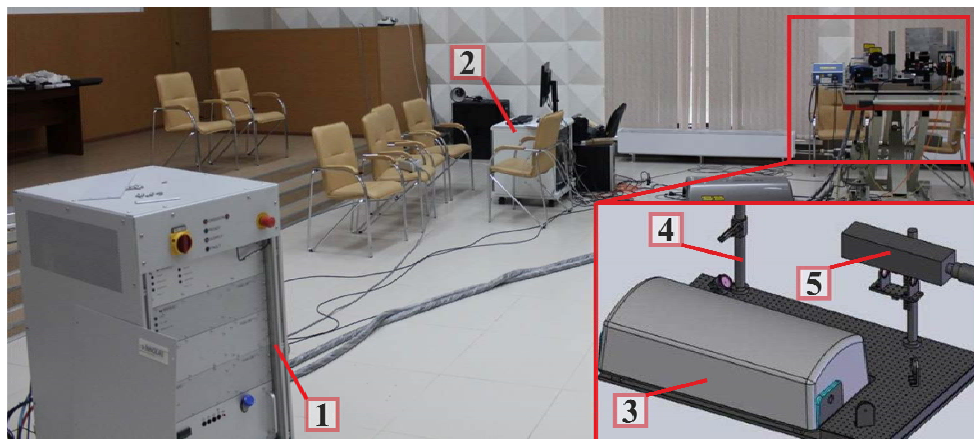
Fig. 5. General view of the PulsESPI System

Рис. 5. Общий вид системы PulsESPI
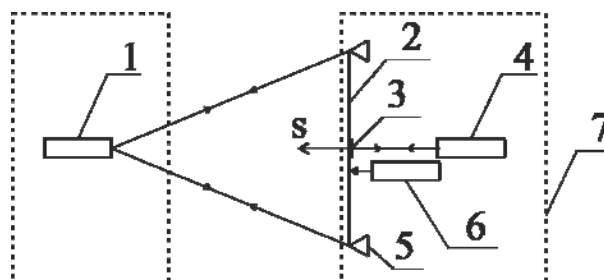
Fig. 6. Test bench layout of the PulsESPI

Рис. 6. Схема стенда для испытаний системы PulsESPI
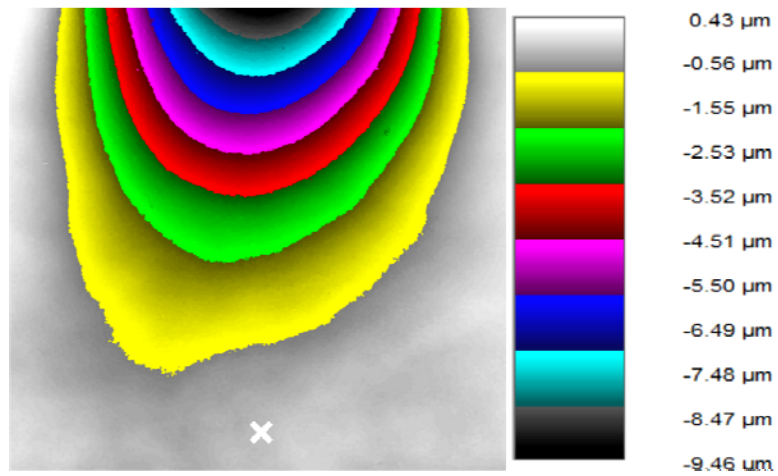
Fig. 7. Object deformation map. Test 1 (deformation at point 0 microns)

Рис. 7. Карта деформаций объекта (деформация в точке 0 мкм)
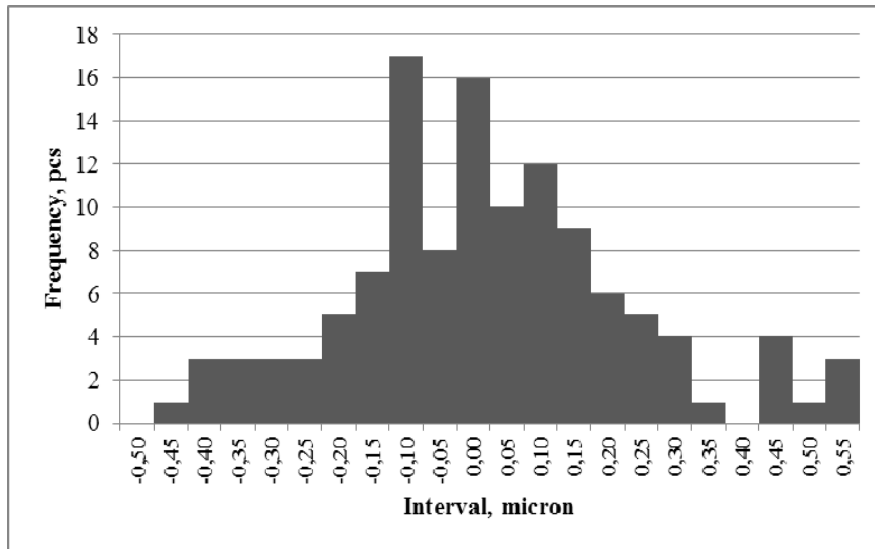
Fig. 8. Error frequency histogram. Test 1

Рис. 8. Гистограмма частот ошибок
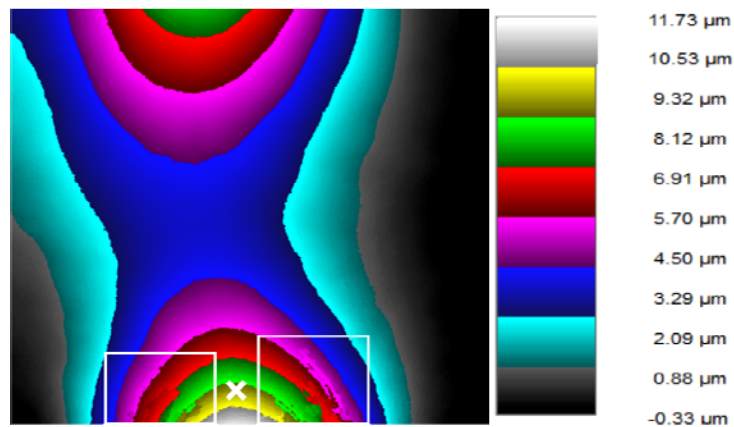
Fig. 9. Object deformation map. Test 2 (deformation at point 10 microns)

Рис. 9. Карта деформаций объекта (деформация в точке 10 мкм)

215
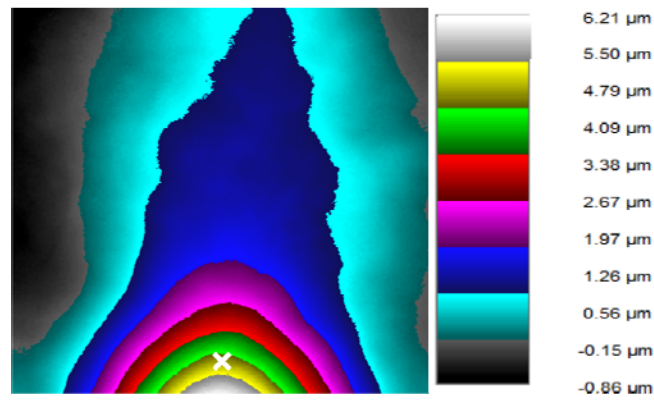
Fig. 10. Object deformation map. Test 3 (deformation at point 5 microns)

Рис. 10. Карта деформаций объекта (деформация в точке 5 мкм)
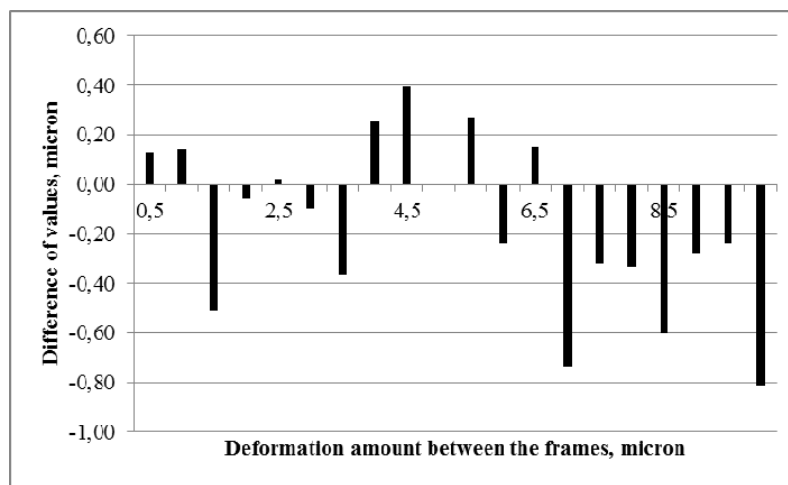
Fig. 11. The difference between the measurements of the Renishaw XL-80 interferometer and the PulsESPI System. Test 2

Рис. 11. Разница показаний интерферометра Renishaw XL-80 и системы PulsESPI
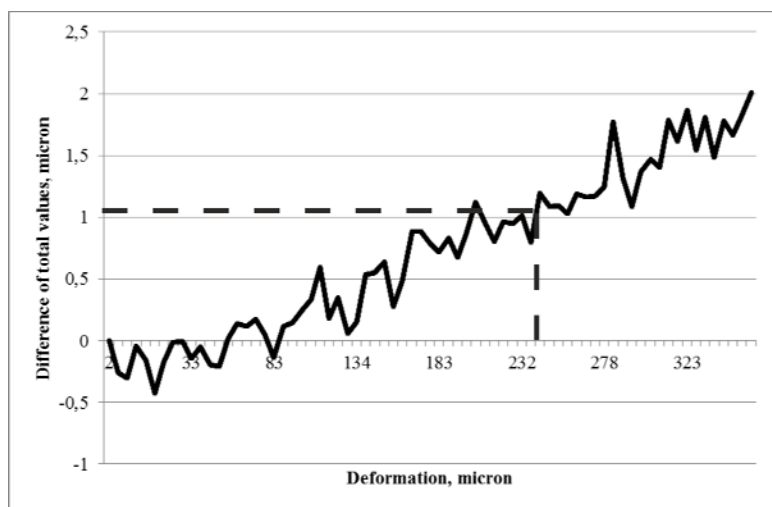
Fig. 12. Difference of total measurements of the Renishaw XL-80 interferometer and the PulsESPI System. Test 2

Рис. 12. Разница суммарных показаний интерферометра Renishaw XL-80 и системы PulsESPI

A possible reason for the appearance of an accumulating error is the instability of the temperature of the room in which the tests were conducted.

When tested in conditions simulating the impact factors of outer space two changes will occur in the optical measurement scheme: a window will be added, by means of which optical radiation will be brought inside the vacuum unit and the refractive index of the medium will change.

The presence of a vacuum has a positive effect on the measurements, since there will be no air flow, and the change in the temperature of the medium will not affect it. Due to the relativity of measurements, the window will not introduce an error in the measurement results. Error will occur only if there is a temperature gradient on the window [17].

Conclusion. As part of this work, the study of the PulsESPI measuring system was carried out, based on the method of electronic speckle pattern interferometry. This method performs the inspection of changes of the object surface relative to the initial state. To test the PulsESPI system for the purpose of studying the metrological characteristics, a test bench has been developed. As a result of testing, the following data were obtained: the maximum deformation between two consecutive measurements (frames) is of no more than 5 μm (with a larger step, the fringes gap occurs and, accordingly, the deformation value is calculated incorrectly); the maximum total deformation for the entire test period, at which the error does not exceed ± 1 μm, is no more than 200 μm. The results obtained and the chosen measurement method allow us to speak about the possibility of using this system for high-precision inspection of thermal deformations of large-sized objects, such as reflectors and elements of mirror systems of spacecraft under conditions of simulation of space impact factors.

References

1. Franson M. *Optika speklov* [Speckle optics]. Moscow, Mir Publ., 1980, 171 p.

2. De la Torre I. M., Hernandez-Montes M. del S., Flores-Moreno J. M., Santoyo F. M. Laser speckle based digital optical methods in structural mechanics: A review. *Optics and Lasers in Engineering*, 2016, Vol. 87, P 32–58.

3. Ulyanov S. S. [What is speckle]. *Sorosovskiy Obrazovatel'nyy zhurnal*. 1999, No. 5, P. 112–116 (In Russ.).

4. Arai Y. Three-dimensional shape measurement beyond the diffraction limit of lens using speckle interferometry. *Journal of modern optics*. 2018, Vol. 65, No. 16, P. 1866–1874.

5. Aksenov E. A., Shmatko A. A., Zvorsky V. I., Kravchuk A. S. [Noncontact speckle interferometric meter for small displacements]. *Radioelectronic and computer systems*. 2008, No. 1 (28), P. 15–19.

6. Stetson K. A. Vibratory strain field measurement by transverse digital holography. *Applied Optics*. 2015, Vol. 54, No. 27, P. 8207–8211.

7. Pedrini G., Tiziani H. J. Double-pulse electronic speckle interferometry for vibration analysis. *Applied optics*. 1994, Vol. 33, No. 34, P. 7857–7863.

8. Vest Ch. *Golograficheskaya interferometriya* [Holographic interferometry]. Moscow, Mir Publ., 1982, 504 p.

9. Kujawinska M., Wojciak J. Spatial phase shifting techniques of fringe pattern analysis in photomechanics. *Second International Conference on Photomechanics and Speckle Metrology*, Proc. SPIE, 1991, Vol. 1554B, P. 503–513.

10 Cookson T. J., Butters J. N., Pollard H. C. Pulsed laser in electronic speckle pattern interferometry. *Optics and Laser Technology*. 1978, Vol. 10, P. 119–124.

11. Tyrer J. R. Application of pulsed holography and double pulsed electronic speckle pattern interferometry to large vibrating engineering structures. *Optics in Engineering Measurement*. 1985, Vol. 599, P. 181–185.

12. Spooren R. Double-pulse subtraction TV holography. *Optical Engineering*. 1992, Vol. 31, No. 5, P. 1000–1007.

13. Pedrini G., Pfister B., Tiziani H. Double pulse-electronic speckle interferometry. *Journal of Modern Optics*. 1993, Vol. 40, No. 1, P. 89–96.

14. Van der Auweraer H., Steibichler H., Haberstok C. et al. Industrial applications of pulsed-laser ESPI vibration analysis. *Proceedings of the International Modal Analysis Conference – IMAC*, Kissimmee, FL, United States, 2001, Vol. 1, P. 490–496.

15. Nösekabel E. H., Ernst T., Haefker W. Measurement of the Thermal Deformation of a Highly Stable Antenna with Pulse ESPI. *18th International Congress on Photonics in Europe*, Proc. SPIE, Munich, Germany, Proc. SPIE, 2007, Vol. 6616, P. 18–21.

16. Ernst T., Linke S., Lori M., Fasold D., Haefker W., Nösekabel E-H., Santiago-Prowald J. Highly Stable Q/V Band Reflector Demonstrator Manufacturing and Testing. *Proc. of 29th ESA Antenna Workshop*, ESTEC, Noordwijk, Netherlands, 2007.

17. Zavyalov P. S., Senchenko E. S., Chugui Yu. V., Mikhalkin V. M., Khalimanovich V. I. [Thermodeformation measurement of spacecraft elements by laser speckle interferometry]. *Materialy XVIII Mezhdunar. nauch. konf. "Reshetnevskie chteniya"* [Materials XVIII Intern. Scientific. Conf "Reshetnev reading"]. Krasnoyarsk, 2014, Vol. 1, No. 18, P. 82–83 (In Russ.).

Библиографические ссылки

1. Франсон М. Оптика спеклов. М. : Мир, 1980. 171 с.

2. Laser speckle based digital optical methods in structural mechanics: A review / De la Torre I. M., Hernandez-Montes M. del S., Flores-Moreno J. M. [et al.] // Optics and Lasers in Engineering. 2016. Vol. 87. P 32–58.

3. Ульянов С. С. Что такое спеклы // Соросовский образовательный журнал. 1999. № 5. С. 112–116.

4. Arai Y. Three-dimensional shape measurement beyond the diffraction limit of lens using speckle interferometry // Journal of modern optics. 2018. Vol. 65, No. 16. P. 1866–1874.

5. Бесконтактный спекл-интерферометрический измеритель малых смещений / Е. А. Аксёнов, А. А. Шматко, В. И. Зворский [и др.] // Радіоелектронні і комп'ютерні системи. 2008. № 1 (28). С. 15–19.

6. Stetson K. A. Vibratory strain field measurement by transverse digital holography // Applied Optics. 2015. Vol. 54, No. 27. P. 8207–8211.

7. Pedrini G., Tiziani H. J. Double-pulse electronic speckle interferometry for vibration analysis // Applied optics. 1994. Vol. 33, No. 34. P. 7857–7863.

8. Вест Ч. Голографическая интерферометрия. М. : Мир, 1982. 504 с.

9. Kujawinska M., Wojciak J. Spatial phase shifting techniques of fringe pattern analysis in photomechanics // Second International Conference on Photomechanics and Speckle Metrology. Proc. SPIE, 1991. Vol. 1554B. P. 503–513.

10. Cookson T.J., Butters J. N., Pollard H.C. Pulsed laser in electronic speckle pattern interferometry // Optics and Laser Technology. 1978. Vol. 10. P. 119–124.

11. Tyrer J. R. Application of pulsed holography and double pulsed electronic speckle pattern interferometry to large vibrating engineering structures // Optics in Engineering Measurement. 1985. Vol. 599. P. 181–185.

12. Spooren R. Double-pulse subtraction TV holography // Optical Engineerin. 1992. Vol. 31, No. 5. P. 1000–1007.

13. Pedrini G., Pfister B., Tiziani H. Double pulse-electronic speckle interferometry // Journal of Modern Optics. 1993. Vol. 40, No. 1, P. 89–96.

14. Industrial applications of pulsed-laser ESPI vibration analysis / Van der Auweraer H., Steibichler H., Haberstok C. [et al.] // Proceedings of the International Modal Analysis Conference – IMAC, Kissimmee, FL, United States, 2001. Vol. 1. P. 490–496.

15. Nösekabel E. H., Ernst T., Haefker W. Measurement of the Thermal Deformation of a Highly Stable Antenna with Pulse ESPI // 18th International Congress on Photonics, Munich, Germany. Proc. SPIE, 2007. Vol. 6616. P. 18–21.

16. Highly Stable Q/V Band Reflector Demonstrator Manufacturing and Testing / Ernst T., Linke S., Lori M. [et al.] // Proc. of 29th ESA Antenna Workshop, ESTEC, Noordwijk, Netherlands, 2007.

17. Измерение термодеформаций элементов космических аппаратов методом лазерной спекл-интерферометрии / П. С. Завьялов, Е. С. Сенченко, Ю. В. Чугуй [и др.] // Решетневские чтения : материалы XVIII Междунар. науч. конф. (11–14 ноября 2011, г. Красноярск) : в 3 ч. / под общ. ред. Ю. Ю. Логинова ; Сиб. гос. аэрокосмич. ун-т. Красноярск, 2014. Т. 1, № 18. С. 82–83.

Zavyalov Peter Sergeevich – Cand. Sc., Director, Head of Laboratory; Technological Design Institute of Scientific Instrument Engineering SB RAS. E-mail: zavyalov@tdisie.nsc.ru.

Kravchenko Maxim Sergeevich – Junior Researcher; Technological Design Institute of Scientific Instrument Engineering SB RAS. E-mail: max@tdisie.nsc.ru.

Urzhumov Vitaliy Viktorovich – Engineer; Technological Design Institute of Scientific Instrument Engineering SB RAS. E-mail: urzhumov@tdisie.nsc.ru.

Kuklin Vyacheslav Aleksandrovich – Head of Department 345; JSC "Academician M. F. Reshetnev "Information Satellite Systems". E-mail: VAK345@iss-reshetnev.ru.

Mikhalkin Vladimir Mikhailovich – Deputy Director – Chief Engineer of the Industrial Center for Large-sized Foldable Mechanical Systems; JSC "Academician M. F. Reshetnev "Information Satellite Systems". E-mail: mikhalkin@iss-reshetnev.ru.

Завьялов Пётр Сергеевич – кандидат технических наук, директор, заведующий лабораторией; Конструкторско-технологический институт научного приборостроения СО РАН. E-mail: zavyalov@tdisie.nsc.ru.

Кравченко Максим Сергеевич – младший научный сотрудник; Конструкторско-технологический институт научного приборостроения СО РАН. E-mail: max@tdisie.nsc.ru.

Уржумов Виталий Викторович – инженер; Конструкторско-технологический институт научного приборостроения СО РАН. E-mail: urzhumov@tdisie.nsc.ru.

Куклин Вячеслав Александрович – начальник отдела 345; АО «Информационные спутниковые системы» имени академика М. Ф. Решетнёва». E-mail: VAK345@iss-reshetnev.ru.

Михалкин Владимир Михайлович – заместитель директора – главный инженер отраслевого центра крупногабаритных трансформируемых механических систем; АО «Информационные спутниковые системы» имени академика М. Ф. Решетнёва». E-mail: mikhalkin@iss-reshetnev.ru.

THE METHOD OF THE DISK FRICTION DETERMINING
OF LOW MASS FLOW CENTRIFUGAL PUMPS

A. A. Zuev[1], V. P. Nazarov[1], A. A. Arngold[2], I. M. Petrov[2]

[1] Reshetnev Siberian State University of Science and Technology
31, Krasnoyarsky Rabochy Av., Krasnoyarsk, 660037, Russian Federation
[2] JSC "Krasnoyarsk machine-building plant"
29, Krasnoyarsky Rabochy Av., Krasnoyarsk, 660123, Russian Federation
E-mail: dla2011@inbox.ru

Low mass flow centrifugal pumps are currently widely used in the energy supply system of liquid rocket engines, the engines of correction, docks, consisting of on-Board power sources on-Board sources power supply system of fuel components in the in gas generator systems for inflating fuel tanks, and in temperature control systems of aircraft and spacecraft.

When designing low mass flow centrifugal pumps for aerospace purposes, methods for calculating and optimizing the flow rate are often used corresponding to the design methods of full-size centrifugal pumps, which limits the mode and design potential of pumps and affects their energy characteristics and reliability. Reliability requirements often lead to the need to reserve units and fuel-supply systems.

Despite the large amount of research works, the issues of reliable design of low mass flow centrifugal pumps with high energy and operational parameters for spacecraft and aircraft remains an urgent task.

The article analyses the operational parameters of low mass flow centrifugal pumps used in aircraft and spacecraft power systems. Taking into account working fluid used and the temperature range, it was found that a laminar rotational flow with Reynolds number characteristic $\mathrm{Re} = 10^3 \div 3 \cdot 10^5$ is realized in the lateral cavity between the impeller and the pump housing.

The determination of power losses on disk friction of the impeller technique is developed taking into account design features and the applied schemes. Equations for determining the disk friction coefficients are consistent with the dependencies obtained by other authors. The obtained equations for the laminar rotational flow made it possible to determine the dependences for the resistance moment and the disk friction power of the impeller determining of a low mass flow centrifugal pump.

Keywords: disk friction, power balance, low mass flow centrifugal pump, dynamic spatial boundary layer.

МЕТОДИКА ОПРЕДЕЛЕНИЯ ДИСКОВОГО ТРЕНИЯ МАЛОРАСХОДНЫХ
ЦЕНТРОБЕЖНЫХ НАСОСОВ

А. А. Зуев[1], В. П. Назаров[1], А. А. Арнгольд[2], И. М. Петров[2]

[1] Сибирский государственный университет науки и технологий имени академика М. Ф. Решетнева
Российская Федерация, 660037, просп. им. газ. «Красноярский рабочий», 31
[2] АО «Красноярский машиностроительный завод»
Российская Федерация, 660123, просп. им. газ. «Красноярский рабочий», 29
E-mail: dla2011@inbox.ru

Малорасходные центробежные насосы в настоящее время находят широкое применение в системах топливоподачи жидкостных ракетных двигателей малой тяги, двигателях коррекции и ориентации космических аппаратов, в составе бортовых источников мощности, газогенераторных системах надува топливных баков, системах терморегулирования летательных и космических аппаратов.

При проектировании малорасходных центробежных насосов аэрокосмического назначения зачастую используют методы расчета и оптимизации проточной части в большей степени соответствующие расчетным методикам полноразмерных центробежных насосов, что ограничивает режимный и конструктивный потенциал насосов и влияет на их энергетические параметры и надежность. Требования обеспечения надежности зачастую приводят к необходимости резервирования агрегатов и систем топливоподачи.

Поэтому, несмотря на большой объем проведенных научно-исследовательских работ, разработка методики проектирования малорасходных центробежных насосов с высокими энергетическими и эксплуатационными параметрами аппаратов остается актуальной задачей ракетного двигателестроения.

В статье проведен анализ режимных параметров малорасходных центробежных насосов, используемых в энергетических системах летательных и космических аппаратов. С учетом используемых рабочих тел и диапазона температурного режима выявлено, что в полости между рабочим колесом и корпусом насоса реализуется ламинарное вращательное течение с характерными числами Рейнольдса в диапазоне $\mathrm{Re} = 10^3 \div 3 \cdot 10^5$.

С учетом конструктивных особенностей и применяемых схем разработана методика определения потерь мощности на дисковое трение рабочего колеса. Выражения для определения коэффициентов дискового трения согласуются с результатами, полученными другими авторами. Полученные выражения для ламинарного вращательного течения позволили определить математические зависимости для определения момента сопротивления и мощности дискового трения рабочего колеса малорасходного центробежного насоса.

Ключевые слова: дисковое трение, баланс мощности, малорасходный центробежный насос, динамический пространственный пограничный слой.

Introduction. A lot of research works [1–9], including low-flow centrifugal pumps [10–20], are devoted to methods of calculating, modelling, and designing centrifugal pumps for liquid rocket engines (LRE). In [1], an experimental characteristic of the rotational speed effect on the impeller speed is considered. In [4–7], the effect of the blade channel on the centrifugal pump performance is researched. The article [9] is devoted to design methods, as well as to the influence of geometrical and operational parameters on the velocity fields and performance distribution of low mass flow centrifugal pumps.

In research works by A. V. Bobkov [10–14], an analysis of the miniaturization of centrifugal-type superchargers on the kinematic parameters of the working fluid, which allow taking into account the factors of small size of the structure, has been carried out; the possibilities of increasing the efficiency of small-sized centrifugal electric pump units by reducing the rotor friction losses and the possibility of the pressure characteristics increasing were considered. In the works of V. V. Dvirny [15; 16] methods for improving supply units and the need to ensure a long life of low-flow blowers are considered. In the studies of M. V. Kraev and E. M. Kraeva [17–19], methods for calculating the energy parameters of low mass flow pumps units are given, the main operational factors are identified, areas of semi-open rational use and open-type impellers that provide high values of energy parameters low flow systems are defined.

However, despite the large amount of research, the method development for designing low mass flow centrifugal pumps with high energy and operational parameters for spacecraft and aircraft remains an urgent task in the field of rocket engine building.

Design and operating parameters characteristics. Low mass flow centrifugal pumps are currently widely used in the energy supply system of liquid rocket engines, the engines of correction, docks, consisting of on-Board power sources on-Board sources power supply system of fuel components in the in gas generator systems for inflating fuel tanks, and in temperature control systems of aircraft and spacecraft.

Low mass flow centrifugal pumps are characterized by the following parameters:

– working fluid consumption does not exceed $\dot{V} = 300 \cdot 10^{-6}$ м³/с;

– low discharge coefficient (the absolute velocity ratio of the meridional component to the circumferential component at the exit of the impeller)

$$\frac{c_{2m}}{u_2} \leq 0.1 ;$$

– rotor speed of the pump from 3000 to 10000 rpm;

– impeller diameter does not exceed 0.05 m;

– speed ratio is in the range $n_s = 40 \div 80$ [20].

As a rule, an electric drive is used as a drive for low mass flow centrifugal pumps (including thermal control systems (TCS)). The electric drive uses brushless DC motors. The frequency of the drive shaft rotation is characterized by the rotation speed $\omega = 314 \div 1047$ с⁻¹. The required resource of low-flow pumps with ball-bearing is 40000–155000 hours of operation (from 4.5 to 18 years). To ensure the required resource, the design schemes of low-flow electric pump units (EPU) with supply elements redundancy are being developed [16].

The working fluids of EPU are various technical fluids: water-glycerine solvents, RM distillate oils, LZ-TK-2 coolant, etc. [19]. The temperature range of thermal control systems operability with LZ-TK-2 coolant is from -90 to +60 °C, and for immersed pumps which supply RM distillate oil is from +2 to 220 °C. Due to the wide range of working fluids used and operating temperatures, the kinematic viscosity of the fluids varies within $\nu = 1 \cdot 10^{-3} \div 0.7 \cdot 10^{-6}$ м²/s.

Setting a research problem. Known methods of designing centrifugal pumps do not provide conditions for the similarity of the processes implemented in the flow parts of the EPU and full-size turbopump units (TPU) of liquid-propellant rocket engines (LRE). In order to increase the reliability of the energy characteristics calculation, a refinement of the used calculation dependencies

and the development of EPU design methods for the considered standard sizes are required.

Further, the EPU power balance will be considered. The output power of a low mass flow centrifugal pump is defined as

$$N_O = N_{req} - N_{mech} - N_D - N_{leak} - N_{hydr},$$

where N_{req} – required power, N_{mech} – mechanical power loss, $N_{Д}$ – impeller disk friction power, N_{leak} – leakage power of the working fluid through the seals and N_{hydr} – hydrodynamic power loss.

It is important to note that disk losses for low mass flow centrifugal pumps can reach 10% and depend on the type of working fluid and operating temperatures significantly.

Further, in the article, the methodology for determining the ratio of disk loss and power loss to disk friction and the EPU disk resistance moment will be considered.

Disk friction coefficient determination. The turbulent flow regime between the rotating impeller disk and the pump housing meets Reynolds criterion $Re = 5 \cdot 10^5$, for laminar mode $Re < 10^5$. The Reynolds criterion for the lateral cavity between the impeller and the pump housing is defined as

$$Re = \frac{\omega D_2^2}{4\nu},$$

Taking into account the geometrical and regime parameters and working fluid physicomechanical characteristics for thermal control systems, the range for the Reynolds criterion will be defined as $Re = 10^3 \div 3 \cdot 10^5$, which corresponds to the laminar flow regime.

In the implementing laminar flow process the velocity distribution in the dynamic boundary layer is determined as

$$\frac{u}{U} = 1 - \left(1 - \frac{y}{\delta}\right)^m,$$

for laminar flow, the profile degree is $m = 2 \div 5$.

Fig. 1 shows the distribution of laminar flow velocity profiles.

Fig. 2 shows a photograph of the laminar boundary layer. From fig. 1 and 2 it can be concluded that the presented velocity distribution function in the laminar boundary layer agrees well with experiment.

Depending on the degree of the velocity profile m there is a need to redefine the dependence of the friction induced shear stress near the wall surface in the boundary conditions of the laminar boundary layer τ_0. The equation for the law of friction of the gradient profile of the distribution of the velocity component in the boundary layer for laminar flow is written as

$$\frac{\tau_0}{\rho U^2} = 0.293 \left(\frac{U \delta^{**}}{\nu}\right)^{-0.5}.$$

When considering the pulse thickness loss equation for the gradient velocity distribution profile

$$\delta^{**} = \frac{m\delta}{(m+1)(2m+1)},$$

the friction induced shear stress for a rectilinear uniform flow is defined as

$$\tau_0 = 0.293 \rho U^2 \left(\frac{U}{\nu} \frac{m\delta}{(m+1)(2m+1)}\right)^{-0.5}.$$
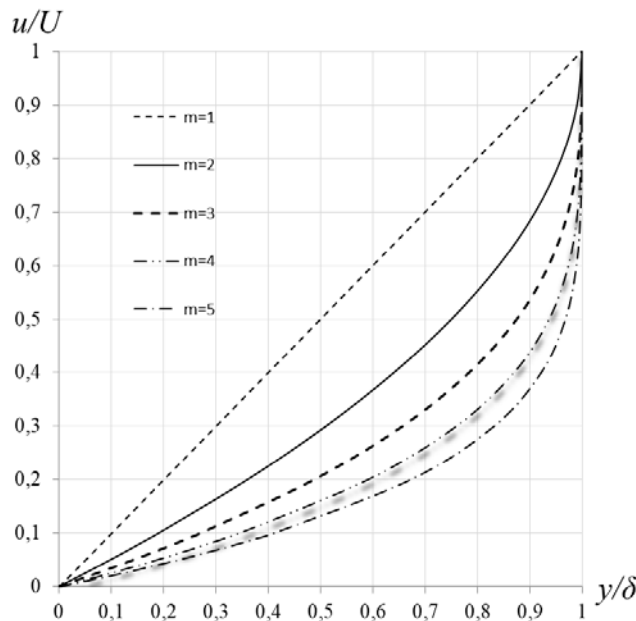
Fig. 1. Distribution of laminar flow velocity profiles

Рис. 1. Распределение профилей скорости
ламинарного течения потока
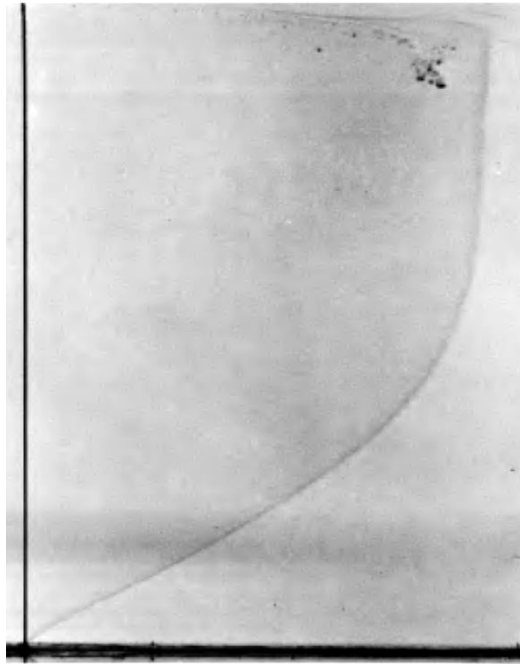
Fig. 2. The velocity distribution profile
of the laminar boundary layer

Рис. 2. Профиль распределения скорости
ламинарного пограничного слоя

When considering the case of the working fluid flow in the channel between the rotating disk and the fixed wall, it is necessary to take into account the stream core angular velocity and the disk. If the circumferential component of the absolute flow velocity on the wall is

$$U_w = \omega_c R ,$$

then the circumferential friction stress on the wall is defined as

$$\tau_{0\alpha}^w = 0.293\rho(\omega_c R)^2\left(\frac{\omega_c R}{\nu}\delta_{\alpha w}^{**}\right)^{-0.5} .$$

If the circumferential component of the flow velocity on the disk is

$$U_D = (\omega_D - \omega_c)R ,$$

then the circumferential friction stress on the disk will be equal to

$$\tau_{0\alpha}^D = 0.293\rho\left[(\omega_D - \omega_c)R\right]^2\left(\frac{(\omega_D - \omega_c)R}{\nu}\delta_{\alpha D}^{**}\right)^{-0.5} .$$

The considered case refers to the flow at which the distribution of the circumferential velocity component corresponds to the equation $\dfrac{U}{R} = \omega = \text{const}$.

The thickness of the pulse loss in the circumferential direction with an arbitrary profile degree for the laminar flow wall can be defined as

$$\delta_{\alpha w}^{**} = 0.04535\left(\frac{4M^2 - 7L}{1+H}\right)^{0.4}\left(\frac{2}{J} + \frac{1}{L}\right)^{0.8}\left(\frac{\nu}{\omega}\right)^{0.2}R^{0.6} .$$

After transforming this equation, the thickness of the loss of momentum in the circumferential direction on the wall for laminar flow is obtained

$$\delta_{\alpha w}^{**} = D1\frac{1}{\text{Re}_c^{\frac{1}{5}}}R^{\frac{4}{5}} ,$$

where

$$D1 = 0.04535\left[\frac{\dfrac{8m\left(47m^2 + 12m + 1\right)}{(3m+1)^2(5m+1)} - }{\dfrac{14m(m+1)\left(7032m^4 + 2602m^3 + 413m^2 + 32m + 1\right)}{(3m+1)(4m+1)(5m+1)(6m+1)(7m+1)(8m+1)}} - \dfrac{}{\left(\dfrac{2m+1}{m}\right)+1}\right]\times$$

$$\times\left[\frac{2(3m+1)(4m+1)(5m+1)}{(m+1)(47m+1)} + \frac{(3m+1)(4m+1)(5m+1)(6m+1)(7m+1)(8m+1)}{2m(m+1)\left(7032m^4 + 2602m^3 + 413m^2 + 32m + 1\right)}\right]^{0,8} .$$

The thickness of the momentum loss in the circumferential direction with an arbitrary degree of profile for a disk with a laminar flow is

$$\delta_{\alpha D}^{**} = \left(\frac{5}{3}\frac{0.01256}{\sqrt{\dfrac{(1+H)J}{3LJ + 4L(K - 2J)}}}\left(\frac{2}{J} + \frac{1}{L}\right)\right)^{0.8}\left(\frac{\nu}{\omega}\right)^{0.2}R^{0.6} .$$

Further, the thickness of the momentum loss in the circumferential direction on the disk is obtained as

$$\delta_{\alpha D}^{**} = D2 \frac{1}{\mathrm{Re}_{D-c}^{\frac{1}{5}}} R^{\frac{4}{5}},$$

where

$$D2 = \left[0.0185 \frac{\left[\frac{2(3m+1)(4m+1)(5m+1)}{(m+1)(47m+1)} + \frac{(3m+1)(4m+1)(5m+1)(6m+1)(7m+1)(8m+1)}{2m(m+1)(7032m^4+2602m^3+413m^2+32m+1)} \right]}{(m+1)\left(\frac{2m+1}{m}+1\right)(47m+1) \sqrt{\left[\frac{8m(m+1)}{(3m+1)(5m+1)}\left(\frac{(m+1)(47m+1)}{(4m+1)} - \frac{2m(47m^2+12m+1)}{(3m+1)}\right) \times \frac{\times \left(7032m^4+2602m^3+413m^2+32m+1\right)}{(6m+1)(7m+1)(8m+1)} - \frac{6m(m+1)^2(47m+1)(7032m^4+2602m^3+413m^2+32m+1)}{(3m+1)(4m+1)(5m+1)(6m+1)(7m+1)(8m+1)}\right]}} \right]^{0,8}.$$

The velocity distribution profile m for practically important cases (which are realized with laminar flow in the cavity between the impeller and the pump) is summarized in tab. 1.

Taking into account the obtained equations for the impulse loss thickness in the circumferential direction, the tangential friction stresses on the wall for laminar flow are defined as

$$\tau_{0\alpha}^{w} = \frac{0.293 \rho \nu^2 \mathrm{Re}_c^{\frac{8}{5}}}{(D1)^{\frac{1}{2}} R^2},$$

and the laminar disk is defined as

$$\tau_{0\alpha}^{D} = \frac{0.293 \rho \nu^2 \mathrm{Re}_{D-c}^{\frac{8}{5}}}{(D2)^{\frac{1}{2}} R^2}.$$

The velocity profile distribution m for practically important cases is summarized in tab. 2 for the frictional stresses of the laminar flow.

The friction coefficient equation for the wall and disk of the impeller with a laminar flow is expressed as

$$C_{fr} = \frac{\tau R^2}{\rho \mathrm{Re}^2 \nu^2}.$$

Then the friction coefficient for the wall in the circumferential direction with a laminar flow is defined as

$$C_{fr\alpha}^{w} = \frac{0.293}{(D1)^{\frac{1}{2}} \mathrm{Re}_c^{\frac{2}{5}}},$$

and the friction coefficient for a disk in the circumferential direction with a laminar flow is

$$C_{fr\alpha}^{D} = \frac{0.293}{(D2)^{\frac{1}{2}} \mathrm{Re}_{D-c}^{\frac{2}{5}}}.$$

Tab. 3 is for coefficient determining of the disk friction and the wall in the circumferential direction with a laminar flow depending on the degree of the velocity distribution profile. This table can be used for engineering calculations convenience m.

The loss coefficient of disk friction during laminar flow is defined as

$$C_M = C_{fr\alpha}^{w} + C_{fr\alpha}^{D}.$$

For the working fluid flow case in the lateral cavity between the working disk and the centrifugal pump housing, the angular core velocity is determined as $\omega_c = 0,5\omega_D$. Then the loss of disk friction coefficient laminar flow with laminar flow is defined as

$$C_M = \frac{1}{\left(0.5 \mathrm{Re}_D\right)^{\frac{2}{5}}} \left(\frac{0.293}{(D1)^{\frac{1}{2}}} + \frac{0.293}{(D2)^{\frac{1}{2}}} \right).$$

Tab. 4 is for determining the laminar flow disk friction loss rate and it demonstrates the analysis of the obtained dependence and comparison with obtained results by other authors.

Fig. 3 presents the disk friction coefficient dependence for the laminar flow of the working fluid at Re < 10^5.

Table 1

**Thickness of impulse loss on the wall and disk in the circumferential direction,
for practically important cases in laminar flow**

№	m	$\delta_{\alpha w}^{**}$	$\delta_{\alpha D}^{**}$
1	2	$\dfrac{0.13612}{\mathrm{Re}_c^{\frac{1}{5}}} R^{\frac{4}{5}}$	$\dfrac{0.27349}{\mathrm{Re}_{D-c}^{\frac{1}{5}}} R^{\frac{4}{5}}$
2	3	$\dfrac{0.20609}{\mathrm{Re}_c^{\frac{1}{5}}} R^{\frac{4}{5}}$	$\dfrac{0.44887}{\mathrm{Re}_{D-c}^{\frac{1}{5}}} R^{\frac{4}{5}}$
3	4	$\dfrac{0.2708}{\mathrm{Re}_c^{\frac{1}{5}}} R^{\frac{4}{5}}$	$\dfrac{0.6382}{\mathrm{Re}_{D-c}^{\frac{1}{5}}} R^{\frac{4}{5}}$
4	5	$\dfrac{0.3321}{\mathrm{Re}_c^{\frac{1}{5}}} R^{\frac{4}{5}}$	$\dfrac{0.83828}{\mathrm{Re}_{D-c}^{\frac{1}{5}}} R^{\frac{4}{5}}$

Table 2

**Tangential friction stresses on the wall and disk in the circumferential direction,
for practically important cases in laminar flow**

№	m	$\tau_{0\alpha}^{w}$	$\tau_{0\alpha}^{D}$
1	2	$\dfrac{0.794158\rho v^2 \operatorname{Re}_c^{\frac{8}{5}}}{R^2}$	$\dfrac{0.560269\rho v^2 \operatorname{Re}_{D-c}^{\frac{8}{5}}}{R^2}$
2	3	$\dfrac{0.645415\rho v^2 \operatorname{Re}_c^{\frac{8}{5}}}{R^2}$	$\dfrac{0.437328\rho v^2 \operatorname{Re}_{D-c}^{\frac{8}{5}}}{R^2}$
3	4	$\dfrac{0.563045\rho v^2 \operatorname{Re}_c^{\frac{8}{5}}}{R^2}$	$\dfrac{0.366766\rho v^2 \operatorname{Re}_{D-c}^{\frac{8}{5}}}{R^2}$
4	5	$\dfrac{0.508432\rho v^2 \operatorname{Re}_c^{\frac{8}{5}}}{R^2}$	$\dfrac{0.320017\rho v^2 \operatorname{Re}_{D-c}^{\frac{8}{5}}}{R^2}$

Table 3

**Friction coefficient on the wall and disk in the circumferential direction,
for practically important cases with laminar flow**

№	m	$C_{fr\alpha}^{w}$	$C_{fr\alpha}^{D}$
1	2	$\dfrac{0.794158}{\operatorname{Re}_c^{\frac{2}{5}}}$	$\dfrac{0.560269}{\operatorname{Re}_{D-c}^{\frac{2}{5}}}$
2	3	$\dfrac{0.645415}{\operatorname{Re}_c^{\frac{2}{5}}}$	$\dfrac{0.437328}{\operatorname{Re}_{D-c}^{\frac{2}{5}}}$
3	4	$\dfrac{0.563045}{\operatorname{Re}_c^{\frac{2}{5}}}$	$\dfrac{0.366766}{\operatorname{Re}_{D-c}^{\frac{2}{5}}}$
4	5	$\dfrac{0.508432}{\operatorname{Re}_c^{\frac{2}{5}}}$	$\dfrac{0.320017}{\operatorname{Re}_{D-c}^{\frac{2}{5}}}$

Table 4

Disk friction coefficient, for practically important cases with laminar flow

№	m	G. Shlikhting	Cimbus, K. Smiden	F. SHul'tc-Grunov	C_M
1	2				$\dfrac{1.787844}{\operatorname{Re}^{\frac{2}{5}}}$
2	3	$\dfrac{3.87}{\operatorname{Re}^{\frac{1}{2}}}$	$\dfrac{3.14}{\operatorname{Re}}\dfrac{R}{z}$,	$\dfrac{2.67}{\operatorname{Re}^{\frac{1}{2}}}$	$\dfrac{1.429221}{\operatorname{Re}^{\frac{2}{5}}}$
3	4		$\dfrac{R}{z} = 0.02$ (radius to gap ratio)		$\dfrac{1.227351}{\operatorname{Re}^{\frac{2}{5}}}$
4	5				$\dfrac{1.093553}{\operatorname{Re}^{\frac{2}{5}}}$

If $m = 2$ and the gradient function of laminar flow agrees well with the dependence of G. Shlikhting [21], then the maximum deviation of the disk friction parameter does not exceed 7 %. If Re = 10^3 the difference is 5 %, and if Re = 10^5 the difference is 7 %. In general, all dependencies are in the region of the confidence span defined by various authors and are in the parameter domain for disk friction coefficients from 0.113 to 0.027, depending on the Re criterion (fig. 3). It is important to note that when designing flow parts it is necessary to choose the turbulence transition which depends on the boundary conditions of the flows.

Fig. 4 shows the dependence on the disk friction coefficients, the friction coefficient for the wall in the circumferential direction and the friction coefficient for the disk in the circumferential direction of the laminar flow required for the flow parts design and for the power balance of low mass flow centrifugal pumps determining.

The radial element of the tangential friction stress is formed by the circumferential and consumable components taking into account the bottom lines slope and leaks through the sealing elements.

Radial stress of friction on the wall is

$$\tau_{0R}^w = \tau_{0Rp}^w + \tau_{0R\alpha}^w$$

and radial friction stress on the disk is

$$\tau_{0R}^D = \tau_{0Rp}^D + \tau_{0R\alpha}^D .$$

Radial stress of friction from the circumferential component is

$$\tau_{0R\alpha} = \varepsilon\tau_{0\alpha} ,$$

where ε – tangent of the bottom slope angle.

The radial friction stress will be determined depending on the flow rate associated with the amount of leakage through the sealing elements, and the dependence on the structure is similar to straight linear flow

$$\tau_0 = 0.01256\rho V_r^2 \left(\frac{V_r}{\nu} \frac{m\delta}{(m+1)(m+2)} \right)^{-0.25} ,$$

where V_p – flow rate.

The one side resistance moment of the low mass flow centrifugal pump working disk is defined as

$$M_D = 2\pi \int_{R1}^{R2} \tau_{0\alpha} r^2 dr = C_M \rho R_2^5 \omega_D^2 .$$
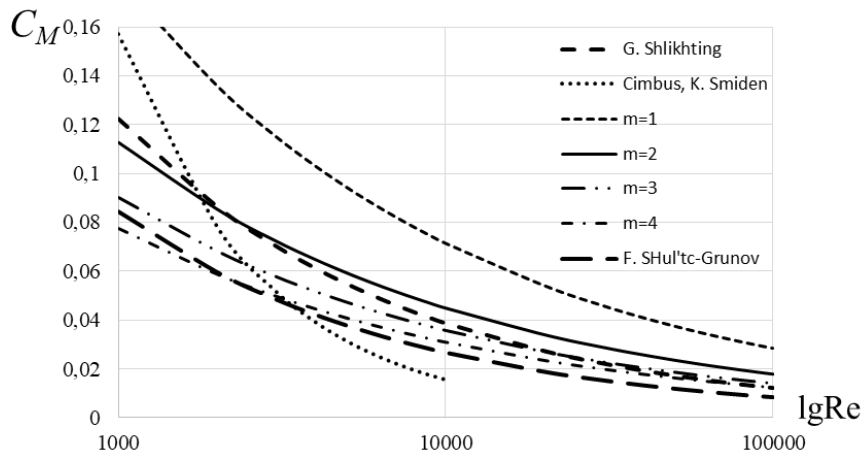

Fig. 3. Coefficient of disk friction laminar flow

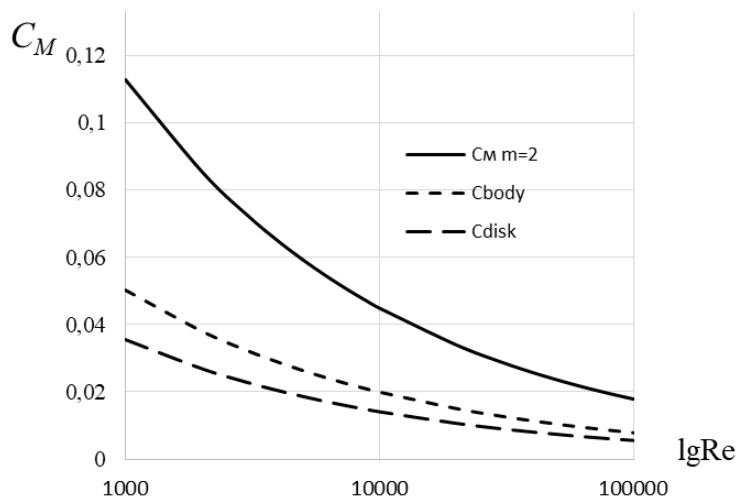Рис. 3. Коэффициент дискового трения ламинарного течения

Fig. 4. Coefficient of disk friction

Рис. 4. Коэффициент дискового трения

Then the impeller disk friction power on one side of the low mass flow centrifugal pump is defined as

$$N_{frD} = M_D \omega_D .$$

Conclusion. The analysis of low mass flow centrifugal pump operating parameters used in aircraft and spacecraft power systems was carried out. After analysing the working fluid characteristics and the temperature range, it was revealed that a laminar rotational flow with Reynolds numbers $Re = 10^3 \div 3 \cdot 10^5$ is conducted in the cavity between the impeller and the pump.

The method for determining the power losses due to disk friction of the impeller with design features and the applied schemes was developed. The equations for disk friction coefficient determining are consistent with the results of other authors. The obtained equations for the laminar rotational flow established mathematical dependencies to determine the resistance moment and power of the impeller disk friction of a low mass flow centrifugal pump.

References

1. Valentini, D., Pace, G., Pasini, A., Torre, L., Hadavandi, R., & d' Agostino, L. (2017). Fluid-induced rotordynamic forces on a whirling centrifugal pump. European Journal of Mechanics – B/Fluids, 61, P. 336–345. Doi: 10.1016/j.euromechflu.2016.09.004.

2. Liu, M., Tan, L., & Cao, S. (2019). Theoretical model of energy performance prediction and BEP determination for centrifugal pump as turbine. Energy. Doi: 10.1016/j.energy.2019.01.162.

3. Sengpanich, K., Bohez, E. L. J., Thongkruer, P., & Sakulphan, K. (2019). New mode to operate centrifugal pump as impulse turbine. Renewable Energy. Doi: 10.1016/j.renene.2019.03.116.

4. Ding, H., Li, Z., Gong, X., & Li, M. (2018). The influence of blade outlet angle on the performance of centrifugal pump with high specific speed. Vacuum. Doi: 10.1016/j.vacuum.2018.10.049.

5. Skrzypacz, J., & Bieganowski, M. (2018). The influence of micro grooves on the parameters of the centrifugal pump impeller. International Journal of Mechanical Sciences, 144, P. 827–835. Doi: 10.1016/j.ijmecsci.2017.01.039.

6. Zhang, N., Liu, X., Gao, B., Wang, X., & Xia, B. (2019). Effects of modifying the blade trailing edge profile on unsteady pressure pulsations and flow structures in a centrifugal pump. International Journal of Heat and Fluid Flow, 75, P. 227–238. Doi: 10.1016/j.ijheatfluidflow.2019.01.009.

7. Chen, H., He, J., & Liu, C. (2017). Design and experiment of the centrifugal pump impellers with twisted inlet vice blades. Journal of Hydrodynamics, Ser. B, 29(6), P. 1085–1088. Doi: 10.1016/s1001-6058(16)60822-3.

8. Yu, R., & Liu, J. (2018). Failure analysis of centrifugal pump impeller. Engineering Failure Analysis, 92, P. 343–349. Doi: 10.1016/j.engfailanal.2018.06.003.

9. Salehi, S., Raisee, M., J. Cervantes, M., & Nourbakhsh, A. (2018). On the flow field and performance of a centrifugal pump under operational and geometrical uncertainties. Applied Mathematical Modelling, 61, P. 540–560. Doi: 10.1016/j.apm.2018.05.008.

10. Bobkov A. V. [The influence of the factor malorazmernyj to the design of the supercharger centrifugal type]. *Uspekhi sovremennoy nauki.* 2017. Vol. 4. No. 2. P. 127–130 (In Russ.).

11. Bobkov A. V. [A geometric criterion of optimizing the design of blade machines]. *Mezhdunarodnyy zhurnal prikladnykh i fundamentalnykh issledovaniy.* 2013. No. 6. P. 49 (In Russ.).

12. Bobkov A. V. [Energy expediency of increasing the number of stages in a small centrifugal electric pump unit]. *Sovremennyye problemy nauki i obrazovaniya.* 2012. No. 4. P. 84 (In Russ.).

13. Bobkov A. V., Tsvetkov E. O. [Improving the pressure qualities of the centrifugal pump thermal control system]. *Mezhdunarodnyy zhurnal prikladnykh i fundamentalnykh issledovaniy.* 2012. No. 10. P. 110 (In Russ.).

14. Bobkov A. V., Tsvetkov E. O. [Features of balance of power losses in electric pump units of spacecraft thermal control systems]. *Izvestiya Samarskogo nauchnogo tsentra Rossiyskoy akademii nauk.* 2011. Vol. 13. No. 1–2. C. 290–292 (In Russ.).

15. Dvirnyy V. V., Krushenko G. G., Golovanova V. V., Dvirnyy G. V., Petyayeva N. N., Kirianova K. A. [Improvement of units for heat transportation in spacecraft]. *Issledovaniya naukograda.* 2016. No. 3–4 (18). P. 12–16 (In Russ.).

16. Dvirnyy V. V., Dvirnyy G. V., Khnykin A. V., Golovanova V. V., Krushenko G. G. [Providing long lasting resource of economical compressors]. *Issledovaniya naukograda.* 2014. No. 3 (9). P. 12–20 (In Russ.).

17. Krayeva E. M. [Energy parameters of high-speed low-flow pumps]. *Vestnik Moskovskogo aviatsionnogo instituta.* 2011. Vol. 18. No. 3. P. 104 (In Russ.).

18. Krayeva E. M. [Calculation of energy parameters of high-speed centrifugal pumps of low speed]. *Izvestiya vysshikh uchebnykh zavedeniy. Aviatsionnaya tekhnika.* 2010. No. 1. P. 48–50 (In Russ.).

19. Krayeva E. M. [To calculation of operating parameters of centrifugal pumps of low speed]. *Vestnik SibCAU.* 2009. No. 2 (23). P. 168–170 (In Russ.).

20. Bobkov A. V., Katalazhnova N. I., Kachalov A. A. [TCalculation of field lines ratio specific speed centrifugal blower spacecraft]. *Uspekhi sovremennogo estestvoznaniya.* 2004. No. 4. P. 50–51 (In Russ.).

21. Shlikhting G. *Teoriya pogranichnogo sloya* [The theory of the boundary layer]. Moscow, Science Publ., 1974. 712 p.

Библиографические ссылки

1. Fluid-induced rotordynamic forces on a whirling centrifugal pump / D. Valentini, G. Pace,. Pasini A. [et al.] // European Journal of Mechanics – B/Fluids. 2017. Vol. 61. P. 336–345. Doi: 10.1016/j.euromechflu.2016.09.004.

2. Liu M., Tan L., Cao S. Theoretical model of energy performance prediction and BEP determination for centrifugal pump as turbine // Energy. 2019. Vol. 172. P. 712–732. Doi:10.1016/j.energy.2019.01.162.

3. New mode to operate centrifugal pump as impulse turbine / K. Sengpanich, E. L. J. Bohez, P. Thongkruer, K. Sakulphan // Renewable Energy. 2019. Vol. 140. P. 983–993. Doi: 10.1016/j.renene.2019.03.116.

4. The influence of blade outlet angle on the performance of centrifugal pump with high specific speed / H. Ding, Z. Li, X. Gong, M. Li // Vacuum. 2019. Vol. 159. P. 239–246. Doi: 10.1016/j.vacuum.2018.10.049.

5. Skrzypacz J., Bieganowski M. The influence of micro grooves on the parameters of the centrifugal pump impeller // International Journal of Mechanical Sciences. 2018. Vol. 144. P. 827–835. Doi: 10.1016/j.ijmecsci.2017.01.039.

6. Effects of modifying the blade trailing edge profile on unsteady pressure pulsations and flow structures in a centrifugal pump / N. Zhang, X. Liu, B. Gao [et al.] // International Journal of Heat and Fluid Flow. 2019. Vol. 75. P. 227–238. Doi:10.1016/j.ijheatfluidflow.2019.01.009.

7. Chen H., He J., Liu C. Design and experiment of the centrifugal pump impellers with twisted inlet vice blades // Journal of Hydrodynamics. Ser. B. 2017. No. 29(6). P. 1085–1088. Doi: 10.1016/s1001-6058(16)60822-3.

8. Yu R., Liu J. Failure analysis of centrifugal pump impeller // Engineering Failure Analysis. 2018. Vol. 92. P. 343–349. Doi: 10.1016/j.engfailanal.2018.06.003.

9. On the flow field and performance of a centrifugal pump under operational and geometrical uncertainties / S. Salehi, M. Raisee, M. J. Cervantes, A. Nourbakhsh // Applied Mathematical Modelling. 2018. Vol. 61. P. 540–560. Doi: 10.1016/j.apm.2018.05.008.

10. Бобков А. В. Влияние фактора малоразмерности на конструкцию нагнетателя центробежного типа // Успехи современной науки. 2017. Т. 4, № 2. С. 127–130.

11. Бобков А. В. Геометрический критерий оптимизации конструкции лопаточной машины // Международный журнал прикладных и фундаментальных исследований. 2013. № 6. С. 49.

12. Бобков А. В. Энергетическая целесообразность увеличения числа ступеней в малоразмерном центробежном электронасосном агрегате // Современные проблемы науки и образования. 2012. № 4. С. 84.

13. Бобков А. В., Цветков Е. О. Повышение напорных качеств центробежного насоса системы терморегулирования // Международный журнал прикладных и фундаментальных исследований. 2012. № 10. С. 110.

14. Бобков А. В., Цветков Е. О. Особенности баланса потерь мощности в электронасосных агрегатах систем терморегулирования космических аппаратов // Известия Самарского науч. центра РАН. 2011. Т. 13, № 1–2. С. 290–292.

15. Совершенствование агрегатов для транспортировки тепла в космических аппаратах / В. В. Двирный, Г. Г. Крушенко, В. В. Голованова [и др.] // Исследования наукограда. 2016. № 3–4 (18). С. 12–16.

16. Обеспечение длительного ресурса малорасходных нагнетателей / В. В. Двирный, Г. В. Двирный, А. В. Хныкин [и др.] // Исследования наукограда. 2014. № 3 (9). С. 12–20.

17. Краева Е. М. Энергетические параметры высокооборотных насосов малого расхода // Вестник Московского авиац. ин-та. 2011. Т. 18, № 3. С. 104.

18. Краева Е. М. Расчет энергетических параметров высокооборотных центробежных насосов малой быстроходности // Известия вузов. Авиационная техника. 2010. № 1. С. 48–50.

19. Краева Е. М. К расчету эксплуатационных параметров центробежных насосов малой быстроходности // Вестник СибГАУ. 2009. № 2 (23). С. 168–170.

20. Бобков А. В., Каталажнова Н. И., Качалов А. А. Расчет полей линий уровня коэффициента быстроходности центробежного нагнетателя космического аппарата // Успехи современного естествознания. 2004. № 4. С. 50–51.

21. Шлихтинг Г. Теория пограничного слоя. М. : Наука, 1974. 712 с.

Zuev Alexander Alexandrovich – Cand. Sc., associate Professor, Department of Aircraft Engines; Reshetnev Siberian State University of Science and Technologies. E-mail: dla2011@inbox.ru.

Nazarov Vladimir Pavlovich – Cand. Sc., Professor, Department of Aircraft Engines, Reshetnev Siberian State University of Science and Technologies. E-mail: nazarov@mail.sibsau.ru.

Arngold Anna Anatolievna – Department of Special Connectors and Instruments, Krasnoyarsk Machine-Building Plant. E-mail: arngoldanna@mail.ru.

Petrov Ivan Mikhaylovich – Deputy chief designer for engines, propulsion systems and power plants, Krasnoyarsk Machine-Building Plant. E-mail: petroof777@mail.ru.

Зуев Александр Александрович – кандидат технических наук, доцент, доцент кафедры двигателей летательных аппаратов; Сибирский государственный университет науки и технологий имени академика М. Ф. Решетнева. E-mail: dla2011@inbox.ru.

Назаров Владимир Павлович – кандидат технических наук, профессор, заведующий кафедрой двигателей летательных аппаратов; Сибирский государственный университет науки и технологий имени академика М. Ф. Решетнева. E-mail: nazarov@.sibsau.ru.

Арнгольд Анна Анатольевна – начальник бюро спецсоединителей, приборов и пультов аппаратуры; АО «Красноярский машиностроительный завод». E-mail: arngoldanna@mail.ru.

Петров Иван Михайлович – заместитель главного конструктора по двигателям, двигательным установкам и энергоустановкам; АО «Красноярский машиностроительный завод». E-mail: petroof777@mail.ru.

DEVELOPMENT OF INTERFACE MODULE EMULATOR ARCHITECTURE FOR SPACECRAFT LIFE SUPPORT SYSTEMS

V. A. Komarov, P. V. Semkin

JSC "Academician M. F. Reshetnev "Information Satellite Systems"
52, Lenin St., Zheleznogorsk, Krasnoyarsk region, 662972, Russian Federation
E-mail: VKomarov@iss-reshetnev.ru

The article gives an analysis of special characteristics of ground-based experimental evaluation of on-board radio-electronic equipment, taking the control unit of up-to date spacecraft on-board control complex as the test objective. The focus is the problem of providing testing procedures of the specific software employed in design and manufacture process. A solution of the problem is worked out on the basis of performance of a hardware-software complex which emulates interface modules for the computing module of control unit. According to the general operation algorithm of the control unit, the developed complex is regarded as a multi-user system. The main functional requirements for hardware-software emulator, regarded as the corresponding queuing system, are also defined. The results of the experiments with the computer module operation prompted the requirements for the emulator response time from the point of view of its operation stability in real strict-time mode. In order to ensure the required efficiency of operation, the emulated functions of the interface modules are classified according to the severity level of their execution determinacy. The results of experimental evaluation of the service channel hardware design variants when applying multi-functional reconfigurable input-output digital devices allowed to develop a hardware-software emulator structural circuit based on operation parallelism of programmable integrated logic circuits and flexibility of software reconfiguration. The realization of emulated functions of selected classes within the available architecture was carried out using the corresponding hardware blocks and software module. The presented analysis of the emulator response limits was performed with the application of National Instruments technologies. The results of the developed hardware-software emulator evaluation and practical application, as well as other possible ways of applying the proposed approach for tests of spacecraft on-board radio-electronic equipment and space system components were also analyzed.

Keywords: practical evaluation, spacecraft electronic equipment, multi-user system, software- hardware modeling.

РАЗРАБОТКА АРХИТЕКТУРЫ ЭМУЛЯТОРА ИНТЕРФЕЙСНЫХ МОДУЛЕЙ СОПРЯЖЕНИЯ СИСТЕМ ЖИЗНЕОБЕСПЕЧЕНИЯ КОСМИЧЕСКИХ АППАРАТОВ

В. А. Комаров, П. В. Семкин

АО «Информационные спутниковые системы» имени академика М. Ф. Решетнева»
Российская Федерация, 660041, г. Железногорск Красноярского края, ул. Ленина, 52
E-mail: VKomarov@iss-reshetnev.ru

Рассмотрена специфика наземной экспериментальной отработки бортовой радиоэлектронной аппаратуры на примере блока управления бортового комплекса управления современных космических аппаратов. Сформулирована проблема обеспечения процесса тестирования его программного обеспечения в процессе проектирования и изготовления. Предложено решение обозначенной проблемы на основе аппаратно-программного комплекса, эмулирующего работу интерфейсных модулей сопряжения для вычислительного модуля блока управления. В соответствии с обобщенным алгоритмом функционирования блока управления разрабатываемый комплекс рассмотрен в виде многопользовательской системы. Определены основные функциональные требования к аппаратно-программному эмулятору как к соответствующей системе массового обслуживания. На основе проведенных экспериментальных исследований процесса функционирования вычислительного модуля

сформулированы требования к времени реакции эмулятора с точки зрения обеспечения его работы в режиме жесткого реального времени. В целях обеспечения требуемой оперативности функционирования проведена классификация эмулируемых функций интерфейсных модулей сопряжения в соответствии со степенью критичности детерминированности их выполнения. По результатам экспериментальной апробации вариантов технической реализации канала обслуживания на основе многофункциональных устройств реконфигурируемого цифрового ввода/вывода разработана структурная схема аппаратно-программного эмулятора, основанная на возможностях параллелизма выполнения операций в программируемых логических интегральных схемах и гибкости программного реконфигурирования. Реализация имитируемых функций выделенных классов в рамках предложенной архитектуры выполнена на основе соответствующих аппаратных блоков и программного модуля. Проведен анализ предельных значений времени реакции эмулятора на примере его реализации с использованием технологий National Instruments. Рассмотрены результаты апробации и внедрения разработанного аппаратно-программного эмулятора, а также дальнейшие направления прикладного применения предложенного подхода в процессе испытаний бортовой радиоэлектронной аппаратуры космических аппаратов и компонентов космических систем.

Ключевые слова: испытания, бортовая радиоэлектронная аппаратура, многопользовательская система, программно-аппаратное моделирование.

Introduction. Hardware-software complex for life support systems control of up-to date long-life spacecraft (SC) are subject to strict requirements concerning their trouble-free operation under destabilizing effects of the open space. One of the units of spacecraft (SC) on-board control complex designed at JSC "Academician M. F. Reshetnev "Information Satellite Systems" features a control unit (CU) comprising a processor module (PM) with a set of interface modules (IM) controlling the corresponding SC systems, components and/or assemblies (reaction-control system, thermal control system, electrical power system, pyro control units, actuators, etc.).

Problem description. Complexity of the PM software operation algorithm and several operating mode options (regular mode, on-board attitude control, etc.) required development of a specialized test complex applicable for ground testing and evaluation [1]. As a rule, the CU PM is a unified module, and the interface modules are made with regard for specific configuration of the corresponding SC service systems; that accounts for significant divergence of the software versions. Data exchange of the SC onboard central computer complex and CU PM is possible, for example, via a multiplex exchange channel, and the exchange of PM and IM is supported by a special internal data exchange interface (IDEI) [1; 2]. This exchange attachment operates special microcircuits or IP-cores, installed in field-programmable gate arrays (FPGA) of IM and performing the functions of the corresponding internal data exchange interface controllers (IDEIC). Fig. 1 presents general block diagram of the control unit.

The PM software testing procedure provides for the possibility of issuing external commands for the PM and the need to ensure two-way data communication of the PM and the corresponding IMs (fig. 1). This dictates the need for ready-made IM units connected to PM, usually featuring many hardware design and operation algorithm variants aimed for different SC. Meeting these requirements in PM software evaluation at the design stage is sometimes impossible, and cost-ineffective anyway, as it induces high expenses for supplying additional IMs [1].

Problem solving description. The problem of providing PM software advanced testing without IM can be solved by applying a special hardware-software complex emulating their performance within the CU. Here are the requirements for the emulator under development.

When the control unit installed in the spacecraft on-board control complex operates at time intervals and in sequence determined by the online leg of PM software algorithm, and by external command sources (OCCC, test instrument system, etc.), processor module of the control unit supports data exchange with corresponding interface modules through internal data exchange interface. Data exchange is performed by calling the corresponding software modules which in their turn call the IMs. Normally, calling each IM involves data recording in control registers – *control data words*, followed by reading the content of IM status register – *status data words*, displaying the issued control inputs execution and current SC systems and components status. Analysis of the state data words is followed by the execution of the corresponding leg of PM software algorithm. Let the control data words generated by the PM software be denoted by the set:

$$\boldsymbol{K}_{\mathrm{DW}} = \left\{ K_i \middle| i = 1, I \right\}, \qquad (1)$$

where I – the number of IM installed in CU; K_i – control data words subset, generated by the respective software module for i IM.

IM-generated status data words are presented in the form of the set:

$$\boldsymbol{Z}_{\mathrm{DW}} = \left\{ Z_i \middle| i = 1, I \right\}, \qquad (2)$$

where Z_i – status data words subset, generated by i IM.

Thus, conversion of IM control data words subset K_i into status data words subset Z_i can be generally expressed as follows:

$$Z_i = f_i \left(K_i \right), \qquad (3)$$

where f_i – ratio function, generally describing the corresponding conversion ($f_i : K_i \mapsto Z_i$). The type of f_i function and the form of its presentation is determined by the functional purpose, hardware design and logic of the corresponding IM.

The collection of ratio functions f_i forms the set:

$$\boldsymbol{F}_{\mathrm{DW}} = \left\{ f_i \middle| i = 1, I \right\}, \qquad (4)$$

where $\boldsymbol{F}_{\mathrm{DW}}$ – set of control data words conversions, realized by the corresponding interface modules installed in the control unit.

In accordance with the introduced designations (expressions (1)–(4)), the developed interface module emulator must ensure the realization of F_{DW} conversion functions set for control data words set K_{DW} generated by the corresponding software modules of the PM software and entering through the internal data exchange interface at random times (fig. 1). In this case, according to the PM software general logic, new control data words are not transferred to the corresponding IM until the status data words generated on the results of the execution of the previous ones are read, or their generation waiting time is not exceeded [2].

In view of the above, the developed IM hardware-software emulator can be regarded as a *multi-user system* operating in an interactive dialogue mode [3–5]. In this system:

– *user terminals (sources of requests)* are PM software modules that generate and exchange data with the corresponding interface modules;

– *requests* are control data words recorded in the corresponding registers;

– *request processing* means performing the conversion of control data words into status data words;

– *response* means status data words generated in the corresponding registers.

General block diagram of the developed interface module emulator as a corresponding closed queuing system is shown in fig. 2 [3; 4].

The main objectives of the queuing system design the article deals with (fig. 2) is the development of its structure and analysis of the main approaches to realization of a service channel aimed at ensuring the required response time $\tilde{t}_r$. The emulator response time $\tilde{t}_r$ is the sum of the in-coming control data words queuing time (K_{DW} set) – $\tilde{t}_q$ and the generation time of status data words (Z_{DW} set) – $\tilde{t}_s$ in correlation with conversion functions set F_{DW} (fig. 2).

The results of experiments with operation of the control unit processor module carried out on the basis of the ground-based debugging complex of onboard electronic equipment [1] helped to determine the following characteristic features of the queuing system shown in fig. 2.

1. The presence of several types of control data words K_i (see expression (1)), generated by the corresponding software modules, and the related time constraints imposed on the generation efficiency of the state data words Z_i.

2. Large-scale change of the time intervals between re-transmitted calls to IM (for example, from 10 us to 200 ms), the probable values of which depend on: the online leg of the PM software algorithm; hardware design and current configuration of the corresponding IM; the current status of SC systems, components, assemblies; CU operation mode [1; 2].
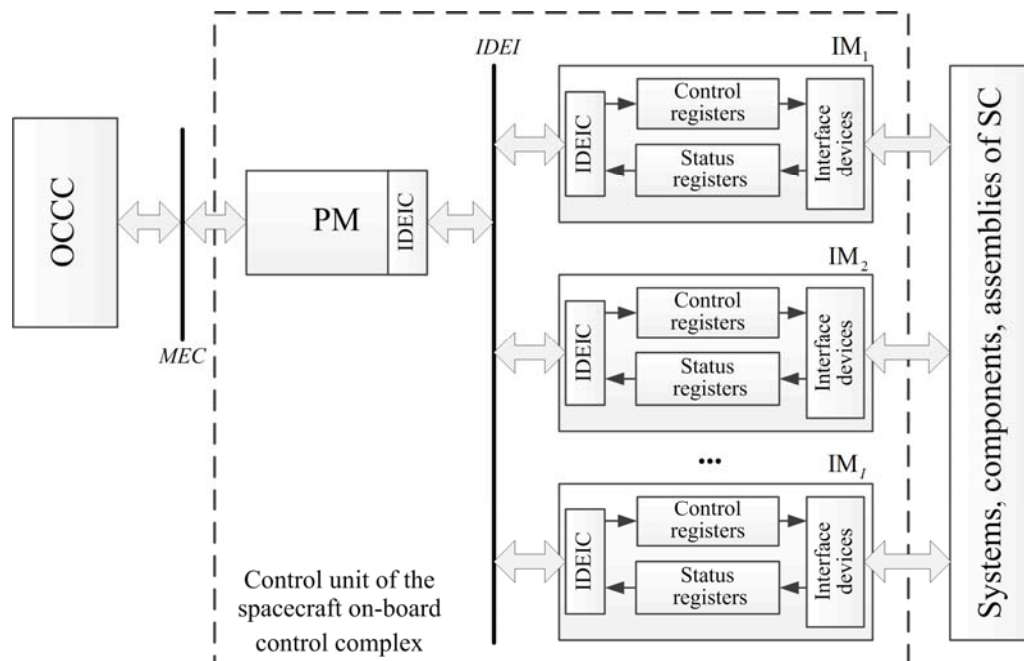
Fig. 1. General block diagram of the control unit of the on-board control complex:
PM – processor module; IDEI – internal data exchange interface; IDEIC – internal data exchange interface controller*; I* – number of control unit interface modules; OCCC – onboard central computer complex; MEC – multiplex exchange channel

Рис. 1. Обобщенная структурная схема блока управления бортового комплекса управления:
ВМ – вычислительный модуль; ВПИ – внутриприборный интерфейс обмена данными; КВПИ – контроллер внутриприборного интерфейса обмена; *I* – число интерфейсных модулей сопряжения блока управления; БЦВК – бортовой центральный вычислительный комплекс; МКО – мультиплекс-ный канал обмена
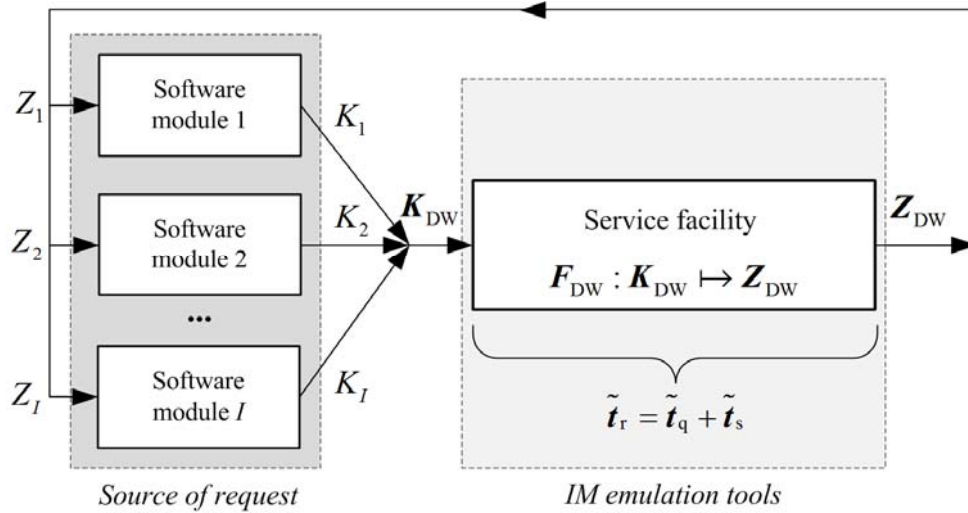
Fig. 2. General block diagram of the interface module emulator as a queuing system

Рис. 2. Обобщенная структурная схема эмулятора интерфейсных модулей
сопряжения как системы массового обслуживания

The analysis of the initial data for IM design, and also for PM software design, helped to determine the following integrated classes of control data words K_{DW}:

– *Class № 1*. The time required by the emulator for generating status data words in the corresponding registers is not more than 12 us ($\tilde{t}_r^{K1} \leq 12$ us);

– *Class № 2*. The time required by the emulator for generating status data words in the corresponding registers exceeds 12 us, but is not more than 150 ms (12 us $< \tilde{t}_r^{K2} < 150$ ms).

Thus, in accordance with the determined special characteristics, hardware-software emulator of interface modules as a closed queuing system must ensure the in-coming request processing determinacy specified by $\tilde{t}_r^{K1}$ and $\tilde{t}_r^{K2}$ values, i. e. realization of real strict-time mode related to PM internal processes in the situation of incomplete empirical data on the incoming traffic parameters [6].

Preliminary evaluation of the service channel based on the programmable integrated logic circuit of the reconfigurable digital input-output device in the form of functional hardware registers linked to the IP- core of the internal interface controller revealed its low processing speed of class No.1 control data words. The corresponding time the control computer requires for reading K_{DW}, program conversion $F_{DW} : K_{DW} \mapsto Z_{DW}$, and recording Z_{DW} values into respective FPGA registers, designed with account for breaks formed with entry of new K_{DW} values, made 10–15 ms (i. e. $\tilde{t}_s = 10$–15 ms) regardless of control data words queuing time.

To ensure the required performance efficiency, a combined emulator architecture based on the features of FPGA operational parallelism and program reconfiguration flexibility was worked out [2; 7]. With the account for the revealed discontinuity of control data words generated by PM and the given classification of speed re-

quirements for status data words generation, K_{DW} and Z_{DW} sets can be presented as follows:

$$K_{DW} = K_{DW}^{K1} \bigcup K_{DW}^{K2}, \qquad Z_{DW} = Z_{DW}^{K1} \bigcup Z_{DW}^{K2},$$

where K_{DW}^{K1} and K_{DW}^{K2} – IM-emulated control data words sets, belonging to the selected classes № 1 and № 2; Z_{DW}^{K1} and Z_{DW}^{K2} – IM-emulated status data words sets, belonging to the selected classes №1 and №2. Respectively:

$$K_{DW}^{K1} = \bigcup_{i=1}^{I} K_i^{K1}, \quad Z_{DW}^{K1} = \bigcup_{i=1}^{I} Z_i^{K1}$$

$$K_{DW}^{K2} = \bigcup_{i=1}^{I} K_i^{K2}, \quad Z_{DW}^{K2} = \bigcup_{i=1}^{I} Z_i^{K2}$$

where K_i^{K1}, K_i^{K2} and Z_i^{K1}, Z_i^{K2} – control data words subsets and generated on their basis state data words subsets, belonging to the selected classes № 1 and № 2 for each i IM. At that $K_i^{K1}, K_i^{K2} \subset K_i$; $Z_i^{K1}, Z_i^{K2} \subset Z_i$ (see expressions (1), (2)).

In a similar way, functional separation of conversion functions set F_{DW} of the selected classes of the processed control data words is performed:

$$F_{DW} = F_{DW}^{K1} \bigcup F_{DW}^{K2},$$

$$F_{DW}^{K1} = \bigcup_{i=1}^{I} f_i^{K1}, f_i^{K1} \subset f_i,$$

$$F_{DW}^{K2} = \bigcup_{i=1}^{I} f_i^{K2}, f_i^{K2} \subset f_i. \tag{5}$$

The developed block diagram of the interface modules hardware-software emulator, taking into account the experimentally revealed discontinuity of the processed control data words, is shown in fig. 3; it comprises a multifunctional unit for reconfigurable digital input-output from FPGA, controlled by the respective industrial computer [8].
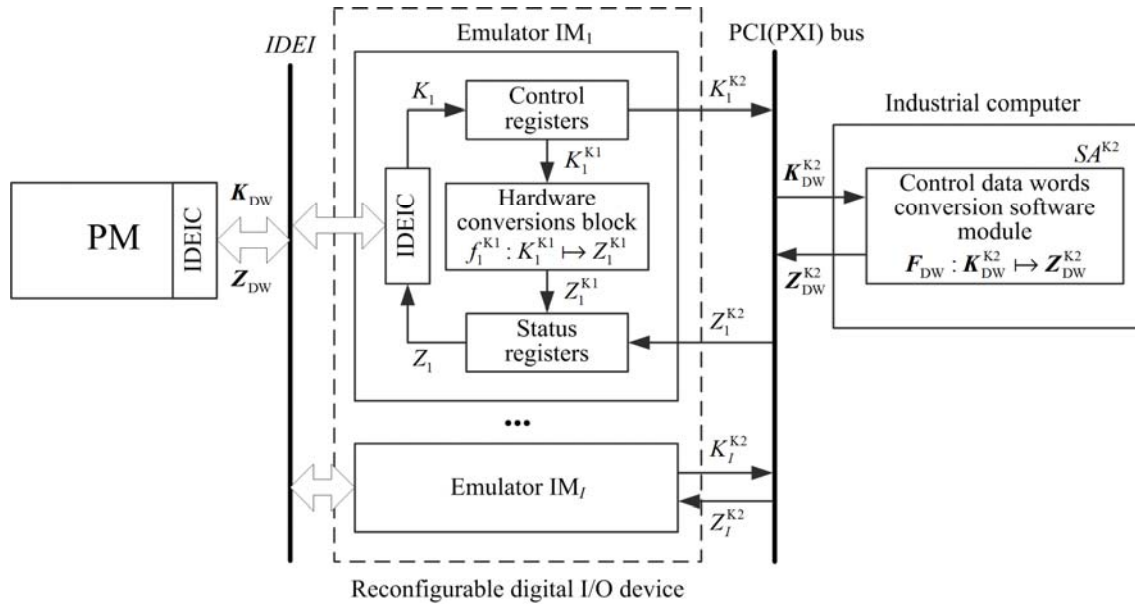
Fig. 3. General block diagram of the interface modules hardware-software emulator
of SC life support system

Рис. 3. Обобщенная структурная схема аппаратно-программного эмулятора интерфейсных
модулей сопряжения систем жизнеобеспечения космического аппарата

General representation of the developed hardware-software interface modules emulator as queuing systems used in processing the corresponding requests (control data words) of № 1 and 2 classes is shown in fig. 4 and 5 respectively [3; 4].

In accordance with the chosen approach, individual service channels realizing ratio functions f_i^{K1} for class No. 1 control data words (see expression (5)) come in the form of hardware conversion units making use of FPGA resources (see fig. 3). This approach ensures determinacy of Z_i^{K1} generation delays and possibility of setting up parallel individual service channels for several emulated interface modules within a single FPGA of the applied reconfigurable digital input-output device.

Ratio functions conversions specified by the F_{DW}^{K2} set (see expression (5)) are realized by the application of the top-level program module SA^{K2}, installed in an industrial computer (see fig. 3). When new K_i^{K2} values enter the control registers, a single interrupt queue is formed for all emulated IMs; in the order of their generation, interrupts are processed in the general software module SA^{K2} by way of reading K_i^{K2}, their conversion and recording Z_i^{K2} in the corresponding hardware registers of FPGA linked with SWUI IP-cores.

The analysis of the probabilistic and temporal characteristics of queuing systems presented in fig.4 and 5 can be performed on the basis of standard approaches [3–5; 9; 10]. Taking into account the necessity of ensuring the developed emulator performance in real strict-time mode ($\tilde{t}_r^{K1} \leq 12$ us, 12 us $< \tilde{t}_r^{K2} < 150$ ms) we analyze the worst

situation of delays in status data words Z_{DW}^{K1} and Z_{DW}^{K2} generation through the example of the developed emulator approbation in IROBO-4000 industrial computer and PCI-7813R device [2; 8].

Class № 1 requests service (performing $F_{DW}^{K1} : K_{DW}^{K1} \mapsto Z_{DW}^{K1}$ conversion) is carried out by means of already developed parallel service devices, the number of which equals the IM number (see fig. 4).

Here the service device is thought of as SWUI IP-core with the corresponding hardware conversion unit making use of FPGA resources. The number of service devices for K_{DW}^{K1} equals the number of IMs in the control unit; that excepts the accumulation of entering requests in the queue; thus, the emulator response time is determined by their service time. For the queuing system presented in fig. 4, the service time of *requests* is determined only by the time of the corresponding data words generation in status registers, and for the given hardware-software emulator implementation variant based on the results of the corresponding FPGA project development the time equals 2 clock-cycles [11–13]:

$$\tilde{t}_r^{K1} = \tilde{t}_s^{K1} = 2 \cdot \frac{1}{f_{cs}} = 2 \cdot \frac{1}{40 \cdot 10^6} = 50 \cdot 10^{-9} \text{s},$$

where f_{cs} – operational clock speed of FPGA project.

When new control data word values K_i^{K2} of No. 2 request class enter the corresponding hardware registers, a unified queue of hardware interrupts is formed for all emulated IMs. The interrupts data are processed in the SA^{K2} software module in the order of their generation (conversion $F_{DW}^{K2} : K_{DW}^{K2} \mapsto Z_{DW}^{K2}$). Maximum delay of

state data words Z_i^{K2} generation when $I = 8$, caused by control data words K_i^{K2} accumulation due to queuing in interrupt processing (see fig. 5) may be determined on account of the above evaluation results of the service channel implementation; the resulting expression is [3–5]:

$$\max\left(\tilde{t}_{\text{r}}^{\text{K2}}\right) = \max\left(\tilde{t}_{\text{q}}^{\text{K2}}\right) + \max\left(\tilde{t}_{\text{s}}^{\text{K2}}\right) =$$

$$= (I-1)\cdot\max\left(\tilde{t}_{\text{s}}^{\text{K2}}\right) + \max\left(\tilde{t}_{\text{s}}^{\text{K2}}\right) = 8\cdot15\cdot10^{-3} = 120\cdot10^{-3} \text{ s.}$$

Thus, the maximum values of response time in status data words generation for $\boldsymbol{K}_{\text{DW}}^{\text{K1}}$ and $\boldsymbol{K}_{\text{DW}}^{\text{K2}}$ obtained in use of the specified hardware-software IM emulator architecture meet the requirements formulated according to the experimental evaluation of PM CU performance. The suggested emulator architecture allows for modification of the implemented in SA^{K2} program module ratio sets $\boldsymbol{F}_{\text{DW}}^{\text{K2}}$ avoiding the FPGA project recompilation, thus providing its flexibility and unification for further industrial application.

Fig. 4. Representation of the hardware-software interface modules emulator
as a queuing system for processing of class No. 1 control data words

Рис. 4. Представление аппаратно-программного эмулятора интерфейсных модулей
сопряжения в виде системы массового
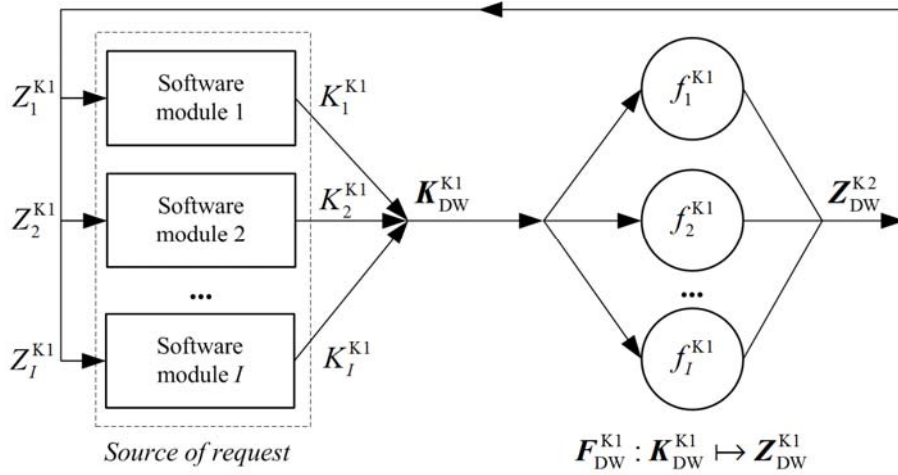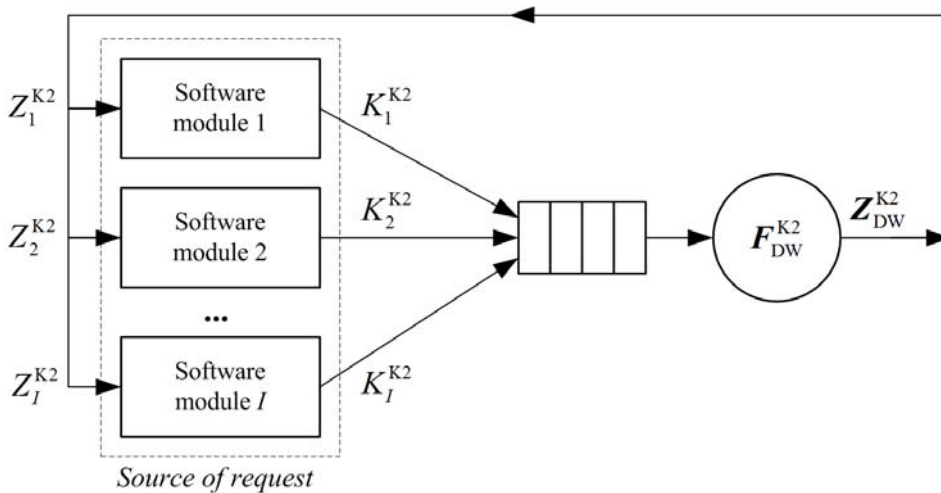обслуживания при обработке слов данных управления класса № 1

Fig. 5. Representation of the hardware-software interface modules emulator as a queuing
system for processing of class No. 2 control data words

Рис. 5. Представление аппаратно-программного эмулятора интерфейсных модулей
сопряжения в виде системы массового обслуживания при обработке слов данных
управления класса № 2

Conclusion. The proposed know-how (fig. 3) has been evaluated and successfully put into operation at the department of astrionics design and test operations of spacecraft control systems in SC "Academician M. F. Reshetnev "Information Satellite Systems" within the ground-based debugging complex of onboard electronic equipment [1; 2; 14; 15]. The debugging complex facilities emulating control unit interface modules of the SC onboard control complex with application of the proposed approach feature a set of unified devices (hardware modules) and the corresponding "FPGA firmware" (developed IMs) that can be independently modified and then compiled in arbitrary order within the corresponding device [11–13].

Application of the PCI-7813R reconfigurable digital input-output board allowed emulation of eight interface modules of the control unit; that reduced the cost of PM software evaluation by several times and shortened its testing time. Further operation of the developed hardware-software emulator proved that the used approaches and developed techniques were correct and efficient [11–15]. The developed hardware-software emulator provides for practical evaluation of regular PM software in the environment simulating real operating conditions of SC; that was achieved by applying certain methods simulating inflight contingency situations for onboard radio-electronic equipment and spacecraft: a number of faults, such as internal interface exchange errors, one of the IMs partial malfunction or failure, SC unit/component/ assembly malfunction, etc. [14; 15].

In general, the evaluated approaches to the method of software and hardware modeling with FPGA application can also be valid for analysis of space systems operation when using special units (components) of ground-based and / or onboard electronic equipment for simulating the changing conditions of transmitting signals via communication channels that depend on the propagation medium, payload characteristics, SC path, etc. [16–18].

References

1. Pichkalev A. V. [The terrestrial debugging complex for onboard radio-electronoc equpment]. *Reshetnevskiye chteniya : materialy XIV Mezhdunar. nauch. konf.* ["Reshetnev readings". Proceed. of XIV Intern. scientific. conf]. Krasnoyarsk, 2010, P. 515–516 (In Russ.).

2. Komarov V. A., Pichkalev A. V. [Application of NI FPGA technologies in testing spacecraft onboard equipment]. *Intellekt i nauka: trudy XI Mezhdunar. nauchn.-prakt. konf. ZHeleznogorsk, 28–29 aprelya 2011 g* [Intellect and science. Proceed. of the XI Intern. scientific-practical. conf., Zheleznogorsk, April 28–29, 2011]. Krasnoyarsk, 2011, P. 146–148 (In Russ.).

3. Takagi H. Queueing analysis. A foundation of performance evaluation. *Finite Systems*. 1993, Vol. II, 560 p.

4. Allen A. O. Probability, Statistics, and Queueing Theory with Computer Science Applications, 2nd ed. Academic Press, New York. 1990, 740 p.

5. Komarov V. A., Sarafanov A. V. [Development of a mathematical model of a multi-user mode of hardware

and software systems operation remote access]. *Informatsionnyye tekhnologii*. 2009, No. 3, P. 67–74 (In Russ.).

6. Burdonov I. B. Kosachev A. S., Ponomarenko V. N. [Real Time Operating Systems]. *Preprinty Instituta sistemnogo programmirovaniya RAN*. Preprint 14, Moscow, 2006, 98 p.

7. Baran E. D. *LabVIEW FPGA. Rekonfiguriruyemyye izmeritel'nyye i upravlyayushchiye sistemy* [LabVIEW FPGA. Reconfigurable measurement and control systems]. Moscow, DMK Press Publ., 2009, 448 p.

8. *Ofitsial'nyy sayt kompanii National Instruments* [Official website of National Instruments] (In Russ.). Available at: http://www.ni.com /ru-ru.html (accessed 16.11.2018).

9. Averill M. Law, David M. Kelton. Simulation modeling and analysis, 4th edition. McGraw-Hill, 2007, 768 p.

10. Komarov V. A., Sarafanov A. V. Simulation of the operation of multiuser distributed measurement and control systems. *Measurement Techniques*. 2011, Vol. 54, No. 2, P. 129–134. Doi: 10.1007/s11018-011-9695-y.

11. Komarov V. A., Yudin V. A., Poleshchuk V. V. *Emulyator interfeysnykh moduley sopryazheniya ispolnitel'nykh ustroystv sistem zhizneobespecheniya KA* [Emulator of interface modules of executive devices of SC life support systems]. Patent RF, No. 2013612869, 2013.

12. Komarov V. A., Yudin V. A., Kazaykin D. S. *Emulyator interfeysnykh moduley sopryazheniya kontrol'no-izmeritel'noy sistemy* [Emulator of interface modules of instrumentation and control system]. Patent RF, No 2013612871, 2013.

13. Komarov V. A., Yudin V. A. *Emulyator interfeysnykh moduley sopryazheniya s analogovymi signalami* [Emulator of analog signal interface module]. Patent RF, No 2013612874, 2013.

14. Nedorezov D. A., Pichkalev A. V., Krasnenko S. S., Nepomnuash O. V. [Application of FPGA for modeling of operation logic of spacecraft onboard radio-electronic equipment]. *Vestnik SibGAU*. 2014, No. 1 (53), P. 133–136 (In Russ.).

15. Nedorezov D. A., Legalov A. I., Nepomnyashchiy O. V., Krasnenko S. S., Ankudinov A. V. [Methodology of mutational testing for ground tests of spacecraft onboard equipment]. *Sistemy i sredstva informatiki*. 2014, Vol. 24, No. 1, P. 73–79 (In Russ.).

16. Leitner J. Space technology transition using hardware in the loop simulation. *Aerospace Applications Conference, 1996. Proceedings*. 1996. IEEE. Vol. 2, P. 303–311.

17. Pu Di, Wyglinski A. M. Digital Communication systems engineering with software-defined radio. Artech House, Boston. 2013, 288 p.

18. Komarov V. A., Pazderin S. O., Matveyenko S. P. *Imitator poleznoy nagruzki kosmicheskogo apparata* [Spacecraft Payload Simulator]. Patent RF, No. 181746, 2018.

Библиографические ссылки

1. Пичкалев А. В. Наземный отладочный комплекс бортовой радиоэлектронной аппаратуры // Решетневские чтения : материалы XIV Междунар. науч.

конф. / Сиб. гос. аэрокосмич. ун-т. Красноярск, 2010. С. 515–516.

2. Комаров В. А., Пичкалев А. В. Применение технологий NI FPGA при испытаниях бортовой аппаратуры космических аппаратов // Интеллект и наука : тр. XI Междунар. научн.-практ. конф., Железногорск, 28–29 апреля 2011 г. Красноярск : Центр информации, 2011. С. 146–148.

3. Takagi H. Queueing analysis. A foundation of performance evaluation // Finite Systems. 1993. Vol. II. 560 р.

4. Allen A. O. Probability, Statistics, and Queueing Theory with Computer Science Applications, 2nd ed. Academic Press, New York. 1990. 740 р.

5. Комаров В. А., Сарафанов А. В. Разработка математической модели многопользовательского режима функционирования аппаратно-программных комплексов с удаленным доступом // Информационные технологии. 2009. № 3. С. 67–74.

6. Бурдонов И. Б. Косачев А. С., Пономаренко В. Н. Операционные системы реального времени. Ин-та системного программирования РАН. Препринт. М., 2006. № 14. 98 с.

7. Баран Е. Д. LabVIEW FPGA. Реконфигурируемые измерительные и управляющие системы. М. : ДМК Пресс, 2009. 448 с.

8. Официальный сайт компании National Instruments [Электронный ресурс]. URL: http://www.ni.com/ru-ru.html (дата обращения: 16.11.2018).

9. Averill M. Law, David M. Kelton. Simulation modeling and analysis, 4th edition. McGraw-Hill, 2007, 768 р.

10. Komarov V. A., Sarafanov A. V. Simulation of the operation of multiuser distributed measurement and control systems // Measurement Techniques. 2011. Vol. 54, No. 2. P. 129.

11. Свидетельство о государственной регистрации программы для ЭВМ № 2013612869 Российская Федерация. Эмулятор интерфейсных модулей сопряжения исполнительных устройств систем жизнеобеспечения КА / В. А. Комаров, В. А. Юдин, В. В. Полещук ; дата рег. 14.03.2013.

12. Свидетельство о государственной регистрации программы для ЭВМ № 2013612871 Российская Федерация. Эмулятор интерфейсных модулей сопряжения контрольно-измерительной системы / В. А. Комаров, В. А. Юдин, Д. С. Казайкин ; дата рег. 14.03.2013.

13. Свидетельство о государственной регистрации программы для ЭВМ № 2013612874 Российская Федерация. Эмулятор интерфейсных модулей сопряжения с аналоговыми сигналами / В. А. Комаров, В. А. Юдин; дата рег. 15.03.2013.

14. Применение ПЛИС для моделирования логики функционирования бортовой радиоэлектронной аппаратуры космических аппаратов/ Д. А. Недорезов, А. В. Пичкалев, С. С. Красненко [и др.] // Вестник СибГАУ. 2014. № 1 (53). С. 133–136.

15. Методология мутационного тестирования для наземных испытаний бортовой аппаратуры космических аппаратов / Д. А. Недорезов, А. И. Легалов, О. В. Непомнящий [и др.] // Системы и средства информатики. 2014. Т. 24, № 1. С. 73–79.

16. Leitner J. Space technology transition using hardware in the loop simulation // Aerospace Applications Conference, 1996. Proceedings., 1996 IEEE. Vol. 2. P. 303–311.

17. Pu Di, Wyglinski A. M. Digital Communication systems engineering with software-defined radio. Artech House, Boston, 2013. 288 p.

18. Пат. 181746 Российская Федерация, МПК H04B 17/391, G01S 19/23. Имитатор полезной нагрузки космического аппарата / В. А. Комаров, С. О. Паздерин, С. П. Матвеенко, № 2017132132 ; заявл. 13.09.2017 ; опубл. 26.07.2018, Бюл. № 21.

Komarov Vladimir Aleksandrovich – Cand. Sc., Docent, head of the complex space systems modeling group; JSC "Academician M. F. Reshetnev "Information Satellite Systems". E-mail: VKomarov@iss-reshetnev.ru

Semkin Petr Vasil'yevich – head of the Department of Design of Space Systems and Communication Complexes, Information Relaying and Special Purpose; JSC "Academician M. F. Reshetnev "Information Satellite Systems". E-mail: psemkin@yandex.ru.

Комаров Владимир Александрович – кандидат технических наук, доцент, начальник группы комплексного моделирования космических систем; АО «Информационные спутниковые системы» имени академика М. Ф. Решетнева». E-mail: VKomarov@iss-reshetnev.ru.

Семкин Петр Васильевич – начальник управления проектирования космических систем и комплексов связи, ретрансляции информации и специального назначения; АО «Информационные спутниковые системы» имени академика М. Ф. Решетнева». E-mail: psemkin@yandex.ru.

CONTROL AND REGULATION EQUIPMENT OF ELECTRIC POWER SYSTEM FOR A PROSPECTIVE PILOTED TRANSPORT SYSTEM

V. V. Savenkov, A. K. Tishchenko, V. N. Volokitin

CJSC "Orbita"
88, Peshe-Streletskaya St., Voronezh, 394038, Russian Federation
E-mail: v.savenkov@orbitaenvo.ru

The aim of this work is to consider solving complex of tasks focused on fulfilling the complicated tactical and technical requirements for regulation and monitoring equipment (RME) of electric power supply system (EPS) for a prospective spacecraft. These requirements are imposed due to the need to ensure high reliability of the equipment during operation under the influence of external factors (vacuum, vibro-impact loads, radiation, absence of convective cooling), as well as to achieve high mass-dimensional parameters of the equipment and its high functionality

The complexity of problem solving lies in the need to ensure conflicting requirements – high levels of energy density, weight and size characteristics, reliability and durability.

These problems fully apply to the RME of the EPS for a prospective piloted transport system (PPTS) which design example shows ways of solving abovementioned problems.

The most rational way of solving these contradictions is to increase the specific energy indicators of the main components of the RME devices – power converters, which can be achieved by using modern power electronic elements, using new materials and semi-finished products, for example, printed circuit boards with a metal heat sink, as well as increasing the layout density design.

Determining solution is to select an optimal structure of the power converter, which provides the best efficiency.

An additional way to reduce the mass-dimensional indicators of the RME is the use of a digital control method, the collection of telemetric information, and the receiving and processing of commands.

At the same time, on the contrary, to ensure the specified reliability of the equipment, it is necessary to use excess reservation at the element level – for power components, and the principles of majority reservation at the functional block level – for control and telemetry schemes.

Using the example of RME, developed by CJSC "Orbita", the main EPS parameters of a new generation spacecraft are shown and most important power supply subsystems are considered in the article: the solar energy control subsystem and the power storage subsystem, ways to build them for meeting specified requirements, taking into account the proposed solutions.

As a result of this work, the optimal structures of power converters – the current regulator of the solar battery and the current regulator of the battery – were selected, the basic principles of power components reservation ensuring the operability of the equipment in case of a single failure of any component without loss of performance and deterioration of RME parameters as a whole are shown.

Block-modular construction method is used for optimal layout and high reliability of the RME, it ensures uniform heat removal from electronic components, which is especially important in vacuum conditions, minimum dimensions and mass optimization of the RME, as well as high mechanical strength of the structure.

The implemented principles of building the RME for PPTS using this approach will allow to increase the active lifetime (ALT) and reliability of the spacecraft with a simultaneous decrease in mass and dimension parameters.

Keywords: prospective transport spacecraft, regulation and control equipment, power supply system.

АППАРАТУРА РЕГУЛИРОВАНИЯ И КОНТРОЛЯ СИСТЕМЫ ЭЛЕКТРОПИТАНИЯ ПЕРСПЕКТИВНОГО ПИЛОТИРУЕМОГО ТРАНСПОРТНОГО КОРАБЛЯ

В. В. Савенков, А. К. Тищенко, В. Н. Волокитин

ЗАО «Орбита»
Российская Федерация, 394038, г. Воронеж, ул. Пеше-Стрелецкая, 88
E-mail: info@orbitaenvo.ru

Целью работы является решение комплекса задач, направленных на выполнение сложных тактико-технических требований, предъявляемых к аппаратуре регулирования и контроля (АРК) систем электропитания (СЭП) перспективных космических аппаратов, обусловленных необходимостью обеспечения высоких показателей надежности аппаратуры при эксплуатации в условиях воздействия внешних воздействующих факторов (вакуум, виброударные нагрузки, радиация, отсутствие конвективного охлаждения), а также достижения высоких массогабаритных показателей аппаратуры и ее высокой функциональности.

Сложность решения задач обусловлена необходимостью обеспечения противоречивых по физической сути требований – высоких показателей энергетической плотности, массогабаритных характеристик, надежности и долговечности.

В полной мере указанные проблемы относятся и к аппаратуре регулирования и контроля системы электропитания перспективного пилотируемого транспортного корабля (АРК ПППТ) нового поколения, на примере проектирования которого показан вариант решения указанных задач.

Наиболее рациональным способом устранения указанных противоречий можно назвать повышение удельных энергетических показателей основных составляющих устройств АРК – силовых преобразователей, которого возможно достичь путем использования современной силовой электронной компонентной базы, применения новых материалов и полуфабрикатов, например, печатных плат с металлическим теплоотводом, а также повышения плотности компоновки при проектировании.

В свою очередь, определяющим решением является выбор оптимальной структуры силового преобразователя, обеспечивающего наилучшую энергетическую эффективность.

Дополнительным путем уменьшения массогабаритных показателей АРК является применение цифрового способа управления, сбора телеметрической информации, приема и обработки команд.

В то же время, напротив, для обеспечения заданных показателей надежности аппаратуры необходимо использовать избыточное резервирование на уровне элементов (для силовых компонентов) и принципы мажоритарного резервирования на уровне функциональных блоков (для схем управления и телеметрии).

На примере разработанной предприятием ЗАО «Орбита» АРК представлены основные параметры СЭП космического корабля нового поколения, рассмотрены важнейшие подсистемы электропитания: подсистема регулирования солнечной энергии и подсистема хранения электроэнергии, способы их построения для реализации заданных требований с учетом предложенных решений.

В результате проведенной работы выбраны оптимальные структуры силовых преобразователей – регулятора тока солнечной батареи и регулятора тока аккумуляторной батареи, представлены основные принципы резервирования силовых компонентов, обеспечивающих работоспособность аппаратуры в случае единичного отказа любого компонента без потери работоспособности и ухудшения параметров АРК в целом.

Для оптимальной компоновки и высокой надежности АРК использованы блочно-модульный способ построения, обеспечивающий равномерный отвод тепла от электронных компонентов, что особенно важно в условиях вакуума, минимизация габаритов и массы АРК, а также высокая механическая прочность конструкции.

Реализованные принципы построения АРК для ПППТ с использованием указанного подхода позволят увеличить срок активного существования (САС), повысить надежность КА с одновременным снижением массогабаритных показателей.

Ключевые слова: перспективный транспортный корабль, аппаратура регулирования и контроля, система электропитания.

Introduction. The development of the RME for a spacecraft (SC) is a multicriteria task, the successful solution of which depends on many factors. At the same time, at this stage of development of the converter and digital circuitry, it is almost impossible to build a single universal design of the RME, which would be easily integrated into the EPS of the SC for various purposes, due to the fact that the EPS of the SC has different voltage levels (EPS with low voltage – up to 50 V, EPS with high voltage – over 100 V) and power levels of the payload (from hundreds of watts to tens of kW).

These factors largely determine the structure, management methods and design features of the RME.

As a rule, the RME of the piloted SC provides with electric power EPS of the SC with a low voltage of 28.5 V or 32.5 V, which is due to the high safety requirements of the crew during the flight, maintenance and repair work, and scheduled tasks carried out with the RME in full-scale space flight. On the other hand, the ARK of the piloted spacecraft is subjected to strict requirements for mass and size, which forms the problem of improving the energy performance of RME power converters, first of all, increasing their efficiency.

The RME is the main link in the electrical power supply system of a prospective reusable piloted transport spacecraft [1], which should replace the piloted space-

ships of the Soyuz series and automatic cargo ships of the Progress series.

Big active lifetime (SAS) (up to 1.5 years), high requirements for reliability (probability of trouble-free operation of the RME is not less than 0.998), multifunctionality, determined the need to choose the optimal structure of the RME for the PPTS and implement unique design solutions in it.

Application of the RME. Together with rechargeable batteries (AB), solar batteries (SB), and onboard cable network the system must provide [2]:

– joint work of SB and AB on the total load;

– power supply of onboard equipment of the PPTS with a constant voltage of 32.5 V of the required quality;

– autonomous charge of each battery with a charging current of a value corresponding to the levels of charge current settings generated by the commands of on-board computer systems (OCS);

– alignment of discharge currents to the total load of parallel operating ABs, with limited discharge current levels;

– the exchange of information with the OCS in terms of receiving and processing commands and transmitting telemetric information via the serial interface bus (SIB) GOST R 52070;

– information exchange via the CAN interface with the AB control module in terms of receiving commands for switching on / off the charge of the battery and transmitting telemetry information from the battery to the RME.

The structure and basic parameters of the RME. The period of active existence of a PPTS is within the limits of 1–1.5 years, while the resource of PPTS must provide its operation both in near-earth orbit and as a part of the near-moon infrastructure.

In this regard, the peculiarities of the operation of PPTS determine rather strict technical requirements for PPTS subsystems, including the RME for:

– weight and size indicators;

– reliability;

– radiation resistance;

– effectiveness;

– energy density.

As a rule, to implement high technical requirements for the RME, the developer of the equipment has to solve many contradictory tasks. For example, increasing of reliability of the RME by reducing the load factor of electronic components (ERI) and redundancy of nodes lead to increase in mass, and increase in efficiency and radiation resistance reduce the energy density and, consequently, worsens mass and dimension parameters of the RME [2–4].

The electrical power supply of the onboard equipment in the PPTS should be provided by a low-voltage EPS with a voltage in the range from 28 V to 32.5 V and with a total power of up to 4000 W.

The implementation of the requirements of the technical specifications in terms of ensuring high reliability and energy density of the RME for the PPTS is performed by applying a block-modular method of building, backup of power elements and nodes, microcontrollers, digital logic. At the same time, the national radiation-resistant element base is used in the construction of the *RME* for the PPTS [2; 5].

The block diagram of the RME for the PPTS and its connection with the EPS of the PPTS is shown in fig. 1.

The block diagram of the ARK for the PPTS contains: 4 current regulators RT1 ... RT4, 4 charge-discharge devices ZRU1 ... ZRU4 (AB current regulators), a voltage regulator SN 32.5 V, 2 filters (one for each independent power bus), a controller.

Subsystem for regulating solar energy. To ensure high energy efficiency requirements, a gallium-arsenide solar battery was used as the primary source of energy with the following main characteristics: the power of one SB at the beginning of a flight is 1800 W, the open-circuit voltage is 100 V, and the short-circuit current is 37 A.

To regulate the current of the solar battery, a parallel type regulator is used, and since a special feature of the chosen type of solar battery compared to silicon-based batteries is an increased electrical capacitance (up to 1 µF), current-limiting circuits are used in the power switch to ensure a smooth current rise trajectory.

The block diagram of the SB current regulator is shown in fig. 2

The current regulator contains: a sensitive element, a feedback signal adder (OS), a PWM signal comparator, a 25 kHz sawtooth voltage generator, a current limiting throttle, a current shunt for measuring the current telemetry signal of the SB, PWM signal drivers (PWM signal amplifiers), the power elements of the regulator presented by field-effect transistors (with series-parallel redundancy) and Schottky diodes.

The regulators are structurally combined by 2 items in 2 power modules with a capacity of 1800 W each, with each current controller having a series-parallel redundancy of the most critical power and control elements. The specific power of each module is 703 W/kg. Each module contains a regulator capable of switching the energy of the SB to two independent power supply buses with the help of switching elements SE (see fig. 1).

The power delivered to the load by each SB current regulator is 900 W.

Energy storage subsystem. The lithium-ion rechargeable battery with the following parameters was used in the energy storage subsystem: operating voltage range – (16.2... 29.5) V; maximum discharge current – 45 A; charging current is steppable, reduced during charging, having six setting levels (20.0; 10.0; 5.0; 2.5; 1.0; 0 A).

The AB current regulator is a charge-discharge device based on direct converters of the raising and lowering types with PWM regulation [6–12].

The block diagram of the AB current regulator is shown in fig. 3

The AB current regulator is a charge-discharge device that contains: a sensitive element, a feedback (OS) adder, a current regulator with current limit, a voltage and current feedback (OS) signals adder, a PWM "CHARGE" comparator, a PWM "DISCHARGE" comparator, a sawtooth voltage generator for PWM – "CHARGE" and PWM – "DISCHARGE" comparators, an electronic fuse on the power field-effect transistor, PWM-signal drivers (PWM-signal amplifiers), power elements of the regulator – field-effect transistors (with parallel redundancy) and Schottky diodes, a current shunt for measuring the current of the AB.
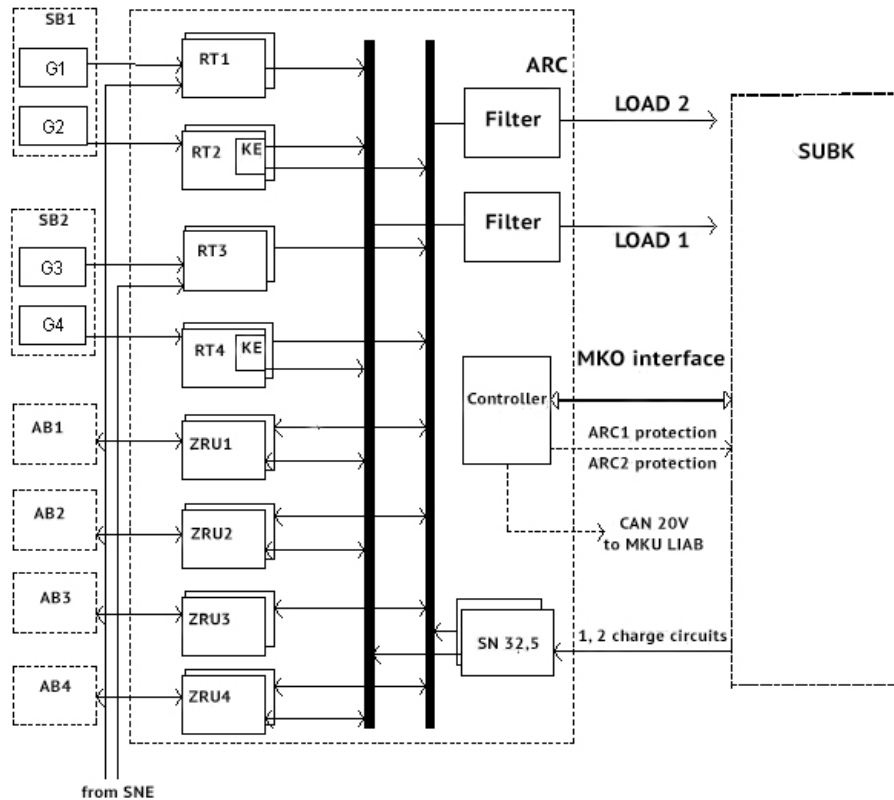
Fig. 1. Block diagram of the RME for the PPTS and its connection with the EPS of the PPTS:
AB1…AB4 rechargeable batteries; SB1, SB2 – solar batteries; G1…G4 – solar generators, SUBK –onboard complex control system of PPTS; MKU LIAB – lithium-ion battery monitoring and control module; SH1, SH2 –independent power lines of PPTS; ELOI –lunar orbital infrastructure elements; EZOI – Earth orbital infrastructure elements; SNE – ground power system

Рис. 1. Структурная схема АРК ПППК и её связи с СЭП ПППК:
АБ1…АБ4 аккумуляторные батареи; СБ1, СБ2 – солнечные батареи; G1…G4 – солнечные генераторы; СУБК – система управления бортовым комплексом ПППК; МКУ ЛИАБ – модуль контроля и управления литий-ионной аккумуляторной батареи; Ш1, Ш2 – независимые шины электропитания ПППК; ЭЛОИ – элементы лунной орбитальной инфраструктуры; ЭЗОИ – элементы земной орбитальной инфраструктуры; СНЭ – система наземного электропитания

Fig. 2. Block diagram of SB current regulator

Рис. 2. Блок-схема регулятора тока СБ

Fig. 3. Block diagram of AB current regulator

Рис. 3. Блок-схема регулятора тока АБ

The design contains 4 pieces of charge-discharge power module, by 2 pcs. of charge-discharge devices each. The module provides 700 W of power, while one device is redundant in each module. The specific power of each charge-discharge module is 284 W/kg.

Control of current power converters of SB and AB is carried out automatically depending on the energy balance on board in accordance with the description given in [13–17].

Constructive and functional features of the RME, ensuring high reliability of the EPS. To increase the reliability of the EPS for the PPTS two independent power supply buses are provided in the RME. In case of failure of any device connected to one bus (for example, as a result of a short circuit), the second bus remains operational, providing power to onboard critical loads up to 2800 W, while part of the solar battery powering the failed bus is switched by one of the current regulators using the SE for a working bus.

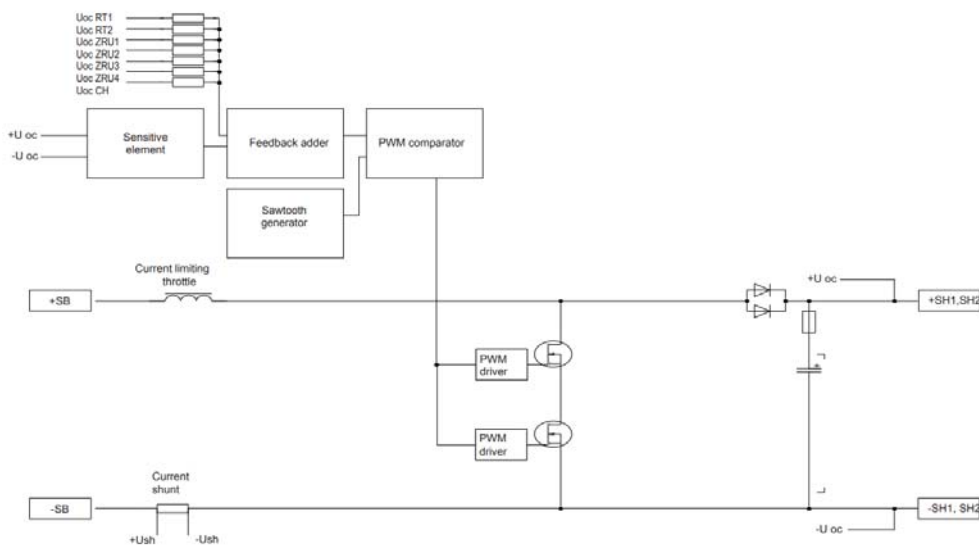The high reliability of the RME for the PPTS is also provided by the use of high-speed electronic short-circuit protection (SC), which may occur in power supply buses described in [12]. In case of a short circuit in the bus, the protection acts in less than 10 μs. In this case, the protection remains active until the cause of the short-circuit fault is completely eliminated.

The use of a digital information transmission channel based on CAN and MPI protocols for transmitting telemetric and control information has significantly reduced the number of electrical connections between the RME and the OCS, on the one hand, and the RME and the AB control module, on the other.

To increase the energy density in the RME, the optimal configuration of power ERI was implemented on the

basis of printed circuit boards with a metal base and ERIs were applied, including power, surface mounted ones.

The applied modern electronic component base, the developed constructive and circuit solutions have provided the optimal operational, energy and mass-dimensional characteristics of the RME. The mass of the RME is 25 kg.

Fig. 4 shows a general view of the ARP for the PPTS.

Conclusion. When constructing the RME for the PPTS of a new generation, the main criteria were considered, allowing to realize the specified characteristics of the EPS for the PPTS. It has been demonstrated that the main points in ensuring the specified technical requirements of the Customer in the development of the RME are: the choice of the optimal structure and circuit design of the RME power converters, the use of modern radiation-resistant components, excessive redundancy of individual elements and majorization of the main functions, active protection from dangerous states (for example, a short circuit in power circuits), a block-modular method of construction of the RME.

As a result, to meet the needs of the development requirements specification, based on many years of experience in creating equipment for regulation and control of EPS systems of spacecraft for various purposes, the design of the ARP for the PPTS was developed, featuring unique circuit design and construction solutions that significantly improved mass and dimensional characteristics of the equipment and increased energy density and efficiency of power converters, ensure good heat dissipation at the same time ensuring high reliability.

The development and application of innovative solutions in building the structure of the ARP for the PPTS allowed to ensure the specified requirements in full measure.
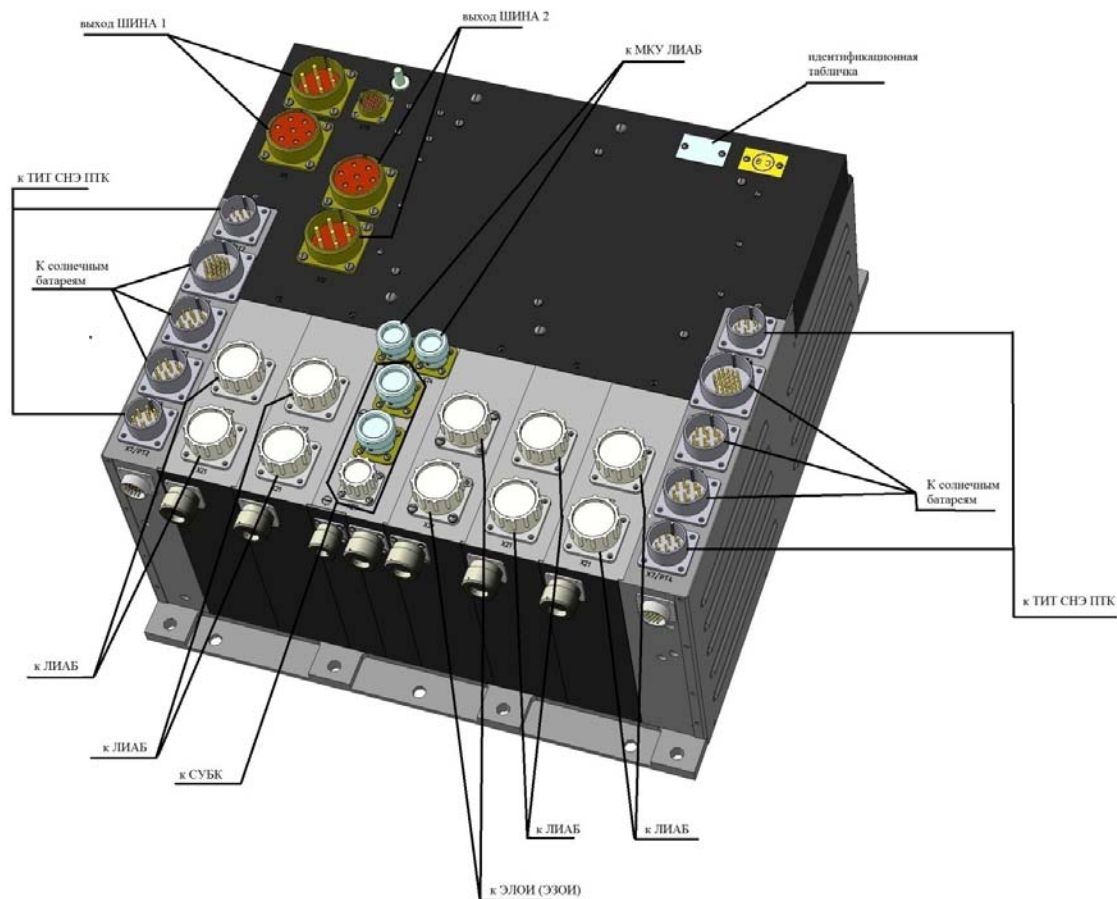
Fig. 4. General view of the RME of the PPTS

Рис. 4. Общий вид АРК ПППТК

References

1. *Pilotiruemyy transportnyy korabl' novogo pokoleniya* [New generation perspective manned transport spacecraft]. Available at: http://kosmolenta.com/index.php/new-tech/ptknp (accessed: 10.02.2019).

2. Orbita, CJSC – Scientific and technical report on part of R&D work "Determinations of suggestions on design and technical requirements implementation for control and regulation equipment (RME) EPS PMTS".

3. Power source control device. Patent WO 2011037170 H02J 7/00 H02H 5/04.

4. Semiconductor device of energy distribution, method and device of regulation (control). Patent USA 2009273239 H02J 1/00.

5. Foreign EEE components radiation resistance database. RSRI "Electrostandard".

6. Orbita, CJSC – Scientific and technical report on part of R&D work "Determinations of suggestions on design and technical requirements implementation for control and regulation equipment (RME) EPS PMTS".

7. Savenkov V. V., Popov A. P. *Zaryadno-razryadnoe ustroystvo* [Charge-discharge equipment]. Patent RF, No. 2217853, 2003.

8. Tishchenko A. K, Livshin G. D., Vlasov F. S. *Zaryadno-razryadnoe ustroystvo* [Charge-discharge equipment]. Patent RF, No. 2306652, 2007.

9. Varenbud L. R., Volokitin V. N., Znov A. M., Tishchenko A. K. *Ustroystvo dlya vyravnivaniya napryazheniya v batarei* [Device for equalizing of the voltage in the battery]. Patent RF, No. 120820, 2012.

10. Switchable power supply circuit. Patent USA 2009207634 H02M 3/335 H02M 3/34.

11. Charging and discharging device. Patent China 101997442 H02J 7/00 H02M 1/14 H02M 7/537.

12. Battery method and control device. Patent USA 2011078092 G06F 17/00 H02J 7/00.

13. Tishchenko A. K., Gankevich P. T., Livshin G. D., Savenkov V. V. *Avtonomnaya sistema elektropitaniya* [Autonomous power supply system]. Patent RF, No. 2211478, 2003.

14. Tishchenko A. K., Gankevich P. T., Savenkov V. V., Livshin G. D. *Avtonomnaya sistema elektropitaniya* [Autonomous power supply system]. Patent RF, No. 2152069, 2000.

15. Tishchenko A. K., Savenkov V. V., Gankevich P. T. *Avtonomnaya sistema elektrosnabzheniya* [Autonomous power supply system]. Patent RF, No. 2229191, 2004.

16. Varenbud L. R., Dezhurov S. A., Pyl'nev R. E., Tishchenko A. K. *Apparatura regulirovaniya i kontrolya sistemy elektrosnabzheniya kosmicheskogo apparata* [Control and regulation equipment for power supply system of spacecraft]. Patent RF, No. 117194, 2012.

17. Battery method and control device. Patent USA 2011078092 G06F 17/00 H02J 7/00.

Библиографические ссылки

1. Пилотируемый транспортный корабль нового поколения [Электронный ресурс]. URL: http://kosmolenta.com/index.php/new-tech/ptknp (дата обращения: 10.02.2019).

2. ЗАО «Орбита». Научно-технический отчёт о составной части ОКР «Разработка предложений по конструкции и реализации технических требований для аппаратуры регулирования и контроля (АРК) СЭС ППТС».

3. Power source control device. Patent WO 2011037170 H02J 7/00 H02H 5/04.

4. Semiconductor device of energy distribution, method and device of regulation (control). Patent USA 2009273239 H02J 1/00.

5. База данных по радиационной стойкости электронных компонентов зарубежного производства (РСЭК). РНИИ «Электростандарт».

6. Пат. 2165669 Российская Федерация, (51) МПК (2000.01) H 02 J 7/10. Зарядно-разрядное устройство / Савенков В. В., Тищенко А. К., Лившин Г. Д. № 99127500/09 ; заявл. 21.12.1999 ; опубл. 20.04.2001, Бюл. № 11.

7. Пат. 2217853 Российская Федерация, (51) МПК (2000.01) H 02 J 7/10, H 02 J 9/06. Зарядно-разрядное устройство / Савенков В. В., Попов А. П. № 2001127450/09 ; заявл. 09.10.2001 ; опубл. 27.11.2003, Бюл. № 33.

8. Пат. 2306652 Российская Федерация, (51) МПК (2006.01) H 02 J 7/02. Зарядно-разрядное устройство / Тищенко А. К., Лившин Г. Д., Власов Ф. С. № 2005137604/09 ; заявл. 05.12.2005 ; опубл. 20.09.2007, Бюл. № 26.

9. Пат. 120820 Российская Федерация, (51) МПК (2006.01) H 02 J 7/00. Устройство для выравнивания напряжения в батареи / Варенбуд Л. Р., Волокитин В. Н., Знов А. М., Тищенко А. К. № 2012115171/07 ; заявл. 16.04.2012 ; опубл. 27.09.2012, Бюл. № 27.

10. Switchable power supply circuit. Patent USA 2009207634 H02M 3/335 H02M 3/34.

11. Charging and discharging device. Patent China 101997442 H02J 7/00 H02M 1/14 H02M 7/537.

12. Battery method and control device. Patent USA 2011078092 G06F 17/00 H02J 7/00.

13. Пат. 2211478 Российская Федерация, (51) МПК (2000.01) G 05 F 1/59, H 02 J 1/10, H 02 J 7/34, H 02 J 9/00. Автономная система электропитания / Тищенко А. К., Ганкевич П. Т., Лившин Г. Д., Савенков В. В. № 2001111492/09 ; заявл. 25.04.2001 ; опубл. 10.03.2003, Бюл. № 7.

14. Пат. 2152069 Российская Федерация, (51) МПК (2000.01) G 05 F 1/59, H 02 J 7/34, H 02 J 9/00. Автономная система электропитания / Тищенко А. К., Ганкевич П. Т., Савенков В. В., Лившин Г. Д. № 98119125/09 ; заявл. 21.10.1998 ; опубл. 27.06.2000, Бюл. № 18.

15. Пат. 2229191 Российская Федерация, (51) МПК (2000.01) H 02 J 9/06. Автономная система электроснабжения / Тищенко А. К., Савенков В. В., Ганкевич П. Т. № 2001121618/09 ; заявл. 29.06.2001 ; опубл. 20.05.2004, Бюл. № 14.

16. Пат. 117194 Российская Федерация, (51) МПК (2006.01) G 05 F 1/59. Аппаратура регулирования и контроля системы электроснабжения космического аппарата / Варенбуд Л. Р., Дежуров С. А., Пыльнев Р. Е., Тищенко А. К. № 2012105520/08 ; заявл. 16.02.2012 ; опубл. 20.06.2012, Бюл. № 17.

17. Пат. 2185016 Российская Федерация, (51) МПК (2000.01) H 02 H 3/08, H 02 H 3/087. Электронный предохранитель / Савенков В. В., Ганкевич П. Т., Тищенко А. К., Казановский А. И., Иванов В. Г. № 2000116552/09 ; заявл. 22.06.2000 ; опубл. 10.07.2002, Бюл. № 19.

Savenkov Vladimir Vladimirovich – Cand. Sc. (Engineering), Deputy General Director for Science – Chief designer; CJSC "Orbita". E-mail: v.savenkov@orbitaenvo.ru.

Tishchenko Anatoliy Konstantinovich – Cand. Sc. (Engineering), Head of R&D department of power supply systems; CJSC "Orbita". E-mail: Molibden3@yandex.ru.

Volokitin Vadim Nikolaevich – Cand. Sc. (Engineering), Head of R&D department of control and regulation equipment; CJSC "Orbita". E-mail: volokitin@orbtiaenvo.ru.

Савенков Владимир Владимирович – кандидат технических наук, заместитель генерального директора по науке – главный конструктор; ЗАО «Орбита». E-mail: v.savenkov@orbitaenvo.ru.

Тищенко Анатолий Константинович – кандидат технических наук, начальник научно-исследовательского отдела систем электропитания; ЗАО «Орбита». E-mail: Molibden3@yandex.ru.

Волокитин Вадим Николаевич – кандидат технических наук, начальник научно-исследовательского отдела аппаратуры регулирования и контроля; ЗАО «Орбита». E-mail: volokitin@orbtiaenvo.ru.

MODELING OF THE STRESS-STRAIN STATE OF ROCKET-SPACE TECHNOLOGY STRUCTURAL ELEMENTS MANUFACTURED BY USING ADDITIVE TECHNOLOGIES

E. S. Ushakova

Bauman Moscow State Technical University
5, 2-ya Baumanskaya St., Moscow, 105005, Russian Federation
E-mail: ellizaweta@gmail.com

One of the promising areas for improving the methods of manufacturing structural elements of rocket and space technology is the use of selective laser melting technology which represents a unique opportunity to manufacture metal products by melting powder and producing a one-piece solid phase structure. However, pores and other structural defects can appear in the formed element during laser sintering which causes a decrease in the strength characteristics of the parts produced. An important step in the additive technologies introduction is the development of methodology for the preliminary prediction of the strength characteristics of manufactured structural elements under the influence of mechanical loads with the help of mathematical modeling. The methodology for estimating the material strength reduction of a rocket-space technology element obtained using additive technologies by simulating a porous structure and calculating the characteristics of the stress-strain state is presented.

The proposed mathematical model and the methodology for calculating the specimen loading on the basis of the distortion energy theory allow calculating the stress-strain state in the process of numerical simulation for different values of the pore diameter. The reduction in yield strength due to the material porosity of the part is estimated using a coefficient equal to the ratio of equivalent stresses arising when a load is applied to a specimen manufactured using traditional and additive technologies. The value of the introduced coefficient characterizes the structure of the grown product and is considered as a function of the random arrangement of pores in the specimen under study. The appearance of pores is the result of a combination of factors: the composition and dispersion of the original metal powder, feed rate, removal distance and laser power during sintering, part orientation and sintering direction, the height of the level of powder deposited on a special base before sintering, etc.

The paper evaluates the reduction in strength for the working part of a series of tensile test specimens grown from metal powder of different dispersity. The non-linear nature of the dependence of the yield strength on the particle diameter of the original metal powder is established. The maximum value of the yield strength corresponds to the specimen with the minimum value of the total surface area of the pores.

Keywords: additive technologies, liquid rocket engine, combustion chamber, porosity, stress-strain state, yield strength.

МОДЕЛИРОВАНИЕ НАПРЯЖЕННО-ДЕФОРМИРОВАННОГО СОСТОЯНИЯ КОНСТРУКЦИЙ РАКЕТНО-КОСМИЧЕСКОЙ ТЕХНИКИ, ИЗГОТОВЛЕННЫХ С ИСПОЛЬЗОВАНИЕМ АДДИТИВНЫХ ТЕХНОЛОГИЙ

Е. С. Ушакова

Московский государственный технический университет имени Н. Э. Баумана
Российская Федерация, 105005, г. Москва, 2-я Бауманская ул., 5
E-mail: ellizaweta@gmail.com

Одним из перспективных направлений совершенствования методов изготовления конструктивных элементов ракетно-космической техники является применение технологии селективного лазерного плавления, которая дает уникальную возможность изготавливать изделия из металла посредством расплавления порошка и получения сплошной твердофазной структуры. Однако при лазерном спекании в формируемом элементе могут образовываться поры и прочие дефекты структуры, что вызывает снижение прочностных характеристик изготавливаемых деталей. Важным этапом при внедрении аддитивных технологий является разработка ме-

тодов предварительного прогнозирования прочностных характеристик изготавливаемых элементов конструкции в условиях воздействия механических нагрузок с помощь математического моделирования. Представлена методика оценки снижения прочности материала элемента конструкции ракетно-космической техники, полученного с использованием аддитивных технологий с помощью моделирования пористой структуры и расчета характеристик напряженно-деформированного состояния.

Предложенные математическая модель и методика расчета нагружения образца, основанная на теории энергии формоизменения, позволяют провести расчёт напряженно-деформированного состояния в процессе численного моделирования для разных значений диаметра пор. Снижение предела текучести в связи с пористостью материала детали оценивается с помощью коэффициента, равного отношению эквивалентных напряжений, возникающих при приложении нагрузки к образцу, изготовленному посредством традиционных и аддитивных технологий. Значение введенного коэффициента характеризует структуру выращенного изделия и рассматривается как функция случайного расположения пор в исследуемом образце, появление которых является результатом влияния совокупности факторов: состав и дисперсность исходного металлического порошка, скорость подачи, расстояние выведения и мощность лазера при спекании, ориентация детали и направление спекания, высота уровня порошка, нанесенного на специальное основание перед спеканием и др.

В работе проведена оценка снижения прочности для рабочей части серии образцов для испытаний на растяжение, выращенных из металлического порошка различной дисперсности. Установлен нелинейный характер зависимости предела текучести от диаметра частиц исходного металлического порошка. Максимальное значение предела текучести соответствует образцу с минимальным значением суммарной площади поверхности пор.

Ключевые слова: аддитивные технологии, жидкостной ракетный двигатель, камера сгорания, пористость, напряженно-деформированное состояние, предел текучести

Introduction. Currently, improving manufacturability and reducing the cost of manufacturing rocket-space technology (RST) structural elements are important scientific and technical challenges. The disadvantage of traditional methods of manufacturing the most heavily loaded units of a liquid-propellant rocket engine (LRE) – combustion chambers (CCs) – is the problem of ensuring the reliability of structures and controlling their quality due to the use of a large number of soldered joints in manufacturing as well as the need to manufacture expensive tooling. For example, only the process of electroerosive deposition of the "artificial" roughness creating turbulence in the coolant flow on the bottom of the cooling tract channels of the CC inner shell lasts 900 n / h [1].

One of the promising directions of improving the methods of manufacturing the rocket-space technology structural elements is the use of additive technologies (AT) [2]. Their main advantages include: manufacturing objects of complex shape with high accuracy, optimizing time spent on manufacturing, using a combination of metal powders (for example, BrH08 + stainless steel) in order to obtain strength characteristics corresponding to the operating conditions of the grown product [3].

The development of additive technologies, in particular, the technology of selective laser melting (SLM), represents a unique opportunity to manufacture metal products by melting powder and obtaining a one-piece solid phase structure [4]. The use of SLM technology allows increasing the material utilization rate to almost 99 % and, thereby, reducing the cost of production [5]. However, during SLM pores and other structural defects (non-melts, cracks, inclusions, etc.) may appear in the formed element, which causes a decrease in the strength characteristics of the parts produced. One of the objects of RST where the introduction of AT seems to be promising is the LRE chamber.

Since the working process in the LRE is characterized by relatively large values of pressure and temperature in

the CC [6], an important step in the introduction of AT is the development of methods for preliminary prediction of the strength characteristics of manufactured structural elements under the influence of mechanical loads using mathematical modeling.

The purpose of this work is to develop a methodology for evaluating the strength reduction of the material obtained using additive technologies by modeling the porous structure and calculating the characteristics of the stress-strain state (SSS).

Mathematical model. The methodology for assessing the strength reduction of parts manufactured using additive technologies on the basis of the SSS determination in the process of numerical simulation using the distortion energy theory (Mises-Huber-Genki theory) [7] has been developed. According to this methodology it is assumed that the specimen begins to break (or to become unacceptably deformed) under the condition $\sigma_{eq} \geq \sigma_{yield}$, where σ_{eq} is von Mises equivalent stress arising in the part under the action of a given load, σ_{yield} is the yield strength of the material of the part.

A safety factor – the ratio of yield strength to equivalent stress σ_{yield} determined, for example, according to Mises [7] – can be used as a characteristic of the strength reliability of a RST product:

$$K_s = \frac{\sigma_{yield}}{\sigma_{eq}}.$$

The reduction of the yield strength $\sigma_{yield.add}$ of the RST structural element material grown from metal powder is taken into account using the coefficient n (<1):

$$\sigma_{yield.add} = n \cdot \sigma_{yield}.$$

Then the safety factor for parts made using additive technology will be determined by the formula:

$$K_{s.add} = \frac{\sigma_{yield.add}}{\sigma_{eq}} = \frac{n \cdot \sigma_{yield}}{\sigma_{eq}}. \tag{1}$$

In this formulation, the value of the coefficient n characterizes the structure of the grown product and is considered as a function of the random arrangement of pores in the specimen under study. The appearance of pores is the result of the influence of a combination of factors: the composition and dispersion of the original metal powder, feed rate, removal distance and laser power during sintering, part orientation and sintering direction, the height of the level of the powder deposited on a special base before sintering, etc. [8–12].

Pores (as well as cracks, non-melts, etc.) in the structure of any material are local sharp changes in the uniformity of shape and rigidity of the product structure and lead to local increase in the value of internal stresses. Consequently, the value of the equivalent stress $\sigma_{eq.pore}$ caused by a given load for a part with pores will be higher than the value for a monolithic part σ_{eq} made of material with the same physical and mechanical properties. The safety factors for the cases considered are determined by the formulas:

$$K_{s.solid} = K_s = \frac{\sigma_{yield}}{\sigma_{eq}};$$

$$K_{s.pore} = \frac{\sigma_{yield}}{\sigma_{eq.pore}}; \qquad (2)$$

$$K_{s.solid} > K_{s.pore}.$$

By presenting a part grown from metal powder as a monolithic one with the presence of local inhomogeneities in the material structure it is possible to consider the values of safety factors from formulas (1) and (2): $K_{s.add} = K_{s.pore}$ to be equal. Then, in accordance with the idea of the physical meaning of the coefficient n, its value will be equal to the ratio of equivalent voltages:

$$\frac{n \cdot \sigma_{yield}}{\sigma_{eq}} = \frac{\sigma_{yield}}{\sigma_{eq.pore}};$$

$$n = \frac{\sigma_{eq}}{\sigma_{eq.pore}}.$$

Consequently, the decrease in the tensile strength of a metal part made by the method of SLM is due to increase in the value of equivalent stresses as compared to a metal part made using traditional methods.

The porosity of the part material is determined by the formula:

$$\varepsilon_{pore} = 1 - k_{lay},$$

where: $k_{lay} = 1 - \dfrac{V_{pore}}{V}$ is the packing factor, V is part volume, V_{pore} is the pore volume in the part material.

Calculation model of the specimen loading. Structural cryogenic steel AISI 316L the mechanical properties [13] of which are listed in Table 1 is considered as a material of the structural RST element.

The porous structure of the specimen created by the method of selective laser sintering from ASIS 316L steel was studied in [14]. The relationship between the structure of the grown material and the sintering and the dispersion modes of the original metal powder was experimentally established in this work. A complex configuration of pores can be approximated by a set of spherical surfaces on the basis of a number of images obtained on the surface of thin sections of material specimens. In the first approximation we will consider the diameter and distance between pores commensurate with the diameter of a metal particle d_p (fig. 1):

$$d_{pore} \approx 2 \cdot d_p, \quad h_{pore} \approx 2 \cdot d_{pore}.$$

In this paper it is expedient to evaluate the reduction in strength for a specimen of a material and not for the design of a LRE chamber as a whole. For this purpose a series of specimens for tensile test were modeled according to GOST 1497–84 [15]. The dimensions the specimens correspond to type 3, number 9 (fig. 2).

The results of the stress-strain state calculations. Assuming that the applied load is evenly distributed over the cross section the strength calculation was carried out directly for a cylindrical fragment of the specimen working part ($h = 0.5$ mm, $V = 3.534$ mm^3, fig. 2) grown from AISI 316L powder of the following series of diameters: $d_{pi} = 60; 90; 120; 150; 180; 210; 240; 270; 300$ microns (fig. 3). The calculated values of the packing factors k_{layi} for each element are presented in tab. 2 A fragment of the working part was fixed on the surface of the rear end; a tensile load was applied along the normal to the surface of the front end. An example of a finite-element model of a calculation object with $d_p = 60$ μm in the form of a computational grid using tetrahedral elements with a total number of $\sim 6 \cdot 10^4$ is shown in fig. 4. Verification of the calculated diagram of porous specimens tension (fig. 5) was carried out using an experimental diagram for steel [15]. Comparison of dependences shows satisfactory coincidence of the qualitative nature of the calculated and experimental diagrams for elastic and the beginning of plastic deformations.

Table 1

Steel AISI 316L mechanical properties at T = 20 ^{o}C

Density	Yield strength	Tensile strength	Young's modulus	Poisson's ratio
$\rho, \dfrac{kg}{m^3}$	σ_{yield}, MPa	$[\sigma_{tens}]$, MPa	E, GPa	μ
7860	300	570	200	0,26

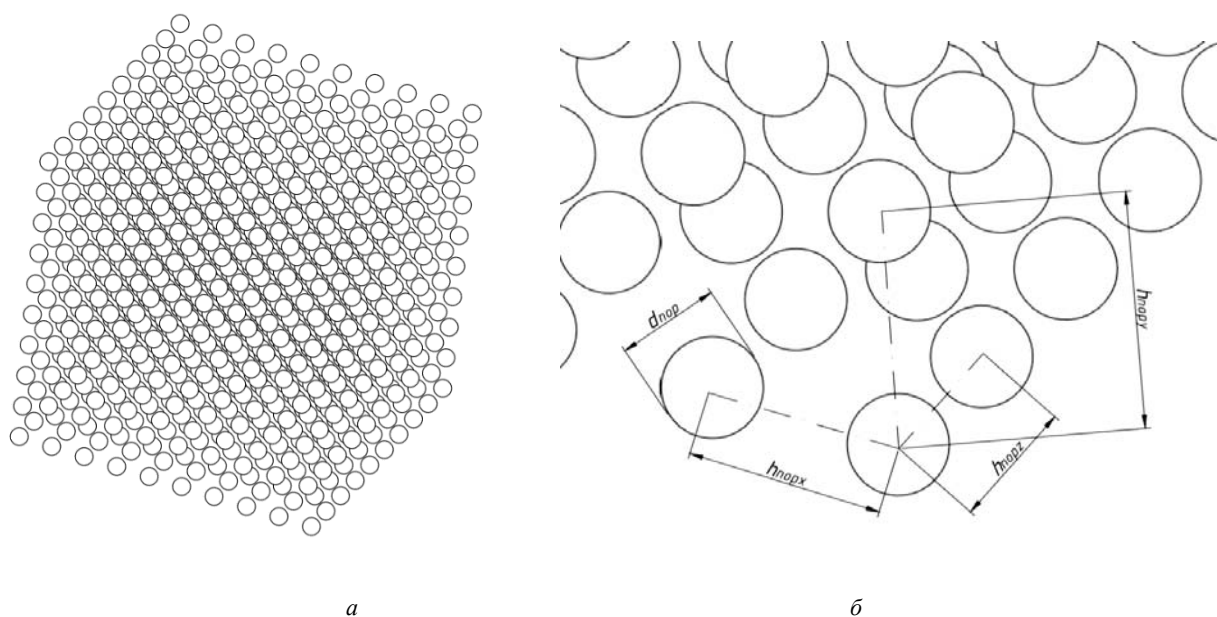*a*   *б*

Fig. 1. Scheme of distribution (*a*) and geometrical characteristics (*b*)
of pores in the object under study

Рис. 1. Схема распределения (*а*) и геометрические характеристики пор (*b*)
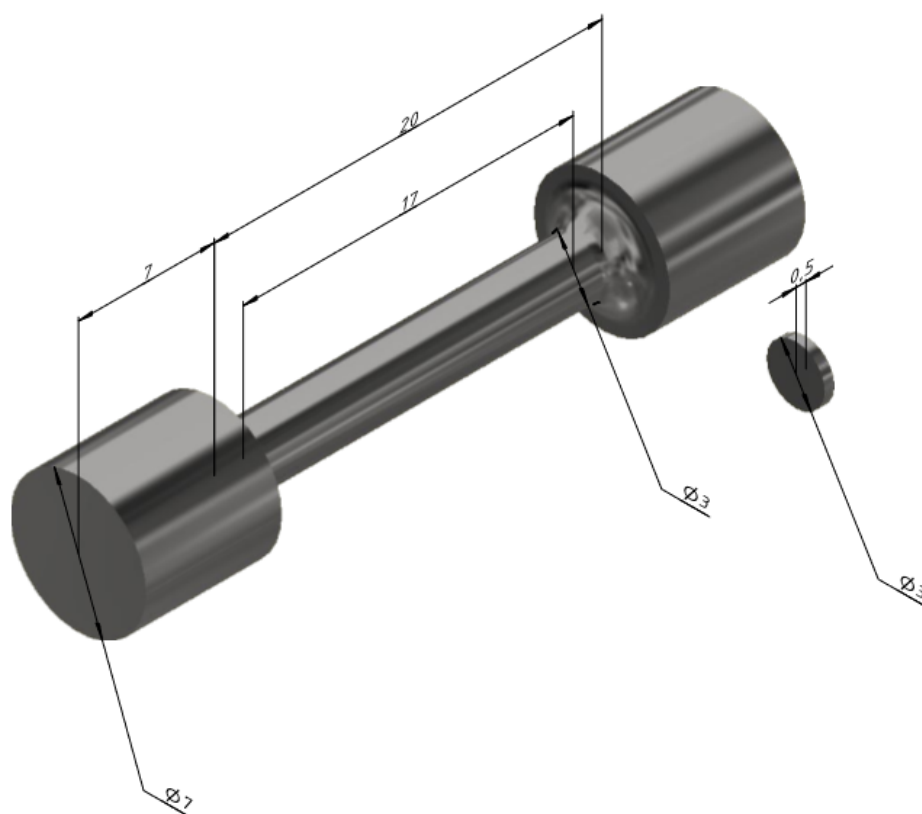в объекте исследования

Fig. 2. 3D-model of the object under study
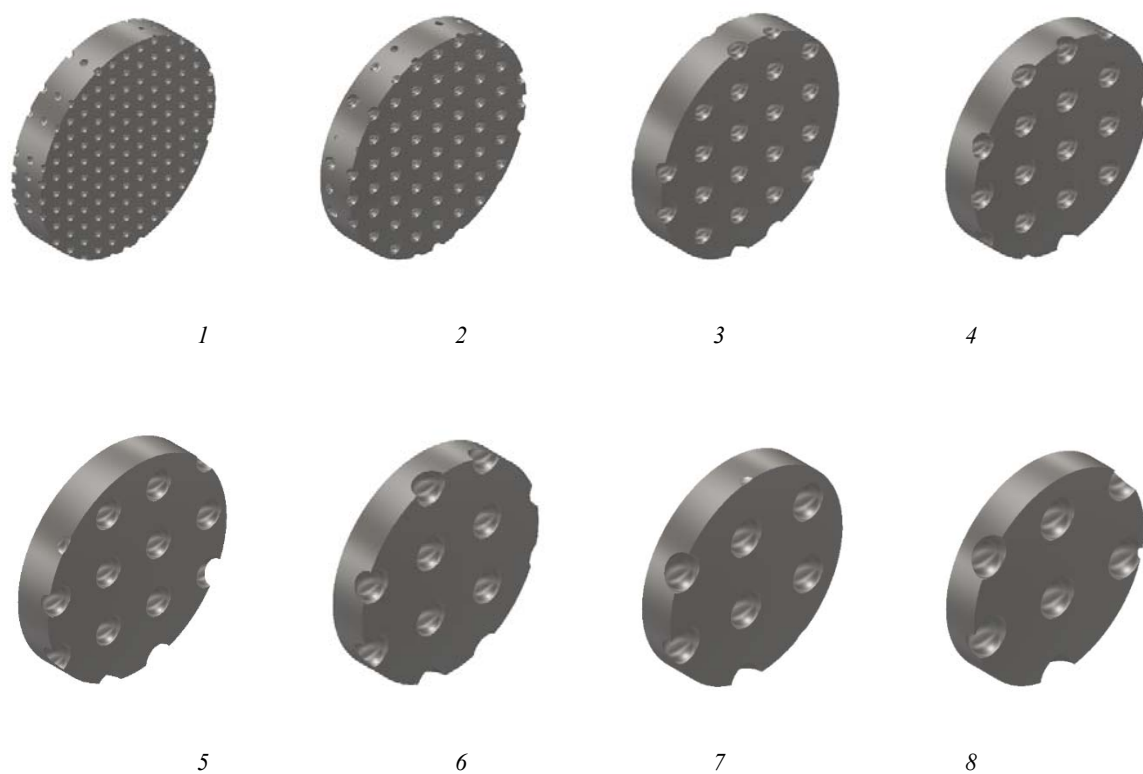
Рис. 2. 3D-модель объекта исследования

Fig. 3. 3-D models of porous specimens grown from metal powder with d_{pi}:
60 μm (*1*), 90 μm (*2*), 150 μm (*3*), 180 μm (*4*), 210 μm (*5*), 240 μm (*6*), 270 μm (*7*), 300 μm (*8*)

Рис. 3. 3-D модели пористых образцов выращенных из металлического порошка с d_{pi}:
60 мкм (*1*), 90 мкм (*2*), 150 мкм (*3*), 180 мкм (*4*), 210 мкм (*5*), 240 мкм (*6*), 270 мкм (*7*), 300 мкм (*8*)
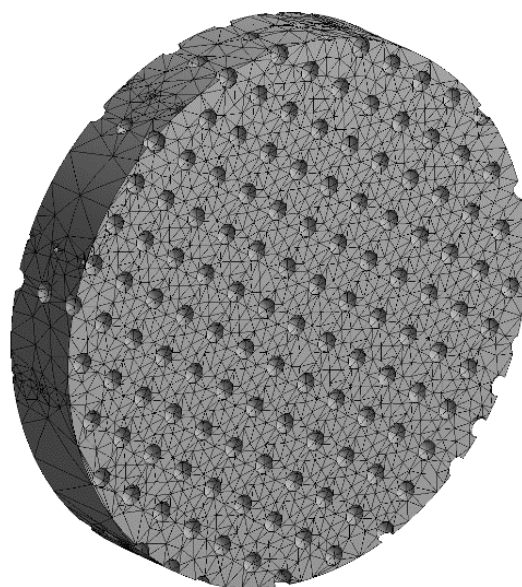
Fig. 4. A finite-element model in the form of a structured grid
of the calculation object at $d_p = 60$ μm

Рис. 4. Конечно-элементная модель в виде структурированной
сетки объекта расчета при $d_p = 60$ мкм

The value of the equivalent stress $\sigma_{eq.porei}$ (tab. 2) arising from the application of tensile load equal to $F = 2000$ N is obtained as a result of a series of calculations for each specimen. The values of the coefficient n_i and the yield strength $\sigma_{yield.porei}$ are presented in tab. 2. The dependence of the value of the yield strength on the particle diameter (hence, on the pore diameter) is nonlinear (fig. 6). The existence of an extremum can be explained by the opposite influence of geometrical parameters on the value of the surface area of the pores in the entire volume of the specimen. The total area of spherical surfaces is proportional to the number of pores in the specimen and at the same time to the diameter of each pore d_{porei}. The smaller the specified diameter of the initial metal powder particle is, the smaller the diameter and surface area of the pore formed in the SLM are, but the smaller the distance between the pores ($h_{pore} \approx 2 \cdot d_{pore}$) is, the greater their number is, and, therefore, the larger the total surface area of pores is.

The maximum value of the yield strength ($\sigma_{yield.p.max} = 291.9$ MPa) corresponds to the specimen with the highest value of the packing coefficient ($k_{lay\ max} = 0.956$), that is, the specimen with the minimum total surface area of pores.
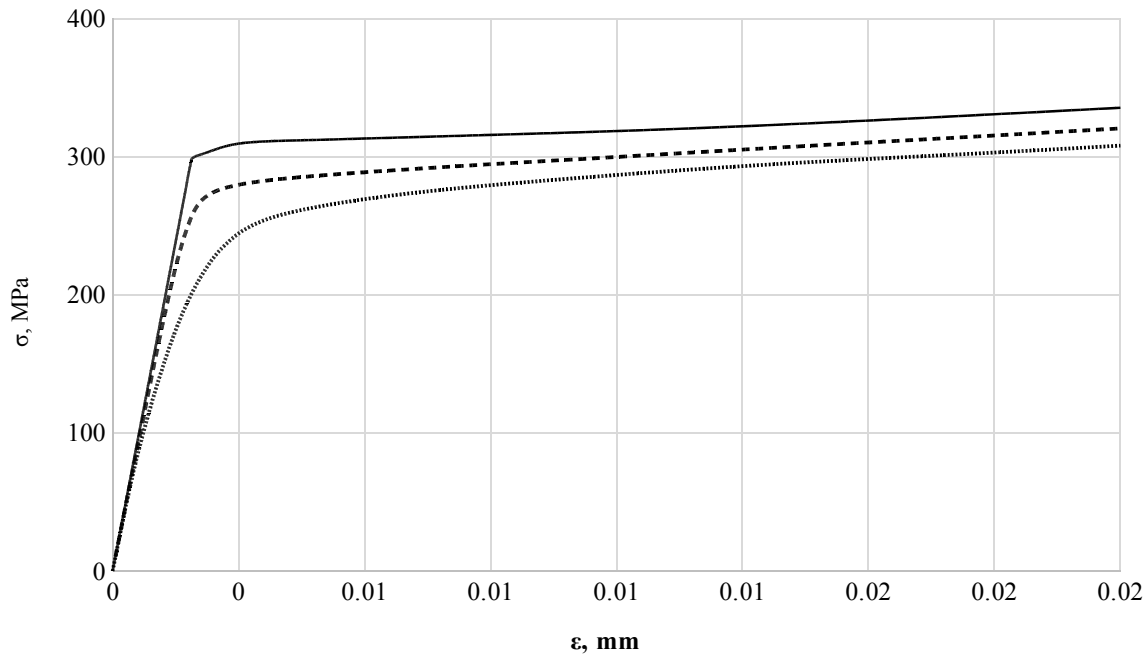

Fig. 5. The calculated diagram of the specimen stress-strain state with:
$1 - d_p = 0$ μm; $2 - d_p = 180$ μm; $3 - d_p = 300$ μm

Рис. 5. Расчетная диаграмма напряженно-деформированного состояния образца при:
$1 - d_p = 0$ мкм; $2 - d_p = 180$ мкм; $3 - d_p = 300$ мкм

Table 2

The results of the yield strength calculation for porous specimens

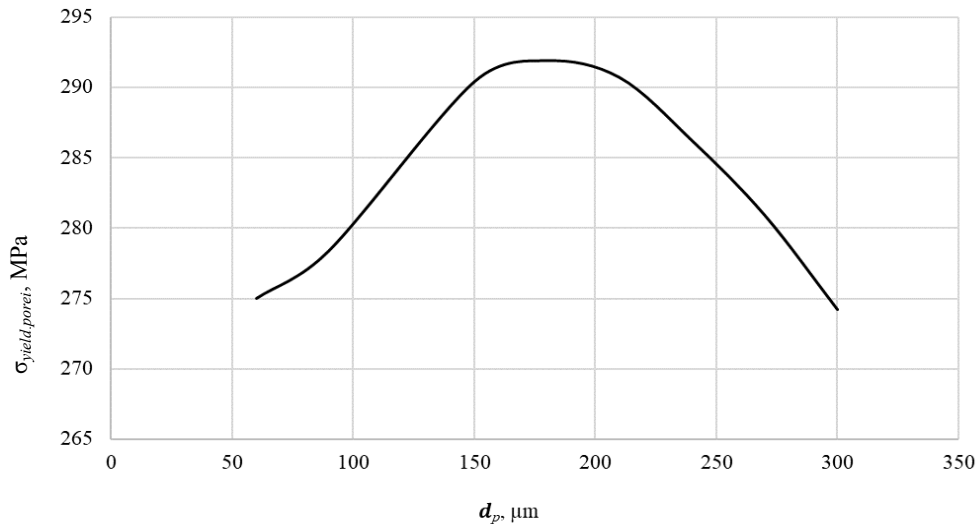| №	d_{pi}	$\sigma_{eq.porei}$	n_i	$\sigma_{yield.porei}$	k_{layi}
	mkm	MPa	–	MPa	–
1	60	254.4	0.917	275.0	0.929
2	90	251.3	0.928	278.4	0.929
3	150	240.8	0.968	290.4	0.955
4	**180**	**239.6**	**0.973**	**291.9**	**0.956**
5	210	240.7	0.969	290.7	0.944
6	240	244.5	0.954	286.2	0.939
7	270	249.1	0.936	280.9	0.929
8	300	255.1	0.914	274.2	0.914
	0 (monolithic)	233.2	1	300.0	1

Fig. 6. The dependence of the specimen yield strength value
on the metal powder particle diameter

Рис. 6. Зависимость значения предела текучести образца
от диаметра частиц металлического порошка

Conclusion. The paper considers the methodology of evaluating the reduction of the strength of the RST structural element material obtained by the SLM method by modeling the porous structure and calculating the characteristics of the stress-strain state. During the calculation it was found that the value of the total surface area of the pores in the material due to the size of the original metal powder particles is directly proportional to the value of the equivalent stress $\sigma_{eq.porei}$ arising in the object under study when tensile load is applied.

The dispersion value of the metal powder d_p is determined using tensile testing of a series of metal specimens. The value determined provides the minimum total surface area of pores in the material structure resulting from laser beam sintering, thereby causing greater value of the yield strength $\sigma_{yield.pore}$ of the part. The optimum value of the powder dispersion for steel AISI 316L in the preparation of specimens for tensile is $d_{p\ opt} = 150...200$ microns.

References

1. Artemov A. L. [Development of design and technology solutions for additive manufacturing of prototype inner lining for combustion chamber of multifunctional liquid-propellant rocket engine]. *Kosmicheskaya tekhnika i tekhnologii.* 2017, No. 1, P. 50–62 (In Russ.).

2. Abdullin M. I., Basyrov A. A., Nikolaev A. V. [Metal filled compositions for 3D printing]. *Universum: khimiia i biologiia.* 2015, No. 11(18). Available at: http://7universum.com/ru/nature/ archive/item/2701 (accessed 05 July 2017).

3. Grigoryanc A. G., Kazaryan M. A., Lyabin N. A. *Lazernaya precizionnaya mikroobrabotka materialov* [Laser Precision Micromachining]. Moscow, Fizmatlit Publ., 2017, 413 p.

4. Elistratova A. A., Korshakevich I. S., Tikhonenko D. V. [3D-printing technologies: advantages and disadvantages]. *Reshetnevskie chteniia. Sbornik materialov*

XVIII Mezhdunarodnoi nauchno-prakticheskoi konferentsii [Reshetnev readings. The collection of materials of XVIII International scientific and practical conference]. Krasnoyarsk, 11–14 November 2014, SibSAU Publ., 2014, P. 557–559.

5. Zlenko M. A., Popovich A. A., Mutylina I. N. *Additivnye tekhnologii v mashinostroenii* [Additive technologies in mechanical engineering]. Saint-Petersburg, Izd-vo Politekhnicheskogo universiteta Publ., 2013, 223 p.

6. Mosolov S. V., Sidlerov D. A. [Comparative analysis of the characteristic features of operational process in liquid rocket engine combustion chamber with jet-centrifugal and cebtrifugal-centrifugal injectors by means of numerical simulation]. *Vestnik MGTU im. N. E. Baumana. Ser. Mashinostroenie.* 2016, No. 2, P. 60–71 (In Russ.).

7. Meiz Dzh. *Teoriia i zadachi mekhaniki sploshnykh sred* [Theory and problems of continuum mechanics]. Moscow, LKI Publ., 2007, 320 p.

8. Galimova L. A., Atroshchenko V. V., Smirnov V. V. et al. [Structure and properties of stainless steel specimens received by method of selective sintering]. *Vestnik Bashkirskogo universiteta: matematika i mekhanika.* 2016, No. 2, P. 258–263 (In Russ.).

9. Hendrickson J. W. Use of Direct Metal Laser Sintering for Tooling in High Volume Production. USU Library, Logan, Utah, 2015. 35 p.

10. Torrado A. R., Roberson D. A. Failure Analysis and Anisotropy Evaluation of 3D-Printed Tensile Test Specimens of Different Geometries and Print Raster Patterns. *Journal of Failure Analysis and Prevention.* 2016, No. 1, P. 154–164.

11. Delgado J., Ciurana J., Rodríguez C. A. Influence of process parameters on part quality and mechanical properties for DMLS and SLM with iron-based materials. *The International Journal of Advanced Manufacturing Technology.* 2012, Vol. 60, No. 5–8, P. 601–610.

12. Smith D. H. et al. Microstructure and mechanical behavior of direct metal laser sintered Inconel alloy 718. *Materials Characterization*. 2016, Vol. 113, P. 1–9.

13. Features of Local Corrosion of AISI316L Steel Manufactured by Selective Laser Melting. Kuznetsov P. A., Krasikov A. V., Staritsyn M. V., Mushnikova S. Y., Parmenova O. N. *Protection of Metals and Physical Chemistry of Surfaces*. 2018, Vol. 54, No 3, P. 484–489.

14. Gu D., Shen Y. Processing conditions and microstructural features of porous 316L stainless steel components by DMLS. *Applied Surface Science*. 2008, Vol. 255, No. 5, P. 1880–1887.

15. *GOST 1497–84 Metally. Metody ispytanij na rastyazhenie* [State Standard 1479-84. Metals. Tensile test methods]. Moscow, Standartiform, 2005, 24 p.

Библиографические ссылки

1. Отработка конструктивных и технологических решений для изготовления опытных образцов внутренней оболочки камеры сгорания многофункционального жидкостного ракетного двигателя с использованием аддитивных технологий / Артемов А. Л. [и др.] // Космическая техника и технологии. 2017. № 1. С. 50–62.

2. Абдуллин М. И., Басыров А. А., Николаев А. В. Металлополимерные композиции для 3D печати // Universum: химия и биология. 2015. № 11(18). URL: http//7universum.com/ru/nature/archive/item/2701 (дата обращения 20 декабря 2018).

3. Григорьянц А. Г., Казарян М. А., Лябин Н. А. Лазерная прецизионная микрообработка материалов : монография. М. : Физматлит, 2017. 413 с.

4. Елистратова А. А., Коршакевич И. С., Тихоненко Д. В. Технологии 3D-печати: преимущества и недостатки // Решетневские чтения : сб. матер. XVIII Междунар. науч.-практ. конф. (Красноярск, 11–14 ноября 2014 г.) / СибГАУ. Красноярск, 2014. С. 557–559.

5. Зленко М. А., Попович А. А., Мутылина И. Н. Аддитивные технологии в машиностроении. СПб. : Изд-во Политехн. ун-та, 2013. 223 с.

6. Мосолов С. В., Сидлеров Д. А. Анализ особенностей рабочего процесса в камерах сгорания ЖРД со струйно-центробежными и центробежно-центробежными форсунками // Вестник МГТУ им. Н. Э. Баумана. Сер. «Машиностроение». 2016. № 2. С. 60–71.

7. Мейз Д. Теория и задачи механики сплошных сред. М. : Изд-во ЛКИ, 2007. 320 с.

8. Галимова Л. А., Атрощенко В. В., Смирнов В. В., Чуракова А. А., Гундеров Д. В., Заманова Г. И. Структура и механические свойства образцов из нержавеющей стали, полученных методом селективного спекания // Вестник Башкирского ун-та: математика и механика. 2016. № 2. С. 258–263.

9. Hendrickson J. W. Use of Direct Metal Laser Sintering for Tooling in High Volume Production. USU Library, Logan, Utah, 2015. 35 p.

10. Torrado A. R., Roberson D. A. Failure Analysis and Anisotropy Evaluation of 3D-Printed Tensile Test Specimens of Different Geometries and Print Raster Patterns // Journal of Failure Analysis and Prevention. 2016. No. 1. P. 154–164.

11. Delgado J., Ciurana J., Rodríguez C. A. Influence of process parameters on part quality and mechanical properties for DMLS and SLM with iron-based materials // The International Journal of Advanced Manufacturing Technology. 2012. Vol. 60, No. 5–8. P. 601–610.

12. Smith D. H. et al. Microstructure and mechanical behavior of direct metal laser sintered Inconel alloy 718 // Materials Characterization. 2016. Vol. 113. P. 1–9.

13. Features of Local Corrosion of AISI316L Steel Manufactured by Selective Laser Melting / P. A. Kuznetsov, A. V. Krasikov, M. V. Staritsyn [et al.] // Protection of Metals and Physical Chemistry of Surfaces. 2018. Vol. 54, No. 3. P. 484–489.

14. Gu D., Shen Y. Processing conditions and microstructural features of porous 316L stainless steel components by DMLS // Applied Surface Science. 2008. Vol. 255, No. 5. P. 1880–1887.

15. ГОСТ 1497–84 Металлы. Методы испытаний на растяжение. М. : Стандартиформ, 2005. 24 с.

Ushakova Elizaveta Sergeevna – is a technician of NIIEM and an employee of the Department of Rocket Engines; Bauman Moscow State Technical University. E-mail: ellizaweta@gmail.com.

Ушакова Елизавета Сергеевна – техник НИИЭМ, сотрудник кафедры ракетных двигателей, Московский государственный технический университет имени Н. Э. Баумана. E-mail: ellizaweta@gmail.com.

SOLAR THERMAL PROPULSION SYSTEMS WITH VARIOUS HIGH-TEMPERATURE POWER SOURCES

S. L. Finogenov *, A. I. Kolomentsev

Moscow Aviation Institute (National Research University)
4, Volokolamskoe shosse, A-80, GSP-3, Moscow 125993 Russian Federation
*E-mail: sfmai2015@mail.ru

The paper provides an overview of space thermal propulsion (STP) systems using concentrated solar energy as the main source of power. The paper considers solar thermal rocket engines of various configurations including those with afterburning of hydrogen heated in the "concentrator – absorber" system (CAS) with various oxidizers. Together with hydrogen the oxidizers form high-energy fuel compositions with a high value of ratio of components mass flow-rates which allows reducing the dimension of the CAS. The extreme dependences of the engine thrust on the specific impulse are shown for various values of the hydrogen heating temperature and the oxidizer-to-fuel ratio. The coefficients of the regression dependencies for the efficiency of a two-stage absorber and an absorber with the maximum non-isothermal heating having the highest possible energy efficiency are presented. The algorithms for calculating the main design parameters of the STP system as a part of a spacecraft (SC) are given, taking into account the ballistic parameters of the multi-turn transfer trajectory with multiple active segments applied to the STP systems having an energy-efficient non-isothermal CAS. The engine configurations with thermal heat accumulation and possible afterburning of heated hydrogen are also considered. Thermal accumulation allows accumulating energy in the solar-absorber during passive movement in the illuminated portions of the transfer orbits regardless of the lighting conditions of the apsidal orbit portions where the engine is turned on. Suitable heat-accumulating phase transition materials (HAM) such as the eutectic alloy of boron and silicon as well as refractory beryllium oxide are selected for different phases of the interorbital transfer to the geostationary Earth orbit (GEO). The main characteristics of different configurations of the STP systems in the problem of placing a spacecraft (SC) into high-energy GEO orbits are shown. A model of the SC-STP system operation is given taking into account ballistic parameters and the possibility of accumulating thermal energy. It is shown that the oxidizer-to-fuel ratio in STP systems with thermal energy storage (TES) increases with the decrease of the interorbital transfer time. The STP configurations with a two-stage TES showing a large energy-mass efficiency at moderate values of the solar concentrator accuracy parameter are considered.

Keywords: solar thermal propulsion, solar high-temperature heat source, concentrator-absorber system, thermal energy storage, hydrogen afterburning, ballistic efficiency.

СОЛНЕЧНЫЕ ТЕПЛОВЫЕ РАКЕТНЫЕ ДВИГАТЕЛИ С РАЗЛИЧНЫМИ ВЫСОКОТЕМПЕРАТУРНЫМИ ИСТОЧНИКАМИ МОЩНОСТИ

С. Л. Финогенов*, А. И. Коломенцев

Московский авиационный институт (национальный исследовательский университет)
Российская Федерация, 125993, г. Москва, А-80, ГСП-3, Волоколамское шоссе, 4
*E-mail: sfmai2015@mail.ru

В статье приводится обзор космических тепловых ракетных двигателей, использующих концентрированную солнечную энергию как основной источник мощности. Рассматриваются солнечные тепловые ракетные двигатели (СТРД) разных схем, в том числе с дожиганием нагретого в системе «концентратор – приемник» (КП) водорода различными окислителями, образующими с водородом высокоэнергетические топливные пары с высоким значением соотношения массовых расходов компонентов, что позволяет уменьшить размерность

системы КП. Показаны экстремальные зависимости тяги двигателя от удельного импульса при различных значениях температуры нагрева водорода и коэффициента избытка окислителя. Приводятся коэффициенты регрессионных зависимостей для КПД двухступенчатого приемника и приемника с предельной неравнотемпературностью нагрева, обладающим предельно возможной энергетической эффективностью. Приведены алгоритмы расчета основных проектных параметров СТРД в составе космического аппарата (КА) с учетом баллистических параметров многовитковой переходной траектории с множественными активными сегментами применительно к СТРД с энергетически выгодной неравнотемпературной системой КП. Также рассматриваются схемы двигателя с тепловым аккумулированием тепла и возможным дожиганием нагретого водорода. Тепловое аккумулирование позволяет накапливать энергию в светоприемнике-аккумуляторе во время пассивного движения на освещенных участках переходных орбит вне зависимости от условий освещенности апсидальных участков орбиты, на которых осуществляется включение двигателя. Для различного времени межорбитального перелета на геостационарную орбиту (ГСО) выбираются целесообразные теплоаккумулирующие фазопереходные материалы (ТАМ) типа эвтектического сплава бора и кремния, а также тугоплавкого оксида бериллия. Показаны основные характеристики разных схем СТРД в задаче выведения КА на высокоэнергетические орбиты типа ГСО. Приведена модель операции системы «КА-СТРД» с учетом баллистических параметров и возможностью аккумулирования тепловой энергии. Показано, что коэффициент избытка окислителя в СТРД с тепловым аккумулятором (ТА) возрастает при уменьшении времени межорбитального перелета. Рассмотрены схемы СТРД с двухступенчатым ТА, показывающим большую энергомассовую эффективность при умеренных значениях параметра точности солнечного концентратора.

Ключевые слова: солнечный тепловой ракетный двигатель, солнечный высокотемпературный источник тепла, система «концентратор – приемник», тепловой аккумулятор, дожигание водорода, баллистическая эффективность.

Introduction. Modern cosmonautics is characterized by the requirements to reduce the cost of placing SC into high working orbits by developing new energy-efficient interorbital transportation vehicles (ITV). Currently there is a steady global trend of increasing the mass and dimensional resources of a geostationary SC associated with the payback period of equipment. Therefore the development of highly efficient engines for ITV using alternative energy sources including solar energy is a highly topical problem.

Nowadays the levels of energy-mass perfection of traditional chemical rocket engines (liquid-propellant rocket engine (LPRE), solid-propellant rocket engine (SPRE)) are close to the limit in many respects, and engines with high specific impulses (nuclear rocket engine (NRE), electric jet engine EJE) have restrictions on the conditions of their use. One of the ways to increase the efficiency of thermal rocket engines is to increase the enthalpy of the fuel due to solar radiation as the most accessible source of energy in near-Earth space. STP systems can have a fairly simple configuration and better energy characteristics compared to chemical rocket engines.

Taking into account the high energy efficiency of direct conversion of solar radiation into the enthalpy of the working fluid it seems appropriate to study the energy possibilities of using STP systems with a high-temperature "concentrator-absorber" system (CAS).

The construction of a STP system requires the solution of complex scientific and technical problems, such as the development of an efficient high-temperature solar heat source (CAS and thermal accumulation capability) with the required energy-mass characteristics, optimal matching of its characteristics with SC parameters and ballistic parameters, ensuring engine orientation conditions including CAS tracking for the Sun, and a number of other tasks.

On the basis of the analysis of Russian and foreign works it has been shown that STP systems are considered primarily as systems including an isothermal CAS [1–6]. Particular solutions and approximation formulas that do not fully reflect the appropriate parameters of the CAS when matching engine characteristics with the main SC design parameters and ballistic parameters are given for non-isothermal solar absorbers [7]. Only oxygen is considered as an oxidizer for STP with afterburning. Graphite [5] is primarily considered as a heat-accumulating material (HAM) for a STP system TES; the expedient characteristics of such an engine when it is integrated into the SC are not shown and the configurations with hydrogen afterburning with various oxidizers are not considered in the works with the proposed phase transition batteries [4; 8].

Simple hydrogen STP system. Let us consider the issues of creating a single-component hydrogen STP system with a CAS as a source of power. An STP system is considered as an engine for ITV from a low orbit to a high-energy one using the example of a geostationary Earth orbit (GEO). The mathematical formulation of the problem of placing a SC with a STP system to high working orbits is presented. The main relevant parameters of the STP system having the greatest impact on the efficiency criterion, that is, on the maximum mass of the payload (PL) M_{PL} on the GEO are selected. It is shown that the relevant parameters include the tolerance of the $\Delta\alpha$ mirror concentrator (accuracy according to O. I. Kudrin [7]) and the heating temperature of the high-temperature part of the absorber T_o assumed to be equal to the hydrogen heating temperature T_{H_2}. It is shown that they significantly depend on the interorbital transfer time, while the optimum temperature T_{H_2} decreases with a decrease in the interorbital maneuver time, and the

optimal parameter $\Delta\alpha$ increases. The optimal ratios of these parameters are revealed.

The CAS of three main configurations is considered: an isothermal one-stage system (OSS); a system with two stages of heating hydrogen in the absorber (TSS); a multistage system with non-uniform heating of hydrogen (MSS). Formally the problem statement is as follows:

$$\psi = \arg\max_{\psi \in \Psi, Z} \left[M_{PL}(\psi) \begin{vmatrix} T_\Sigma = fix \\ x_0 = fix \\ x_\kappa = fix \end{vmatrix} \right], \qquad (1)$$

where $\psi = \langle T_o; \Delta\alpha \rangle$ is the vector of the STP relevant parameters belonging to the set of alternative values Ψ and Z and subject to optimization to ensure the maximum M_{PL} at fixed values of the interorbital transfer time T_Σ and phase coordinates of the initial and final orbits x_0, x_κ.

The algorithm for selecting the relevant parameters for maximizing the mass of PL is considered in detail in [9]. The model takes into account the masses of SC and the engine according to known regression dependencies [10]. The accuracy of determining the PL mass is sufficient to make a decision on the choice of the preferred alternative among competing ITVs. The results of calculations on the example of various solar absorbers are shown in fig. 1–6

[11] as applied to the "Soyuz-2-1b" launch vehicle (LV). Here the conventional diameter of a mirror means its full dimensions (mid-mirror) collecting solar radiation into a focal light spot falling on a radial-type solar absorber.

If the efficiency of the isothermal (one-stage) absorber is determined simply by using the well-known formulas given in [7; 12], then for engineering calculations of the two-stage absorber efficiency the regression dependencies are proposed which are determined by the power series coefficients $a_i = f(T_{H_2})$:

$$\eta = \Sigma a_i \cdot \Delta\alpha^i, \quad i = 0...k. \qquad (2)$$

The values of the coefficients of the series depending on the heating temperature of hydrogen are presented in tab. 1.

STP systems with a non-isothermal CAS. The uneven heating of hydrogen in a non-isothermal absorber corresponds to a Gaussian diagram of the solar energy distribution in the focal light spot. For extremely uneven heating of the coolant in the absorber in the absence of radial heat transfer an assumption was made about the axisymmetric exponential distribution of the radiant flux in the focal light spot, which corresponds to the experimental aberrograms of real parabolic mirrors [7; 12–14].

Table 1

Coefficients for determining the two-stage absorber efficiency

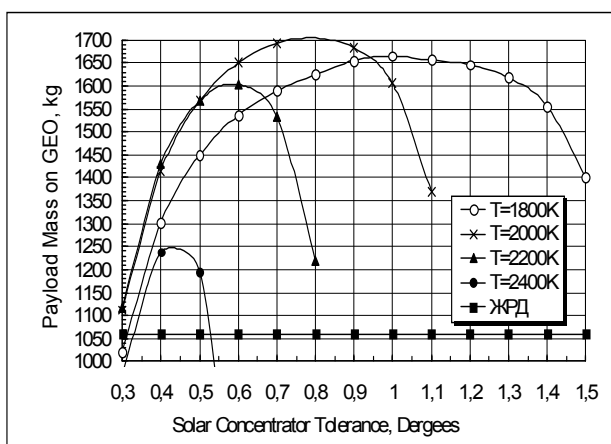| T_{H2}, K	2000	2200	2500	2800	3000	3200
a_0	0.9160	0.8269	0.7877	0.7369	0.6891	0.6432
a_1	−0.3210	−0.9587	−0.0803	−0.3021	−0.4621	−0.2234
a_2	0.6896	−0.2633	−0.4654	0.0623	0.7874	1.1895
a_3	−0.0013	0.0362	0.2233	−0.0955	−0.7816	−2.7105

Fig. 1. The dependence of PL mass on the GEO
on the concentrator tolerance for an isothermal absorber

Рис. 1. Зависимость массы ПН на ГСО
от параметра точности концентратора
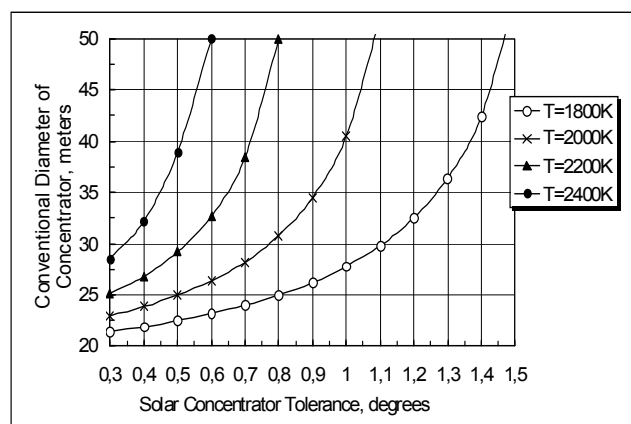для равнотемпературного приемника

Fig. 2. The dependence of the mirror conventional diameter
on the concentrator tolerance for an isothermal absorber

Рис. 2. Зависимость условного диаметра зеркала
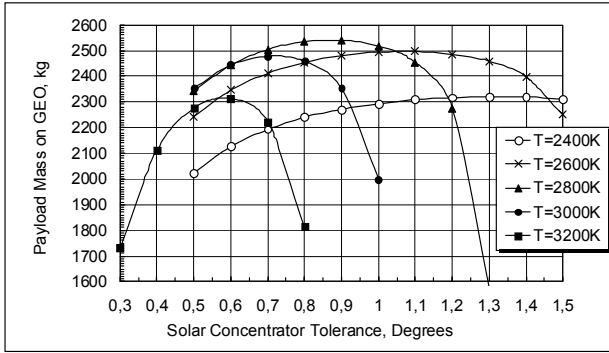от параметра точности для равнотемпературного
приемника

Fig. 3. The dependence of PL mass on the GEO
on the concentrator tolerance for a two-stage absorber

Рис. 3. Зависимость массы ПН на ГСО
от параметра точности концентратора
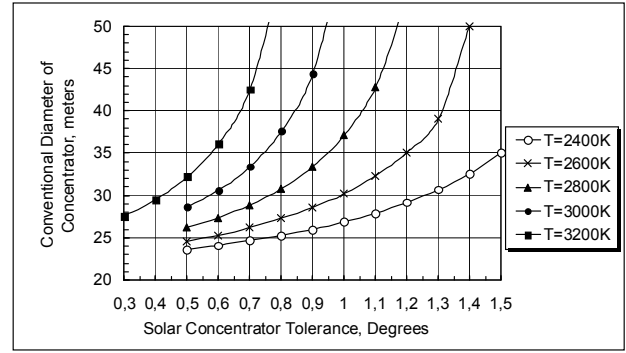для двухступенчатого приемника

Fig. 4. The dependence of the mirror conventional diameter
on the concentrator tolerance for a two-stage absorber

Рис. 4. Зависимость условного диаметра зеркала
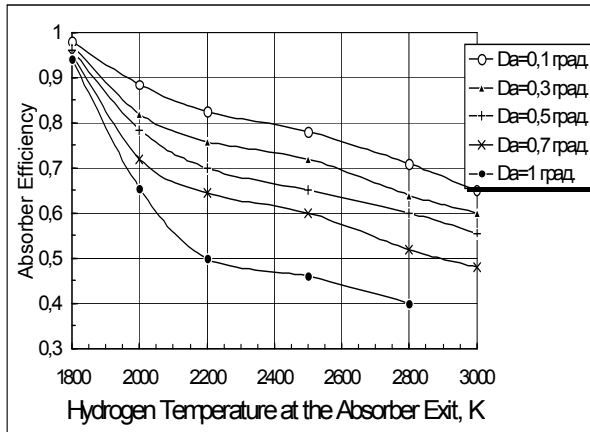от параметра точности для двухступенчатого приемника

Fig. 5. The dependence of a two-stage absorber efficiency
on exit temperature for different values of $\Delta\alpha$ (denoted as Da)

Рис. 5. Зависимость КПД двухступенчатого приемника
от температуры на выходе для различных значений $\Delta\alpha$
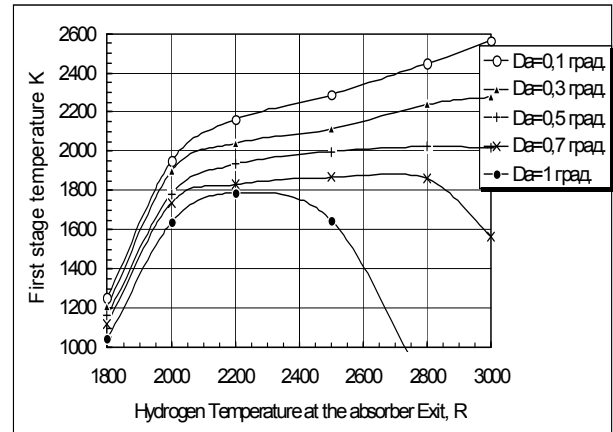(обозначен как Da)

Fig. 6. The dependence of the absorber first stage
temperature on final hydrogen temperature

Рис. 6. Зависимость температуры первой ступени
приемника от конечной температуры водорода

The temperature distribution over the radius of such an absorber can be described by a differential equation according to O. I. Kudrin [7]:

$$\frac{dT}{dr} = 2BT_{cond}rT^4(r) - 2.4\frac{a_s T_{cond}}{\cos^2\Theta}r\exp\left(\frac{-1.2r^2}{\cos^2\Theta}\right), \quad (3)$$

where T is the temperature of the absorber (assumed to be equal to the heating temperature of hydrogen); r is the relative radius of the absorber; a_S is the effective absorption coefficient of solar radiation; B is a complex that takes into account the reciprocal self-radiation of the absorber, the optical parameters of the concentrator and the characteristics of solar radiation:

$$B = \frac{\varepsilon_{eff}\sigma_o \sin^2(\alpha_o + \Delta\alpha)}{\Im_o\eta_r \sin^2(2\Theta)}. \quad (4)$$

Here ε_{eff} is the effective emissivity of the absorber; $\alpha_o = 32'$ is the apparent angular size of the Sun at the level of the Earth's orbit; σ_o is the Stefan-Boltzmann constant; Q is the opening angle (aperture) of the mirror; $\Im_o = 1360$ Вт/м^2 is the surface power of solar radiation (solar constant) at the level of the Earth's orbit; η_r is the reflection coefficient of the mirror surface of the concentrator.

The boundary conditions are written as $T(r = 1) = T_{start} = 20$ K, that is, the temperature at the periphery of the absorber is equal to the temperature of the hydrogen evaporated in the tank. Then $T(r = 0) = T_{output}$ is the exit

(final) temperature of heated hydrogen achieved in the central part of the absorber.

In equation (3) there is a "conventional temperature" T_{cond} characterizing the ratio of the increase in the hydrogen temperature provided that all the concentrated solar energy is used to heat it. The ratio of the actual temperature of hydrogen at the outlet (minus the temperature of the hydrogen coming from the tank) to the conventional temperature determines the efficiency of the heating process. Conventional temperature depends on the area of the mirror concentrator and the mass flow rate of gas. The area of the mirror is determined, in its turn, by the efficiency of the CAS, which depends on temperature and its optical-geometric parameters including the parameter $\Delta\alpha$. Therefore, the determination of the absorber efficiency and the final gas temperature is an iterative process requiring the specification of the initial conventional diameter of the concentrator and the flow characteristics of the engine.

Differential equation (3) in the general case has no analytical solution. In his work O. I. Kudrin [7] shows only two particular solutions restricted by a narrow application scope. In the present work equation (3) is solved numerically by Runge – Kutta – Fellberg method of order 4 and 5.

Comparing the approximate formulas for the efficiency of a non-isothermal CAS mentioned in the works of O. I. Kudrin [7] with the results of numerical integration one can note that the approximate formulas give a good result only for sufficiently accurate mirrors and not too high absorber temperatures. However, such values are not optimal from the standpoint of maximum PL mass when using stepped absorbers and they depend on the flight time. To determine the efficiency of the non-isothermal absorber one can propose more accurate dependences based on the results of the numerical integration of equation (3). Approximation formulas that allow simple determining the efficiency of a non-isothermal absorber depending on the tolerance at different hydrogen heating temperatures T_{H_2} are determined by the coefficients $a_i = f(T_{H_2})$ of the power series (2) (tab. 2).

Fig. 7 presents the results of numerical simulation of the process of heating hydrogen to 3000 K. The dependences of the conventional temperature on the tolerance $\Delta\alpha$ are shown in fig. 8. It can be seen that the allowable value of the parameter $\Delta\alpha$ decreases with increasing the final hydrogen heating temperature. The excess of this parameter leads to a substantially non-linear increase in the conventional temperature and, as a result,

to sharp decrease in the efficiency of the CAS accompanied by the increase in the size of the concentrator and its mass.

Fig. 9 presents the absorber efficiency values depending on the initially specified temperature refined during the iterative recalculation when integrating equation (3) for different values of the parameter $\Delta\alpha$. The nature of these curves depends, among other things, on the conventional temperature indirectly determined by the parameter $\Delta\alpha$. Under the condition of the STP system thrust constancy the increase in $\Delta\alpha$ leads to decrease in the hydrogen temperature at the outlet (fig. 10).

In tab. 3–5 [11] it is shown that the optimal hydrogen temperature and the optimal accuracy of the solar concentrator decrease, and the size of the solar concentrator increases with decrease in the time of the interorbital transfer.

At the same time, the requirements for the angular accuracy β of the dynamic tracking of the Sun position by the CAS which can be provided with modern technical means are reduced.

Fig. 11 shows a flowchart of the algorithm for optimal matching the STP characteristics with a non-isothermal absorber with the main design SC parameters (upper stage) and trajectory parameters that provide the maximum PL mass at a given interorbital transfer time [13].

STP systems with afterburning of heated hydrogen. Let us consider a STP system where hydrogen heated in the considered CAS is afterburnt by oxidizers which together with hydrogen form high-energy fuel compositions with a large stoichiometric mass flow rate of the components, which makes it possible to reduce the consumption of heated hydrogen for a given thrust and thereby reduce the required mirror size [15]. In addition to oxygen, fluorine (stoichiometric ratio with hydrogen $K_{mo} = 18.86$) and hydrogen peroxide ($K_{mo} = 12.09$) are considered as oxidizers.

Such a STP system with afterburning can be considered as a liquid rocket engine with increased enthalpy of fuel. In contrast to a purely chemical engine in a STP system the thermal energy of heated hydrogen accounts for a significant proportion in the total enthalpy of fuel, therefore the heating value of the fuel affects the specific impulse to a lesser extent, and the choice of oxidizer can be carried out with better reason taking into account the value of the ratio of the components mass flow rates. In addition, the increased density of the fuel $H_2 + F_2$ or $H_2 + H_2O_2$ facilitates placing the spacecraft into the original reference orbit.

Table 2

Coefficients for definition of non-isothermal absorber efficiency

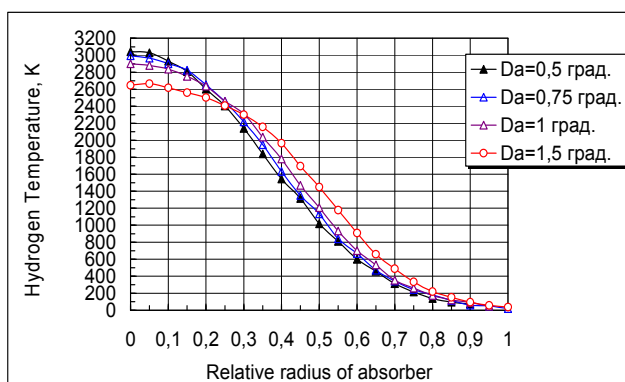| $T_{H2,}$ K	2500	2800	3000	3200	3500	3800
a_0	0.8304	0.8189	0.8149	0.8108	0.8047	0.7935
a_1	−0.0233	−0.0209	−0.0487	−0.0919	−0.1978	−0.3459
a_2	−0.0723	−0.1549	−0.1988	−0.2426	−0.2875	−0.3045
a_3	0.0024	0.0207	0.0311	0.0435	0.0573	0.0624

Fig. 7. The dependence of hydrogen heating temperature
on the absorber relative radius

Рис. 7. Зависимость температуры нагрева водорода
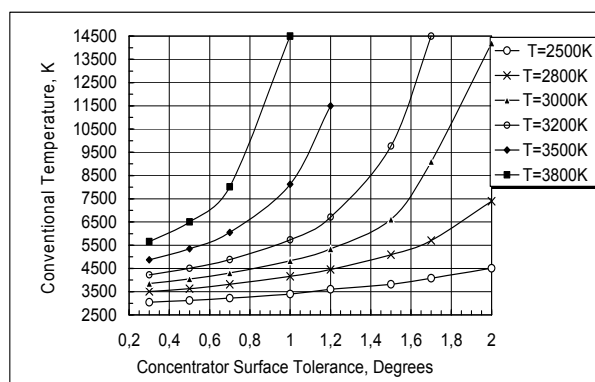от относительного радиуса приемника

Fig. 8. The dependence of conventional temperature
on concentrator tolerance

Рис. 8. Зависимость условной температуры
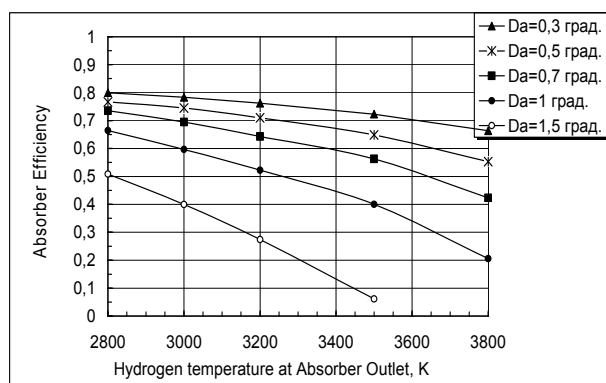от параметра точности концентратора

Fig. 9. The dependence of extremely non-isothermal
absorber efficiency on the specified outlet temperature

Рис. 9. Зависимость КПД предельно-
неравнотемпературного приемника от заданной
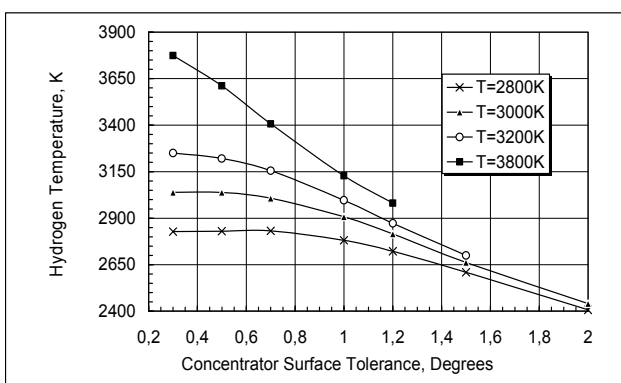температуры на выходе

Fig. 10. The dependence of hydrogen temperature
on concentrator tolerance for different specified initial
heating temperature

Рис. 10. Зависимость температуры водорода
от параметра точности для разных заданных
начальных температур нагрева

Table 3

Characteristics of spacecraft with a STP system for an isothermal absorber

Mission Time, days	Absorber Temperature, K	Concentrator Tolerance $\Delta\alpha$, deg.	Conventional Mirror Diameter, meter	Payload Mass on GEO, kg	Angular accuracy β, degrees
60	2200	0.64°	20.8	1640	1.25°
40	2100	0.7°	23.7	1510	1.3°
20	1900	1.0°	33.0	1270	1.6°

Table 4

Characteristics of spacecraft with a STP system for a two-stage absorber

Mission Time, days	Absorber Temperature, K	Concentrator Tolerance $\Delta\alpha$, deg.	Conventional Mirror Diameter, meter	Payload Mass on GEO, kg	Angular accuracy β, degrees
60	3000	0.77°	24.0	2180	1.39°
40	2800	0.9°	27.6	2050	1.53°
20	2600	1.1°	37.9	1810	1.74°

Table 5

Characteristics of spacecraft with a STP system for non-isothermal absorber

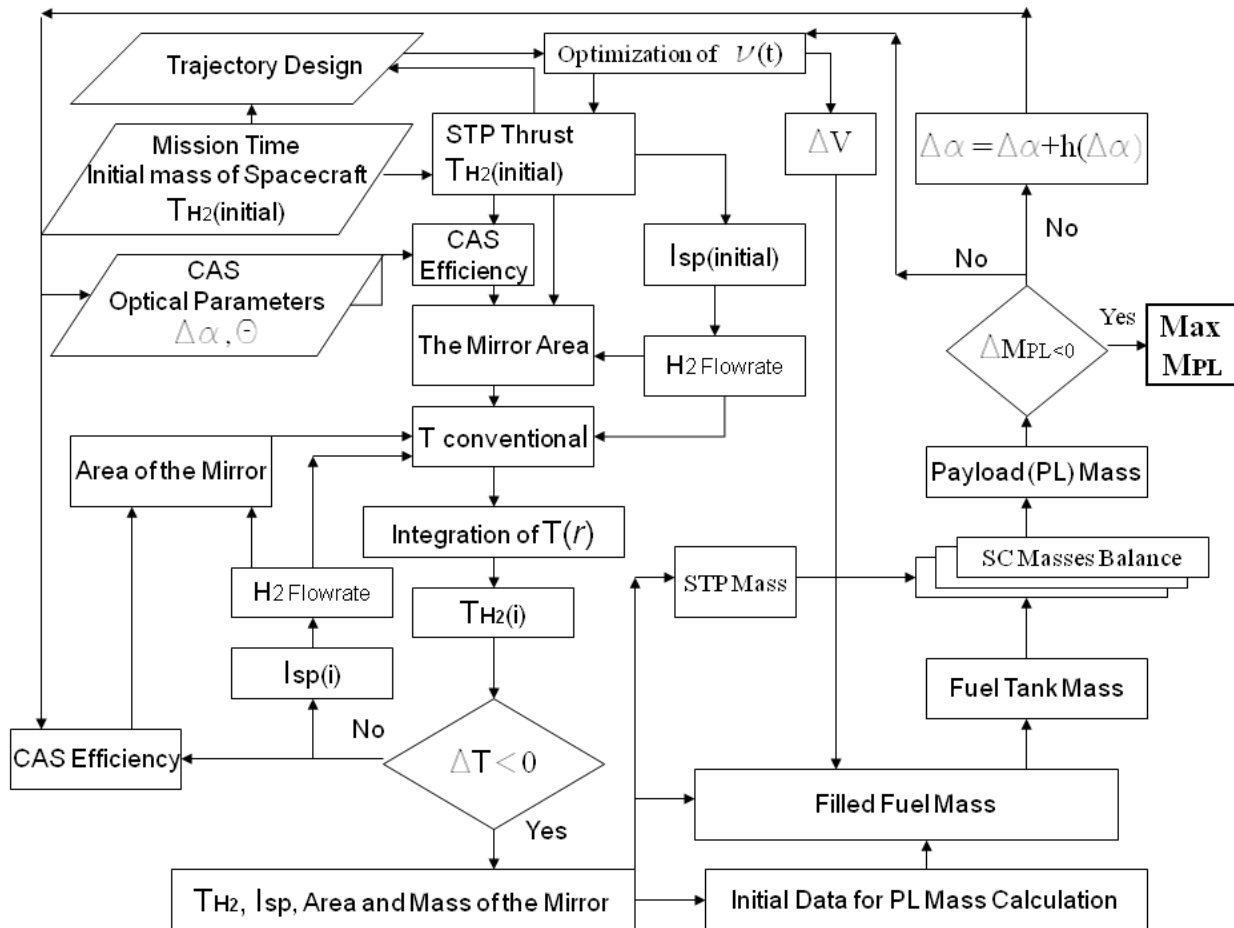| Mission Time, days	Absorber Temperature, K	Concentrator Tolerance Δα, deg.	Conventional Mirror Diameter, meter	Payload Mass on GEO, kg	Angular accuracy β, degrees
60	3800	0.86°	25.4	2600	1.48°
40	3600	1.0°	30.4	2480	1.64°
20	3200	1.4°	41.9	2230	2.0°

Fig. 11. The algorithm of optimal agreement of STP characteristics with SC

Рис. 11. Алгоритм оптимального согласования характеристик СТРД с КА

Opportunities of using oxygen and fluorine as oxidizers for a STP system as applied to the "Proton-M" launch vehicle are compared. As it can be seen from fig. 12, the mass efficiency of the space stage with the fluorine-hydrogen STP provides a gain in PL mass of more than 25 % with an oxidizer-to-fuel ratio $\alpha = 0.1$ ($K_m = 0.19$) in the case of an isothermal absorber, when appropriate values of $\alpha < 0.15$ compared with the use of an oxygen-hydrogen booster with an oxygen-hydrogen liquid-propellant rocket engine KVD-1 when using light inflatable film mirrors. The use of an extremely non-isothermal absorber allows increasing the mass efficiency of the engine and significant expanding the range of α

values at which a steady gain in the PL mass is maintained.

The graphs in fig. 13 show noticeably smaller paraboloid concentrator sizes in the case of a fluoride-hydrogen STP compared to an oxygen-hydrogen one. The difference may be over 25 %.

The calculations show a lower mass efficiency of the STP use with $H_2 + H_2O_2$ fuel in comparison with the use of fluorine or oxygen. The area α where the gain of STP with hydrogen peroxide over LPRE remains depends on the type of a CAS. The choice of the appropriate value of the oxidizer-to-fuel ratio at which the concentrator size is significantly reduced with an acceptable decrease in mass

efficiency is very important. This takes into account the degree of temperature non-uniformity of the absorber and the type of the concentrator.

STP optimal thrust. On the basis of M. S. Konstantinov's works [16; 17] it is shown that the values of the characteristic velocity for each pair $(j;I_y)$ with optimized 3-segment many-revolution transfer can be used for further calculations for reactive accelerations j from 2.5 to 12.5 mm/s^2 with I_y from 600 to 900 s, which is typical for SC with STP.

However, in the case of STP with afterburning the same specific impulse can be provided by various combinations of the hydrogen heating temperature and the ratio of its mass flow rate to the flow rate of the oxidizer [18]. The energy-mass efficiency of a SC with such an engine can vary greatly. High-temperature heating (up to 2600–2800 K) is more advantageous with components mass flow-rate ratios in the range K_m = 3.2–4 in order to achieve a moderate value of the specific impulse I_y = 600 s. The nominal mirror diameter can be significantly (up to 40 %) reduced and the PL mass can be increased by 35 % for a low-temperature CAS (heating is not higher than 2000 K). In this case, the possible PL mass equal to 1950 kg is more than 1.8 times greater than that for the liquid-propellant booster of the "Fregat" type (the SC mass on the GEO is 1060 kg). Refined mass calculations of PL on the GEO were carried out for the optimized trajectory (fig. 14).

Taking into account the minimized (each time) values of the characteristic velocity it is possible to find the local maximum of the PL mass for each specific impulse value. For example, the specific impulse I_y = 600 s corresponds to the optimal thrust of 100 N, and for I_y = 900 s the optimal thrust is 70–80 N.

STP with TES. Let us consider a STP system with a CAS including TES which accumulates heat energy in the illuminated passive portions of each transfer orbit and gives it to hydrogen when the engine is turned on in the apsidal portions of the transfer orbits. This simplifies the task of selecting powered portions regardless of the light conditions and simplifies the desired guidance of the CAS to the Sun. The analysis [8; 19] showed that the feasible HAM should be searched between high-temperature HAM such as beryllium oxide and less refractory substances such as the eutectic 3BeO*2MgO. The eutectic boron alloy with silicon B*Si [8] belongs to such substances with an intermediate melting point and a high energy intensity.

A mathematical model of SC with STP operation has been developed to calculate and optimally match the engine characteristics with the "CA-TES" system, the main design SC parameters and orbital parameters [20] taking into account the thermophysical properties and transient processes in HAM [12; 21]. The mathematical model is designed as a software package and consists of five blocks (fig. 15).

The block (A) includes deterministic external factors. The ballistic block (Б) includes algorithms for solving the ballistic problem of determining the total flight time and the dynamic problem of determining the cost of the characteristic speed of the maneuver. Block (В) determines the main design SC parameters and

calculation of the PL mass. Block (Г) includes calculation of energy-mass and geometric characteristics of STP with the "CA-TES" system and the possibility of hydrogen afterburning. Block (Д) includes coordination of the main design parameters of the STP and the SC and their optimization together with the parameters of motion control for identifying the extremum of the objective function of the operation (maximizing the PL mass) under the restriction of flight time.

The analysis of the operation of a SC with STP showed that the following parameters of the "CA-TES" system can be chosen as relevant ones at the stage of exploratory research: (a) the ratio of the energy intensity TES Q_a to the area (or mass) of the mirror F_3 (or the ratio of the masses of the concentrator and TES M_K / M_{TA}) and (b) the accuracy parameter of the mirror $\Delta\alpha$. Formally the problem of choosing the optimal relevant parameters of STP with TES in a SC is as follows:

$$\psi = \arg \max_{\psi \in \Psi, U} \left[M_{PL}(\psi) \begin{vmatrix} T_\Sigma = fix \\ x_0 = fix \\ x_\kappa = fix \\ T_0 = fix \end{vmatrix} \right], \qquad (5)$$

where $\psi = <\Delta\alpha, M_\kappa / M_{TA}>$ is the vector of optimized relevant parameters of STP with TES, T_0 is the temperature of the absorber-accumulator taken to be equal to the melting temperature of the HAM under consideration, M_κ / M_{TA} is the ratio of masses of the concentrator and TES, x_0, x_κ are the phase coordinates of the SC, T_Σ is the interorbital transfer time, Ψ, U is the set of alternatives. The mathematical model of optimization of the main design parameters of the "SC-STP" technical system with the TES is shown in fig. 16.

The optimal mass ratios of the concentrator and TES are different for different HAMs, and they increase as their melting temperature increases. For example, for the eutectic 3BeO*2MgO the optimum M_κ / M_{TA} is 0.2, while for the B*Si alloy the optimum value M_κ / M_{TA} is 0.3–0.4, and for the refractory beryllium oxide M_κ / M_{TA} = 0.9 (fig. 17). The effect the concentrator tolerance on the PL mass is shown in fig. 18, whence it follows that there exist ranges of the parameter $\Delta\alpha$ optimal values depending on the melting point of particular HAM [19]. As the melting temperature of HAM increases, the optimum parameter $\Delta\alpha$ decreases (the optimum concentration of solar radiation increases), since greater accuracy dramatically augments the specific mass of the mirror reducing the PL mass due to the increase in engine mass, and the decrease in accuracy diminishes the efficiency of the CAS which requires larger area and mass of the mirror and also leads to a drop in the PL.

Reducing the time of the mission trip leads to a sharp decrease in the mass efficiency of the upper stage with the STP which is explained by significant increase in the mass of the CA and TES systems (fig. 19, 20).

STP with TES and hydrogen afterburning. Let us consider the effectiveness of the use of STP with TES and

afterburning of hydrogen heated in TES with oxygen and fluorine. The problem has the following formalized formulation:

$$\psi = \arg \max_{\psi \in \Psi, U, \Xi} \left[M_{PL}(\psi) \begin{vmatrix} T_{\Sigma} = fix \\ x_0 = fix \\ x_{\kappa} = fix \\ T_0 = fix \end{vmatrix} \right], \qquad (6)$$

where $\psi = <\alpha, \Delta\alpha, M_{\kappa}/M_{TA}>$ is the vector of optimized relevant parameters of STP with TES, T_0 is the temperature of the absorber-accumulator taken to be equal to the melting temperature of the HAM under consideration, x_0, x_{κ} are the phase coordinates of the SC, T_{Σ} is the interorbital transfer time, Ψ, U, Ξ is the set of alternatives.
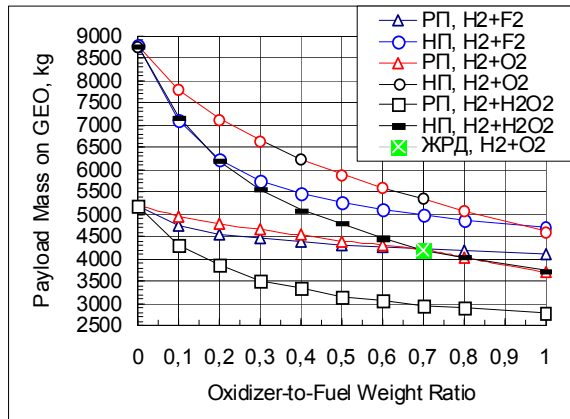

Fig. 12. The dependence of PL mass
on oxidizer-to-fuel ratio when using different oxidizers
for hydrogen afterburning

Рис. 12. Зависимость массы ПН от коэффициента
избытка окислителя при использовании различных
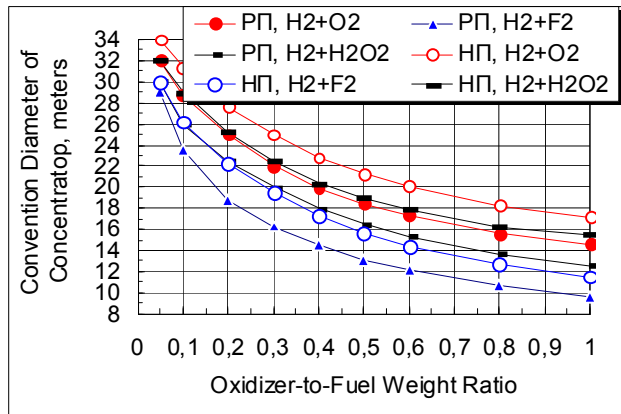окислителей для дожигания водорода

Fig. 13. The dependence of the convention concentrator
diameter on oxidizer-to-fuel ratio when using different
oxidizers for hydrogen afterburning

Рис. 13. Зависимость диаметра параболоидного
концентратора от коэффициента избытка окислителя
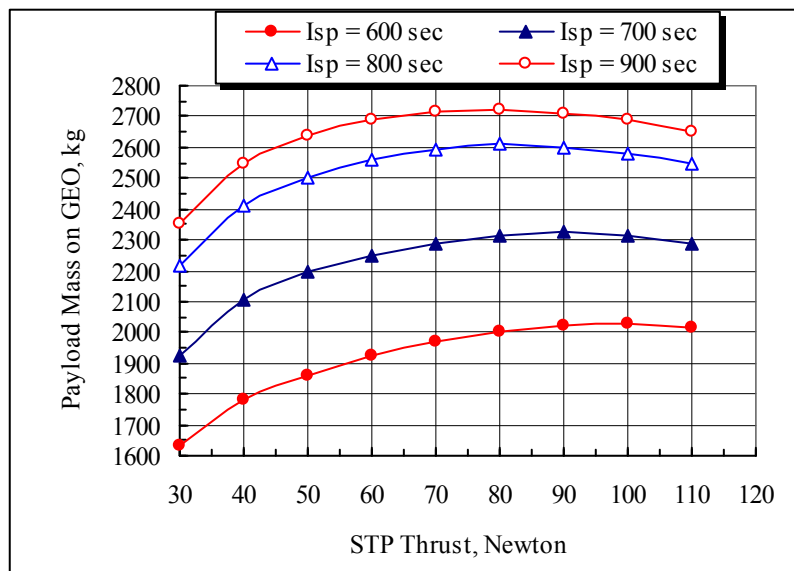при использовании различных окислителей
для дожигания водорода

Fig. 14. The dependence of PL mass on the GEO on STP thrust:
hydrogen temperature is 2800K, concentrator tolerance is $\Delta\alpha = 1°$,
time of placing on the GEO is 30 days

Рис. 14. Зависимость массы ПН на ГСО от тяги СТРД:
температура водорода – 2800 К, параметр точности – $\Delta\alpha = 1°$,
время выведения на ГСО – 30 суток

Structure of Multi-Level Mathematical Model of "Spacecraft-STP" Operation
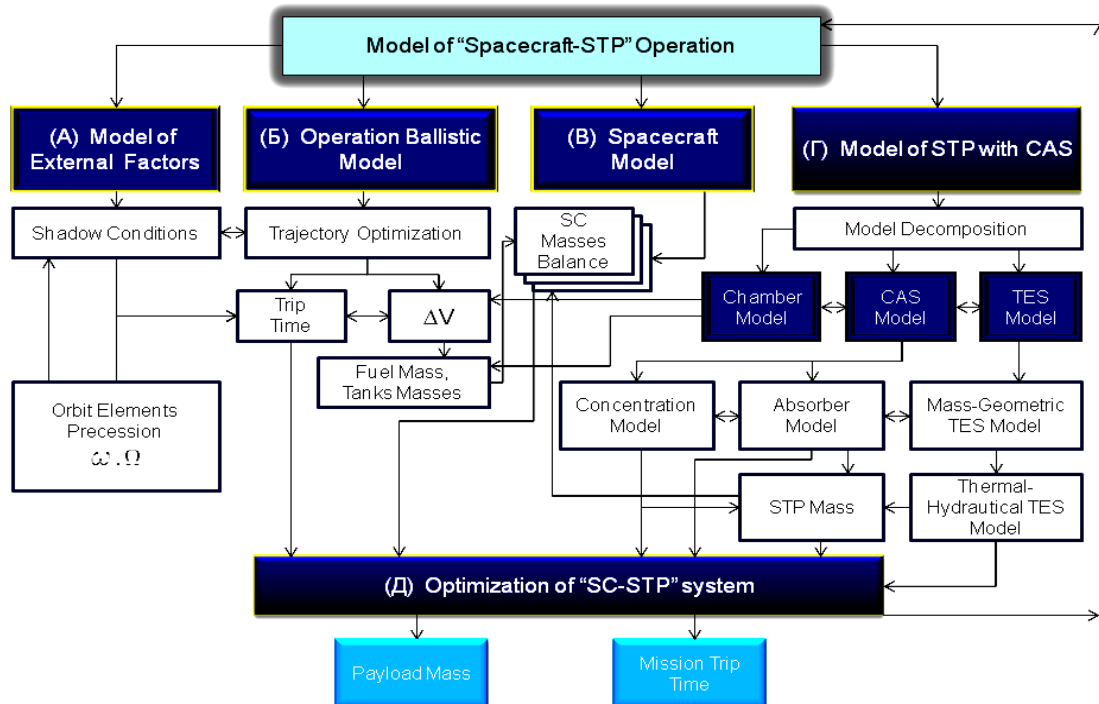

Fig. 15. The block-diagram of a mathematical model of a "SC-STP" technical system operation

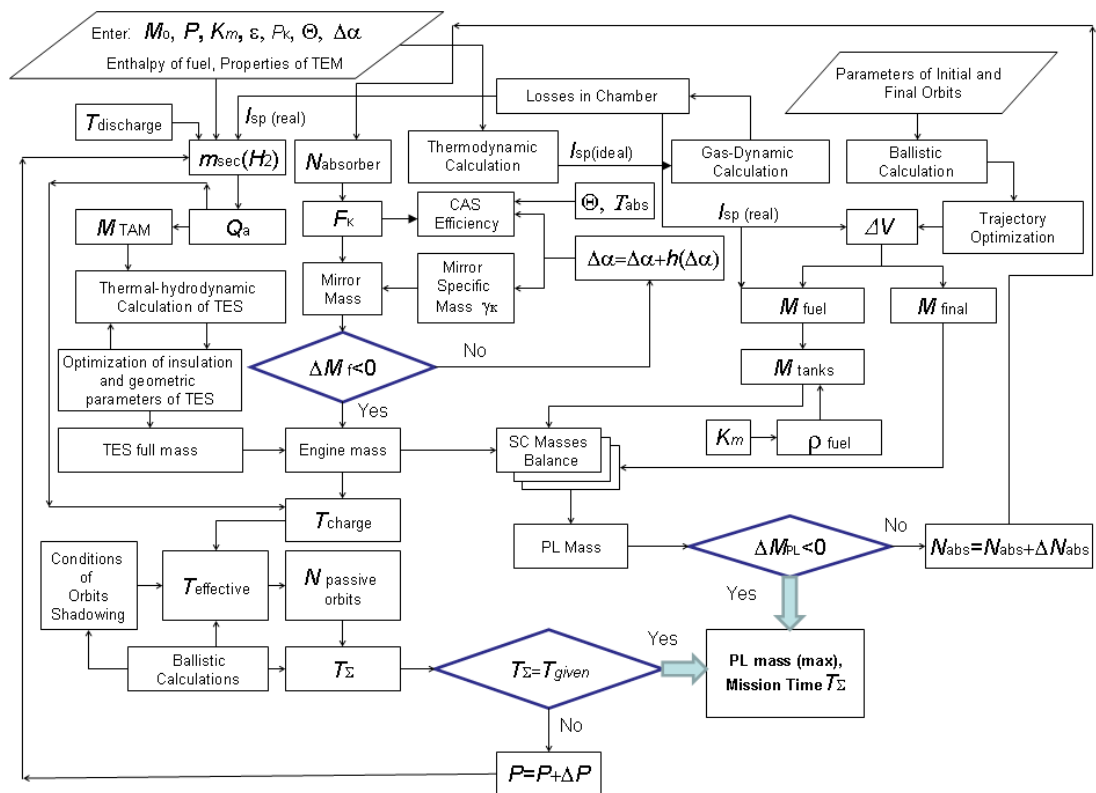Рис. 15. Блок-схема математической модели операции технической системы «КА-СТРД»

Fig. 16. The mathematical model of optimization of the main design parameters
of the "SC-STP" technical system with TES

Рис. 16. Математическая модель оптимизации основных проектных параметров
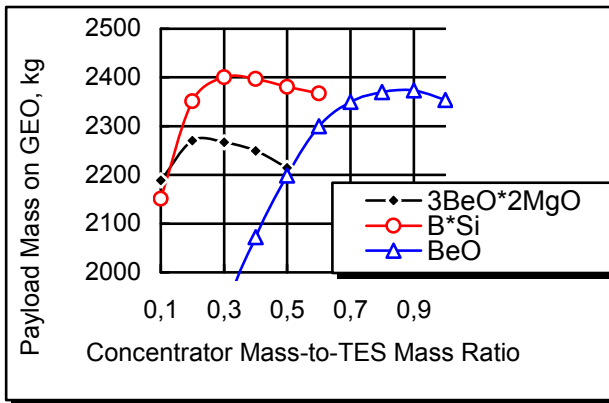технической системы «КА-СТРД» с ТА

Fig. 17. The dependence of the PL mass on the mass ratio
of the concentrator and TES for high-temperature HAM

Рис. 17. Зависимость массы ПН от соотношения масс
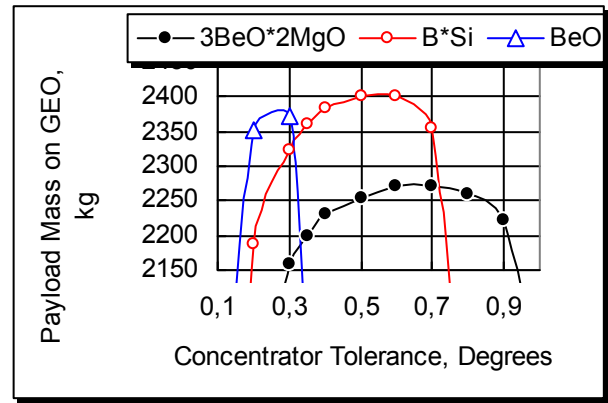концентратора и ТА для высокотемпературных ТАМ

Fig.18. The dependence of the PL mass
on the concentrator surface tolerance

Рис. 18. Зависимость массы ПН от параметра
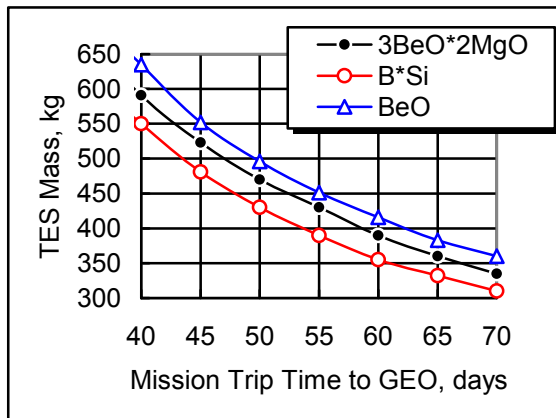точности зеркала

Fig. 19. The dependence of the TES mass
on the time of placing into the GEO

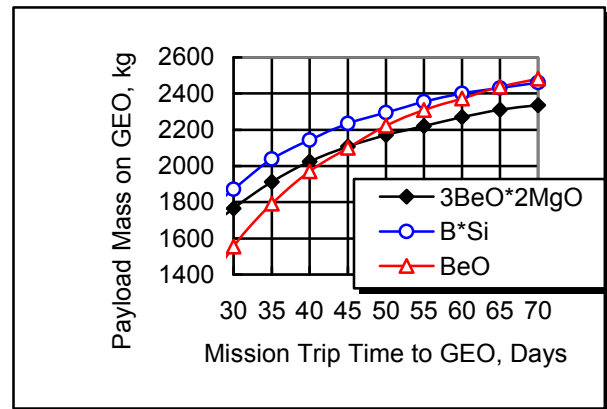Рис. 19. Зависимость массы ТА от времени
выведения на ГСО

Fig. 20. The dependence of the PL mass on the time
of placing into the GEO

Рис. 20. Зависимость массы ПН от времени выведения
на ГСО

The results of calculations according to the presented mathematical model (fig. 16) showed that when choosing an eutectic alloy of boron and silicon as HAM the appropriate value of the ratio $Q_a/F_з$ is about 3.2 MJ/m^2 with the optimum value of the accuracy parameter $\Delta\alpha = 0.5°$ and the selected rational value of the angular aperture of the mirror paraboloid $\Theta = 60°$ [20; 22]. This corresponds to the ratio of the energy intensity Q_a to the mirror mass of about 2.8 MJ/kg which ensures the maximum of the operation objective function – the PL mass. The quantitative estimation of the allowable reduction in the dimension of the "CA-TES" system is clearly demonstrated in fig. 21, 22 in the coordinates $\{M_{PL}; Dк\}$ (from right to left according to the indicated points – the increase of α from 0 to 1 in increments of 0.1).

It is shown that there are various ranges of reasonable values of α for the considered oxidizers corresponding to

the largest PL (fig. 23). The results of similar calculations for the case of using beryllium oxide as HAM [2] are given as a comparative example in fig. 24.

Here the ratio $Q_a/N_{abs} = 22–24$ MJ/kW ($Q_a/F_к = 7,5$ MJ/m^2) corresponds to the optimal interorbital transfer with the choice of the concentrator tolerance $\Delta\alpha = 0.25°$. The results of the comparison show higher efficiency of the boron-silicon alloy with the same values of the oxidizer-to-fuel ratio over the entire considered time interval of the interorbital transfer. Compared to the promising combined ITVs that use high and low thrust engines for "raising" a SC on the GEO the gain in PL mass can be up to 450 kg with the same interorbital transfer time of 60 days.

STP with two-stage TES. In order to reduce the TES mass it may be advisable to use TES with two heating stages [8]. The efficiency of such a system is greater than that of an isothermal system; therefore in such a STP

system it is possible to use, for example, refractory beryllium oxide BeO in a high-temperature stage with a significantly less accurate mirror having lower specific mass. Combinations of phase transition HAM with high latent heat of melting, for example, lithium hydride LiH in the low-temperature stage (melting point is 961 K, latent heat of melting is about 2540 kJ/kg* K) and BeO (melting point is 2804 K, latent heat of melting is 2840 kJ/kg*K) [3] are selected for construction of such an STP system. As it follows from the graphs in fig. 25–27, the PL mass on the GEO does not have an extremum within the ratio of the mirror mass to the TES mass 0.05–1 for the range $K_m = 0$–1.6 and for the case $K_m = 0$ it has a significant gain in PL mass on the GEO over other types of STP when the time of interorbital transfer is 60 days.
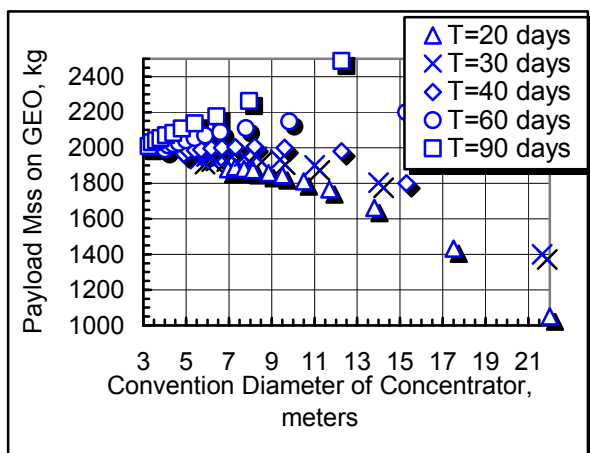

Fig. 21. The PL mass and the concentrator conventional diameter for different time of placing into the GEO while afterburning hydrogen with fluorine

Рис. 21. Масса ПН и условный диаметр концентратора для различного времени выведения на ГСО при дожигании водорода фтором
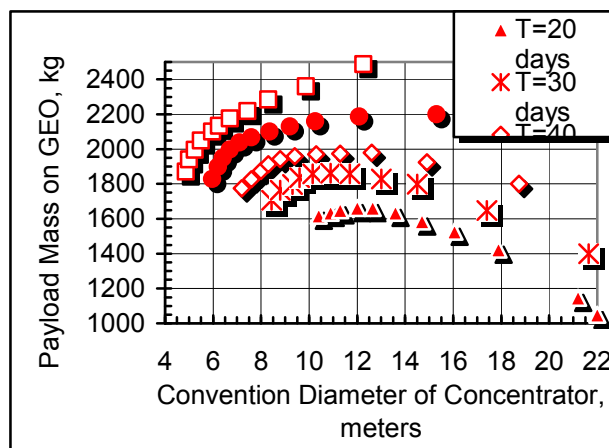

Fig. 22. The PL mass and the conventional diameter of the concentrator for different time of placing into the GEO while afterburning hydrogen with oxygen

Рис. 22. Масса ПН и условный диаметр концентратора для различного времени выведения на ГСО при дожигании водорода кислородом
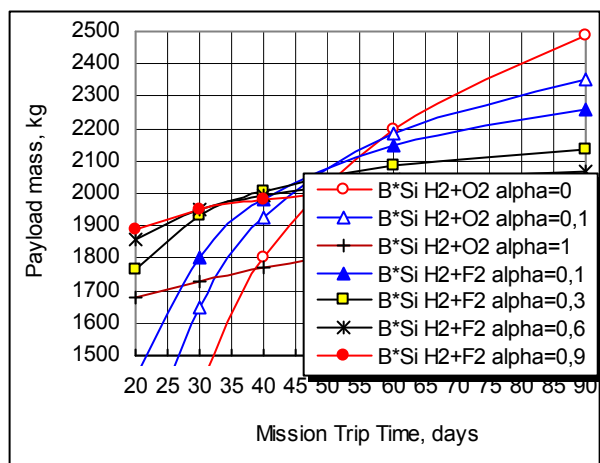
Fig. 23. The dependence of the PL mass on the time of placing into the GEO while afterburning hydrogen with oxygen and fluorine. HAM is the alloy B*Si

Рис. 23. Зависимость массы ПН от времени выведения на ГСО при дожигании водорода кислородом и фтором. ТАМ – сплав B*Si
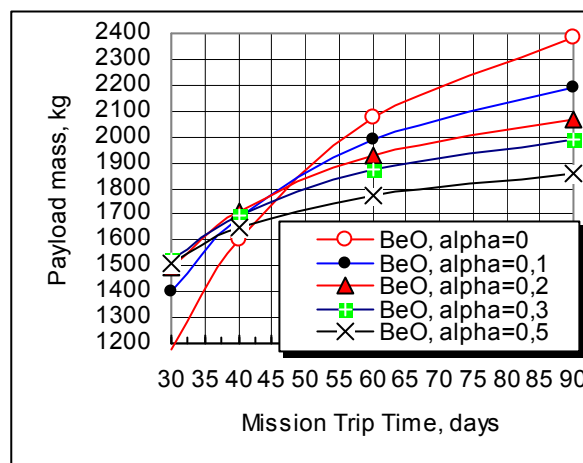

Fig. 24. The dependence of the PL mass on the time of placing into the GEO when using beryllium oxide as HAM and afterburning hydrogen with oxygen

Рис. 24. Зависимость массы ПН от времени выведения на ГСО при использовании в качестве ТАМ оксида бериллия и дожигании водорода кислородом
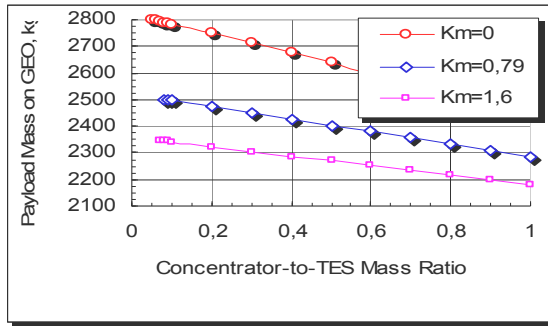
Fig. 25. The dependence of PL mass on the GEO
on the ratio of the mirror mass to the TES mass
for the values of $K_m = 0$–1.6

Рис. 25. Зависимость массы ПН на ГСО
от отношения массы зеркала к массе ТА
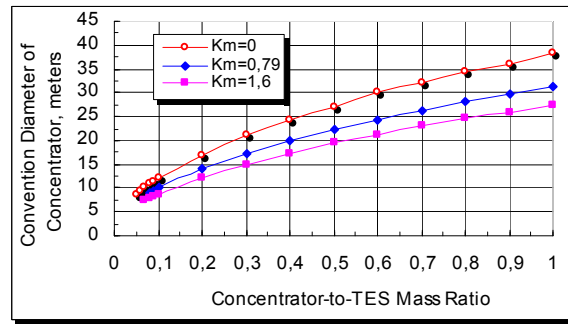для значений $K_m = 0$–1,6

Fig. 26. The dependence of the concentrator
conventional diameter on the ratio of the mirror mass
to the TES mass for the values of $K_m = 0$–1.6

Рис. 26. Зависимость условного диаметра концентратора
от отношения массы зеркала к массе ТА
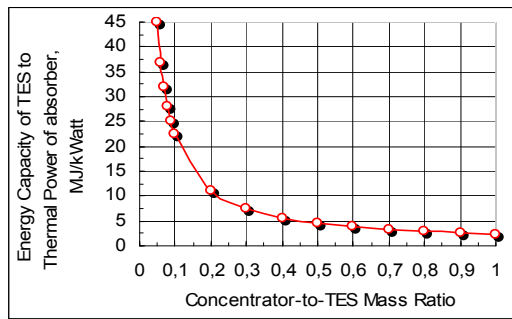для значений $K_m = 0$–1,6

Fig. 27. The dependence of the ratio of TES energy
intensity to the absorber thermal power on the ratio
of the mirror mass to the TES mass

Рис. 27. Зависимость отношения энергоемкости ТА
к тепловой мощности приемника от отношения
массы зеркала к массе ТА

Conclusion. Rocket engines of configurations using solar energy in the CA system are considered. Numerical solutions are obtained for the problem of temperature distribution over the radius of the extremely non-isothermal absorber which made it possible to compile refined regression dependencies to determine its efficiency. The authors also obtained regression dependences for determining the efficiency of a two-stage absorber convenient for engineering calculations. The possibilities of improving the engine performance while using such absorbers to improve the flight efficiency of the SC are determined. Techniques for optimal matching the STP characteristics with various types of CAS and the main design SC parameters and ballistic parameters in the problem of interorbital transfer to high working orbits using the example of a GEO for different homing time have been developed. The dependences of the optimal temperature of hydrogen heating in the CAS on the time of SC placing into the GEO are revealed. It is shown that the optimal temperature of hydrogen and the optimal accuracy of the solar concentrator decrease, and the size of the solar concentrator increases with the reduction of the multi-turn interorbital transfer time.

Besides oxygen, fluorine and hydrogen peroxide are also proposed to be used as expedient oxidizers. Together

with hydrogen they form high-energy fuel compositions with a large stoichiometric ratio of components flow-rates as applied to the STP configuration with afterburning. It is shown that when afterburning with these oxidizers the dimension of the CAS can be significantly reduced. The authors present the analysis of the flight characteristics of the SC with STP with hydrogen afterburning, including those with heating in a stepped CAS. It is shown that there are extremal dependences of the STP thrust on the specific impulse.

The expedient combinations of the concentrator accuracy parameter and the ratio of the solar concentrator mass to the TES mass for the HAMs considered are shown. It is shown that the ratio of the mirror mass to the TES mass can be expressed by the ratios of the TES energy intensity to the thermal power of the absorber or to the concentrator diameter as determining the time of the interorbital transfer. The optimal values of these parameters providing the maximum possible PL mass are given. The problems of optimal coordination of the characteristics of the STP with TES and the main design SC parameters and ballistic parameters in the transfer to high working orbits are posed and solved using the example of the GEO for different transfer time.

Mathematical models and software algorithms have been developed for the operation of the "STP with TES – SC" technical system and the optimization of its main design parameters. The expedient values of the concentrator tolerance and the ratio of the TES energy intensity to the absorber thermal power or the concentrator diameter when afterburning the heated in TES hydrogen with oxygen or fluorine were selected as a result of the calculation using the proposed model. The problems of optimal coordination of the characteristics of STP with TES and afterburning hydrogen with various oxidizers together with the main design parameters of the spacecraft and ballistic parameters in the transfer to high working orbits have been posed and solved. It is shown that the expedient values of the oxidizer-to-fuel ratio for the considered variants of STP with TES increase with decreasing time of the interorbital transfer.

Mass-geometric and energetic parameters of STP with a two-stage system "CA-TES" are considered. They show the possibility of using high-temperature TES such as

beryllium oxide to provide a high specific impulse at moderate values of the solar concentrator tolerance. In this case the PL mass can be significantly increased compared with other types of STP at acceptable solar concentrator tolerance.

References

1. Wassom S. R., Lester D. M., Farmer G., Holmes M. Solar Thermal Propulsion IHPRPT Demonstration Program Status. 37th Joint Propulsion Conference and Exhibit. Salt Lake City, UT, USA. July 08–11, 2001. AIAA Paper, 2001, No. 2001–3735.

2. Finogenov S. L., Kolomentsev A. I. [Solar thermal propulsion with beryllium oxide latent fusion thermal energy storage and hydrogen after-burning]. *Vestn. Mosk. Gos. Tekh. Univ. im. N.E. Baumana, Mashinostr.* 2018, Vol. 25, No. 3, P. 107–115 (In Russ.).

3. Finogenov S. L, Kudrin O. I., Nikolenko V. V. Solar Thermal Propulsion with High-Efficient "Absorber-Thermal Storage" System. IAF Paper 1997, No S.06.05. 48th International Astronautical Congress, October 6-10, 1997, Turin, Italy.

4. Gilpin M. R, Scharfe D. B., Young M. P., Webb R. Experimental Investigation of Latent Heat Thermal Energy Storage for Bi-Modal Solar Thermal Propulsion. 12th International Energy Conversion Engineering Conference. Cleveland, OH, USA. July 28–30, 2014. AIAA Paper, 2014. № 2014–3832. Available at: https://arc.aiaa.org/doi/10.2514/6.2014-3832./

5. Koroteev A. S. et al. Kick Stages with Solar Heat Propulsion Systems for Increase of Middle-Class Soyuz Launchers Competitiveness. Proc. of the 6th International Symposium on Propulsion for Space Transportation: Propulsion for Space Transportation of the XXIst Century. Versailles, France. May 2002.

6. Leenders H. C. M., Zandbergen B. T. C. Development of a solar thermal thrusters system. 59th IAC Congress, Glasgow, Scotland, 2008. Paper IAC-08-D1.1.01.

7. Kudrin O. I. *Solnechnye vysokotemperaturnye kosmicheskie energodvigatel'nye ustanovki.* [Solar high-temperature space power plants]. Moscow, Mashinostroenie Publ., 1987. 247 p.

8. Fedik I. I., Popov E. B. [Power-propulsion plant based on solar thermal storage] *Sbornik dokladov III Mezhdunarodnogo soveshchaniya po problemam energoakkumulirovaniya i ekologii v mashinostroenii, energetike i na transporte* [Proc. III Int. Conference on problems of energy storage and ecology in mechanical engineering, energetic and transport]. Moscow, IMASH RAS, 2002. P. 282–292 (In Russ.).

9. Finogenov S. L., Kolomentsev A. I. [About choice of scheme and parameters of solar thermal propulsion]. *Aerospace MAI Journal.* 2017, Vol. 24, No. 1, P. 63–75 (In Russ.).

10. Safranovich V. F., Emdin L. M. *Marshevye dvigeteli kosmicheskikh apparatov. Vybor tipa i parametrov* [Sustainer engines for space vehicles. Choice of type and parameters]. Moscow, Mashinostroenie Publ., 1980, 240 p.

11. Finogenov S. L., Kolomentsev A. I. [Parameters selection of solar thermal rocket engine under flight time limitation]. *Aerospace MAI Journal.* 2016, Vol. 23, No. 3, P. 58–68 (In Russ.).

12. Grilihes V. A., Matveev V. M., Poluehktov V. P. *Solnechnye vysokotemperaturnye istochniki tepla dlya kosmicheskikh apparatov* [Solar high-temperature heat sources for space vehicles]. Moscow, Mashinostroenie Publ., 1975, 248 p.

13. Finogenov S. L., Kolomentsev A. I. [Nonisothermal Concentrator-Absorber System Performances for Solar Thermal Propulsion]. *Vestn. Mosk. Gos. Tekh. Univ. im. N.E. Baumana, Mashinostr.* 2017, No. 2, P. 66–83 (In Russ.). DOI: 10.18698/0236-3941-2017-2-66-83.

14. Finogenov S. L., Kolomentsev A. I., Nazarov V. P. [Solar thermal propulsion with different types of „concentrator-absorber" system]. *Vestnik SibGAU.* 2016, Vol. 17, No. 3, P. 738–747 (In Russ.).

15. Finogenov S. L., Kolomentsev A. I., Kudrin O. I. [Use of different oxidizers for afterburning of hydrogen heated in rocket engine by solar energy]. *Vestnik SibGAU.* 2015, Vol. 16, No. 3, P. 680–689 (In Russ.).

16. Konstantinov M. S., Min Thein [Optimisation of spacecraft injection trajectory into GEO for transportation system having specific impulse of 600-900 sec]. *Trudy MAI.* 2017, No. 95 (In Russ.). Available at: http://trudymai.ru/published.php?ID=84516.

17. Finogenov S. L., Kolomentsev A. I., Konstantinov M. S. [Performances of spacecraft with solar thermal propulsion]. *Vestnik KGTU im. A. N. Tupoleva.* 2017, No. 2 (74), P. 62–69 (In Russ.).

18. Finogenov S. L. [Choice of performances of solar thermal propulsion in the task of optimal injection into GEO]. *Vestnik KGTU im. A. N. Tupoleva.* 2018, No. 1 (75), P. 74–79 (In Russ.).

19. Finogenov S. L., Kolomentsev A. I. [The choice of heat-accumulating materials for solar thermal propulsion]. *Vestnik SibGAU.* 2016, Vol. 17, No. 1, P. 161–169 (In Russ.).

20. Finogenov S. L. [Conception of solar thermal propulsion with latent heat thermal energy storage and afterburning of hydrogen with fluorine]. *Vestn. Mosk. Gos. Tekh. Univ. im. N.E. Baumana, Mashinostr.* 2018, No. 3 (120), P. 44–63 (In Russ.). DOI: 10.18698/0236-3941-2018-3-44-63.

21. Levenberg V. D., Tkach M. P., Gol'strem V. A. *Accumulirovanie tepla.* [Heat accumulating]. Kiev, Tehnika Publ., 1991, 112 p.

22. Finogenov S. L., Kolomentsev A. I. [Performances of solar thermal propulsion with thermal energy storage and hydrogen afterburning]. *Vestn. Mosk. Gos. Tekh. Univ. im. N. E. Baumana, Mashinostr* [Herald of the Bauman Moscow State Tech. Univ., Mech. Eng.]. 2018, No. 7 (121), P. 55–70 (In Russ.). DOI: 10.18698/0236-3941-2018-3-55-70.

Библиографические ссылки

1. Wassom S. R., Lester D. M., Farmer G., Holmes M. Solar Thermal Propulsion IHPRPT Demonstration Program Status // 37th Joint Propulsion Conference and Exhibit. Salt Lake City, UT, USA (July 08-11, 2001). AIAA Paper. 2001. № 2001–3735.

2. Финогенов С. Л., Коломенцев А. И. Солнечный тепловой ракетный двигатель с оксид-бериллиевым фазопереходным тепловым аккумулятором и дожиганием водорода // Вестник Московского авиационного института. 2018. Т. 25, № 3. С. 107–115.

3. Finogenov S. L, Kudrin O. I., Nikolenko V. V. Solar Thermal Propulsion with High-Efficient "Absorber-Thermal Storage" System // IAF Paper 1997, No S.06.05. 48th International Astronautical Congress (October 6–10, 1997). Turin, Italy.

4. Gilpin M. R, Scharfe D. B., Young M. P., Webb R. Experimental Investigation of Latent Heat Thermal Energy Storage for Bi-Modal Solar Thermal Propulsion // 12th International Energy Conversion Engineering Conference. Cleveland, OH, USA. July 28-30, 2014. AIAA Paper, 2014. № 2014-3832 [Электронный ресурс]. URL: https://arc.aiaa.org/doi/10.2514/6.2014-3832.

5. Koroteev A. S. et al. Kick Stages with Solar Heat Propulsion Systems for Increase of Middle-Class Soyuz Launchers Competitiveness // Proc. of the 6th International Symposium on Propulsion for Space Transportation: Propulsion for Space Transportation of the XXIst Century. Versailles, France. May 2002.

6. Leenders H. C. M., Zandbergen B. T. C. Development of a solar thermal thrusters system // 59th IAC Congress, Glasgow, Scotland, 2008. Paper IAC-08-D1.1.01.

7. Кудрин О. И. Солнечные высокотемпературные космические энергодвигательные установки. М. : Машиностроение, 1987. 247 с.

8. Федик И. И., Попов Е. Б. Двигательно-энергетическая установка на солнечных тепловых аккумуляторах // Сб. науч. докладов III Междун. совещания по проблемам энергоаккумулирования и экологии в машиностроении, энергетике и на транспорте. М. : ИМАШ РАН, 2002. С. 282–292.

9. Финогенов С. Л., Коломенцев А. И. О выборе схемы и параметров солнечного теплового ракетного двигателя // Вестник Московского авиационного института. 2017. Т. 24, № 1. С. 63–75.

10. Сафранович В. Ф., Эмдин Л. М. Маршевые двигатели космических аппаратов. Выбор типа и параметров. М. : Машиностроение, 1980. 240 с.

11. Финогенов С. Л., Коломенцев А. И. Выбор параметров солнечного теплового ракетного двигателя при ограничении на время полета // Вестник Московского авиационного института. 2016. Т. 23, № 3. С. 58–68.

12. Грилихес В. А., Матвеев В. М., Полуэктов В. П. Солнечные высокотемпературные источники тепла для космических аппаратов. М. : Машиностроение, 1975. 248 с.

13. Финогенов С. Л., Коломенцев А. И. Характеристики неравнотемпературных систем концентратор-приемник солнечного теплового ракетного двигателя // Вестник МГТУ им. Н. Э. Баумана. Сер. «Машиностроение». 2017. № 2. С. 66–83. DOI: 10.18698/0236-3941-2017-2-66-83.

14. Финогенов С. Л., Коломенцев А. И., Назаров В. П. Солнечный тепловой ракетный двигатель с различными типами системы «концентратор – приемник» // Вестник СибГАУ. 2016. Т. 17, № 3. С. 738–747.

15. Финогенов С. Л., Коломенцев А. И., Кудрин О. И. Использование различных окислителей для дожигания водорода, нагреваемого в ракетном двигателе за счет солнечной энергии // Вестник СибГАУ. 2015. Т. 16, № 3. С. 680–689.

16. Константинов М. С., Мин Тейн. Оптимизация траектории выведения космического аппарата на геостационарную орбиту для транспортной системы с удельным импульсом двигателя 600–900 с. // Труды МАИ. 2017. № 95 [Электронный ресурс]. URL: http://trudymai.ru/published.php?ID=84516.

17. Финогенов С. Л., Коломенцев А. И., Константинов М. С. Характеристики космического аппарата с солнечным тепловым ракетным двигателем // Вестник КГТУ им. А. Н. Туполева. 2017. № 2 (74). С. 62–69.

18. Финогенов С. Л. Выбор характеристик солнечного теплового ракетного двигателя в задаче оптимального перелета на геостационарную орбиту // Вестник КГТУ им. А. Н. Туполева. 2018. № 1 (75). С. 74–79.

19. Финогенов С. Л., Коломенцев А. И. Выбор теплоаккумулирующего материала для солнечного теплового ракетного двигателя // Вестник СибГАУ. 2016. Т. 17, № 1. С. 161–169.

20. Финогенов С. Л. Концепция солнечного теплового ракетного двигателя с фазопереходным тепловым аккумулятором и дожиганием водорода фтором // Вестник МГТУ им. Н. Э. Баумана. Сер. «Машиностроение». 2018. № 3 (120). С. 44–63. DOI: 10.18698/0236-3941-2018-3-44-63.

21. Левенберг В. Д., Ткач М. П., Гольстрем В. А. Аккумулирование тепла. Киев : Тэхніка, 1991. 112 с.

22. Финогенов С. Л., Коломенцев А. И. Характеристики солнечного теплового ракетного двигателя с тепловым аккумулятором и дожиганием водорода // Вестник МГТУ им. Н. Э. Баумана. Сер. «Машиностроение». 2018. № 4 (121). С. 55–70. DOI: 10.18698/0236-3941-2018-3-55-70.
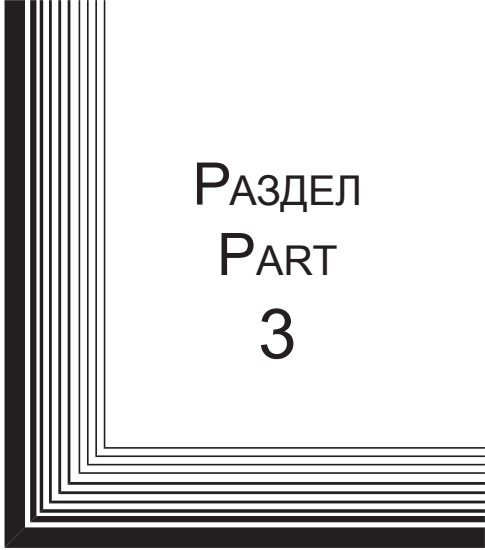
Финогенов Сергей Леонардович – старший научный сотрудник; Московский авиационный институт (Национальный исследовательский университет), кафедра 202 «Ракетные двигатели». E-mail: sfmai2015@mail.ru.

Коломенцев Александр Иванович – кандидат технических наук, профессор; Московский авиационный институт (Национальный исследовательский университет), кафедра 202 «Ракетные двигатели». E-mail: a.i.kolomentsev@yandex.ru.

Finogenov Sergei Leonardovich – Senior researcher of Department 202 "Rocket Engines"; Moscow Aviation Institute (National Research University). E-mail: sfmai2015@mail.ru.

Kolomentsev Alexander Ivanovich – Cand. Sc. Professor, Professor of Department 202 "Rocket Engines", Moscow Aviation Institute (National Research University). E-mail: a.i.kolomentsev@yandex.ru.

ТЕХНОЛОГИЧЕСКИЕ
ПРОЦЕССЫ
И МАТЕРИАЛЫ

TECHNOLOGICAL
PROCESSES
AND MATERIALS SCIENCE

THE PROCESS OF NANOMODIFYING CAST ALUMINUM ALLOY INGOTS FOR COMPONENTS OF AEROSPACE VEHICLES

G. G. Krushenko[1, 2], V. P. Nazarov[2], S. N. Reshetnikova[2], G. V. Dvirnyi[2]

[1]Institute of computational modeling SB RAS
44, Akademgorodok, Krasnoyarsk, 660036, Russian Federation
[2] Reshetnev Siberian State University of Science and Technology
31, Krasnoyarsky Rabochy Av., Krasnoyarsk, 660037, Russian Federation
E-mail: genry@icm.krasn.ru

Currently, increasing attention has been paid to such a class of materials as nanopowders (NP) of chemical compounds, which are ultra-thin formations of not more than 100 nm in size. Such attitude to these materials is explained by the fact that they have unique physical, chemical and mechanical properties significantly different from the properties of materials of the same chemical composition in a massive state, and these properties can be transferred to some extent from them or with their participation to the products.

The existing methods of introducing NP into metal melts could not be used due to their special properties in comparison with coarse powders, and therefore a new method of their introduction into the melt was developed, excluding direct contact of NP particles with oxygen and unhindered penetration of particles into the melt through the oxide layer. The essence of the method was as follows. In the aluminum container filled up with aluminum particles or deformable aluminum alloys D1 or D16 and various NP (nitrides, carbides, oxides, etc.), and this composition was pressed into the rod, with its help NP was introduced into the melt during casting of aluminum ingots and deformable aluminum alloys.

The results of the study showed that this excludes the appearance of cracks in the ingots, as well as improves their technological and mechanical properties.

Keywords: aluminum alloys, ingots, nanopowders, improvement of technological and mechanical properties.

НАНОМОДИФИЦИРОВАНИЕ АЛЮМИНИЕВЫХ СПЛАВОВ ПРИ ЛИТЬЕ СЛИТКОВ, ДЕФОРМИРУЕМЫХ В АЭРОКОСМИЧЕСКИЕ ИЗДЕЛИЯ

Г. Г. Крушенко[1,2], В. П. Назаров[2], С. Н. Решетникова[2], Г. В. Двирный[2]

[1]Институт вычислительного моделирования СО РАН
Российская Федерация, 660036, г. Красноярск, Академгородок, 44
[2]Сибирский государственный университет науки и технологий имени академика М. Ф. Решетнева
Российская Федерация, 660037, г. Красноярск, просп. им. газ. «Красноярский рабочий», 31
E-mail: genry@icm.krasn.ru

В последнее время все большее внимание уделяется такому классу материалов, как нанопорошки (НП) химических соединений, которые представляют собой сверхтонкие образования размерами не более 100 нм. Такое отношение к этим материалам объясняется тем, что они обладают уникальными физико-химическими и механическими свойствами, существенно отличающимися от свойств материалов одного и того же химического состава в массивном состоянии, и эти свойства могут быть в определенной степени переданы от них или с их участием продуктам.

Существующие способы введения НП в металлические расплавы не могли быть использованы вследствие наличия у них особых свойств по сравнению с более крупными порошками, в связи с чем был разработан новый способ их введения в расплав, исключающий прямой контакт частиц НП с кислородом и беспрепятственное их

проникновение в расплав через окисную пленку. Суть способа заключалась в следующем. В алюминиевый контейнер засыпали частицы алюминия или алюминиевых деформируемых сплавов Д1 или Д16 и различные НП (нитриды, карбиды, оксиды и др.) и подвергали эту композицию прессованию в пруток, с помощью которого НП и вводили в расплав при литье слитков из алюминия и алюминиевых деформируемых сплавов.

Результаты исследования показали, что при этом исключается появление в слитках трещин, а также повышаются их технологические и механические свойства.

Ключевые слова: алюминиевые сплавы, слитки, нанопорошки, повышение технологических и механических свойств.

Introduction. In recent years, more attention has been paid to such a class of materials as nanopowders (NP) of chemical compounds, which are ultrafine crystalline or amorphous formations with 100 nm in size (1 nm = $= 10^{-9}$ m) [1]. Such an attitude to these materials is explained by the fact that they have unique physicochemical and mechanical properties that differ significantly from the material properties of the same chemical composition in a massive state, and these properties can be transferred to the products obtained from them or with their help [2].

History. There is various information regarding the proposal of the term "nanotechnology" [3]. Thus, according to [4], the first who not only proposed (in 1950) a new term – molecular engineering, but also predicted the creation of nanomolecular devices, was an electrical engineer at the Massachusetts Institute of Technology A. R. von Hippel). In 1959, the Nobel Prize laureate, physicist Richard Feynman, in his famous lecture published in 1960 [5], pointed to the possible significant prospects for designing at the scale of atoms and molecules that can be achieved as a result of obtaining materials and devices molecular scale (atomic-molecular scale) and noted that to control the properties of these small nanostructures ("nano" – structures), it will be necessary to create a new class of miniature tools.

In the early 1980s, an engineer at the Massachusetts Institute of Technology, K.E. Drexler proposed approaches, physical principles for obtaining complex nanoscale structures [6]. Later on this topic, he published several monographs, including [7], in which he outlined the prospects for the application of molecular technology (molecular manufacturing technology) opportunities in a number of industries. In this monograph, he used the term "nanotechnology" (nanotechnology) to describe the vision of the subject by R. Feynman and the technologies for implementing his idea. It is believed [8] that N. Taniguchi from the University of Tokyo, in a report made in 1974 at a conference of the Japanese Society of Precise Engineering on the coming transition to processing with ultrahigh precision, defined the term "nanotechnology" [9] as a technology that ensures "extra" high precision and "ultra fine" sizes about 1 nm (1 nanometer = 10^{-9} m). He defined the term "nanotechnology" the following way: "nanotechnology mainly consists of the processing of separation, consolidation, and deformation of materials the size of one atom or one molecule" [10].

Today publications on the use of NPs in the creation of products, both on a metal and an elastomer basis appear [11–13]. The first author's certificate on the invention on the use of NP for grinding the structure of

aluminum alloys [14] was obtained in 1981 (priority from 10.17.79). According to the results of the technologies developed on the use of NP for improving the quality of metal products manufactured in various ways from various metals and alloys, 25 USSR author certificates and patents of the Russian Federation for inventions were obtained. Most of the work was done to crush the structure and, as a result, increase the level of mechanical properties of products from aluminum cast alloys (shaped casting and liquid stamping) and cast iron (shaped casting), aluminum and deformable aluminum alloys during casting of ingots in a semi-continuous manner. The process of grinding the structural components of the alloys at the macro and micro levels is called modifying. The result of the modification of metal compositions is the improvement of the technological properties at the stage of obtaining products, as well as improvement of the strength and plastic characteristics of the finished products, especially in the case of using NP for this purpose.

The method of introducing nanopowders into metal melts. Existing methods of introducing powdered additives into metal melts could not be taken using NP due to their special properties as compared to coarse powders, and therefore a fundamentally new method of their introduction into the melt was developed [14], which excluded direct contact of powder particles with oxygen in the process of their introduction, penetration of particles through the oxide layer, exclusion of aggregation and controlled dosing by weight.

The essence of the method was as follows. In a thin-walled aluminum container (diameter 165 mm, height 235 mm, wall thickness 2 mm) pellets of aluminum or aluminum deformable alloys D1 or D16 with a diameter of 1.5–3.0 mm, obtained by centrifugal spraying, were poured. The same container was filled up to 3.0 wt. % NP by weight of the granules. Nitrides, carbonitrides, oxides, carbides, and other high-strength refractory chemical compounds with particle sizes up to 100 nanometers were used as NP.

The opening in the container was closed with a lid, installed in an installation with an eccentric axis of rotation, and it was rotated, as a result the surface of the granules was clad with nanopowder particles.

Then this container was heated, placed in a container of a hydraulic press and with a pressing force of 100–120 ton-force the rods were pressed with a speed of 3.5 cm/sThe rods obtained in this way had a thin-walled surface (tenths of mm), the quality of which (roughness) was almost the same as the surface of profiles pressed from compact aluminum billets made from ingots.

And their volume consisted of densely pressed fibers (see the figure). This is explained by the fact that, due to the presence of NP particles on the granule surface during the extrusion process, the granules were deformed separately from each other, which is confirmed by the results of a microscopic study of the surface of clad aluminum particles and fibers. It turned out that the fibers are completely covered with NP particles firmly embedded in their surface. At the same time, the purity of the surface of such a bar was the same with a rod extruded from a compact aluminum billet obtained from an ingot. In rods $\varnothing 9.5$ mm there were from 1100 to 1200 densely compacted fibers with a cross section of 0.005–0.075 mm^2, the length of which, depending on the size of the aluminum particles, is in the range of 400–3200 mm.
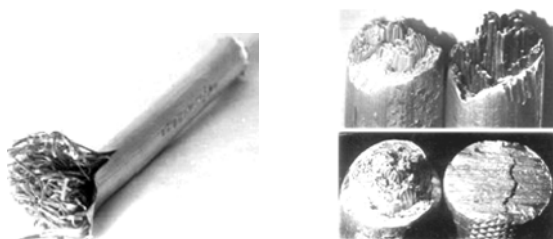
A typical type of modifying rod $\varnothing$ 9.5 mm, pressed from the composition of aluminum granules + NP

Типичный вид модифицирующего прутка $\varnothing$ 9,5 мм, отпрессованного из композиции алюминиевые гранулы + НП

In the process of conducting experiments under production conditions, it was found that regardless of the chemical composition of the NP, their crystal system and class, symmetry elements, space group, structural type, lattice period, density, melting temperature and other parameters considered, they all had a similar modifying effect.

Modification of aluminum and aluminum alloys with nanopowders during casting of ingots in a semi-continuous manner. A rather common defect of ingots cast in a semicontinuous method from aluminum and wrought aluminum alloys is the occurrence of cracks in the process of crystallization – crystallized or hot cracks, and after complete solidification of the metal – cold cracks. According to [15], on flat ingots, cracks are located on the surface of both the bottom part and the bottom part with a transition to wide faces, where their direction coincides with the direction of the casting. These cracks are formed as a result of violations of the speed and temperature of the casting due to uneven cooling around the perimeter of the ingot. On round ingots, cracks are classified as follows: a) central (due to rapid cooling of the peripheral layers with a sufficiently strong core that resists shrinkage of the outer layers); b) radial – located in the middle part of the ingot and develop from the periphery to the center (they appear only at the initial moment of cooling of the ingot with water, when the bottom of the well is above the belt of direct cooling of the ingot with water; upon subsequent cooling

these cracks are tightly compressed); c) circular cracks – occur in the zone of change in the character of the grain structure and more often on ingots with a columnar structure (the reason is a big difference in the cooling rates of the crust near the wall of the mold and the metal in the middle of the ingot from the direct effect of cooling water). The occurrence of cracks is associated [16] with the occurrence of internal stresses during solidification of the ingot, due to the presence of a temperature gradient in the cross section and height of the ingot, which leads to non-simultaneous crystallization of the outer and inner volumes of the metal and as a result of difficult shrinkage of the first peripheral and then the inner layers. It is believed that hot cracks appear due to the low ductility of the alloy in the solid-liquid state, and cold – due to low elongation in the hardened state. It has been noted that hot cracks do not occur if the elongation in the solid-liquid state is more than 0.3 %, and cold – if its value is more than 1.5 %. The magnitude of the stresses in this case is determined by the elastic and plastic deformations that occur in the considered volume of the metal under the influence of adjacent layers, which are cooled with a different speed. This phenomenon is aggravated by a significant heterogeneity of the structure over the section of the ingot, characterized by three zones: a thin peripheral layer of the ingot that forms at the surface of the water-cooled crystallizer, has the smallest structure, then comes a layer of large columnar crystals directed to the center of the ingot, and the central zone consisting of coarse disoriented crystals. Such a structure is a characteristic of large-sized ingots, during casting of which cracks often occur. Most of the defect in the continuous casting of steel ingots also refers to cracks [17]. To a greater degree, the occurance of cracking increases [18] when aluminum liquid charge, delivered to the mixtures of casting section directly from the electrolyzers, is used for casting ingots (economically more advantageous technological scheme due to the exclusion of the operation of preparing alloys by melting solid charge). The reason for this is the formation of a coarse-crystalline structure of ingots, which is associated with the deactivation of nucleating agents at high temperature (1173–1223 K) of electrolysis aluminum supplied directly to the mixer It has been established that with an increase in the grade (purity) of aluminum, the ingot rejects for cracks increase, which is associated with the formation of a coarse-crystalline structure.

In order to identify the causes of cracks and establish optimal casting conditions that reduce the risk of this defect by the method of multidimensional correlation analysis [19], the ingot defects were calculated for cracks cast from A6 aluminum [20]. For active control of the technological process, a mathematical model of the connection of the number of ingots (optimization parameter, U, %) of two standard sizes was investigated: I – 347 × 1325 mm and II – 347 × 1630 rejected on cracks along a wider face, with controlled molding parameters (X_1 – casting speed, mm / min and X_2 – casting temperature), with the ratio of impurities of Fe: Si (X_3) and including the element-modifier (X_4, %). Digital expressions of all factors were fixed in 264 heats. As

a result of the calculations, linear regression equations were obtained, which relate the number of ingot defects for cracks to the factors influencing its appearance.

For an ingot of type I, an equation was obtained:

$$U = -791.4 + 0.376X_1 + 1.152 X_2 - 0.11X_3 - 130X_4. \quad (1).$$

For ingot type II:

$$U = -961.0 + 2.38X_1 + 1.25 X_2 - 0.09X_3 - 1390X_4. \quad (2).$$

The coefficient of multiple correlation for equation (1) was 0.71 and 0.869 for equation (2), which indicates a significant proportion of the studied factors in the volume of active factors. The close dependence of the level of defect on cracks on the studied factors turned out to be much more than its dependence on each of them separately and on the close connection of factors with each other. The magnitudes of the coefficients in the equations and the sign in front of them indicates the relative magnitude and direction of the influence of the effect of the corresponding factor on the optimization parameter (reduction or increase in the defect). The values of the pair correlation coefficients between Y and X_1, X_2 and X_4 are close, which indicates that these factors have approximately the same effect on the ingot defect on cracks. So, for an ingot, the cross section of 347 × 1325 mm, the bond between Y and X_3 is weak (ryx$_3$ = –0,027), which is explained by the compliance with the required value (> 1) of the ratio Fe: Si – average 1.24, and for an ingot with a cross section of 347 × 1630 mm, this relationship was much closer (ryx$_3$ = –0.0476) which, when casting such ingots, requires a stricter respect for the ratio Fe:Si. Using the obtained equations, nomograms were calculated and constructed, which allow us to predict the expected level of defect on cracks during the smelting process and adjust the casting technological parameters (casting speed and temperature, Fe: Si ratio, titanium content), respectively, to reduce the ingot defect for cracks [20]. Experimental verification gives a very satisfactory convergence of the estimated number of defects with the actual. Good convergence is also observed in the case of introducing into the calculation the water pressure in the cooling system of ingots with dimensions of 295 × 1230 × 2400 mm made from A7 aluminum. Analysis of the initial information showed that when casting ingots of type I, the content of titanium in different heats varies in the range of 0.01–0.028 %, for type II – in the range of 0.014–0.027 %. The calculation of defects for cracks using the regression equations found for the lower and upper titanium contents with the stability of the other factors showed a significant influence of this factor. So, for ingot I, at the lower level of titanium, a defect for cracks is predicted to 24.9 %, at the top – it decreases to 1.45 %, for II, respectively, 21.16 and 3.09 %.

When working with commonly used ligatures, obtained in the form of relatively massive ingots containing titanium modifying element, or with a titanium sponge, which dissolve for quite a long time, incommensurable with the casting speed of the ingot, it is not possible to change this factor (X_4 – titanium, %) affect the reduction of defects for cracks. In the case of the use of rod modifying ligatures that can be made with any desired diameter, their dissolution occurs at a rate commensurate with any of the ingot casting speed adopted by the technology (from 60 to 90 mm/min), while ensuring stable and equal content of modifying element in any volume of metal in the ingot.

The negative consequences of the use of the liquid charge are prevented by the introduction of modifiers into the melt, in particular, titanium, less often in its pure form, more often in the volume of aluminum-titanium master alloys. When titanium interacts with liquid aluminum in the melt, nucleating particles of TiAl$_3$ compound appear, which leads to a refinement of the structure, and, consequently, to an increase in the plasticity of the hardened and hardening metal, and as a result – to a decrease in the ingot defect due to cracks. Analysis of 9857 ingots cast at Krasnoyarsk Aluminum Smelter 347 × 1325 mm and 347 × 1630 mm and weighing up to five tons showed that the smallest number of defects on cracks (2.0–4.5 %) provides a titanium content in the range of 0.030–0.035 %. Moreover, it is also known that the occurrence of cracks in ingots is also influenced by the ratio of Fe and Si impurities present in aluminum. Without going into a hypothesis explaining this phenomenon, it can be noted that in order to reduce defects on cracks, it is recommended that the iron content be higher than the silicon content by 0.02–0.05 %. On the same number of ingots, we found that the smallest number of them is with cracks (1.1–1.3 %) with the same titanium content is characterized by the ratio Fe: Si in the range 1.0 : 1.2. Due to the fact that cutting of large-sized ingots at the plant for studying their structure was not possible, it was studied on sample tests simultaneously cast with ingots with an estimate of the size of the macro grain detected on thin sections according to a developed scale. So, for the smallest grain (area of about 0.5 mm^2) I point was taken, and for grain with an area of about 100 mm^2, V point was taken. Comparison of the obtained data showed that the number of ingots with cracks correlates with the grain size on samples: with an increase in the grain size, the number of ingots with cracks increases. So, if with a structure characterized by II point, the defect does not exceed 2.2 %, then with V point, the defect reaches 21.0 %. It should be noted that not all ingots are finally rejected for this type of defect, some types of cracks, especially shallow ones, are cut down and the cutting site is cleaned. Nevertheless, there is a danger of production of ingots with cracks undetected on the surface for further processing by pressure, where this defect at the technological stages is not always detected and can get into the finished product, and lead to negative consequences in operation.

Despite the relatively high efficiency of titanium for grinding the structure and reducing the likelihood of cracks in the ingots, this method has a significant disadvantage, that titanium is introduced either as a titanium sponge or as a pig ligature into a liquid metal in a mixer-forehearth or in the distributing mixer, where these components, firstly, dissolve for quite a long time (hours), secondly, despite the mixing of the melt, titanium is

unevenly distributed over the volume of the bath, which is reflected in its distribution over the height of the ingot, and, consequently, on the degree of grinding of the grain and further – on the technological properties of the ingot and on the mechanical and operational characteristics obtained from these products (sheet, profile, forgings).

Modifying technology. We applied a technology implemented under production conditions, firstly, eliminating the long standing of the melt in the mixer, and, secondly, ensuring the same content of the modifying agent throughout the entire ingot. As mentioned earlier, from the composition consisting of aluminum and NP particles, rods were pressed, which were wound onto a bobbin, and their continuous dosed introduction, coordinated with the volumetric flow rate of the poured metal, was carried out either into the chute or into the junction box in automatic mode using designed installation, consisting of: reel, which serves for winding the rod, electric motor, gearbox, feeding unit of rod and guide tube. The feed speed of the rod into the melt was consistent with the volume flow rate of the metal and was adjusted by changing the number of revolutions of the drive shaft on which the reel was mounted, using an autotransformer. At the same time, the number of NP injected did not exceed 0.05 mass. %, and the consumption of the rod was 20–25 kg per ton of metal. In order to determine the algorithm for automatic control of the rate of introduction of a modifying rod into the melt during ingot casting, which provides the required amount of modifier (NP) in the alloy, such factors as casting temperature (X_2) and Fe: Si ratio (X_3), which are usually not subject to significant fluctuations ingot casting process, taken as stable. Building on the coordinate plane a system of points M_i (X_i, Y_i, where X_i is the mass flow rate of aluminum when casting an ingot, Q, kg; Y_i – titanium content, Ti, kg) showed that the points are located on a line very close to a straight line. Therefore, we can assume that between X_i, (T_i, kg) and U_i, (Q, kg) there is a linear relationship like $Y = a + bX$, where a and b are constant. Based on this assumption, a calculation was made by which an empirical relationship was obtained: $Y = –0.2304 + 0.00055X$, the value of the correlation coefficient for which ($r = 0.9996$) confirms the existence of a close, straightforward relationship of the required titanium content in aluminum with volume flow of the latter. The coefficient of determination in this case was $d = r^2 \times 100$ % = 99.92 %. As an example, the established linear dependence of the melt flow rate and the titanium content in it was transformed into the operating parameters of the casting process of an ingot with a cross section of 400 × 1560 mm, respectively, into the casting speed and the feed speed of the rod alloy. This largest ingot produced by the company was chosen as the object of testing the technology of introducing bar ligatures due to the largest amount of defect on cracks in its bottom part and reaching a wide edge, which is associated with a relatively slow crystallization rate of the metal, contributing to the formation of a large cristal structure. In order to test the installation's ability to provide a high bar feed rate, a ligature with a low content of – Al – 1.95 % Ti modifier was used, commensurate

with the content of NP in rods. At the adopted ingot casting speed (70 mm/min), the volume flow rate of aluminum was 135 kg / min, which required, in order to ensure the content of titanium in aluminum A7 provided for by technical documentation, to introduce a rod with a diameter of 8 mm (the weight of the one running meter is 0.144 kg) at a speed of 4 m/min (4.27 kg per 1 ton of aluminum). Such a rod feed rate ensured introduction of about 0.008 % Ti into the melt in addition to the titanium sponge previously injected into the mixer (about 0.018 % Ti), which in total turned out to be close to the required titanium content, which was determined by chemical analysis – 0.027 % Ti. It is easy to obtain a similar empirical dependence of the feed speed of a rod with different content of the modifying agent on the volume flow rate of aluminum. On thin chargesof the bottom part of the samples with a diameter of 75 mm and a height of 40 mm, cast simultaneously with the casting of the ingot, it was found that the average area of the macrograin of the original aluminum A7 containing 0.018 % Ti is 1.24 mm^2, and the additional introduction is 0.008 % Ti rod ligature reduces it to 0.082 mm^2 (15.1 times). The fact that such an effect of grinding grain was obtained precisely due to the additionally introduced modifier –titanium is evidenced by the fact that when introduced into the same melt when casting the same ingot, a 10 mm diameter rod made of aluminum of the AD0 brand with the same volume feed with a titanium-containing rod, the area grain decreases only 2.4 times (to 0.051 mm^2). At the same time, the depth of the peripheral zone of the columnar crystals of the sample of the original aluminum is 3.5 mm (9.3 % of the sample diameter); when introducing the aluminum rod AD0, it decreases to 2.0 mm (1.75 times) and when modifying with a titanium rod, it is completely absent.

The influence of the type of modifier on the grinding of grain and the mechanical properties of aluminum alloys. Preliminary experiments were carried out under production conditions when pouring from 973 K into metal form samples with a diameter of 60 mm and a height of 300 mm of an aluminum wrought alloy D16 prepared in a liquid charge and taken from a pre-chamber 20-ton mixer from a temperature of 1003 K to a filling bucket with a capacity of 4 kg the subsequent introduction into the melt of various NP in the volume of modifying rods with a diameter of 8 mm, pressed from the granules of the alloy D16 and various NP. The study of charges prepared on the cross-sections of the cast samples showed the effect of grinding grain when using all types of modifying substances, but to a greater degree this effect is observed when modifying the NP. So, if, when a sample rod is brought into the melt, pressed only from granules, the grain is crushed 1.3 times, and the rod pressed out of REM – 1.7 times, then all used NP grind the grain 2–3 times. The effect of the modifying additive on the size of the macrograin in the cross section of a chill sample with a diameter of 60 mm, 300 mm high, cast in a chill mold of alloy D16: 1 – without modification; modifying rod pressed from granules: 2 – alloy D16; 3 – rare-earth metals (Al + 11,0 % La; Al + 11,0 % Ce); modifying bar is pressed out of granules

of alloy D16 and nanopowder: 4 – Si_3N_4; 5 – SiC; 6 – $V_{0,75}N_{0,25}$ (with an impurity V_2O_3); 7 – SiC (with an impurity SiO_2);8 – B_4C (with an impurity BN); 9 – $Cr_3C_{1,6}N_{0,4}$ (with an impurity Cr_2O_3 + C); 10 – B_4C; 11 – TaN; 12 – SiC (with an impurity SiO_2 + Si). The effectiveness of the modifying impact of the NP was confirmed under production conditions when casting ingots on a continuous casting installation when they were introduced into the melt in the automatic mode in the amount of modifying rods.

Thus, when casting ingots with a diameter of 420 mm from AMg6 alloy at a speed of 60 mm / min at 968 K with the adding of a rod into the mold under a metal stream, it was found that if the standard modifying additive (Al-Ti ingot) the average grain size makes up 0,322 мм², then when modifying the NP BN it decreases to 0.146 mm² (2.2 times), NP SiC – to 0.123 mm² (2.6 times), and NP TaN – to 0.078 mm² (4.1 times).

When casting ingots with a diameter of 190 mm from alloy D16, a modifying rod with a diameter of 6 mm was pressed from the granules of the alloy D16 and NP SiC. Rods with a diameter of 12 mm were pressed from homogenized ingots (holding for 6 hours at 753–773 K, air cooling), and after quenching (holding for 15 minutes at 763...773 K, cooling in water), standard cylindrical specimens were carved from them. Analysis of the test results showed that the SiC NP crushes the macrograin over the ingot cross section on average 1.7 times (from 0.35 for the alloy modified by the factory technology to 0.20 mm²), and by c of the ingot radius – 2.3 times (from 0.35 to 0.15 mm²). The temporal resistance $\sigma_в$ in the samples of the modified NP SiC alloy increased by 2.3 %, the yield strength $\sigma_в$ – by 11.0 %, and the relative elongation δ by 31.6 %. The microstructure did not show significant differences from the usual alloy. During casting of ingots with a diameter of 480 mm from D1 alloy, the effect of introducing into the melt NP SiC, B_4C and $V_xC_yN_z$ was investigated. Modifying rods with a diameter of 10 mm were pressed from both D1 alloy granules and from these granules and NP on a rod-shaped horizontal hydraulic press P8743B with a force of 2000 tf at a speed of 2 mm/min. The ingots were cast at 983 K at a speed of 32.36 mm / min, homogenized (the mode is indicated above) and cut into blanks 800 mm long, which were then heated in an IN600 furnace to 653–673 K and on a P4757 press with a force of 700 tf, they were pressed into an intermediate product with a diameter of 100 mm. Of the three sections of this product (loose, medium and tightening) blanks with a length of 250 mm were cut, heated them to 633...653 K and on the press P8739 with a force of 800 tf extruded profile 100–59 (corner with a shelf width of 20 mm). Mechanical properties were tested on three corners cut from the above-mentioned hardened corners (as indicated above) in the VZP-1 vertical tempering furnace. Comparison of the results of testing the mechanical properties of different parts of the profile (output, medium and tightening), pressed from similar parts of the intermediate product, showed that modifying with all the above mentioned NPs in all cases gives mechanical properties higher than conventional technology provides. The study of the structure of the

transverse templates of ingots showed that the highest degree of grinding grain provides NP $V_xC_yN_z$. At the same time, there were no significant differences in the microstructure of the alloy modified by various NPs.

Due to the fact that the filtering used at the enterprise to remove non-metallic inclusions from the melt leads to the enlargement of the macrograin ingots, work was carried out to eliminate this undesirable phenomenon using NP. At the same time, ingots of 280 mm in diameter were cast from the AMg6 alloy at 983–993 K at a speed of 6 mm/min with the filtration of the melt in an upward flow, ingots with a diameter of 280 mm were cast through successively installed meshes from glass fabric SSF-4 and SFF-0.06. Modifying bar with a diameter of 10 mm, containing NP SiC or B_4C, or $V_xC_yN_z$, injected into the mold under a stream of metal coming from the transfer case. For comparison, ingots were cast with the introduction of a rod pressed only from pellets into the mold. The cast ingots were homogenized (holding for 6 hours at 753–773 K; cooling in air), after which they were cut into blanks 700 mm long, heated to 673–683 K and pressed on a horizontal press into profile PC13820-2. Of the three sections of the profile (output, medium and tightening) cut samples for testing mechanical properties. The macrostructure was studied on the ingot transverse templates. The results of tests of mechanical properties showed that, in general, NPs lead to an increase in the relative elongation. So, if δ for ingots cast from filtered metal by factory technology is 19.1 %, then NP B_4C increases it to the greatest extent до 29.4 % (by 24,6 %), NP $V_xC_yN_z$ – to 22.6 % (by 23.4 %) and NP SiC – to 21.8 % (by 14.1 %), then a rod of granules – to 21.6 % (13.2 %). There is also an increase in yield strength $\sigma_{0,2}$. So, if for an ingot cast with filtration according to factory technology, its value is 230 MPa, then NP SiC increases $\sigma_в$ to 247 MPa (by 5.2 %), NP $V_xC_yN_z$ – for 250 MPa (by 8.5 %), granulated rod is up to 233 MPa (by 1.3 %), and NP B_4C does not change this characteristic. Temporary resistance $\sigma_в$ does not change in all types of NP and with the introduction of the rod of granules. The study of the structure of the ingots showed that the filtration of the alloy enlarges the macrograin, whereas the introduction of the NPs studied into the melt after filtration leads to its sharp grinding and to the formation of a homogeneous structure over the section.

Modification of the structure of ingots for forgings. The obtained positive results with the introduction of NP into the melt during the casting of ingots, from which further extrusion methods were used to extrude a profile of different cross sections, served as the basis for testing this technology during the casting of ingots intended for the manufacture of forgings from them. For this purpose, when casting ingots of $\varnothing$420 mm from AMg6 alloy, the melt was modified with a rod of 10 mm containing one of NP – SiC, BN or TaN. The ingots were cast at 973 K at a speed of 60 mm / min with the introduction of the rod into the transfer case. Cast ingots were homogenized (holding for 6 hours at 753–773 K; air cooling), then they were cut into workpieces 750 mm long, turned to $\varnothing$380 mm and, after preheating to 703 K, forgings were

obtained with a force of 1250 tf deformation ξ = 62 % according to the scheme: upsetting the workpiece in a disc coil → forging disc coil on a rod → secondary sedimentation of a rod in a disc coil KP-10-27. The structure was studied on templates cut from an ingot and from a disc coil. Metal contamination by nonmetallic inclusions was estimated from fractures of technological samples (40 × 40 × 120 mm) cut from transverse templates, as a result of which it was found that the least contamination is characteristic of serial ingots – ΣF_{inc}= 10 mm^2, whereas with the introduction of rods containing NP BN, SiC, TaN, this characteristic significantly increases – to 23.5; 24.0 and up to 38 mm^2, which exceeds the requirements of technical documentation. When analyzing the macro-structure of cross-section templates, it was found that ingots cast by serial technology with the introduction of a rod of granules are characterized by a heterogeneous structure: fine grain around the periphery, then a columnar structure (width 50–90 mm) follows, and behind it – fine-grained structure. The introduction of any of the NPs prevents the formation of a columnar structure, and according to the degree of impact, the most effective of them was NP TaN grain refinement 4.1 times as compared to serial ingots (from 0.322 to 0.073 mm^2), then NP SiC – 2.6 times (up to 0.123 mm^2) and NP BN – 2.2 times (up to 0.146 mm^2). Analysis of the microstructure did not reveal any special differences in the internal structure of the grain of serial ingots and ingots of a metal modified by NP. At the same time, in all ingots, close microporosity is observed. The study of macrosections and kinks of templates of forgings made of modified NP alloy showed the presence of non-metallic inclusions (total area ΣF_{inc}, mm^2) and stroke bundles associated with the presence of oxide layers in the metal (total length, mm), respectively, on charges – from 4 up to 9 mm^2 and from 10 to 24 mm, at fractures – from 5 to 6.5 mm^2 and from 18 to 28 mm, which meets the requirements of technical documentation, but at the same time exceeds the number of defects for a serial forging, on the macrosections of which no defects were found, there is a part of fan structure with an area of 25 mm^2; at fractures, the area of nonmetallic inclusions ΣF_{inc} is only 2 mm^2. The mechanical properties of specimens cut from forgings according to the required documentation of the scheme in the fractional, transverse and altitudinal directions turned out to be quite close to the properties of serial forgings, and in some cases even exceeded them, especially the relative elongation. Macrograin forgings made from ingots modified by NPs turned out to be smaller than forgings made from serial ingots and from ingots cast from an alloy into which a bar of granules was introduced. Thus, as a result of the research described above, it was found that as a result of the introduction of various refractory materials into the liquid alloy AMg6, the grain size of the nonmetallic inclusions increases, as well as the number of laminations (in forgings). A possible reason for their existence can be considered the use of modifying rods of granules as a basis, which contribute to the volume of this product a large amount of aluminum oxide Al2O3, which is present

on their surface, and gases, present (hydrogen) on the surface. It should be noted that in all our studies, non-metallic inclusions and delaminations were not observed on the products pressed from ingots cast from alloys modified by various NPs. By the way, this fact does not at all indicate in favor of the absence of non-metallic inclusions (aluminum oxide particles Al_2O_3) in the volume of compacts – their number, both in the original ingots modified by NP, and in the compacts or forgings obtained from them, remains almost the same but in the process of obtaining products from ingots, these oxides are crushed and evenly distributed over the volume of the deformed metal.

Conclusion. As a result of the use of a new type of modifiers – nanopowders of refractory chemical compounds, and the developed method of their introduction into metal melts in the volume of rods pressed from the composition "aluminum particles + nanopowders", the mechanical properties of the products obtained by the pressure treatment of ingots cast with the semicontinuous method from aluminum and aluminum alloys were improved.

References

1. Moskvichev V. V., Krushenko G. G., Burov A. E. et al. *Nanopoproshkovye tekhnologii v mashinostroenii.* [Nanoporoshkov engineering technologies]. Krasnoyarsk, Sibirskiy federal'nyy universitet Publ., 2013, 186 p.

2. Gusev A. I. [Effects of the nanocrystalline state in compact metals and their compounds]. *UFN.* 1998, Vol. 168, No. 1, P. 55–83 (In Russ.).

3. Krushenko G. G. [History, status and prospects of nanotechnology development]. *Nanotekhnika.* 2006, No. 4, P. 16–22 (In Russ.).

4. Rouvray D. H. Is the future nano? *Chemistry in Britain.* 2000, No.12, P. 27–32.

5. Feynman R. P. There's plenty of room at the bottom. *Engineering and Science.* 1960, Vol. 23, No. 2, P. 22–36.

6. Drexler K. E. Molecular engineering:An approach to the development of general capabilities for molecular manipulation. *Proceedings of the National Academy of Sciences.* 1981, Vol. 78, No. 9, P. 5275–5278.

7. Drexler K. E. Engines of Creation: The Coming Era of Nanotechnology. New York, Anchor-Doubleday, 1986, 298 p.

8. Nanotechnology. Integrated Processing Systems for Ultra-Precision and Ultra-Fine Products, Ed. Taniguchi N. Oxford: Oxford University Press, 1996, 406 p.

9. Taniguchi N. On the Basic Concept of NanoTechnology. *Proc. Intern. Conf. Prod. Eng.* Tokyo: Part II, Japan Society of Precision Engineering, 1974. P. 18–23.

10. Visser G. W. Nanotechnology, what is it? Sixth Session. Forum VI, Plenary Session Nanotechnology and manufactured nanomaterials: opportunities and challenges. Le Meridien President, Dakar, Senegal. Available at: http:// lenta.ru/articles/2008/05/16/nano/ (accesed 04.07.2018).

11. Saburov V. P., Cherepanov A. N., Krushenko G. G. et al. *Plazmokhimicheskiy sintez ul'tradispersnykh*

poroshkov i ikh primenenie dlya modifitsirovaniya metallov i splavov [Plasma chemical synthesis of ultrafine powders and their application for modification of metals and alloys]. Novosibirsk, Nauka Publ., 1995, 344 p.

12. Zhukov M. F., Cherskiy I. N., Krushenko G. G. et al. *Uprochnenie metallicheskikh, polimernykh i elastomernykh materialov ul'tradispersnymi poroshkami* plazmokhimicheskogo *sinteza* [Hardening of metal, polymer and elastomeric materials by ultrafine powders of plasma chemical synthesis]. Novosibirsk, Nauka Publ., 1999, 312 p.

13. Moskvichev V. V., Makhutov N. A., Krushenko G. G. et al. *Treshchinostoykost' i mekhanicheskie svoystva konstruktsionnykh materialov tekhnicheskikh system* [Crack resistance and mechanical properties of structural materials of technical systems]. Novosibirsk, Nauka Publ., 2002, 234 p.

14. Krushenko G. G., Musokhranov Yu. M., Yamskikh I. S. et al. *Sposob modifitsirovaniya liteynykh alyuminievykh splavov evtekticheskogo tipa* [Method of modification of casting aluminum alloys of eutectic type]. Patent SU, no. 831840, 1981.

15. Krushenko G. G., Padalka V. A., Ryabinko A. V. et al. [Atlas of casting defects of ingots made of aluminum and aluminum deformable alloys, cast by semi-continuous method]. *Tsvetnaya metallurgiya*. 1998, No. 11–12, P. 42 (In Russ.).

16. Dobatkin V. I. *Slitki alyuminievykh splavov.* [Ingots of aluminum alloys]. Moscow, Metallurgizdat Publ., 1960, 176 p.

17. Goly-Probst A., Sturmer U. Increased caster productivity with the B. O. P. S. breakout prediction system. *Metals, Mining & More*. 2000, No. 3, P. 6.

18. Krushenko G. G., Terekhov V. N., Kuznetsov A. N. [Continuous casting of ingots with the use of molten aluminum and alloys]. *Tsvetnye metally*. 1975, No. 11, P. 49–51 (In Russ.).

19. Ezekiel M., Fox K. A. Methods of correlation and regression. New York: Wiley, 1963. 562 p.

20. Krushenko G. G., Kuznetsov A. N. [Reduction of aluminum ingot scrap on cracks when working on liquid charge]. *Tsvetnye metally*. 1976, No. 5, P. 52–53 (In Russ.).

Библиографические ссылки

1. Нанопопрошковые технологии в машиностроении / В. В. Москвичев, Г. Г. Крушенко, А. Е. Буров [и др.]. Красноярск : Сиб. федер. ун-т, 2013. 186 с.

2. Гусев А. И. Эффекты нанокристаллического состояния в компактных металлах и их соединениях // УФН. 1998. Т. 168, № 1. С. 55–83.

3. Крушенко Г. Г. История, состояние и перспективы развития нанотехнологий // Нанотехника. 2006. № 4. С. 16–22.

4. Rouvray D. H. Is the future nano? // Chemistry in Britain. 2000. № 12. P. 27–32.

5. Feynman R. P. There's plenty of room at the bottom // Engineering and Science. 1960. Vol. 23, No. 2. P. 22–36.

6. Drexler K. E. Molecular engineering:An approach to the development of general capabilities for molecular manipulation // Proceedings of the National Academy of Sciences. 1981. Vol. 78, No. 9. P. 5275–5278.

7. Drexler K. E. Engines of Creation: The Coming Era of Nanotechnology. New York : Anchor-Doubleday, 1986. 298 p.

8. Nanotechnology. Integrated Processing Systems for Ultra-Precision and Ultra-Fine Products / Ed. Taniguchi N. Oxford : Oxford University Press, 1996. 406 p.

9. Taniguchi N. On the Basic Concept of NanoTechnology // Proc. Intern. Conf. Prod. Eng. Tokyo : Part II, Japan Society of Precision Engineering, 1974. P. 18–23.

10. Visser G. W. Nanotechnology, what it? Sixth Session. Forum VI, Plenary Session Nanotechnology and manufactured nanomaterials: opportunities and challenges. Le Meridien President, Dakar, Senegal [Электронный ресурс]. URL: http://lenta.ru/articles/2008/05/16/nano/. (дата обращения 04.07.2018).

11. Плазмохимический синтез ультрадисперсных порошков и их применение для модифицирования металлов и сплавов / В. П. Сабуров, А. Н. Черепанов, Г. Г. Крушенко [и др.]. Новосибирск : Наука, 1995. 344 с.

12. Упрочнение металлических, полимерных и эластомерных материалов ультрадисперсными порошками плазмохимического синтеза / М. Ф. Жуков, И. Н. Черский, Г. Г. Крушенко [и др.]. Новосибирск : Наука, 1999. 312 с.

13. Трещиностойкость и механические свойства конструкционных материалов технических систем / В. В. Москвичев, Н. А. Махутов, Г. Г. Крушенко [и др.]. Новосибирск : Наука, 2002. 234 с.

14. Способ модифицирования литейных алюминиевых сплавов эвтектического типа : а. с. СССР 831840: МПК А1 С22С 1/06 / Крушенко Г. Г., Мусохранов Ю. М., Ямских И. С. и др. Заявка № 2831160 от 17.10.1979, Бюл. 1981. № 19.

15. Атлас литейных дефектов слитков из алюминия и алюминиевых деформируемых сплавов, отливаемых полунепрерывным способом / Г. Г. Крушенко, В. А. Падалка, А. В. Рябинко [и др.] // Цветная металлургия. 1998. № 11–12. С. 42.

16. Добаткин В. И. Слитки алюминиевых сплавов. М. : Металлургиздат, 1960. 176 с.

17. Goly-Probst A., Sturmer U. Increased caster productivity with the B.O.P.S. breakout prediction system // Metals, Mining & More. 2000. № 3. P. 6.

18. Крушенко Г. Г., Терехов В. Н., Кузнецов А. Н. Непрерывное литье слитков с применением жидкого алюминия и лигатур // Цветные металлы. 1975. № 11. С. 49–51.

19. Ezekiel M., Fox K. A. Methods of correlation and regression. New York : Wiley, 1963. 562 p.

20. Крушенко Г. Г., Кузнецов А. Н. Уменьшение брака алюминиевых слитков по трещинам при работе на жидкой шихте // Цветные металлы. 1976. № 5. С. 52–53.

Krushenko Genrikh Gavrilovich – Dr. Sc., Prof., Ch. Researcher, Institute of Computational Modeling SB RAS; Professor, Reshetnev Siberian University of Science and Technology. E-mail: genry@icm.krasn.ru.

Nazarov Vladimir Pavlovich – Ph. D., Professor, Department of Aircraft Engines, Reshetnev Siberian State University of Science and Technologies. E-mail: nazarov@mail.sibsau.ru.

Reshetnikova Svetlana Nikolaevna – Cand. Sc., Head of Methodical study of dissertation councils; Reshetnev Siberian University of Science and Technology. E-mail: ambre2014650@yandex.ru.

Dvirnyy Guriy Valer'yevich – Cand. Sc., Associate Professor of the Department "Mechanical Engineering"; Reshetnev Siberian University of Science and Technology. E-mail: dg1802@mail.ru.

Крушенко Генрих Гаврилович – доктор технических наук, профессор, главный научный сотрудник, Институт вычислительного моделирования СО РАН; профессор кафедры двигателей летательных аппаратов; Сибирский государственный университет науки и технологий имени академика М. Ф. Решетнева. E-mail: genry@icm.krasn.ru.

Назаров Владимир Павлович – кандидат технических наук, профессор, заведующий кафедрой двигателей летательных аппаратов; Сибирский государственный университет науки и технологий имени академика М. Ф. Решетнева. E-mail: nazarov@sibsau.ru.

Решетникова Светлана Николаевна – кандидат технических наук, заведующий методическим кабинетом при диссертационных советах; Сибирский государственный университет науки и технологий имени академика М. Ф. Решетнева. E-mail: ambre2014650@yandex.ru.

Двирный Гурий Валерьевич – кандидат технических наук, доцент кафедры технологии машиностроения; Сибирский государственный университет науки и технологий имени академика М. Ф. Решетнева. E-mail: dg1802@mail.ru.

THE RESEARCH OF THERMOPHYSICAL PROPERTIES OF THE WORKING ENVIRONMENT FOR ABRASIVE-EXTRUSION PROCESSING

E. B. Pshenko[1]*, I. Ya. Shestakov[1], I. A. Remizov[2], T. A. Veretnova[3]

Reshetnev Siberian State University of Science and Technology
31, Krasnoyarsky Rabochy Av., Krasnoyarsk, 660037, Russian Federation
Krasnoyarsk State Medical University behalf of Professor V. F. Voyno-Yasenetsky
1, Partizan Zheleznyaka, Krasnoyarsk, 660022, Russian Federation
Siberian Federal University
79, Svobodny Av., Krasnoyarsk, 660041, Russian Federation
*E-mail: pshenko-64@mail.ru

The most important resource for improving the performance of parts is the reduction of the surface roughness. One of the promising ways to reduce the surface roughness is the abrasive extrusion processing. When developing the AEP technology, it is necessary to know the flow rate (pressure) of the WE, which depends on the viscosity of the latter. In turn, the viscosity of the WE is determined by its temperature. The temperature of the working environment at AEP can be calculated if the coefficients of thermal conductivity and thermal diffusivity of the WE are known. The working environment for AEP consists of two components, therefore, the coefficient of thermal conductivity can be calculated by known formulas. However, the calculation error is significant, therefore, the experimental determination of the above-mentioned coefficients is required. The installations for the coefficients research have been presented, the methods of conducting experiments have been developed. After mathematical processing of the experiments results by means of the AdvanceGrapher v. 2.11, the dependences of the thermal conductivity and thermal diffusivity on the abrasive concentration have been obtained. The studies of the thermophysical properties of the working environment have shown that the values of thermal conductivity and thermal diffusivity of the WE are mainly determined by the concentration of abrasive grains in the working environment. The direct dependence of these coefficients on the degree of filling the working environment with abrasive grains has been established.

Keywords: abrasive extrusion processing, working environment, thermal conductivity and thermal diffusivity coefficients.

ИССЛЕДОВАНИЕ ТЕПЛОФИЗИЧЕСКИХ СВОЙСТВ РАБОЧЕЙ СРЕДЫ ДЛЯ АБРАЗИВНО-ЭКСТРУЗИОННОЙ ОБРАБОТКИ

Е. Б. Пшенко[1]*, И. Я. Шестаков[1], И. А. Ремизов[2], Т. А. Веретнова[3]

[1]Сибирский государственный университет науки и технологии имени академика М. Ф. Решетнева
Российская Федерация, 660037, Красноярск, просп. им. газ. «Красноярский рабочий», 31
[2]Красноярский государственный медицинский университет имени профессора В. Ф. Войно-Ясенецкого
Российская Федерация, 660022, Красноярск, ул. Партизана Железняка, 1
[3]Сибирский федеральный университет
Российская Федерация, 660041, г. Красноярск, просп. Свободный, 79
*E-mail: pshenko-64@mail.ru

Важнейшим ресурсом повышения эксплуатационных характеристик деталей является уменьшение шероховатости поверхности. Одним из перспективных способов снижения шероховатости поверхности является абразивно-экструзионная обработка (АЭО). При разработке технологии АЭО необходимо знать расход (давление) рабочей среды (РС), который зависит от вязкости последней. В свою очередь вязкость РС определяется её температурой. Температуру РС при АОЭ можно рассчитать, зная коэффициенты теплопроводности

и температуропроводности РС. РС при АЭО состоит из двух компонентов, поэтому рассчитать коэффициент теплопроводности можно по известным формулам. Однако погрешность расчётов значительна, поэтому требуется экспериментальное определение вышеупомянутых коэффициентов. Представлены установки для исследования коэффициентов, разработаны методики проведения опытов. После математической обработки результатов экспериментов с помощью программы AdvanceGrapher v. 2.11 получены зависимости коэффициентов теплопроводности и температуропроводности от концентрации абразива. Проведенные исследования теплофизических свойств рабочей среды показали, что величины коэффициентов теплопроводности и температуропроводности РС, в основном, определяются концентрацией абразивных зерен в рабочей среде. Установлена прямая зависимость этих коэффициентов от степени наполнения рабочей среды абразивными зернами.

Ключевые слова: абразивно-экструзионная обработка, рабочая среда, коэффициенты теплопроводности и температуропроводности.

Introduction. Now there exists the whole class of parts containing open and closed channels of a variable cross-section to which surface layer condition the increased design requirements are imposed. These are aircraft parts (low thrust engine nozzles, impellers of turbopump units), high-precision transport parts (nozzles, sprayers), technical equipment parts (stamps, compression molds, matrixes, nozzles of thermoplastic automatic machines), etc.

The most important resource of the increase in production characteristics of parts is the decrease of roughness of a surface and ensuring parallelism of its direction along the flow of components as well as the removal of tensile and compressive stresses.

The practice of finishing processing showed that the most productive and effective for the formation of the surface layer (SL) of figurine channels is the abrasive-extrusion processing (AEP) which consists in the movement (remolding) of viscoelastic, filled with the abrasive grains (AG) working environment (WE) under the pressure 5–12 MPa along the processed channel surface [1–5].

When developing the AEP technology it is necessary to know the flow rate (pressure) of the WE which depends on the viscosity of the latter [6; 7]. The viscosity of the WE in turn is defined by its temperature. The WE temperature at AEP can be calculated knowing thermal conductivity and thermal diffusivity coefficients of the WE. The working environment at AEP consists of two components, therefore it is possible to calculate a thermal conductivity coefficient by Odelevsky's [8], Misnara's [9], Burger's [10] formulas. The authors [11] consider that Odelevsky's formula is the most universal. The researchers of heat conductivity of composites offer a simple formula for the coefficient calculation, the method of "inversion" [12].

It has been established [13] that the thermal conductivity coefficient significantly depends on the concentration of abrasive and slightly depends on other factors.

Research method and equipment. The experimental determination of a thermal conductivity coefficient of the WE was carried out by means of the flat layer method [14] on the installation (fig. 1). The working environment contained a viscoelastic component (high-molecular silicone rubber) and abrasive grains (silicon carbide black of graininess 100 or alundum white of graininess 50). During the experiments the content of abrasive grains was changing from 10 to 80 % (on volume basis) with a 15 % interval.

The working environment 3 in the form of the disk with $\delta = 1 \cdot 10^{-2}$ m thickness is located between the heater 1 and the fridge 5. The insulating ring containing the additional security heater 4, which provides one-dimensionality of the heat flux, is located outside. For the same purpose the ratio δ/D (D – the disk diameter equal to $16 \cdot 10^{-2}$ m) has been chosen small. To measure the temperature difference the thermocouples 2 were used.

It is known that at a one-dimensional heat flux through the flat layer the thermal conductivity is calculated

$$\lambda = Q_{\text{т}}\delta / F \cdot (T_1 - T_2)], \qquad (1)$$

where $Q_{\text{т}}$ – the heat flux of the heater; δ – the sample thickness; F – the surface area; T_1 and T_2 – the temperatures of "hot" and "cold" sample surfaces (working environment).

Therefore for thermal conductivity research by this method the heat flux close to one-dimensional one through the layer of the working environment under study was created and measured and the temperature difference between layer borders was measured as well.

As the temperatures were measured not on sample surfaces, but at some distance from them inside the heater and the fridge, then the temperature differential corrections in the heater layer ΔT_1 and the fridge ΔT_2 were made to the measured temperature difference ΔT_{meas} The corrections are determined by formulas:

$$\Delta T_1 = Q_{\text{т}}\delta_1 / (F \cdot \lambda_1); \qquad (2)$$

$$\Delta T_2 = Q_{\text{т}}\delta_2 / (F \cdot \lambda_2), \qquad (3)$$

where δ_1 and $\delta_2 = 2 \cdot 10^{-3}$ м – distances from a thermocouple junction to the sample surface in the heater and the fridge respectively; λ_1 and λ_2 – thermal conductivity of heater and fridge materials (for steel 12X18H10T $\lambda_1 = \lambda_2 = 15.2$ W/m $\cdot$ K).

Taking into account these corrections the calculation formula is:

$$\lambda = \frac{Q_{T^\delta}}{F\left[\Delta T_{ism} - \dfrac{Q_T}{F}\left(\dfrac{\delta_1}{\lambda_1} + \dfrac{\delta_2}{\lambda_2}\right)\right]}. \qquad (4)$$

The graph of the dependence of the thermal conductivity coefficient on the concentration of abrasive is presented in fig. 2.

After the experiments results mathematical processing by means of the Advance Grapher v. 2.11 the dependences of thermal conductivity coefficients on concentration of abrasive have been received for alundum white:

$$\lambda_{ek} = -0.046 - 0.045 \cdot Ka + 0.008 \cdot Ka^2 - 5.6 \cdot 10^{-5} Ka^3; \quad (5)$$

for silicon carbide black:

$$\lambda_{\text{кк}} = -0.322 - 0.016 \cdot Ka + 0.013 \cdot Ka^2 - 8.56 \cdot 10^{-5} Ka^3. \quad (6)$$

Except for the abrasive concentration as the factors of variation the grain size (Ba) – the abrasive graininess in the range of 25–100 microns and T_{slave} – the temperature of the working environment in the range of 20–60 ^{0}C were studied.
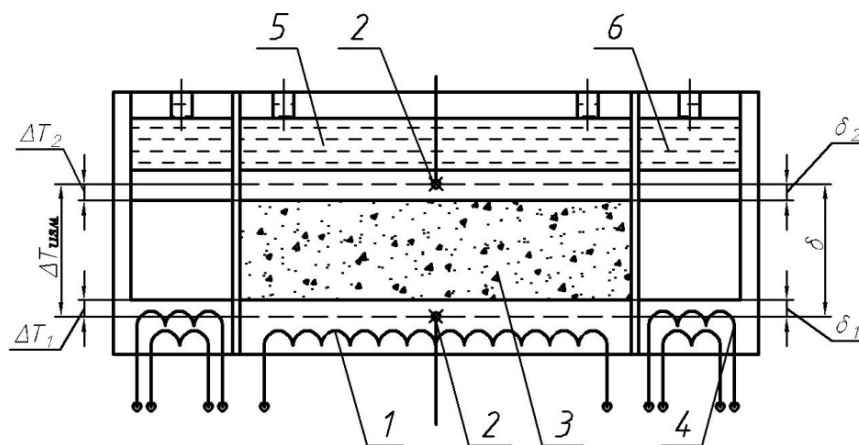

Fig. 1. Installation diagram for determining the coefficient of thermal conductivity
by the method of a flat layer:
1 – heater; *2* – thermocouples; *3* – sample under test (working environment);
4 – security heater; *5* – fridge; *6* – fridge security ring

Рис. 1. Схема установки для определения коэффициента теплопроводности
методом плоского слоя:
1 – нагреватель; *2* – термопары; *3* – исследуемый образец (рабочая среда); *4* – охранный
нагреватель; *5* – холодильник; *6* – охранное кольцо холодильника
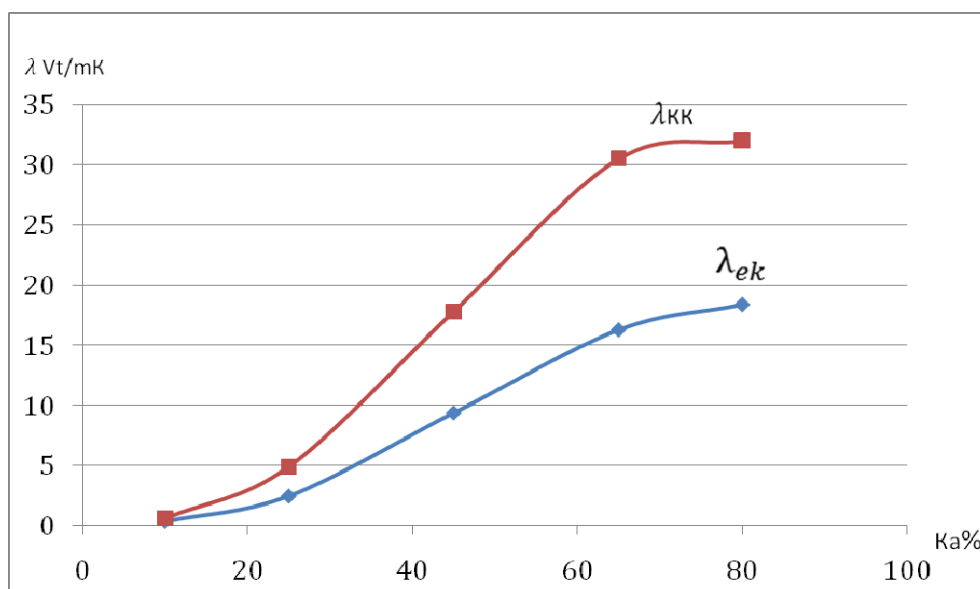

Fig. 2. Dependence of the coefficient of thermal conductivity of the working environment
on the concentration of abrasive

Рис. 2. Зависимость коэффициента теплопроводности рабочей среды
от концентрации абразива

As a result of the experiments it has been established that the thermal conductivity coefficient of the WE in the specified interval of change of abrasive graininess and temperature changes no more than by 3 %. Therefore these factors can not be considered when developing technological processes of AEP.

Calculation results of the thermal conductivity coefficient of working environments by Odelevsky's, Misnara's formulas give the error of the required value determination in the comparison with the experimental one more than 60 %, by the inversion method the error makes 20–45 % in the specified range of abrasive concentration research. Such inaccuracy of thermal conductivity determination coefficient is unacceptable at projection of AEP technology.

The formulas for calculation of thermal diffusivity of composites have not been found now, therefore this parameter was defined experimentally.

To determine the thermal diffusivity coefficient of the working environment the method based on the measurement of the heating rate and time lag of the maximum (minimum) temperature on the free surface of a sample relative to the moment of switching on (switching off) the input into the sample power was used [15].

The working environment limited by a metal cylinder with the height of 11 mm and the diameter of 160 mm was used as a sample. The experiments were carried out on the installation (fig. 3). The installation consists of the heating element 1 with 100 W power on which the sample – the working environment 2 in the cylinder 3 was located. The measurement of temperatures was performed by means of thermocouples 4 in three different points which are located at the free surface of the sample on the depth of 1 mm. The thermocouples were located on one circular axis with the 20 mm diameter located concentrically relatively the center of the sample cylinder. The operation of the heating element was controlled by means of the thermocouple 5. Fixing of measurement results was carried out via the analag-to-digital converter 6 to the personal computer 7 on the virtual digital oscillograph.

The measurements were carried out in intervals 20–60 °C that is the operating temperature at AEP. The data received from three thermocouples were averaged to decrease a random error of measurement due to possible heterogeneity of a working environment structure. The graphs of change of the input electric power and temperature are provided on the oscillogram (fig. 4)

The thermal diffusivity coefficient of samples was calculated by formula:

$$\alpha = \delta^2 / (\Delta t - K) \cdot \sigma, \tag{7}$$

where δ – the thickness of the studied sample, 0.01 m; Δt – the time which passed between switching on (switching off) the power of the heater and the achievement of a maximum (minimum) temperature on the sample surface, c; K – the time constant of the measurement circuit defined on the model, 0.5 c: σ – the dimensionless coefficient depending on the input power in our installation $\sigma = 8 \cdot 10^{-4}$.

After the mathematical processing of experiments results by means of the AdvanceGrapher v. 2.11 the dependences of thermal diffusivity coefficients on the abrasive concentration have been received for alundum white:

$$\alpha_{\text{ек}} = -6.3 \cdot 10^{-5} + 9.09 \cdot 10^{-6}\text{Ka} +$$
$$+ 1.14 \cdot 10^{-6}\text{Ka}^2 - 6.75 \cdot 10^{-9}\text{Ka}^3; \tag{8}$$

for silicon carbide black:

$$\alpha_{\text{кк}} = -3.02 \cdot 10^{-4} + 5.09 \cdot 10^{-5}\text{Ka} +$$
$$+ 1.3 \cdot 10^{-6}\text{Ka}^2 - 2.94 \cdot 10^{-9}\text{Ka}^3. \tag{9}$$

The dependence of a thermal diffusivity coefficient of the working environment on the abrasive concentration is presented in fig. 5.
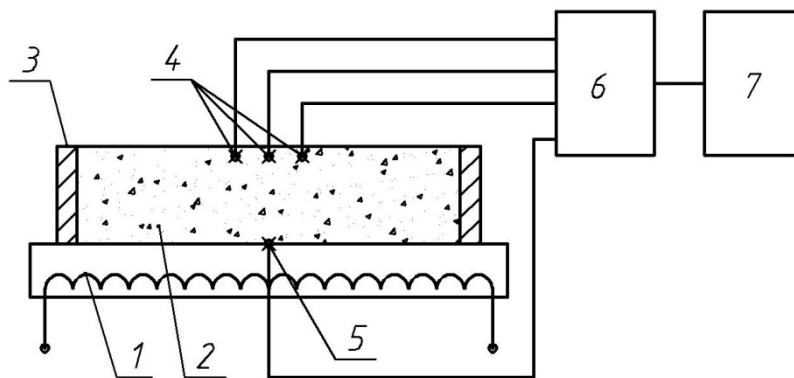

Fig. 3. Installation diagram for determining the coefficient of temperature and conductivity:
1 – heater; *2* – sample under test (working medium); *3* – cylinder; *4* – termocouple;
5 – control thermocouple; *6* – analog-to-digital converter; *7* – personal computer

Рис. 3. Схема установки для определения коэффициента температуропроводности:
1 – нагреватель; *2* – исследуемый образец (рабочая среда); *3* – цилиндр;
4 – термопары; *5* – контрольная термопара; *6* – аналагово-цифровой
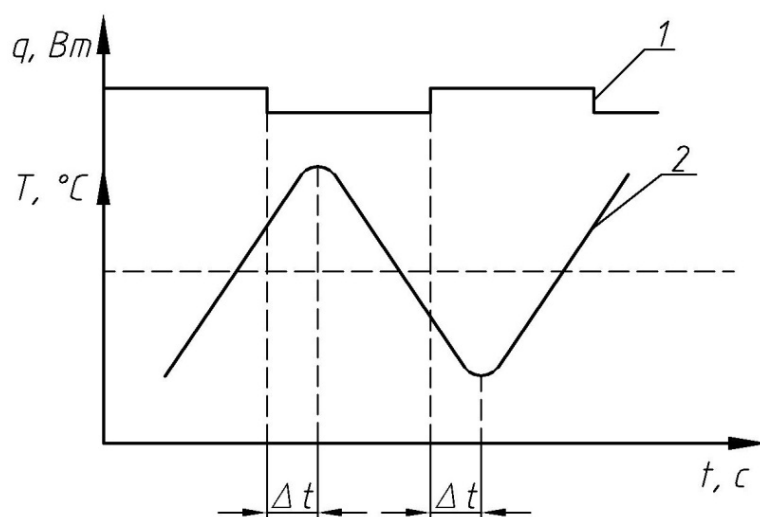преобразователь; *7* – персональный компьютер

Fig. 4. Oscillograms of power and temperature:
1 – graph of changes in input power; *2* – graph of temperature changes
on the free surface of the sample; Δ*t* – measured time lag of the maximum
(minimum) temperature, s

Рис. 4. Осциллограмма мощности и температуры:
1 – график изменения вводимой мощности; *2* – график изменения
температуры на свободной поверхности образца; Δ*t* – измеряемое
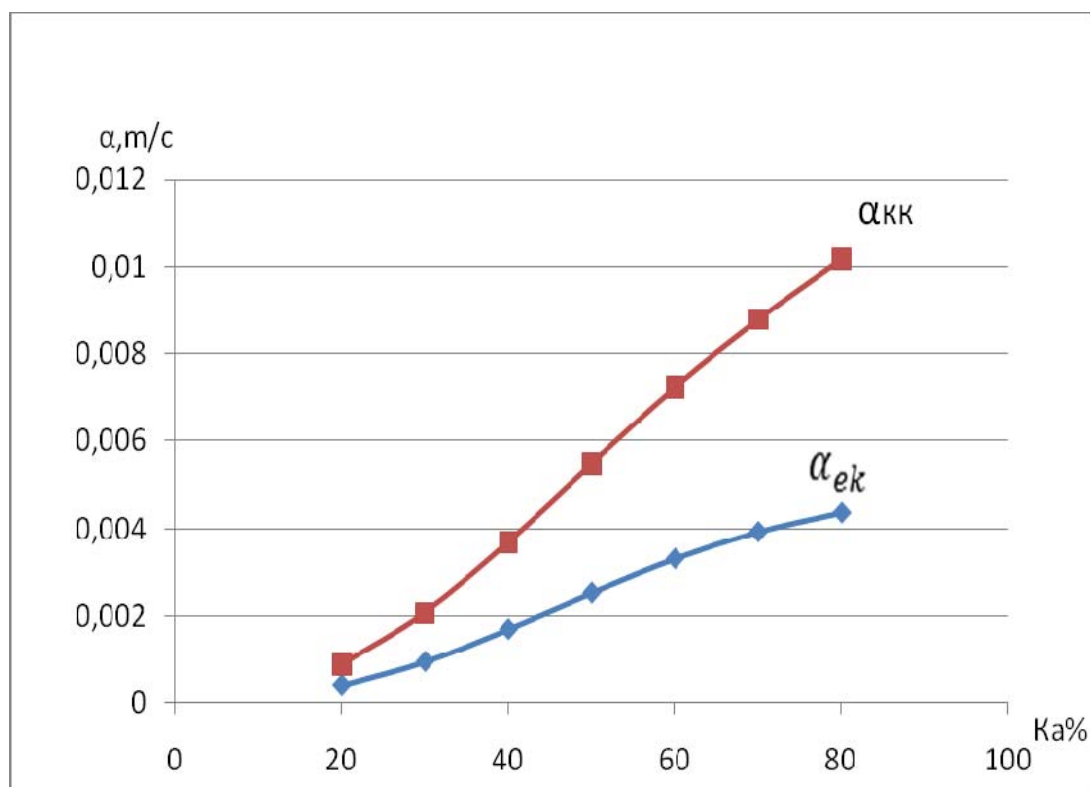временное запаздывание максимума (минимума) температуры, с

Fig. 5. Dependence of the thermal diffusivity of the working environment
on the abrasive concentration

Рис. 5. Зависимость температуропроводности рабочей среды от концентрации абразива

281

Similarly to the thermal conductivity coefficient, the grain size (Ba) – the abrasive graininess in the range of 25–100 microns and T_{slave} – the temperature of the working environment in the range of 20–60 °C were studied as the factors of variation for thermal diffusivity.

As a result of the experiments it has been established that thermal diffusivity insignificantly depends on the operating temperatures, the abrasive values and other factors not bound to the structure of the WE. In this connection, these factors were excluded from consideration.

Conclusion. The conducted research of thermal properties of the working environment have shown that the values of thermal conductivity and thermal diffusivity of the WE are generally defined by the concentration of abrasive grains in the working environment. The direct dependence of these coefficients on the degree of filling the working environment with abrasive grains has been established

References

1. Pshenko E. B., Narushevich D. A., Struzik E. S. [Study of the effect of processing temperature on the process of abrasive-extrusion honing]. *Reshetnevskie chteniya: Materialy IX Mezhdunarodnoy nauchnoy konferentsii* [Reshetnev Readings. Proceedings of the IXth International Scientific Conference]. Krasnoyarsk, SibSAU, 2005, P. 166–167 (In Russ.).

2. Pshenko E. B. [Development of methods for determining the calorimetric properties of the working environment during abrasive-extrusion honing]. *Reshetnevskie chteniya: Materialy IX Mezhdunarodnoy nauchnoy konferentsii* [Reshetnev Readings: Proceedings of the XI International Scientific Conference]. Krasnoyarsk, SibSAU, 2007, P. 198–199 (In Russ.).

3. Levko V. A., Lubnin M. A., Snetkov P. A., Pshenko E. B., Turilov D. M. Research the influence finishing canal shape to flow media for abrasive flow machining process. *Vestnik SibGAU.* 2009, No. 5 (26), P. 93–99 (In Russ.).

4. [Nonlinear Finite Element Analysis of Elastomers] (In Russ.). Available at: http://www.mscsoftware.ru/products/marc (accessed: 10.09.2016).

5. Snetkov P. A., Levko V. A., Pshenko E. B., Lubnin M. A. [Experimental determination factor to viscosity, elasticity and plasticity media for abrasive flowmachining process]. *Vestnik SibGAU.* 2009, No. 5 (26), P. 99–103 (In Russ.).

6. Dulnev G. N., ZarichnyakYu. P. *Teploprovodnost' smesey I kompozitsionnykh materialov* [Thermal conductivity of mixtures and composite materials]. Leningrad, Energiya Publ., 1974, 230 p. (In Russ.).

7. Mysnar A. *Teploprovodnost' tverdykhtel, zhidkostey, gazoviikhkompozitsiy* [Thermal conductivity of solids, liquids, gases and their compositions]. Moscow, Mir Publ., 1968, 221 p. (In Russ.).

8. Chudnovsky A. F. *Teplofizicheskie kharakteristiki dispersnykh materialov* [Thermophysical characteristics of dispersed materials]. Moscow, Fizmatgiz Publ., 1962, 340 p. (In Russ.).

9. Kirillov V. N., Efimov V. A., Donskoy A. A. [Thermal conductivity of the systems silicone-organic elastomer-powdered mineral filler]. *IFZH.* Vol. XXIII, No. 3, 1972, 400 p. (In Russ.).

10. Mikheev V. A., Sulaberidze V. Sh., Mushenko V. D. [The study of thermal conductivity of composite materials based on silicone with fillers]. *News of universities. Instrument making.* 2015, Vol. 58, No. 7, P. 571–575 (In Russ.).

11. Liang Fang, Jia Zhao, Kun Sun, Degang Zheng, Dexin Ma Temperature as sensitive monitor for efficiency of work in abrasive flow machining. *Wear.* 2009, Vol. 266, Iss. 7–8. P. 678–678.

12. Uhlmann E., Schmiedel C., Wendler J. Simulation of the Abrasive Flow Machining. Process CFD (Computational fluid dynamics). *Procedia CIRP.* 2015, Vol. 31, P. 209–214. 15th CIRP Conference on Modelling of Machining Operations (15th CMMO).

13. Levko V. A. *Nauchnye osnovy abrazivno-ekstruzionnoy obrabotki detaley* [Scientific bases abrasive extrusion machining parts]. Krasnoyarsk, SibSAU Publ., 2015, 222 p.

14. Sysoev S. K., Sysoev A. S. *Ekstruzionnoe khoningovanie detaley letatel'nykh apparatov; teoriya, issledovaniya, praktika* [Extrusion honing of aircraft parts; theory, research, practice]. Krasnoyarsk, SibSAU Publ., 2005, 220 p.

15. Levko V. A. [Features of the rheology of the working environment for abrasive extrusion processing]. *Vestnik SibGAU.* 2005, No. 7, P. 96–100 (In Russ.).

16. Levko V. A. [Abrasive extrusion processing. The modern level, problems and directions of development]. *Izvestiya Tomskogo politekhnicheskogo universiteta.* 2006, Vol. 309, No. 6, P. 125–129 (In Russ.).

Библиографические ссылки

1. Пшенко Е. Б., Нарушевич Д. А., Струзик Е. С. Исследование влияния температуры обработки на процесс абразивно-экструзионного хонингования // Решетневские чтения : материалы IX Междунар. науч. конф. Красноярск : СибГАУ, 2005. С. 166–167.

2. Пшенко Е. Б. Разработка методики определения калориметрических свойств рабочей среды при абразивно-экструзионном хонинговании // Решетневские чтения : материалы XI Междунар. науч. конф. Красноярск : СибГАУ, 2007. С. 198–199.

3. Research the influence finishing canal shape to flow media for abrasive flow machining process / V. A. Levko, M. A. Lubnin, P. A. Snetkov [et al.] // Вестник СибГАУ. 2009. № 5 (26). С. 93–99.

4. Nonlinear Finite Element Analysis of Elastomers [Электронный ресурс]. URL: http://www.mscsoftware.ru/products/marc (дата обращения 10.09.2016).

5. Experimental determination factor to viscosity,elasticity and plasticity media for abrasiveflow machining process / P. A. Snetkov, V. A. Levko, E. В. Pshenko, M. A. Lubnin // Вестник СибГАУ. 2009. № 5 (26). С. 99–103.

6. Дульнев Г. Н., Заричняк Ю. П. Теплопроводность смесей и композиционных материалов. Л. : Энергия, 1974. 230 с.

7. Миснар А. Теплопроводность твёрдых тел, жидкостей, газов и их композиций. М. : Мир, 1968. 221 с.

8. Чудновский А. Ф. Теплофизические характеристики дисперсных материалов. М. : Физматгиз, 1962. 340 с.

9. Кириллов В. Н., Ефимов В. А., Донской А. А. Теплопроводность систем кремнийорганический эластомер-порошкообразный минеральный наполнитель // ИФЖ. Т. XXIII, № 3. 1972. 400 с.

10. Михеев В. А., Сулаберидзе В. Ш., Мушенко В. Д. Исследование теплопроводности композиционных материалов на основе силикона с наполнителями // Известия вузов. Приборостроение. 2015. Т. 58, № 7. С. 571–575.

11. Liang Fang, Jia Zhao, Kun Sun, Degang Zheng, Dexin Ma. Temperature as sensitive monitor for efficiency of work in abrasive flow machining // Wear. 2009. Vol. 266, Iss. 7–8. P. 678–678.

12. Uhimann E., Schmiedel C., Wendler J. CFD (Computational fluid dynamics) Simulation of the Abrasive Flow Machining Process Procedia // CIRP. 2015. Vol. 31. P. 209–214.

13. Левко В. А. Научные основы абразивно-экструзионной обработки деталей : монография / Сиб. гос. аэрокосмич. ун-т. Красноярск, 2015. 222 с.

14. Сысоев С. К., Сысоев А. С. Экструзионное хонингование деталей летательных аппаратов; теория, исследования, практика : монография / Сиб. гос. аэрокосмич. ун-т. Красноярск, 2005. 220 с.

15. Левко В. А. Особенности реологии рабочей среды при абразивно-экструзионной обработке // Вестник СибГАУ. 2005. № 7. С. 96–100.

16. Левко В. А. Абразивно-экструзионная обработка. Современный уровень, проблемы и направления развития // Известия Томского политехн. ун-та. 2006. Т. 309. С. 125–129.

Pshenko Elena Borisovna – Cand. Sc., Associate Professor at the Department of Mechanical Engineering Technology; Reshetnev Siberian State University of Science and Technology. E-mail: pshenko-64@mail.ru.

Shestakov Ivan Yakovlevich – Dr. Sc., Associate Professor, Professor, Reshetnev Siberian State University of Science and Technology. E-mail: yakovlevish@mail.ru.

Remizov Igor Anatolyevich – Cand. Sc., Associate Professor, Krasnoyarsk State Medical University named after professor V. F. Voyno-Yasenetsky.

Veretnova Tatyana Anatolyevna– Cand. Sc., Head of the correspondence department; Siberian Federal University.

Пшенко Елена Борисовна – кандидат технических наук, доцент кафедры технологии машиностроения; Сибирский государственный университет науки и технологий имени академика М. Ф. Решетнёва. E-mail: pshenko-64@mail.ru.

Шестаков Иван Яковлевич – доктор технических наук, профессор, доцент; Сибирский государственный университет науки и технологий имени академика М. Ф. Решетнёва. E-mail: yakovlevish@mail.ru.

Ремизов Игорь Анатольевич – кандидат физико-математических наук, доцент; Красноярский государственный медицинский университет имени профессора В. Ф. Войно-Ясенецкого.

Веретнова Татьяна Анатольевна – кандидат технических наук, начальник заочного отделения; Сибирский федеральный университет.

MATHEMATICAL MODEL OF A LINEAR ELECTRODYNAMIC ENGINE OPERATION ON IMPACT WITH ACCOUNT FOR ELASTIC DEFORMATION OF THE HARDENED SURFACE

N. A. Shvaleva[*], A. A. Fadeev, T. T. Eresko

Reshetnev Siberian State University of Science and Technology
31, Krasnoyarsky Rabochy Av., Krasnoyarsk, 660037, Russian Federation
* E-mail: natalyashvaleva@ya.ru

Operational characteristics of contacting elements of cars and mechanisms are by far defined by a layer quality indicators at the surfaces of contact. One of the ways of increasing details durability, including missile and space equipment details, is the superficial plastic deformation (SPD). In the article aspects of dynamic ways of hardening from the position of the wave theory of blow are considered.

The construction of a shock stand on the basis of a linear electrodynamic drive with a size of 60 mm, operating in a shock-pulse mode, as well as a well-known mathematical model of the workflow – the movement of the armature with the tool at the moment of striking the surface. This model does not fully describe the operation process since the mass of the striker taken into account equaled 1 kg, which does not characterize the process of the impact tool, the purpose of which is the object deformation (for example, work hardening with the aim of surface material sealing or breakdown of the hole in it, or applying license plates markers).

The mathematical model that describes the movement of the armature with the tool, taking into account the elastic deformation of the hardened surface was obtained. In the course of the performed calculation, the magnitude of the elastic deformation of the hardened surface was calculated from the dynamic component of the force impulse applied to it through the indenter (the tip of the impact tool).

The layout of the shock stand with the equipment used, are offered. Experiments on the signal recording with various arrangements of piezoelectric transducers on the anvil – the hardened surface (diagrams of the sensors location are given) were carried out.

Keywords: blow, mathematical model, elastic deformation, contact spot, linear electrodynamic engine, counter-body, indenter.

МАТЕМАТИЧЕСКАЯ МОДЕЛЬ РАБОТЫ ЛИНЕЙНОГО ЭЛЕКТРОДИНАМИЧЕСКОГО ДВИГАТЕЛЯ ПРИ УДАРЕ С УЧЕТОМ УПРУГОЙ ДЕФОРМАЦИИ УПРОЧНЯЕМОЙ ПОВЕРХНОСТИ

Н. А. Швалева[*], А. А. Фадеев, Т. Т. Ереско

Сибирский государственный университет науки и технологий имени академика М. Ф. Решетнева
Российская Федерация, 660037, г. Красноярск, просп. им. газ. «Красноярский рабочий», 31
* E-mail: natalyashvaleva@ya.ru

Эксплуатационные характеристики контактирующих элементов машин и механизмов в значительной степени определяются показателями качества слоя у поверхностей контакта. Одним из способов повышения прочности деталей, в том числе деталей ракетно-космической техники, является поверхностное пластическое деформирование (ППД). В статье рассмотрены аспекты динамических способов упрочнения с позиции волновой теории удара.

Представлена конструкция ударного стенда на базе линейного электродинамического привода с типоразмером 60 мм, работающего в ударно-импульсном режиме, а также известная математическая модель рабочего процесса – движения якоря с инструментом в момент удара бойка о поверхность. Данная модель в полной мере не описывает процесс работы, так как масса бойка учитывалась равной 1 кг, что не характеризует процесс работы ударного инструмента, целью которого является деформация объекта (например, наклеп с целью поверхностного уплотнения материала или пробой отверстия в нем, или нанесение номерных маркеров).

Получена математическая модель, которая описывает движение якоря с инструментом с учетом упругой деформации упрочняемой поверхности. В ходе выполненного расчета вычислена величина упругой деформации упрочняемой поверхности по динамической составляющей силового импульса, прикладываемого к нему через индентор (наконечник ударного инструмента).

Представлена схема ударного стенда, используемое оборудование. Были проведены эксперименты по регистрации сигнала с различным расположением пьезодатчиков на наковальне – упрочняемой поверхности (схемы расположения датчиков приведены). Выполнено сравнение расчетных данных по показаниям осциллографа с теоретическими данными математической модели, где выявлено расхождение и объяснены возможные факторы его возникновения. Несмотря на расхождения и недостатки, расчеты и проведенный опыт указывают на наличие упругой деформации, а значит, ударная установка может найти применение при обработке поверхностно – пластическим деформированием ударными способами рабочих поверхностей деталей, в том числе деталей ракетно-космической техники.

Ключевые слова: удар, математическая модель, упругая деформация, пятно контакта, линейный электродинамический двигатель, контр-тело, индентор.

Introduction. Currently in order to increase durability of car details, including missile and space equipment details, dynamic ways of superficial plastic deformation (SPD) are widely applied with shock deformation impact on the processed surface in conditions of faltering contact, ensuring the most effective way of enhancing operational properties of car details, improving fatigue durability and hardness of a detail surface under the influence of impact load [1]. Stamping is one of the examples of dynamic SPD.

It is known that one of the main characteristics of dynamic loading efficiency under SPD is the share of energy of blow used for elasto-plastic deformation of the processed material in a deformation zone. According to the wave theory the blow is considered as a form of flat acoustic waves extending on the collided bodies and having the period, amplitude and duration. The period of such a wave is called a shock impulse, the form of which represents the change of amplitude in time. The form of an impulse defines efficiency of dynamic loading [2].

Therefore, in the research of bodies' interaction, dynamic contact tasks including those connected with shock impact are the most interesting and challenging. For a more detailed description of shock interaction nature (especially relevant in engineering practice) the rheological model needs to solve not only contact problems, but also to consider the wave phenomena [3; 4].

In mechanical engineering for SPD implementation via dynamic methods devices with mechanical or pneumatic drive have found broad application. Also, linear electric drives of shock action due to high specific energy of blow and speed have been widely adopted [5; 6]. For example, for stamping and sealing devices [7; 8] have been used.

Construction of a shock stand on the basis of a linear electrodynamic drive. The design of the shock stand on the basis of the linear electrodynamic drive (LEDD) operating in the shock – pulse mode is known to have been developed by the SIBGAU team [9]. The design and the analytical model of the electrodynamic engine is given in the work [10]. For this stand there is an equation describing the movement of the armature with the tool at the moment of striking the surface [11] developed on the basis of a process functioning algorithm [12] and a design technique of a linear engine [13].

Description of mathematical model of shock process. The equation describing the movement of an armature with the tool taking into account elastic deformation of material [14] is known. In this equation weight of the striker m_b equaled 1 kg. For further calculations for mathematical model of shock process and pilot study to compare the size of elastic deformation of the hardened surface, received as a result of mathematical modeling and during the experiment, it is required to specify the striker weight and parameters of shock process. In the right member of equation the first member characterizes the total dynamic effort arising under speed change of an armature with the tool. The second member of the equation characterizes the static effort developed by an armature engine winding. The third member of the equation is defined by the size of required elastic deformation ($\alpha_{y\text{-}n}$) of the processed material and properties of materials couple (k) "striker – surface" [15].

The research objective is to determine technical specifications of LEDD with a standard size 60 mm (marking 2L60L) and also to determine the extent of elastic deformation of the hardened surface by means of the obtained mathematical model of the impact device operation, and to further compare the rated value of elastic deformation of the hardened surface with the results of the pilot study.

For the description of shock impulse formation, generated in the system: striker – the processed surface in the deformation center, we will enter the following marking: P_u – amplitude impulse stage passing to the processed metal, H; $a_{1.2}$ – the speed of shock wave distribution in the striker and a wave guide respectively, m/s; $\rho_{1.2}$ – material density respectively the strike and a wave guide, kg/m³; $E_{1.2}$ – the elasticity module of material respectively the striker and the wave guide, Pa; $F_{1.2}$ – striker and a wave guide cross-sectional area, in this case we accept equal values; k – resistance factor to introduction.

Let's assume that the shock impulse of irregular shape P_u, having reached the processed surface, is distributed on the passing P_k and the reflected P_o approaches the deformation zone via the tool (striker). The passing impulse forms a dynamic component of the deformation force [15].

$$P_u = P_k + P_o,$$

where

$$P_k = P_u(1 + \psi); \ P_o = P_u\psi; \ P_u = q\frac{C_1 v}{2},$$

where C_1 – striker acoustic rigidity; C_2 – wave guide acoustic rigidity, their relation is determined by formulas:

$$r = C_1 / C_2; \quad C_{1,2} = \rho_{1,2} \cdot a_{1,2} \cdot F_{1,2}.$$

For loading of metals when hardening SPD it is required to consider interaction of the deformation wave with the border under which material properties and the specified radius of curvature are considered by resistance factor to introduction of $k = (2.4...7.5)\ 10^8$ H/m. Coefficients of reflection and deformation wave passing to the loaded surface are defined:

$$\psi = 1 - 2\Delta; \quad \Delta = \exp(-bat),$$

where $b = k/(E_1/F_1)$.

At various acoustic striker and a wave guide hardness, through their contacting border a part of energy from the deformation wave passes. The wave reflected from the border possesses the other left energy. Change of force in the deformation wave as it passes through the border of arms' zones can be characterized by passing and reflection factors.

Expression for determination of passing the q factor, a direct wave of deformation is written as:

$$q = \frac{2}{1+r}.$$

In relation to this case, strikers and a wave guide have the identical cross-sectional area and material, therefore, $\rho_1 = \rho_2$; $a_1 = a_2$; $r = F_1/F_2$.

In the work [16] the dependences confirmed experimentally for calculation of deformation of the hardened material are established. The dependence for elastic deformation is written as:

$$\alpha_y = \frac{\alpha_o}{\sqrt[3]{1 + \dfrac{2h}{\alpha_y}}},$$

where h – residual approximation which is equal to the depth of the reconstructed print, m; α_y – elastic approximation disappearing with the removal of loading caused by elastic reconstruction of the indentor and counterbody, m; α_o – approximation of the tool to the loaded surface at purely elastic power contact (the Hertz formula), m.

These values are found by formulas:

$$h = \frac{P_u}{2\pi R_{pr} H D n_D};$$

$$\alpha_o = \sqrt[3]{\frac{9\pi^2}{16} \cdot \frac{(k_i + k_m)^2 P^2}{R_{pr}}};$$

$$\alpha_y = \frac{\alpha_o}{\sqrt[3]{1 + 2h/\alpha_y}},$$

where R_{pr} – is the specified curvature radius, in relation to this case – infinitely big, m; HD – the plastic hardness of the processed metal, MPa; n_D – dynamic coefficient of plastic hardness where

$$n_D = 0.5 \left(1 - 137\frac{v}{HD} + \sqrt{1 + 2250\frac{v}{HD}} \right);$$

v – striker's speed, m/s; k_i, k_m – elastic constants of the respective indentor and processed metal, 1/MPa.

$$k_i = \frac{1 - \mu_i^2}{\pi E_i}, \quad k_m = \frac{1 - \mu_m^2}{\pi E_m},$$

where E_i, E_m – elasticity module according to indenter and the processed metal, MPa; μ_i, μ_m – Poisson's ratio according to the indenter and the processed metal.

Results of mathematical modeling. During the transformation process the mathematical model (1) which describes operation of the stand based on the linear electrodynamic drive of a standard size 60 mm (mark 2L60L) with regard to elastic deformation of the hardened surface was received .

$$\frac{d^2 x_b}{dt^2} = \left(\frac{z^2 B_z^2}{m_b R_{ya.A}} - \frac{k_D}{m_b} \right) \cdot \frac{dx}{dt} \cdot \left(1 - e^{-\frac{t}{T_m}} \right) +$$
$$+ \frac{z B_z I_{ya}}{m_b} - \left(k \cdot \frac{\alpha_o}{\sqrt[3]{1 + \dfrac{2h}{\alpha_y}}} \right) / m_b, \tag{1}$$

where x_b – striker removal, m; m_b – striker mass, kg; z – anchor design parameter; B_z – magnetic induction in the clearance gap, T; $R_{ya \cdot A}$ – active resistance of the anchor coil, Ohm; k_D – damping factor, H·s/m; t – dispersal time, s; T_m – dispersal time constant, s; I_{ya} – current in the anchor winding, A; k – resistance factor to striker introduction, H/m; α_o – approximation of the tool with the loaded surface at purely elastic power contact, m.

In the process of calculation the size of elastic dynamic deformation amounted to $5.158 \cdot 10^{-9}$. Provided that the tool speed (striker) (according to data sheet) – $v = 4.5$ m/s; full amplitude of shock impulse – $P_u = 13.5$ H; residual approximation $h = 4.892 \cdot 10^{-13}$ m; approximation of the tool and the loaded surface at purely elastic power contact $\alpha_o = 7.291 \cdot 10^{-7}$ m; material of the processed surface – steel 45, striker material – quenched steel 40X.

A specified mathematical model allows to estimate characteristics of linear electrodynamic engine with a standard size of 60 mm operating in shock-pulse mode at the time when the striker hits the hardened surface and also to determine the size of elastic deformation of the hardened surface.

Experiment procedure. The stand is designed on the basis of the linear electrodynamic drive (fig. 1).

The stand consists of the following elements: linear electric motor *1* with a percussion instrument (striker) *3* fixed on the bed with an anvil *4* (with the anvil rigidly fixed on support *6*). Piezoelectric sensors *5* are fixed onto the anvil (hardened surface). Signals from the sensors arrive at the recording device *7* (oscillograph and/or personal computer). The linear engine power is supplied by power supply *2*.

The stand operation: when supplying back feed from the power supply *2* to linear electric motor *1* (the reverse mode) the anchor ejects with the tool (striker) *3* from the inductor's clearance gap and impacts the anvil *4*, equipped with piezoelectric sensors *5*, signal from which is recorded with oscillograph *7*.

Measurement of elastic deformation is done by means of: piezoelectric sensors, ADS-2071MV oscillograph, oscillographic probe.

Experiments on signal recording with various arrangements of piezoelectric sensor on the anvil (counterbody) were made.

Signal recording was done with oscillograph, the signal was transmitted via the probe with attenuation factor 1 : 10.

Sensor layouts are shown in fig. 2. On diagram No. 1 sensors are located on the outer side of the anvil, with sensor No. 1 opposite the working aperture. On diagram No. 2 sensor No. 1 is located inside, with sensor No. 2 on outer side. Oscillograms of impacts are shown in fig. 3 and 4.

Comparison of experimental data with the results of mathematical modeling. The calculated values of the first peak according to oscillograph (fig. 3, 4) and mathematical model are given in the table.

Calculation of elastic deformation according to oscillograph was made with reference to an earlier developed method of transformation factor calculation [5] and the Hooke's law under plane stress condition.

Comparison of estimated data according to oscillograph and theoretical data of mathematical model showed 14 % divergence at the most.
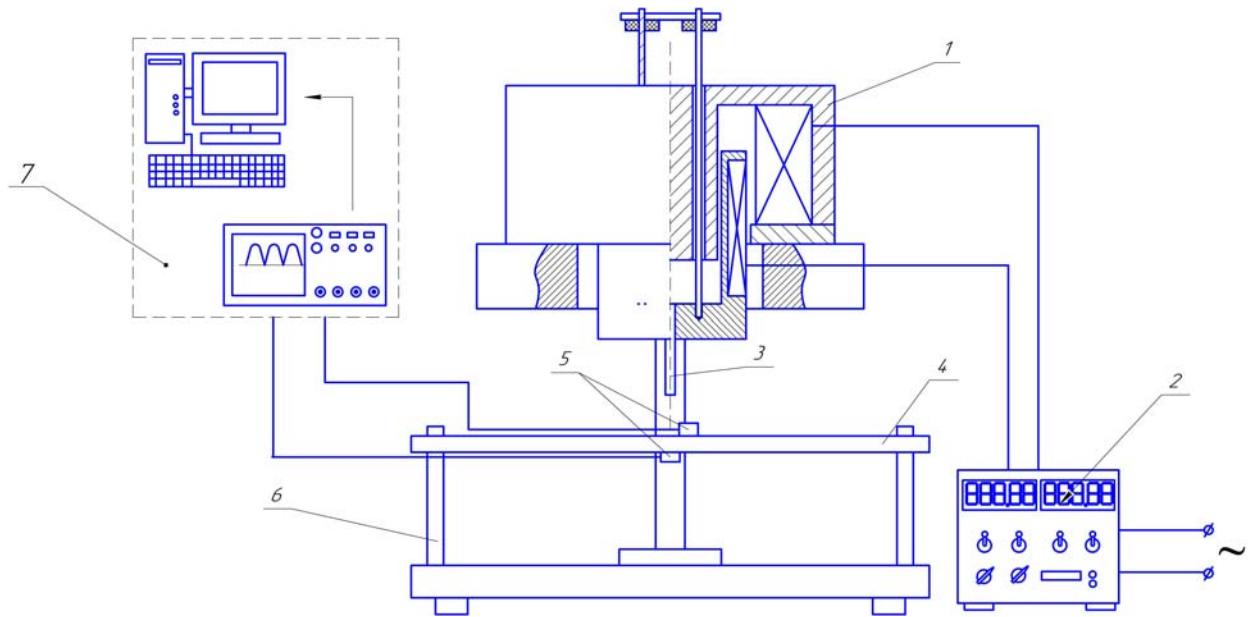

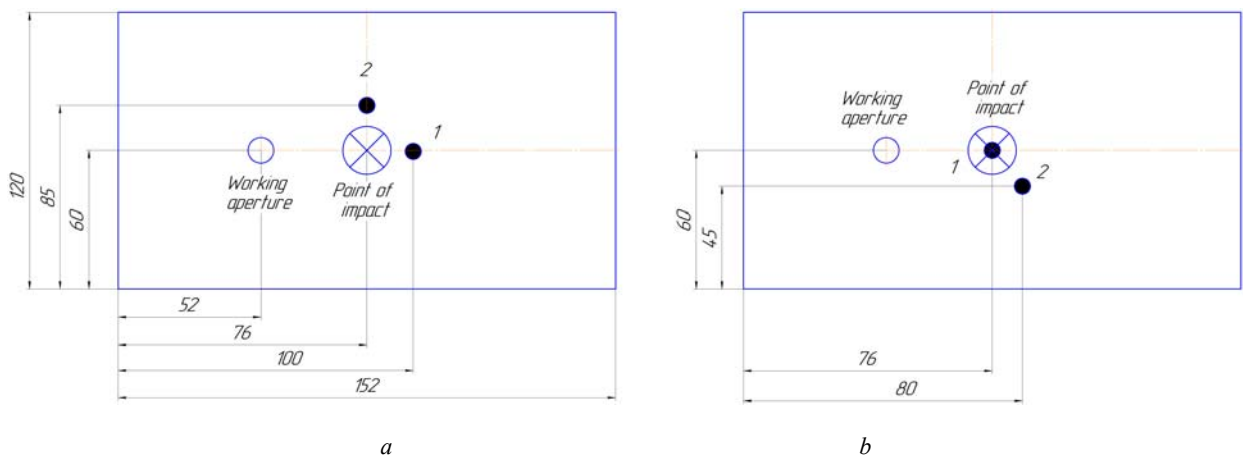Fig. 1. The scheme of the shock stand

Рис. 1. Схема ударного стенда

Fig. 2. Location of sensors:
a – scheme № 1; *b* – scheme № 2

Рис. 2. Схема расположения датчиков:
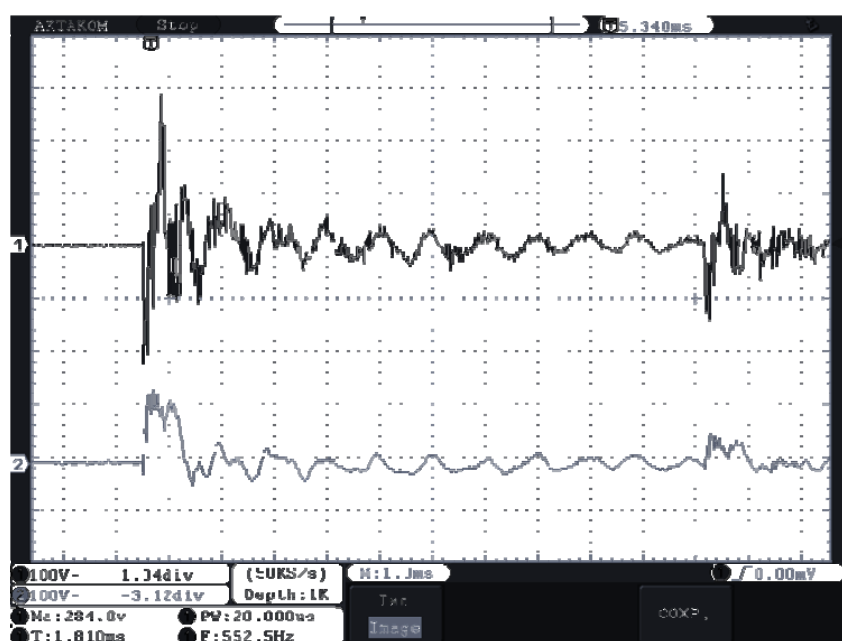*a* – схема № 1; *b* – схема № 2

Fig. 3. Recording of a signal from sensors according to the scheme № 1

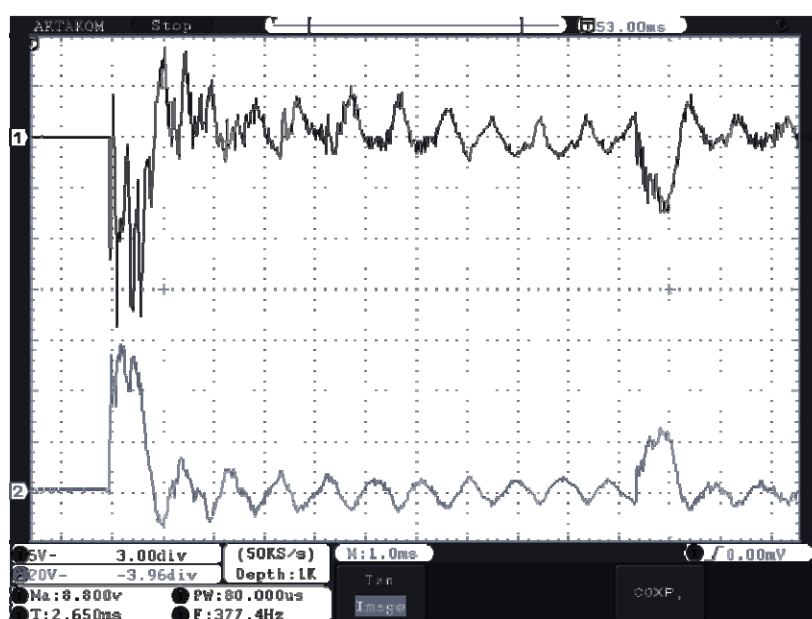Рис. 3. Регистрация сигнала датчиков по схеме № 1

Fig. 4. Recording of a signal from sensors according to the scheme № 2

Рис. 4. Регистрация сигнала датчиков по схеме № 2

Comparative results of the experiment and mathematical modeling

dia-gram	No In seq.	First stress peak value of sensor, B	Length of the first impulse, ms	Increment velocity, m/s	Estimated defor-mation value, m	Experimental defor-mation value, m
a	1	215	0.01			$4.418 \cdot 10^{-9}$
	2	38	0.05	3.3	$5.158 \cdot 10^{-9}$	$3.904 \cdot 10^{-9}$
b	1	12	0.1			$2.466 \cdot 10^{-9}$
	2	55	0.03			$3.39 \cdot 10^{-9}$

Conclusion. While performing the works the mathematical model of the linear electrodynamic engine operation with regard to hardened surface, elastic deformation was developed, also the elastic deformation in a contact spot was calculated. Experiments on signal recording with various arrangements of piezoelectric sensor on a counterbody (anvil) were made. Comparison of estimated data according to oscillograph and theoretical data of mathematical model was made, with the divergence which can be explained by the following factors:

1. Anvil material inhomogeneity: possible defects of the anvil material, work hardening. Another reason is that no defectoscopy of an anvil was applied and an anvil has a long term useful life.

2. Influence from mechanical (elastic) waves, such as: reflection, diffraction. Due to an aperture sensor No. 1 according to the layout 1 is placed in front of it.

3. Recordings of higher harmonics spread in the material made by piezoelectric sensors.

4. Influence of indirect calculation errors on experimental (approximate) dependences.

Despite divergences and shortcomings, it is possible to confirm a rather exact description of elastic deformation formation process in shock – pulse impact of the indenter on the hardened surface. Specified mathematical model of the linear electrodynamic drive operation in the shock - pulse mode allows to calculate parameters of material deformation with the set characteristics of a shock machine, and also to research materials' mechanical properties under various loading conditions.

Reference

1. Kirichek A. V, Solovyev D. L, Afonin A. N, Schubert A., Zaydler H. [Prospects of creating the multilevel surface layer by the deformation hardening] *Izvestiya Yugo-Zapadnogo gosudarstvennogo universiteta. Seriya Tekhnika i tekhnologii*. 2013, No. 4, P. 015–019 (in Russ.).

2. Kirichek A. V, Silantiev S. A. [Determination of the energy parameters of the shock mechanism used to harden the surface of plastic deformation]. *Izvestiya Yugo-Zapadnogo gosudarstvennogo universiteta*. 2014, No. 1 (52), P. 105–111.

3. Zaletdinov A. V. *Matematicheskoye modelirovaniye volnovykh protsessov v tverdykh telakh posle udarnogo vozdeystviya. Kand. Diss.* [Mathematical modeling of wave processes in solids after shock. Cand. Diss.]. Voronezh, 2014. 138 p.

4. Radchenko, A. V. Radchenko P. A. *Udarno-volnovyye protsessy i razrusheniye v anizotropnykh materialakh i konstruktsiyakh: monografiya* [Shock-wave processes and destruction in anisotropic materials and structures: a monograph]. Tomsk, Izd-vo Tom. gos. arkhit.-stroit. un-ta Publ., 2015, 204 p.

5. Fadeev A. A., Chestakov I. Y., Eresko T. T. [Use of the linear electrodynamic actuator for the research of shock interaction of materials]. *Vestnik SibSAU.* 2016, Vol. 17, No. 4, P. 1077–1087 (In Russ.).

6. Kirichek A., Silant'ev S. A. Determination of the Energy Parameters of the Shock Mechanism Used to Harden the Surface by Plastic Deformation. *Applied Mechanics and Materials*. 2015, Vol. 756, P. 85–91.

7. Ugarov G. G., Neiman V. Yu. *Elektromagnitnyy udarnyy instrument* [Electromagnetic percussion instrument]. Patent PF, No. 2099175, 1997.

8. Ugarov G. G., Neiman V. Yu. *Ustroystvo dlya kleymeniya yuvelirnykh izdeliy i instrumenta* [A device for stamping jewelry and tools]. Patent PF, No. 2065360, 1996.

9. Stryuk A. I., Bezyazykov S. A., Shestakov I. A., Shelkovsky O. L. *Elektrodinamicheskiy molot* [Electrodynamic hammer]. Patent PF, No. 2062167, 1996.

10. Chestakov I. Y., Stryuk A. I., Fadeev A. A. *Lineynyye elektrodinamicheskiye dvigateli. Konstruirovaniye. Prakticheskoye ispol'zovaniye* [Linear electrodynamic motors. Designing. Practical use]. Krasnoyarsk, SibGAU Publ., 2011, 148 p.

11. Fadeev A. A., Chestakov I. Y., Eresko T. T. [A mathematical model of the percussion device on the basis of the linear electrodynamic actuator]. *Materialy XVIII Mezhdunar. nauch. konf. "Reshetnevskie chteniya"* [Materials XVIII Intern. Scientific. Conf "Reshetnev reading"]. Krasnoyarsk, 2014, P. 315–316 (In Russ.).

12. Stryuk A. I., Bezyazykov S. A., Shestakov I. A., Shelkovsky O. L. *Sposob upravleniya rabotoy elektrodinamicheskogo molota* [The method of controlling the operation of an electrodynamic hammer]. Patent PF, No. 2062168, 1996.

13. Eresko S. P, Eresko T. T, Fadeev A. A *Sovershenstvovaniye konstruktsiy i metodov proyektirovaniya vibroudarnykh mekhanizmov* [Improvement of designs and methods of design of vibro-shock mechanisms]. Krasnoyarsk, 2017, 190 p.

14. Shvaleva N. A, Fadeev A. A., Eresko T. T. [Mathematical model of the operation of a linear electrodynamic motor upon impact with allowance for elastic deformation]. *Materialy XXII Mezhdunar. nauch. konf. "Reshetnevskie chteniya"* [Materials XVIII Intern. Scientific. Conf "Reshetnev reading"]. Krasnoyarsk, 2018, P. 515–516 (In Russ.).

15. Kirichek A. V., Solov'ev D. L. Lazutkin A. G. *Teknologiya i obirudovanie statiko-impul'snoj obrabotki poverchnosti plasticheskim deformirovaniem: Biblioteka tekhnologa* [Technology and equipment, staticpulse processing surface plastic deformation: a Library technologist]. Moscow, Mashinostroenie Publ., 2004, 228 p.

16. Drozd M. S., Matlin M. M., Sidyakin Yu. I. *Inzhenernye raschety uprugo-plasticheskoy deformatsii* [Engineering analysis of elastic-plastic deformation]. Moscow, Mashinostroenie Publ., 1986, 230 p.

Библиографические ссылки

1. Перспективы создания многоуровневого поверхностного слоя деформационным упрочнением / А. В. Киричек, Д. Л. Соловьев, А. Н. Афонин [и др.] // Известия Юго-Западного гос. ун-та. Серия «Техника и технологии». 2013. № 4. С. 015–019.

2. Киричек А. В., Силантьев С. А. Определение энергетических параметров ударных механизмов, используемых для упрочнения поверхностным пластическим деформированием // Известия Юго-Западного гос. ун-та. 2014. № 1 (52). С. 105–111.

3. Залетдинов А. В. Математическое моделирование волновых процессов в твердых телах после удар-

ного воздействия : дис. ... канд. тех. наук : 05.13.18. Воронеж, 2014. 138 с.

4. Радченко А. В. Радченко П. А. Ударно-волновые процессы и разрушение в анизотропных материалах и конструкциях : монография. Томск : Изд-во Том. гос. архит.-строит. ун-та, 2015. 204 с.

5. Фадеев А. А., Шестаков И. Я., Ереско Т. Т. Использование линейного электродинамического привода для исследования ударного взаимодействия материалов // Вестник СибГАУ. 2016. Т. 17, № 4. С. 1077–1087.

6. Kirichek A., Silant'ev S. A. Determination of the Energy Parameters of the Shock Mechanism Used to Harden the Surface by Plastic Deformation // Applied Mechanics and Materials. 2015. Vol. 756. P. 85–91.

7. Пат. 2099175 РФ, МПК B25D13/00. Электромагнитный ударный инструмент / Г. Г. Угаров, В. Ю. Нейман ; заявитель и патентообладатель Институт горного дела СО РАН ; заявл. 24.02.1995 ; опубл. 20.12.1997, Бюл. № 34.

8. Пат. № 2065360. Устройство для клеймения ювелирных изделий и инструмента / Г. Г. Угаров, В. Ю. Нейман ; опубл. 1996, Бюл. № 32.

9. Пат. 2062167 РФ, МПК B 21 J 7/30. Электродинамический молот / А. И. Стрюк, С. А. Безъязыков, И. А. Шестаков, О. Л. Шелковский ; опубл. 20.06.1996, Бюл. № 7.

10. Шестаков И. Я., Стрюк А. И., Фадеев А. А. Линейные электродинамические двигатели. Конструирование. Практическое использование : монография / Сиб. гос. аэрокосмич. ун.-т. Красноярск, 2011. С. 148.

11. Фадеев А. А., Шестаков И. Я., Ереско Т. Т. Математическая модель работы ударного устройства на основе линейного электродинамического привода // Решетневские чтения : материалы XVIII Междунар. науч.-практ. конф. (Красноярск, 11–14 нояб. 2014 г.) : в 3 ч. Ч. 1 / под общ. ред. Ю. Ю. Логинова ; Сиб. гос. аэрокосмич. ун-т. Красноярск, 2014. С. 315–316.

12. Пат. 20062168 РФ. МПК В 21 J 7/30. Способ управления работой электродинамического молота / А. И. Стрюк, С. А. Безъязыков, И. А. Шестаков, О. Л. Шелковский ; опубл. 20.06.1996, Бюл. № 17.

13. Ереско С. П., Ереско Т. Т., Фадеев А. А. Совершенствование конструкций и методов проектирования виброударных механизмов : монография / СибГУ им. М. Ф. Решетнева. Красноярск, 2017. 190 с.

14. Швалева Н. А., Фадеев А. А., Ереско Т. Т. Математическая модель работы линейного электродинамического двигателя при ударе с учетом упругой деформации // Решетневские чтения : материалы XXII Междунар. науч.-практ. конф. (Красноярск, 12–16 нояб. 2018 г.) : в 2 ч. Ч. 1 / под общ. ред. Ю. Ю. Логинова ; СибГУ им. М. Ф. Решетнева. Красноярск, 2018. С. 515–516.

15. Киричек А. В., Соловьев Д. Л., Лазуткин А. Г. Технология и оборудование статико-импульсной обработки поверхностным пластическим деформированием. М. : Машиностроение, 2004. 287 с.

16. Дрозд М. С., Матлин М. М., Сидякин Ю. И. Инженерные расчеты упруго-пластической деформации. М. : Машиностроение, 1986. 230 с.

Shvaleva Natalya Aleksandrovna – master's degree student, Reshetnev Siberian State University of Science and Technology. E-mail: natalyashvaleva@ya.ru.

Fadeev Aleksandr Aleksandrovich – Cand. Sc., docent, Reshetnev Siberian State University of Science and Technology, E-mail: fadeev.77@mail.ru.

Eresko Tatiana Trofimovna – Dr. Sc., docent, head of Department of Fundamentals of designing machines, Institute of Mechanical Engineering and Mechatronics, Reshetnev Siberian State University of Science and Technology. E-mail: ereskottt@mail.ru.

Швалева Наталья Александровна – магистрант, Сибирский государственный университет науки и технологий имени академика М. Ф. Решетнева. E-mail: natalyashvaleva@ya.ru.

Фадеев Александр Александрович – кандидат технических наук, доцент, заместитель директора; Сибирский государственный университет науки и технологий имени академика М. Ф. Решетнева, Институт машиноведения и мехатроники. E-mail: fadeev.77@mail.ru.

Ереско Татьяна Трофимовна – доктор технических наук, доцент, заведующий кафедрой основ конструирования машин, Сибирский государственный университет науки и технологий имени академика М. Ф. Решетнева. E-mail: ereskottt@mail.ru.